

Advances

in Clinical and Experimental Medicine

MONTHLY ISSN 1899-5276 (PRINT) ISSN 2451-2680 (ONLINE)

advances.umw.edu.pl

2023, Vol. 32, No. 8 (August)

Impact Factor (IF) – 2.1
Ministry of Science and Higher Education – 140 pts
Index Copernicus (ICV) – 168.52 pts



WROCLAW
MEDICAL UNIVERSITY

Advances
in Clinical and Experimental
Medicine



Advances in Clinical and Experimental Medicine

ISSN 1899-5276 (PRINT)

ISSN 2451-2680 (ONLINE)

advances.umw.edu.pl

MONTHLY 2023
Vol. 32, No. 8
(August)

Advances in Clinical and Experimental Medicine (*Adv Clin Exp Med*) publishes high-quality original articles, research-in-progress, research letters and systematic reviews and meta-analyses of recognized scientists that deal with all clinical and experimental medicine.

Editorial Office

ul. Marcinkowskiego 2–6
50-368 Wrocław, Poland
Tel.: +48 71 784 12 05
E-mail: redakcja@umw.edu.pl

Publisher

Wrocław Medical University
Wybrzeże L. Pasteura 1
50-367 Wrocław, Poland

Online edition is the original version
of the journal

Editor-in-Chief

Prof. Donata Kurpas

Deputy Editor

Prof. Wojciech Kosmala

Managing Editor

Marek Misiak, MA

Scientific Committee

Prof. Sabine Bährer-Kohler
Prof. Antonio Cano
Prof. Breno Diniz
Prof. Erwan Donal
Prof. Chris Fox
Prof. Naomi Hachiya
Prof. Carol Holland
Prof. Markku Kurkinen
Prof. Christos Lionis

Statistical Editors

Wojciech Bombała, MSc
Anna Kopszak, MSc
Dr. Krzysztof Kujawa
Jakub Wronowicz, MSc

Manuscript editing

Marek Misiak, MA, Jolanta Prazeres, MA

Prof. Raimundo Mateos
Prof. Zbigniew W. Raś
Prof. Jerzy W. Rozenblit
Prof. Silvana Santana
Prof. James Sharman
Prof. Jamil Shibli
Prof. Michał Toborek
Prof. László Vécsei
Prof. Cristiana Vitale

Section Editors

Anesthesiology

Prof. Marzena Zielińska

Basic Sciences

Prof. Iwona Bil-Lula
Prof. Bartosz Kempisty
Dr. Wiesława Kranc
Dr. Anna Lebedeva

Clinical Anatomy, Legal Medicine, Innovative Technologies

Prof. Rafael Boscolo-Berto

Dentistry

Prof. Marzena Dominiak
Prof. Tomasz Gedrange
Prof. Jamil Shibli

Laser Dentistry

Assoc. Prof. Kinga Grzech-Leśniak

Dermatology

Prof. Jacek Szepietowski

Emergency Medicine, Innovative Technologies

Prof. Jacek Smereka

Gynecology and Obstetrics

Prof. Olimpia Sipak-Szmigiel

Histology and Embryology

Dr. Mateusz Olbromski

Internal Medicine

Angiology

Dr. Angelika Chachaj

Cardiology

Prof. Wojciech Kosmala
Dr. Daniel Morris

Endocrinology

Prof. Marek Bolanowski

Gastroenterology

Assoc. Prof. Katarzyna Neubauer

Hematology

Prof. Andrzej Deptała

Prof. Dariusz Wołowicz

Nephrology and Transplantology

Assoc. Prof. Dorota Kamińska

Assoc. Prof. Krzysztof Letachowicz

Pulmonology

Prof. Anna Brzecka

Microbiology

Prof. Marzenna Bartoszewicz

Assoc. Prof. Adam Junka

Molecular Biology

Dr. Monika Bielecka

Prof. Jolanta Saczko

Neurology

Assoc. Prof. Magdalena Koszewicz

Assoc. Prof. Anna Pokryszko-Dragan

Dr. Masaru Tanaka

Neuroscience

Dr. Simone Battaglia

Dr. Francesco Di Gregorio

Oncology

Prof. Andrzej Deptała

Prof. Adam Maciejczyk

Dr. Marcin Jędryka

Gynecological Oncology

Dr. Marcin Jędryka

Ophthalmology

Dr. Małgorzata Gajdzis

Orthopedics

Prof. Paweł Reichert

Otolaryngology

Assoc. Prof. Tomasz Zatoński

Pediatrics

Pediatrics, Metabolic Pediatrics, Clinical Genetics, Neonatology, Rare Disorders

Prof. Robert Śmigiel

Pediatric Nephrology

Prof. Katarzyna Kiliś-Pstrusińska

Pediatric Oncology and Hematology

Assoc. Prof. Marek Ussowicz

Pharmaceutical Sciences

Assoc. Prof. Marta Kepinska

Prof. Adam Matkowski

Pharmacoeconomics, Rheumatology

Dr. Sylwia Szafraniec-Buryło

Psychiatry

Prof. Jerzy Leszek

Assoc. Prof. Bartłomiej Stańczykiewicz

Public Health

Prof. Monika Sawhney

Prof. Izabella Uchmanowicz

Qualitative Studies, Quality of Care

Prof. Ludmiła Marcinowicz

Radiology

Prof. Marek Sądadek

Rehabilitation

Dr. Elżbieta Rajkowska-Labon

Surgery

Assoc. Prof. Mariusz Chabowski

Assoc. Prof. Mirosław Kozłowski

Prof. Renata Taboła

Telemedicine, Geriatrics, Multimorbidity

Assoc. Prof. Maria Magdalena

Bujnowska-Fedak

Editorial Policy

Advances in Clinical and Experimental Medicine (Adv Clin Exp Med) is an independent multidisciplinary forum for exchange of scientific and clinical information, publishing original research and news encompassing all aspects of medicine, including molecular biology, biochemistry, genetics, biotechnology and other areas. During the review process, the Editorial Board conforms to the "Uniform Requirements for Manuscripts Submitted to Biomedical Journals: Writing and Editing for Biomedical Publication" approved by the International Committee of Medical Journal Editors (www.ICMJE.org). The journal publishes (in English only) original papers and reviews. Short works considered original, novel and significant are given priority. Experimental studies must include a statement that the experimental protocol and informed consent procedure were in compliance with the Helsinki Convention and were approved by an ethics committee.

For all subscription-related queries please contact our Editorial Office: redakcja@umw.edu.pl

For more information visit the journal's website: advances.umw.edu.pl

Pursuant to the ordinance of the Rector of Wrocław Medical University No. 12/XVI R/2023, from February 1, 2023, authors are required to pay a fee for each manuscript accepted for publication in the journal Advances in Clinical and Experimental Medicine. The fee amounts to 990 EUR for original papers and meta-analyses, 700 EUR for reviews, and 350 EUR for research-in-progress (RIP) papers and research letters.

Advances in Clinical and Experimental Medicine has received financial support from the resources of Ministry of Science and Higher Education within the "Social Responsibility of Science – Support for Academic Publishing" project based on agreement No. RCN/SP/0584/2021.



Ministry of Education and Science
Republic of Poland

Czasopismo Advances in Clinical and Experimental Medicine korzysta ze wsparcia finansowego ze środków Ministerstwa Edukacji i Nauki w ramach programu „Społeczna Odpowiedzialność Nauki – Rozwój Czasopism Naukowych” na podstawie umowy nr RCN/SP/0584/2021.



Ministerstwo
Edukacji i Nauki

Indexed in: MEDLINE, Science Citation Index Expanded, Journal Citation Reports/Science Edition, Scopus, EMBASE/Excerpta Medica, Ulrich's™ International Periodicals Directory, Index Copernicus

Typographic design: Piotr Gil, Monika Kołęda

DTP: Wydawnictwo UMW

Cover: Monika Kołęda

Printing and binding: Drukarnia I-BiS Bierońscy Sp.k.

Contents

Editorials

- 829 Idris Demirsoy, Adnan Karaibrahimoglu
Identifying drug interactions using machine learning

Meta-analyses

- 839 Shuheng Yang, Yadong Zhou, Lei Zeng
Regorafenib compared to nivolumab after sorafenib failure in patients with hepatocellular carcinoma: A systematic review and meta-analysis

Original papers

- 847 Zexin Hou, Lili Zhao, Lingjun Zou, Benlan Li
The prognostic value of tumor-infiltrating lymphocytes in non-small cell lung cancer patients who received neoadjuvant chemotherapy followed by surgery
- 855 Shu Wang, YuQi Zhu, Xiaohan Qian, Tianling Ding, Yan Yuan, Yuan Li, Hanfeng Wu, Tong Chen
The outcome of ibrutinib-based regimens in relapsed/refractory central nervous system lymphoma and the potential impact of genomic variants
- 865 Shujun Wang, Weiwei Ding, Ying Du, Qing Qi, Kaiyun Luo, Jianfeng Luan, Yanfei Shen, Baoan Chen
Allogeneic platelet gel therapy for refractory abdominal wound healing: A preliminary study
- 873 Lan Li, Xiaoyan Wu, Lemin He, Rong Luo, LiQiong Lou
Serum levels of SOCS6 are decreased in diabetic retinopathy and are related to severity of the disease
- 881 Sami Bilici, Durdu Altuner, Zeynep Suleyman, Seval Bulut, Cengiz Sarigul, Mine Gulaboglu, Fikret Altindag, Adalet Ozcicek, Cebraail Gursul, Halis Suleyman
Favipiravir-induced inflammatory and hydropic degenerative liver injury in rats
- 889 Xiangyu Qi, Qingbo Guan, Wenjing Zhang, Xinshuang Huang, Chunxiao Yu
The time-dependent adverse effects of a high-fat diet on sperm parameters
- 901 Tomáš Ventruba, Pavel Ventruba, Michal Jeřeta, Jana Žáková, Eva Lousová, Igor Crha, Tereza Souralová, Irena Koutná, Aleš Hampl
The contribution of donated human embryos suitable for the production of embryonic stem cells to increase the quality of life: Selection and preparation of embryos in the Czech Republic
- 909 Nan Wang, Daquan Jiang, Chunxiu Zhou, Xi Han
Alpha-solanine inhibits endothelial inflammation via nuclear factor kappa B signaling pathway

Reviews

- 921 Karolina Fiona Osypko, Michał Piotr Ciszynski, Paweł Kubasiewicz-Ross, Jakub Hadzik
Bone tissue 3D bioprinting in regenerative dentistry through the perspective of the diamond concept of healing: A narrative review

Identifying drug interactions using machine learning

Idris Demirsoy^{1,A–C,F}, Adnan Karaibrahimoglu^{2,D,E}

¹ Department of Computer Engineering, Faculty of Engineering, Uşak University, Turkey

² Department of Biostatistics and Medical Informatics, Suleyman Demirel University, Isparta, Turkey

A – research concept and design; B – collection and/or assembly of data; C – data analysis and interpretation;

D – writing the article; E – critical revision of the article; F – final approval of the article

Advances in Clinical and Experimental Medicine, ISSN 1899–5276 (print), ISSN 2451–2680 (online)

Adv Clin Exp Med. 2023;32(8):829–838

Address for correspondence

Idris Demirsoy

Email: idrisdemirsoy1@gmail.com

Funding sources

None declared

Conflict of interest

None declared

Acknowledgements

Idris Demirsoy would like to thank all the people whose assistance was a milestone in the completion of this project. The author thanks Mondira Bhattacharya for introducing him to people who are expert in their field, Jaishri Meer for providing detailed information about drug–drug interactions and showing him MedDRA system, among others. The author would like to thank Tim Carlson for explaining the clinical drug–drug interactions, among others, Erhan Berber for emphasizing patient view on drug–drug interactions, Balachandra Ambiga for selecting him for the project, and Shereen McIntyre for believing in him and supporting him.

Abstract

The majority of Americans, accounting for 51% of the population, take 2 or more drugs daily. Unfortunately, nearly 100,000 people die annually as a result of adverse drug reactions (ADRs), making it the 4th most common cause of mortality in the USA. Drug–drug interactions (DDIs) and their impact on patients represent critical challenges for the healthcare system. To reduce the incidence of ADRs, this study focuses on identifying DDIs using a machine-learning approach. Drug-related information was obtained from various free databases, including DrugBank, BioGRID and Comparative Toxicogenomics Database. Eight similarity matrices between drugs were created as covariates in the model in order to assess their influence on DDIs. Three distinct machine learning algorithms were considered, namely, logistic regression (LR), eXtreme Gradient Boosting (XGBoost) and neural network (NN). Our study examined 22 notable drugs and their interactions with 841 other drugs from DrugBank. The accuracy of the machine learning approaches ranged from 68% to 78%, while the F1 scores ranged from 78% to 83%. Our study indicates that enzyme and target similarity are the most significant parameters in identifying DDIs. Finally, our data-driven approach reveals that machine learning methods can accurately predict DDIs and provide additional insights in a timely and cost-effective manner.

Key words: prediction, machine learning algorithms, drug–drug interaction, similarity matrices, biostatistics

Received on January 18, 2023

Reviewed on April 3, 2023

Accepted on July 21, 2023

Published online on August 14, 2023

Cite as

Demirsoy I, Karaibrahimoglu A. Identifying drug interactions using machine learning. *Adv Clin Exp Med.* 2023;32(8):829–838. doi:10.17219/acem/169852

DOI

10.17219/acem/169852

Copyright

Copyright by Author(s)

This is an article distributed under the terms of the Creative Commons Attribution 3.0 Unported (CC BY 3.0) (<https://creativecommons.org/licenses/by/3.0/>)

Introduction

A drug interaction occurs when one drug affects another drug by increasing or decreasing its effect. The manipulated effect of the drug might cause unwanted and unexpected side effects. Important pharmacological cycles that impact bioavailability, including assimilation, dissemination, digestion, and discharge, may be influenced by communication.¹ Such associations can incorporate issues like the organization of a medication that raises digestive system motility and decreases the retention of other medications, as well as the rivalry for a similar plasma protein carrier, restraint of the activity of an administered medication, or a communication at the discharge level, which influences the end of one of the medications.² Additionally, pharmacodynamic interactions may take place at the pharmacological level when 2 drugs interact with the same protein, at the signal level involving different signaling pathways, or at the effector level where different pharmacological responses are elicited.³ Hence, it is not feasible to identify or predict all drug interactions. However, it is possible to evaluate and comprehend the most important features affecting drug–drug interactions (DDIs) using the approach proposed in our study. Our method provides satisfactory results and insight into which covariates are most used while identifying DDIs.

Three types of approach are mainly implemented to predict DDI methods using machine learning approaches: 1) a similarity-based approach, 2) a classification-based approach and 3) a text mining approach. Some examples of these methods⁴ use similarity-based modeling with few similarity matrices such as 2D molecular structure, interaction profile, target, and side-effect similarities. On the other hand,⁵ some use a large-scale logistic regression (LR) model to predict potential DDIs. From the chemical–protein interactome (CPI) profile-based similarity to MeSH-based similarity, 10 similarities were used.⁶ Wu

et al. provided a 3-tiered hierarchical text mining approach for Drug-Drug Interaction (DDI) analysis, designed to label essential terms, sentences containing drug interactions, and pairs of interacting drugs.⁶ However, text mining was not preferred by researchers, as they used classification-based approach⁷ to apply a new trend of similarity-based methods. Using the idea proposed by Vilar et al., a weighted similarity network was developed.² Similarly, Rohani and Eslahchi used a feature matrix with only using one machine learning algorithm, a neural network (NN).⁷ Most of these classification-based machine learning algorithms only use either a predictor or multiple predictors which are similar to other researches with LR. We offer to use more predictors with advanced machine learning algorithms.

Predicting DDIs can be investigated as a binary classification problem,^{7,8} where the dependent variable is the interaction or non-interaction; the goal is to correctly label the DDIs. Our method uses feature matrices with classification-based machine learning algorithms, not only to compare different algorithms but also to write and create our dataset, as explained in Feature matrices section. In Materials and methods section, we pointed out where the data was collected and which databases were used. Additionally, we briefly introduced the machine learning algorithms used in the paper. Sample feature matrices are shown in Table 1. The first 2 columns stand for drug 1 and drug 2 names, others represent 8 feature matrices. Each of them, independently, shows how similar 2 drugs are based on a specific feature. Under the drug name, there is a code that stands for the DrugBank ID for that specific drug. It helps to work on drugs based on data structures such as split and merge. In Table 1, DB00176 stands for fluvoxamine which is a serotonin reuptake inhibitor used to treat obsessive-compulsive disorder. Fluvoxamine is also one of the most used antidepressants with cardiovascular drugs.⁹ Therefore, it has been chosen for illustration purposes in Table 1. The drugs in the 2nd column were chosen randomly. For example,

Table 1. Sample feature matrices

Drug 1, DrugBank ID	Drug 2, DrugBank ID	Pathway	MedDRA	Molecular	ATC	Target	Enzyme	PPI	Disease	Y
Fluvoxamine DB00176	norethisterone DB00717	0.881	0.171	0.065	0.000	0.010	0.179	0.211	0.172	1
Fluvoxamine DB00176	candesartan DB13919	0.885	0.112	0.191	0.000	0.015	0.206	0.174	0.071	1
Fluvoxamine DB00176	ergotamine DB00696	0.894	0.145	0.141	0.122	0.018	0.318	0.129	0.237	1
Fluvoxamine DB00176	aldosterone DB04630	0.879	0.050	0.090	0.000	0.008	0.152	0.170	0.163	0
Fluvoxamine DB00176	norfloxacin DB001059	0.886	0.173	0.141	0.000	0.009	0.328	0.232	0.296	1
Fluvoxamine DB00176	ropivacaine DB00296	0.938	0.162	0.188	0.123	0.006	0.336	0.208	0.139	1

MedDRA – Medical Dictionary for Regulatory Activities; ATC – Anatomical Therapeutic Chemical; PPI – protein–protein interaction. The dataset contains 11 columns, the first 2 are drug names. The next 8 columns are feature matrices that show similarities between 2 drugs in the sense of the concept. The final column, Y, shows whether or not 2 drugs are interacting: 1 corresponds to interactions and 0 corresponds to non-interactions.

Table 2. Comparison of the methods based on evaluation metrics

Algorithms	Accuracy	Sensitivity	Specificity	F1 Score	Kappa
Logistic regression	0.6864	0.6837	0.6988	0.7816	0.2641
Neural network	0.7510	0.7501	0.7533	0.8137	0.4154
XGBoost	0.7812	0.7911	0.7613	0.8310	0.5508

XGBoost – eXtreme Gradient Boosting. The largest numbers are bolded.

DB00717 stands for norethisterone, a progesterone used for birth control. The table can read Pathway similarities between them as 0.881, Medical Dictionary for Regulatory Activities (MedDRA) (side effect) similarities as 0.171, ATC similarities as 0.000, enzyme similarities as 0.179, and so on. Feature matrices section explains the methods used to compute each column. In the Data analysis section, the methods of data analysis are described in detail. The data were fitted using 3 machine learning algorithms and the obtained minimum accuracy was 68.64%, the minimum F1 score was 78.16% from LR, the maximum accuracy was 78.12%, and the maximum F1 score was 83.1% from eXtreme Gradient Boosting (XGBoost) (Table 2). In Conclusions section, the importance of features is explained, and the most important covariate for explaining DDIs is plotted for trained data. Finally, future work is discussed.

Materials and methods

When a patient takes numerous medications, clinical DDIs can develop. Clinical toxicity or treatment failures can be caused by these DDIs. Therefore, DDI evaluations are an important element of medication development and the risk–benefit analysis of novel treatments. In their DDI guidance documents, regulatory agencies such as the Food and Drug Administration (FDA) of the USA, the Pharmaceuticals and Medical Devices Agency (PMDA) of Japan, and the European Medicines Agency (EMA) have recommended various methodologies (in vitro, clinical, and in silico) to examine DDI potentials, which can be utilized with patient management strategies. In this project, we conducted non-clinical DDI testing. Therefore, in this paper, publicly available databases were used. The following databases were used:

- DrugBank: A freely available database that stores drug information such as the Anatomical Therapeutic Chemical (ATC) codes enzymes, transporters and interactions;
- TwoSIDES: A freely available database with information about adverse drug reactions, side effects and drug indications;
- BioGRID: A public database that stores and disseminates data on genetic and protein interactions in human models and organisms;
 - PubChem: A reference database for drug structures;
 - UniProt: A database of protein sequences and functions that is open to the public.

Similarity metrics

Distance or similarity metrics were used in a broad range of applications, prompting evaluations of their effectiveness in fields such as texture image retrieval, web page clustering and social media event detection.¹⁰ The 3 most common similarity metrics include the Tanimoto coefficient, the Dice coefficient and the Cosine similarity.

The similarity values obtained using these methods were non-negative and included values between 0 to 1, including 0 and 1. When there was no similarity, a value of 0 was selected, and for many similarities, a value of 1 was chosen. The formulas compute these metrics and more can be found in Bajusz et. al.¹⁰ We mainly used Tanimoto similarity metrics while computing our feature matrices (Equation 1):

$$\text{Tanimoto coefficient} = T(A, B) = \frac{c}{a + b - c} \quad (1)$$

where a is the total number of objects in A, b is the total number of objects in B and c is the number of common objects between A and B, in which A and B stands for the features of drug 1 and drug 2.

Inverse document frequency

In the raw frequency, all terms are given equal importance.¹¹ However, it is known that some terms are repeated frequently, but they are not as important as once thought. Therefore, inverse document frequency (IDF) is a metric for determining whether a phrase is common or uncommon in a corpus of documents.¹² For example, after applying IDF for side effect (MedDRA) similarity, in the beginning, all of the reported side effects are counted, the number of unique side effects is identified, and a frequency table is created. Finally, the IDF of each unique side effect is computed using the following formula (Equation 2):

$$\text{IDF}(t, \text{drugs}) = \log \left[\frac{n}{df(t, \text{drugs})} \right] \quad (2)$$

where N is the total number of documents, t denotes the interest, and df(t, drugs) denotes the number of medicines with the interest. If a side effect is reported frequently, it gets a smaller IDF number because of the natural logarithm of the fraction.

XGBoost

The XGBoost is one of the most preferred classification methods. It is not only computationally fast, but it also gives accurate results when compared to some other algorithms.¹³ The XGBoost is a tree-based algorithm that is similar to a decision tree; however, it uses a parallel computing feature. The XGBoost uses base/weak learners, which are only slightly better than guessing, but combines a bunch of the weak learners to create a strong learner, which is a form of ensemble learning. It weighs each weak learner prediction based on its prediction performance.¹⁴ The XGBoost uses 3 main forms of gradient boosting inside the algorithm. The learning rate is contained in gradient boosting, also known as the gradient boosting machine. For the training, test and validation sets, stochastic gradient boosting operates as a random sub-sample at the row and column level (if applicable). Finally, Regularized Gradient Boosting contains both L1, also known as Lasso regularization, and L2, also known as Ridge regularization. The XGBoost was chosen for this study because of its speed and excellent overall performance. The XGBoost constructs an ensemble of classification trees (as in classification and regression tree (CART)). When adding the t^{th} tree to the ensemble, the objective function for XGBoost can be formulated as follows (Equation 3):

$$\text{Obj}(\theta) = L(\theta) + \Omega(\theta) \quad (3)$$

where $L(\theta)$ denotes the loss function and $\Omega(\theta)$ denotes the regulation function. More details of XGBoost can be found in Chen et al.¹⁵

Neural network

An NN is a computer program that uses algorithms to find patterns in a group of data.¹⁶ It resembles the work of human brain which tries to find relationships between things. In this context, a NN is a type of nervous system that can be biological or artificial.

A simple NN contains 3 layers: input, hidden and output. A layer is a collection of neurons. Usually, the number of hidden layers defines the name of the network. More details about NNs can be found in many valuable sources, such as the study by Paul and Singh.¹⁷ Activation functions are a very important part of NNs since they play a critical role in learning and understanding non-linear relationships between the input and output signals. The activation function in a NN receives a signal from the input, transforms it into an output signal, and sends it to the next layer. Except for the output layer, the rectified linear unit (ReLU) is a piecewise linear function used as an activation function because it has constraints on weights. When the value is less than 0, it takes 0; otherwise, it takes the obtained value.¹⁸ There are a few advantages of using ReLUs. Because of the constraint, taking the inverse of the function is easy. Moreover, ReLU does not activate all neurons, which helps

in fast computation. For the output layer, sigmoid function has been chosen (Equation 4):

$$\text{Sigmoid} = S(x) = \frac{1}{1 + e^{-x}} \quad (4)$$

Sigmoid is mainly chosen because as an output we are interested in interaction (1) and non-interaction (0).¹⁹ In Equation 4, e stands for Euler's number.

Logistic regression

Logistic regression is a statistical model in which dependent variables are categorical and have only 2 levels, such as success/failure and interaction/non-interaction. Principally, LR is suitable to test the hypothesis about relationships between a dichotomous response and one or more categorical or continuous explanatory variables.

Since LR can accommodate multiple-level categorical dependent variables, but we are interested in 2 levels only, we defined the basic LR form as follows (Equation 5):

$$\text{logit}(Y) = \log\left(\frac{\pi}{1 - \pi}\right) = \beta_0 + \beta_1 X \quad (5)$$

where π is the probability of the outcome of interest, β_0 is the intercept, β_1 is the slope, and X is an arbitrary explanatory variable.

The LR-fitted line plot has a sigmoid or S-shaped curve and misrepresents data when using the linear regression line. Hence, LR uses logit, which stands for natural logarithm, to respond to variables. More details on LR can be found in the study by Peng et al.²⁰

Feature matrices

The DDI data were collected from different sources. Drug-Bank database v. 5.6. (<https://go.drugbank.com>; retrieved by June 2020) is a free drug information source that provides over 1.3 million accurate and updated DDIs covering all FDA- and Health Canada-approved drug sources from drug labels and references. Another free source, the Comparative Toxicogenomics Database (<http://ctdbase.org/downloads/>; retrieved June 2020) is used for pathway and disease similarity. The TwoSIDES database (<http://tatonettilab.org/resources/nsides/>; retrieved June 2020) includes the information on adverse effects of the interacting drugs.

The DDI dataset, which was downloaded from Drug-Bank, was transformed into a matrix with dichotomous values [0,1] representing the interaction between 2 drugs. The extra columns take values between 0 and 1, which shows the similarity between the 2 drugs based on specific features such as chemicals, enzymes and proteins. When it comes to predicting new interactions, our method provides DDI predictions using the similarity between known DDIs and new drug pairs. Our basic assumption is that if drug A has a known interaction with drug B and

the similarity between drug B and new drug C is greater than a certain threshold, then drug A will interact with drug C. If the 2 drugs are known to interact, and there is another drug that is comparable to one of the drugs in the DDI pair, the 3rd drug can cause a DDI.

Feature vectors

One of the most important aspects of any statistical learning method is the extraction of a meaningful collection of features. Classic prediction studies primarily consider topological features. Ding et al. points that machine learning-based approaches can be divided into 3 groups.²¹ We combined all these types to create a feature matrix that contains approaches from all these types. In these types of setups, each feature matrix is an explanatory variable. Therefore, it would be beneficial to have as many feature matrices as possible. After an extensive literature review, we found out that creating the following feature matrices is feasible and advantageous.

Molecular structure similarity

To begin with, we present a specified collection of chemicals as simplified molecular-input line-entry system (SMILES) strings obtained from DrugBank. The RDKit was used to transform the SMILES strings into molecular extended connectivity fingerprints (ECFP; Open-Source Cheminformatics Software).²² The two-dimensional Tanimoto similarity measure, also known as the Jaccard similarity measure of the fingerprints, was used to calculate the similarity scores between 2 drug molecules.

ATC similarity

The World Health Organization (WHO) uses the Anatomical Therapeutic Chemical (ATC) classification system, which is a hierarchical classification system that organizes medications by organ or system. The ATC codes were gathered from DrugBank. Rednik's semantic similarity algorithm was used to compute ATC similarity. This type of similarity was evaluated using ATC codes which are shown in Fig. 1. The ATC coding system partitions are based on the biological system or organ on which they target.

Target similarity

Drug targets, such as specific proteins and nucleic acids, are a type of biological macromolecule in the body that has a pharmacodynamic function through interacting with medicines. To predict drug–target interactions (DTIs), several researchers used a single similarity measure for medications and targets, namely chemical structure similarity for pharmaceuticals and amino acid sequence similarity for targets. Amino acid sequences of the target proteins were obtained from the Universal Protein (UniProt) database.

The Anatomical Therapeutic Chemical (ATC) classification system, Centralized medicinal products for human use by ATC code

A - Alimentary tract and metabolism
B - Blood and blood forming organs
C - Cardiovascular system
D - Dermatologicals
G - Genito urinary system and sex hormones
H - Systemic hormonal prep, excluding sex hormones
J - General antiinfectives for systemic use
L - Antineoplastic and immunomodulating agents
M - Musculo-skeletal system
N - Nervous system
P - Antiparasitic products
R - Respiratory system
S - Sensory organs
V - Various

Fig. 1. The Anatomical Therapeutic Chemical (ATC) classification system

Then, the method suggested by Bleakley and Yamanishi²³ was used, namely the Smith–Waterman sequence alignment score between drug target genes computed with BLOSUM62 substitution matrix.²⁴ The scores' geometric means were computed to normalize the score, which was obtained after aligning each sequence (Fig. 2).

Pathway similarity

A drug's target proteins are found in a variety of pathways, which means that a single drug can affect numerous pathways and modify their activities. Pathway information on drugs was obtained from the Comparative Toxicogenomics Database.

We combined this information with DrugBank data. The IDF was used to assign more weight, and the Tanimoto coefficient was utilized to compute pathway similarities between pairs of drugs.

Disease similarity

Identifying drug–disease associations is time-consuming and expensive. Information on diseases associated with drugs was extracted from the Comparative Toxicogenomics Database, in which the diseases associated with drugs were used for representing drug molecules. Then, we combined disease information with the DrugBank database. Finally, IDF was used to assign more weight and Tanimoto similarity was used to compute disease similarity between a pair of drugs.

MedDRA similarity

The MedDRA defines medical terminology to enable sharing of regulatory information. The terminology is used throughout the regulatory process, from pre-market to post-market, as well as for data entry, consultation, evaluation, and presentation. In the feature matrix, MedDRA is used for side-effect similarities. The side-effect information is gathered from TwoSIDES, which is a source of polypharmacy

1 # Entries for the BLOSUM62 matrix at a scale of $\ln(2)/2.0$.

<u>2</u>	A	R	N	D	C	Q	E	G	H	I	L	K	M	F	P	S	T	W	Y	V	B	J	Z	X	*
<u>3</u> A	4	-1	-2	-2	0	-1	-1	0	-2	-1	-1	-1	-1	-2	-1	1	0	-3	-2	0	-2	-1	-1	-1	-4
<u>4</u> R	-1	5	0	-2	-3	1	0	-2	0	-3	-2	2	-1	-3	-2	-1	-1	-3	-2	-3	-1	-2	0	-1	-4
<u>5</u> N	-2	0	6	1	-3	0	0	0	1	-3	-3	0	-2	-3	-2	1	0	-4	-2	-3	4	-3	0	-1	-4
<u>6</u> D	-2	-2	1	6	-3	0	2	-1	-1	-3	-4	-1	-3	-3	-1	0	-1	-4	-3	-3	4	-3	1	-1	-4
<u>7</u> C	0	-3	-3	-3	9	-3	-4	-3	-3	-1	-1	-3	-1	-2	-3	-1	-1	-2	-2	-1	-3	-1	-3	-1	-4
<u>8</u> Q	-1	1	0	0	-3	5	2	-2	0	-3	-2	1	0	-3	-1	0	-1	-2	-1	-2	0	-2	4	-1	-4
<u>9</u> E	-1	0	0	2	-4	2	5	-2	0	-3	-3	1	-2	-3	-1	0	-1	-3	-2	-2	1	-3	4	-1	-4
<u>10</u> G	0	-2	0	-1	-3	-2	-2	6	-2	-4	-4	-2	-3	-3	-2	0	-2	-2	-3	-3	-1	-4	-2	-1	-4
<u>11</u> H	-2	0	1	-1	-3	0	0	-2	8	-3	-3	-1	-2	-1	-2	-1	-2	-2	2	-3	0	-3	0	-1	-4
<u>12</u> I	-1	-3	-3	-3	-1	-3	-3	-4	-3	4	2	-3	1	0	-3	-2	-1	-3	-1	3	-3	3	-3	-1	-4
<u>13</u> L	-1	-2	-3	-4	-1	-2	-3	-4	-3	2	4	-2	2	0	-3	-2	-1	-2	-1	1	-4	3	-3	-1	-4
<u>14</u> K	-1	2	0	-1	-3	1	1	-2	-1	-3	-2	5	-1	-3	-1	0	-1	-3	-2	-2	0	-3	1	-1	-4
<u>15</u> M	-1	-1	-2	-3	-1	0	-2	-3	-2	1	2	-1	5	0	-2	-1	-1	-1	-1	1	-3	2	-1	-1	-4
<u>16</u> F	-2	-3	-3	-3	-2	-3	-3	-3	-1	0	0	-3	0	6	-4	-2	-2	1	3	-1	-3	0	-3	-1	-4
<u>17</u> P	-1	-2	-2	-1	-3	-1	-1	-2	-2	-3	-3	-1	-2	-4	7	-1	-1	-4	-3	-2	-2	-3	-1	-1	-4
<u>18</u> S	1	-1	1	0	-1	0	0	0	-1	-2	-2	0	-1	-2	-1	4	1	-3	-2	-2	0	-2	0	-1	-4
<u>19</u> T	0	-1	0	-1	-1	-1	-1	-2	-2	-1	-1	-1	-1	-2	-1	1	5	-2	-2	0	-1	-1	-1	-1	-4
<u>20</u> W	-3	-3	-4	-4	-2	-2	-3	-2	-2	-3	-2	-3	-1	1	-4	-3	-2	11	2	-3	-4	-2	-2	-1	-4
<u>21</u> Y	-2	-2	-2	-3	-2	-1	-2	-3	2	-1	-1	-2	-1	3	-3	-2	-2	2	7	-1	-3	-1	-2	-1	-4
<u>22</u> V	0	-3	-3	-3	-1	-2	-2	-3	-3	3	1	-2	1	-1	-2	-2	0	-3	-1	4	-3	2	-2	-1	-4
<u>23</u> B	-2	-1	4	4	-3	0	1	-1	0	-3	-4	0	-3	-3	-2	0	-1	-4	-3	-3	4	-3	0	-1	-4
<u>24</u> J	-1	-2	-3	-3	-1	-2	-3	-4	-3	3	3	-3	2	0	-3	-2	-1	-2	-1	2	-3	3	-3	-1	-4
<u>25</u> Z	-1	0	0	1	-3	4	4	-2	0	-3	-3	1	-1	-3	-1	0	-1	-2	-2	-2	0	-3	4	-1	-4
<u>26</u> X	-1	-1	-1	-1	-1	-1	-1	-1	-1	-1	-1	-1	-1	-1	-1	-1	-1	-1	-1	-1	-1	-1	-1	-1	-4
<u>27</u> *	-4	-4	-4	-4	-4	-4	-4	-4	-4	-4	-4	-4	-4	-4	-4	-4	-4	-4	-4	-4	-4	-4	-4	-4	1

Fig. 2. BLOSUM62 – replacement of amino acids

ADRs for combinations of drugs gathered from FDA Adverse Event Reporting System (FAERS) and the DrugBank. We have used IDF weight for the terms and computed Tanimoto coefficient for similarities between pairs of drugs.

Enzyme similarity

Enzyme similarity was computed using the approach applied to target similarity. Amino acid sequences of the enzyme protein were obtained using the UniProt database, and the Smith–Waterman sequence alignment score between drug target genes was computed as suggested by Bleakley and Yamanishi.²³ The geometric mean of the scores was calculated to normalize the score obtained from aligning each sequence.

PPI similarity

Proteins are in charge of all biological systems in a cell, and while many proteins operate on their own, the great majority of them interact with one another to ensure appropriate biological activity. The protein–protein interaction (PPI) network was created, and the closest distance between proteins was computed. Following the suggestions of Rohani

and Eslahchi,⁷ the distances were converted to similarity measurements using the following equation (Equation 6):

$$S(p_1, p_2) = A \times e^{-D(p_1, p_2)} \quad (6)$$

where $S(p_1, p_2)$ is the computed similarity value between 2 proteins, $D(p_1, p_2)$ is the shortest path between these proteins in the PPI network, and A was chosen to be $0.9 \times \exp(1)$. Figure 3 presents one-step interactions between proteins for illustration purposes.

Data analysis

This paper was intended to investigate major cardiovascular drugs and their interactions with other drugs. First, we took few well known drugs and their interaction to other available drugs. Then we added new drug and its interactions with other available. Finally, in the current study, we used 22 drugs in drug 1 column. In the current study, we used 22 drugs as drug 1 and 841 drugs as drug 2, totaling 18,249 data points after removing duplicates. Sample data is shown in Table 1. During the analysis, we used R v. 4.0.2 software (R Foundation for Statistical Computing, Vienna, Austria).

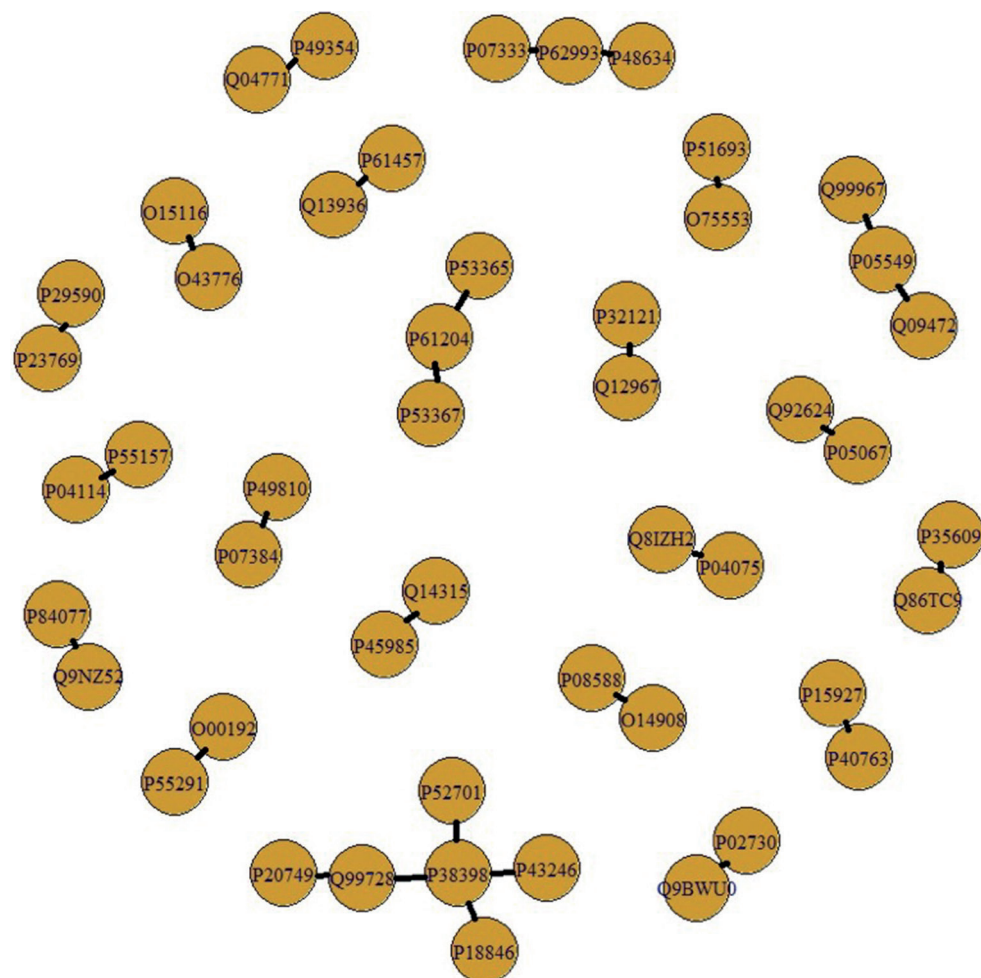


Fig. 3. One-step protein–protein interactions

Checking for multicollinearity is a vital step of data analysis. Multicollinearity indicates which independent variables are not independent of each other, and whether the high correlation between independent variables might cause problems with not only fitting but also interpreting

the results. Therefore, in Fig. 4, the correlation matrix between 8 feature matrices can be observed. The highest correlation is 0.44 between Pathway similarity and Disease similarity. This is followed by a correlation 0.38 between Enzyme similarity and PPI similarity.

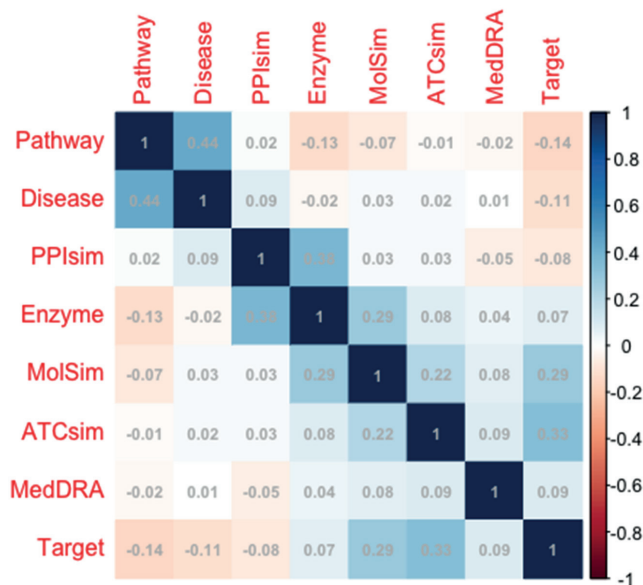


Fig. 4. Correlation matrix between explanatory variables

We checked the assumptions using LR and found that there were no highly influential outliers in the data. Cook’s distance was estimated to verify the finding. Linear relationships between each explanatory variable and the logit of the response variables were checked using the Box–Tidwell method. We have fitted a LR model, which contains both x and $x \cdot \log(x)$ for all of our explanatory variables (x). We then added those interactions into a model and fitted it to LR. We found out that ATC, target, enzyme, and disease do not satisfy linearity assumptions. Their p-values were $<2e-16$, $<2e-16$, $<2e-16$, and 0.01747, respectively. Later, we created new variables using the square of ATC, target, enzyme, and disease. However, ATC was not significant. In the end, we used the square of the target, enzyme and disease variables, and the natural log of ATC. We checked all LR assumptions for new variables and did not notice any problems. Since we have a large dataset, overfitting was not our primary issue. The goodness-of-fit of the LR model was evaluated by using Nagelkerke’s R^2 from the fmsb R package and obtained a value of 0.2199, showing a moderate relationship.

Table 3. Model summary of logistic regression

Parameter	df	Deviance	Resid. Df	Resid. Dev	p-value (> χ)
NULL	–	–	14591	19336	–
Pathway	1	25.88	14590	19311	0.0046
MedDRA	1	473.24	14589	18837	0.0000
MolSim	1	1200.67	14588	17637	0.0000
ATCsim_In	1	251.25	14587	17385	0.0000
Target2	1	323.50	14586	17062	0.0000
Enzyme2	1	275.20	14585	16787	0.0000
PPIsim	1	10.62	14584	16776	0.0022
Disease2	1	10.63	14583	16766	0.0012

df – degrees of freedom; Resid. Df – residual degree of freedom; Resid. Dev – residual deviance.

On the other hand, the model summary presented in Table 3 shows that all covariates are statistically significant.

Classification problems, especially with binary outcomes, were labeled as positive or negative. The decision was made by using a confusion matrix or contingency table, which consist of 4 categories: 1) true positive (TP) occurs when the outcome is successfully classified as positive; 2) true negative (TN) occurs when the outcome is successfully classified as negative; 3) false positive (FP) refers to an outcome as positive when the truth is negative; and 4) false negative (FN) refers to an outcome as negative when the truth is positive. Sensitivity refers to the ability of a test to correctly identify events related to a disease. Specificity, on the other hand, refers to the ability of a test to reliably detect events that occur in the absence of disease. Equations 7–11 has been used to compute these values in Table 2.

$$\text{TPR} = \text{recall} = \frac{\text{TP}}{\text{TP} + \text{FN}} \quad (7)$$

$$\text{FPR} = \frac{\text{FP}}{\text{FP} + \text{TN}} \quad (8)$$

$$\text{Precision} = \frac{\text{TP}}{\text{TP} + \text{FP}} \quad (9)$$

$$\text{Accuracy} = \frac{\text{TP} + \text{TN}}{\text{TP} + \text{TN} + \text{FP} + \text{FN}} \quad (10)$$

$$\text{F1} = 2 \times \frac{\text{Precision} \times \text{Recall}}{\text{Precision} + \text{Recall}} \quad (11)$$

A confusion matrix can be obtained after fitting any machine learning algorithm and obtaining predictions on the test set. An accuracy of algorithm can be checked by computing some measures such as false positive rate (FPR) to indicate the fraction of negative groups which are incorrectly classified as positive. True positive rate (TPR) indicates the fraction of positive groups that are successfully classified as positive. Precision indicates the measure of correctly spotted positive events out of the predicted

positive events. Recall indicates the measure of correctly spotted positive events out of all the actual positive events. Accuracy indicates the measure of all the correctly spotted events. When the ratio of the positive and negative events is close to each other, accuracy is a good indicator to consider. Although it is not always the case for equally numbered groups, in real datasets, mainly positive and negative events are not equal, which indicates imbalanced data. Therefore, an F1 score would be useful in the case of unequal groups and when FPs and FNs are being considered, since mislabeling interactions as non-interactions might cause patient's death.

The dataset is split into branches (80% training and 20% testing). Three machine learning algorithms were used to fit the data in R software using the macOS Ventura 13.3.1 operating system (Apple Inc., Cupertino, USA). Results are shown in Table 2. We used the xgboost package to fit XGBoost, Keras and Tensorflow packages for fitting the NN and, finally, the stats package was used for fitting the LR. A 10-fold cross-validation was carried out independently for each algorithm to validate our models.

Conclusions

We have used 3 popular machine learning algorithms, LR, XGBoost and NN, for solving a classification problem. Each method has its strengths and weaknesses. Logistic regression is a simple algorithm that is easy to implement, interpret and explain. On the other hand, LR has limitations in its ability to capture complex, non-linear relationships between the dependent and independent variables. The XGBoost and NN are commonly preferred blackbox methods. They have high accuracy and power to handle larger datasets but time-consuming hyperparameter tuning and difficult interpretations.

Following the results presented in Table 2, we could say that using XGBoost would be a good machine learning algorithm in this case. We achieved the highest accuracy among all algorithms using XGBoost (78%), which is not surprising because, as we pointed out before, XGBoost

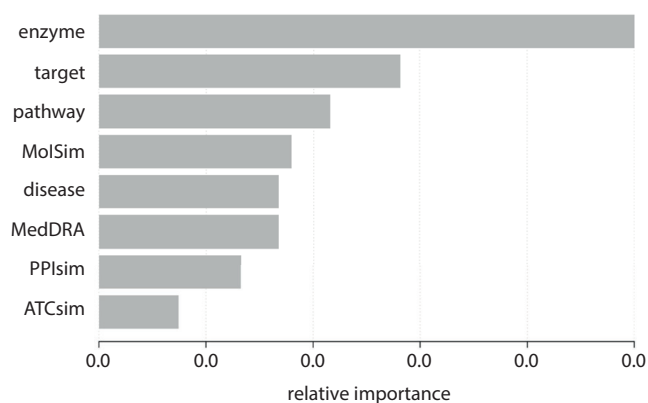


Fig. 5. Feature importance from eXtreme Gradient Boosting (XGBoost)

uses gradient boosting inside the algorithm. Therefore, it is known to retrieve importance scores for each feature. In general, significance assigns a score to each feature that reflects how useful or important it was in the development of the model's enhanced decision trees. The higher the relative relevance of a characteristic, the more often it is used to make critical judgments with decision trees. After the training, `rgb.importance` was used to identify which features have higher importance.²⁵ Feature selection is a widely used approach in machine learning.^{26,27} Enzyme similarity is the most important feature in the model, followed by target similarity (Fig. 5). Finally, ATC similarity is the least important feature. Thus, even if some papers are only focused on molecular similarity, enzyme and target protein similarities are the most vital features when it comes to identifying DDIs.

Kappa is a statistical measure that evaluates the degree of agreement between predicted and actual values. It ranges from -1 to 1 , with 1 indicating perfect agreement, 0 indicating random agreement and -1 indicating complete disagreement. Based on the kappa values reported in Table 2, it is apparent that the XGBoost model exhibits the highest agreement between predicted and actual values, with a kappa value of 0.5508 . This finding suggests that the XGBoost model is capable of predicting outcomes more accurately than the other 2 models. In contrast, the LR model reached the lowest kappa value of 0.2641 . The NN model, with a kappa value of 0.4154 , falls in between the values obtained for the XGBoost and LR models. These results suggest that the NN model is more accurate than the LR model but not as accurate as the XGBoost model in predicting outcomes.

Creating a new feature matrix is computationally requiring more powerful devices; therefore, using excessive feature matrices to identify DDIs in methods would be interesting to investigate if the purpose is solely for feature selection in DDIs. However, we believe that after feature selection, the model would end up with 8 or 9 explanatory variables, which would be similar to the ones used in this paper. Additionally, we compared 3 machine learning algorithms, but every other classification method available

in R programming could be used. Finally, we used 22 drugs as drug 1 and 841 drugs as drug 2 (see Table 1), but it could be expanded to larger numbers with more powerful devices and extra time, as mentioned earlier. Our method creates feature matrices from raw data and is still faster than many other approaches. The method would be vital for scientists in drug development since this is a non-clinical and accurate approach. It would also lower Research and Development (R&D) expenses of pharmaceutical companies. A R-shiny app or another automation system can be created to obtain probability of DDI interaction for chosen drugs. This would help doctors when deciding which drugs to prescribe for a given patient.

Supplementary data

The Supplementary file has 22 folders for each drugs in a drug 1 column in Table 1. The R codes which is used to fit all 3 machine learning algorithms can be found at <https://github.com/iDemirsoy/Understanding-DDI->.

ORCID iDs

Idris Demirsoy  <https://orcid.org/0000-0002-3321-4748>

Adnan Karaibrahimoglu  <https://orcid.org/0000-0002-8277-0281>

References

- Percha B, Altman RB. Informatics confronts drug–drug interactions. *Trends Pharmacol Sci.* 2013;34(3):178–184. doi:10.1016/j.tips.2013.01.006
- Zhang P, Wang F, Hu J, Sorrentino R. Label propagation prediction of drug–drug interactions based on clinical side effects. *Sci Rep.* 2015;5:12339. doi:10.1038/srep12339
- Vilar S, Friedman C, Hripcsak G. Detection of drug–drug interactions through data mining studies using clinical sources, scientific literature and social media. *Brief Bioinform.* 2018;19(5):863–877. doi:10.1093/bib/bbx010
- Vilar S, Uriarte E, Santana L, et al. Similarity-based modeling in large-scale prediction of drug–drug interactions. *Nat Protoc.* 2014;9(9):2147–2163. doi:10.1038/nprot.2014.151
- Fokoue A, Sadoghi M, Hassanzadeh O, Zhang P. Predicting drug–drug interactions through large-scale similarity-based link prediction. In: Sack H, Blomqvist E, d'Aquin M, Ghidini C, Ponzetto SP, Lange C, eds. *The Semantic Web. Latest Advances and New Domains.* Cham, Switzerland: Springer International Publishing; 2016:774–789. doi:10.1007/978-3-319-34129-3_47
- Wu HY, Chiang CW, Li L. Text mining for drug–drug interaction. In: *Biomedical Literature Mining.* New York, USA: Springer New York; 2014:47–75. doi:10.1007/978-1-4939-0709-0_4
- Rohani N, Eslahchi C. Drug–drug interaction predicting by neural network using integrated similarity. *Sci Rep.* 2019;9(1):13645. doi:10.1038/s41598-019-50121-3
- Vilar S, Harpaz R, Uriarte E, Santana L, Rabadan R, Friedman C. Drug–drug interaction through molecular structure similarity analysis. *J Am Med Inform Assoc.* 2012;19(6):1066–1074. doi:10.1136/amiajnl-2012-000935
- Roos J. Cardiac effects of antidepressant drugs: A comparison of the tricyclic antidepressants and fluvoxamine. *Br J Clin Pharmacol.* 1983;15(Suppl 3):439S–445S. doi:10.1111/j.1365-2125.1983.tb02135.x
- Bajusz D, Rácz A, Héberger K. Why is Tanimoto index an appropriate choice for fingerprint-based similarity calculations? *J Cheminform.* 2015;7:20. doi:10.1186/s13321-015-0069-3
- Papineni K. Why inverse document frequency? In: *Second Meeting of the North American Chapter of the Association for Computational Linguistics*; 2001. <https://aclanthology.org/N01-1004.pdf>. Accessed August 15, 2020.

12. Church K, Gale W. Inverse Document Frequency (IDF): A measure of deviations from Poisson. In: Armstrong S, Church K, Isabelle P, Manzi S, Zoukermann E, Yarowsky D, eds. *Natural Language Processing Using Very Large Corpora*. Dordrecht, the Netherlands: Springer Netherlands; 1999:283–295. doi:10.1007/978-94-017-2390-9_18
13. Chen T, He T, Benesty M. Xgboost: Extreme gradient boosting. Melbourne, Australia: University of Melbourne; 2015. <https://cran.ms.unimelb.edu.au/web/packages/xgboost/vignettes/xgboost.pdf>. Accessed August 11, 2020.
14. Demirsoy I. Estimating the Intensity of Point Processes on Linear Networks [doctoral thesis]. Tallahassee, USA: Florida State University; 2020. <https://diginole.lib.fsu.edu/islandora/object/fsu:781648>. Accessed August 15, 2020.
15. Chen T, Guestrin C. XGBoost: A scalable tree boosting system. In: *Proceedings of the 22nd ACM SIGKDD International Conference on Knowledge Discovery and Data Mining*. San Francisco, USA: ACM; 2016: 785–794. doi:10.1145/2939672.2939785
16. Abiodun OI, Jantan A, Omolara AE, Dada KV, Mohamed NA, Arshad H. State-of-the-art in artificial neural network applications: A survey. *Heliyon*. 2018;4(11):e00938. doi:10.1016/j.heliyon.2018.e00938
17. Paul S, Singh A. *Hands-On Python Deep Learning for the Web*. Birmingham, UK: Packt Publishing; 2020. ISBN:978-1-78995-608-5.
18. Agarap AF. Deep learning using rectified linear units (ReLU). *arXiv*. 2018. doi:10.48550/ARXIV.1803.08375
19. Wanto A, Windarto AP, Hartama D, Parlina I. Use of binary sigmoid function and linear identity in artificial neural networks for forecasting population density. *IJISTECH*. 2017;1(1):43. doi:10.30645/ijistech.v1i1.6
20. Peng CYJ, Lee KL, Ingersoll GM. An introduction to logistic regression analysis and reporting. *J Educ Res*. 2002;96(1):3–14. doi:10.1080/00220670209598786
21. Ding H, Takigawa I, Mamitsuka H, Zhu S. Similarity-based machine learning methods for predicting drug–target interactions: A brief review. *Brief Bioinform*. 2014;15(5):734–747. doi:10.1093/bib/bbt056
22. Landrum G. Getting started with the RDKit in Python: The RDKit 2023.03.1 documentation. 2018. <https://www.rdkit.org/docs/GettingStartedInPython.html>. Accessed August 11, 2020.
23. Bleakley K, Yamanishi Y. Supervised prediction of drug–target interactions using bipartite local models. *Bioinformatics*. 2009;25(18): 2397–2403. doi:10.1093/bioinformatics/btp433
24. Noh K, Yoo S, Lee D. A systematic approach to identify therapeutic effects of natural products based on human metabolite information. *BMC Bioinformatics*. 2018;19(Suppl 8):205. doi:10.1186/s12859-018-2196-0
25. Chen T, He T, Benesty M, Khotilovich V. Package ‘Xgboost’. Toronto, Canada: University of Toronto; 2022. <https://cran.utstat.utoronto.ca/web/packages/xgboost/xgboost.pdf>. Accessed August 15, 2020.
26. Chen C, Zhang Q, Yu B, et al. Improving protein–protein interactions prediction accuracy using XGBoost feature selection and stacked ensemble classifier. *Comput Biol Med*. 2020;123:103899. doi:10.1016/j.combiomed.2020.103899
27. Wang Y, Ni XS. A XGBoost risk model via feature selection and Bayesian hyper-parameter optimization. *arXiv*. 2019. doi:10.48550/ARXIV.1901.08433

Regorafenib compared to nivolumab after sorafenib failure in patients with hepatocellular carcinoma: A systematic review and meta-analysis

Shuheng Yang^{1,A–D}, Yadong Zhou^{1,C,D}, Lei Zeng^{2,E,F}

¹ Department of Hepatobiliary Surgery, Chongqing University Fuling Hospital, China

² Department of Hepatobiliary and Pancreatic Surgery, Third Affiliated Hospital of Chongqing Medical University, China

A – research concept and design; B – collection and/or assembly of data; C – data analysis and interpretation;

D – writing the article; E – critical revision of the article; F – final approval of the article

Advances in Clinical and Experimental Medicine, ISSN 1899–5276 (print), ISSN 2451–2680 (online)

Adv Clin Exp Med. 2023;32(8):839–845

Address for correspondence

Lei Zeng

E-mail: christopherhitchens199286@gmail.com

Funding sources

None declared

Conflict of interest

None declared

Received on February 17, 2022

Reviewed on December 9, 2022

Accepted on December 23, 2022

Published online on May 4, 2023

Abstract

Which systemic therapy should be administered following sorafenib failure for patients with advanced hepatocellular carcinoma (HCC) is still a debated issue in clinical practice. This study aimed to compare regorafenib with nivolumab after sorafenib failure in patients with HCC. MEDLINE via PubMed, Scopus and Embase databases were searched for studies published until December 2021. The risk of bias (RoB) was evaluated using the Cochrane Collaboration tool for assessing risk of bias in randomized trials. From a total of 2120 articles, 3 papers were included in this meta-analysis. We found a statistically significant difference in the patient's objective response rate between the regorafenib and nivolumab groups (odds ratio (OR): 0.296, 95% confidence interval (95% CI): 0.161–0.544, $p = 0.000$). A statistically significant difference between regorafenib and nivolumab was not found for disease control rate after sorafenib failure in patients with advanced HCC (OR: 1.111, 95% CI: 0.793–1.557, $p = 0.541$) nor the number of progressive disease events (OR: 0.972, 95% CI: 0.693–1.362, $p = 0.867$). Overall survival (OS) and progression-free survival (PFS) were not calculable. The heterogeneity of the included data was low. Nivolumab monotherapy appears superior to regorafenib after sorafenib failure in patients with advanced HCC.

Key words: hepatocellular carcinoma, sorafenib, regorafenib, nivolumab, meta-analysis

Cite as

Yang S, Zhou Y, Zeng L. Regorafenib compared to nivolumab after sorafenib failure in patients with hepatocellular carcinoma: A systematic review and meta-analysis.

Adv Clin Exp Med. 2023;32(8):839–845.

doi:10.17219/acem/158488

DOI

10.17219/acem/158488

Copyright

Copyright by Author(s)

This is an article distributed under the terms of the Creative Commons Attribution 3.0 Unported (CC BY 3.0) (<https://creativecommons.org/licenses/by/3.0/>)

Introduction

Hepatocellular carcinoma (HCC) is the 6th most common type of malignancy and the most frequent type of liver cancer. It is also the 3rd leading cause of cancer-related deaths worldwide, resulting in nearly 745,000 deaths annually.¹ Hepatitis B virus (HBV), hepatitis C virus (HCV) and other non-viral chronic liver diseases leading to cirrhosis are the most well-known risk factors for HCC.² Although factors such as alcohol use, diabetes and smoking are also considered risk factors for developing HCC, this is less broadly accepted.^{2,3}

Hepatocellular carcinoma is asymptomatic in the early stages; thus, most HCC cases are not recognized until advanced stages which renders this disease incurable in clinical practice.⁴ The best therapy for resectable HCC without portal hypertension is surgery.⁵ In patients who were not ideal candidates for resection according to the Barcelona Clinic Liver Cancer (BCLC) classification, surgical resection was linked to higher survival than locoregional or systemic therapeutic strategies.⁶ However, the majority of patients with HCC do not benefit from surgery and will ultimately need further medical treatment. Sorafenib, a small-molecule multikinase inhibitor, is the most commonly used systemic therapy in patients with HCC. However, it improves the median overall survival (OS) for no more than 2–3 months.^{5,7} Furthermore, at least half of the patients who receive sorafenib as a treatment fail to respond. The lack of second-line treatment for these patients is thus a serious issue.⁸

Multiple immunologic pathways contribute to HCC development by impairing the antitumor immune surveillance of the host.⁹ Nivolumab, a Programmed-Death-1 (PD-1) immune checkpoint inhibitor, has modest single-agent activity in advanced HCC with a favorable 6-month OS rate (72%) and without any significant side effects.^{10,11} An objective response rate of 15–20% was achieved using nivolumab (as opposed to 2–3% in sorafenib) in patients with advanced HCC, irrespective of the line of therapy (CheckMate 040 study).¹²

The hypervascular nature of most HCC tumors and the involvement of multiple angiogenic pathways suggests that these mechanisms may be associated with the progression and pathogenesis of HCC.¹³ Regorafenib, an oral multikinase blocker, inhibits the protein kinases associated with oncogenesis, metastasis, angiogenesis, and tumor immunity.¹⁴ Moreover, regorafenib has a wider range of inhibitory effects compared to other tyrosine kinase inhibitors, and can alter the tumor micro-environment.¹⁵ The RESORCE trial showed that treatment of advanced HCC patients who failed to respond to sorafenib with regorafenib improved median OS compared with placebo (10.6 compared to 7.8 months, respectively).¹⁶

Objectives

This meta-analysis aimed to assess the therapeutic effects of regorafenib compared to nivolumab after sorafenib failure in patients with HCC.

Methods

Data sources and searches

This meta-analysis was performed according to the Preferred Reporting Items for Systematic Reviews and Meta-Analyses (PRISMA) guidelines.¹⁷ An electronic search of MEDLINE via PubMed, Scopus and Embase databases was performed for studies published until December 2021. The search terms were “regorafenib,” “STIVARGA,” “nivolumab,” “OPDIVO,” “hepatocellular carcinoma,” and “HCC”. The search strategy was as follows: TITLE-ABS-KEY (regorafenib) OR TITLE-ABS-KEY (stivarga) AND TITLE-ABS-KEY (nivolumab) OR TITLE-ABS-KEY (opdivo) AND TITLE-ABS-KEY (hepatocellular AND carcinoma) OR TITLE-ABS-KEY (hcc) AND (LIMIT-TO (LANGUAGE, “English”)) AND (LIMIT-TO (SRCTYPE, “j”)).

Study selection

The inclusion criteria for the primary analysis were as follows: all clinical trials that were performed on humans and compared the effects of second-line regorafenib therapy with nivolumab therapy after failure of first-line sorafenib therapy in patients with advanced HCC. Because regorafenib is approved only for HCC patients who have tolerated first-line sorafenib, we only included studies in which such a criterion was considered. Studies that assessed the effects of either only regorafenib or nivolumab therapy (and thus provided no comparison) in advanced HCC were excluded. All duplicate, non-English-language and animal (in vivo) or cell lines (in vitro) papers were excluded as well. Independent data collection was performed by 2 authors and all potentially relevant citations were retrieved in full. These citations were independently evaluated by the same 2 authors for eligibility. Disagreement was resolved by consensus or consultation with the 3rd author.

Data extraction

Pre-designed electronic forms were used to extract all the relevant data from the included articles. Last name of the first author, publication year, study design, mean age of the patients, sex, Child–Pugh class, study outcome(s), and related adverse events (grade III/IV) were extracted from the included studies. The p-value for complete response, partial response, stable disease, objective response (complete response + partial response), progressive

disease, disease control rate (complete response + partial response + stable disease), objective response rate, and odds ratios (ORs) and related 95% confidence intervals (95% CIs) were also extracted. The primary objective of this study was to compare the effects of regorafenib compared to nivolumab after sorafenib failure in patients with HCC using complete response, partial response stable disease, progressive disease, as well as objective response rate, and the secondary objective was to compare the side effects of these 2 regimens.

Study quality

The risk of bias (RoB) was evaluated using the Cochrane Collaboration tool for assessing risk of bias in randomized trials. This tool consists of performance, detection, selection, and attrition assessment, and of reporting bias items.¹⁸

Statistical analyses

All statistical analyses were conducted using Comprehensive Meta-Analysis software v. 2 (Biostat Inc, Englewood, USA). A fixed-effects model was used to pool the study outcomes. Median as well as 95% CI and response rates were used to report time-to-event data and categorical outcomes, respectively. The heterogeneity of the included publications was evaluated using χ^2 and I^2 tests. A value of $I^2 < 25\%$ was considered as low-level heterogeneity. Funnel plots and

Begg and Mazumdar’s test were not used to assess publication bias as the number of included studies was lower than 10. A two-tailed p-value of less than 0.05 was regarded as statistically significant for all comparisons.

Results

Search results

An initial electronic search of the included databases yielded a total of 2120 articles; as a first step of their evaluation, 387 duplicate citations were excluded. Accordingly, the title, abstract and keywords of the remaining 1733 articles were screened. This resulted in the exclusion of a further 1700 publications. Finally, the full texts of the 33 remaining articles were screened and 3 papers were chosen for this meta-analysis (Fig. 1).

General study characteristics

The main characteristics of the included studies are presented in Table 1. All of the included studies were retrospective cohort studies. A total of 676 patients were included in this meta-analysis, with 140 males and 536 females; 383 patients received regorafenib and 230 patients received nivolumab. Most patients had a Child–Pugh class of A or B. The etiology of HCC was predominantly HBV and HCV.

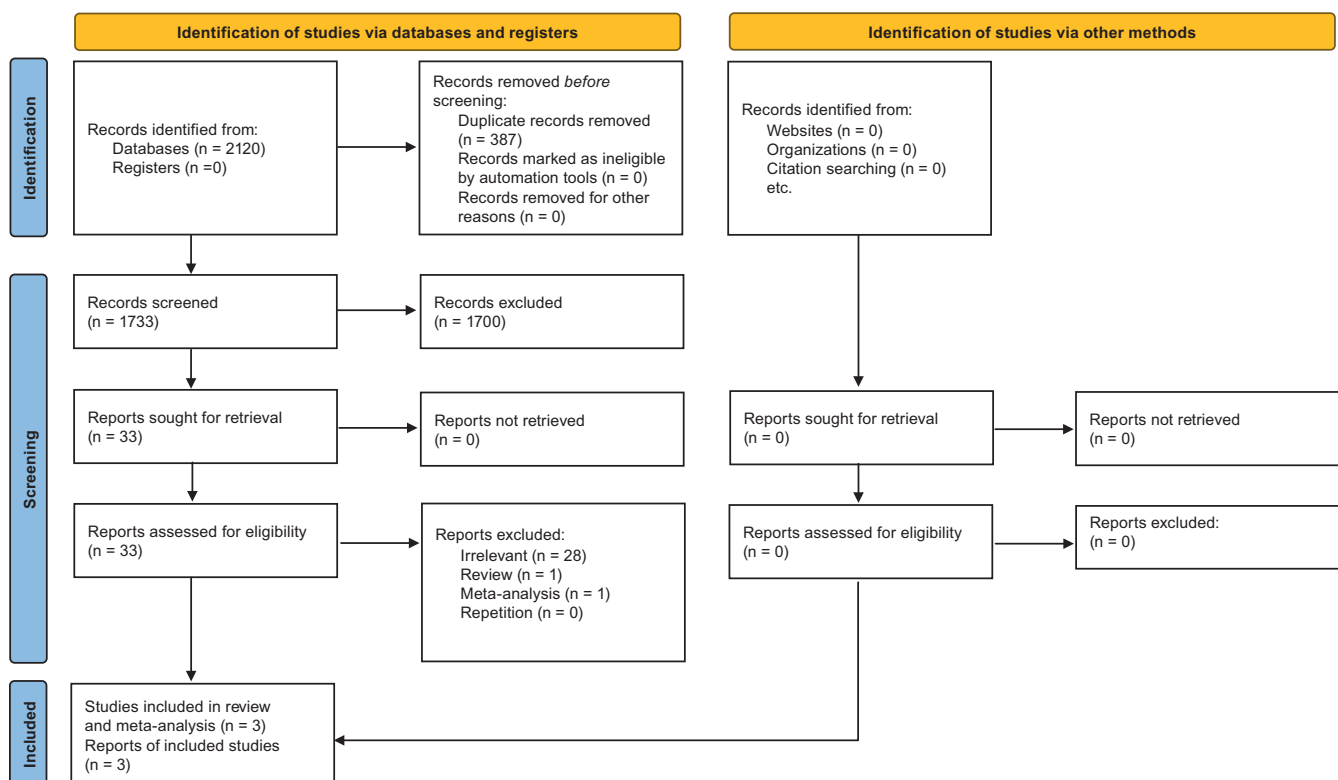


Fig. 1. Preferred Reporting Items for Systematic Reviews and Meta-Analyses (PRISMA) flowchart of study inclusion (From: Page MJ, McKenzie JE, Bossuyt PM, Boutron I, Hoffmann TC, Mulrow CD, et al. The PRISMA 2020 statement: an updated guideline for reporting systematic reviews. *BMJ* 2021;372:n71. doi:10.1136/bmj.n71. More information: <http://www.prisma-statement.org/>)

Table 1. Main characteristics of the included studies (all 3 were retrospective cohort studies)

Study	Number of patients	Gender (male)	Regorafenib (nivolumab)	Child–Pugh class	Etiology	Outcome(s)	Adverse events
Choi et al., 2020 ²⁷	436	109 (327)	223 (150)	A and B	mainly HBV and HCV	Survival outcomes in patients treated with regorafenib and nivolumab after sorafenib failure did not differ significantly.	NM
Lee et al., 2020 ²⁸	150	28 (122)	102 (48)	A, B and C	mainly HBV	The use of nivolumab may be associated with improved OS and better objective response rate as compared to using regorafenib.	Both drugs were well tolerated.
Kuo et al., 2021 ²⁹	90	23 (67)	58 (32)	A and B	mainly HBV and HCV	After sorafenib failure, using nivolumab or regorafenib both resulted in promising treatment outcomes.	The most frequent related adverse event was hand-to-food skin reaction.
Total	676	140 (536)	383 (230)	–	–	–	–

HBV – hepatitis B virus; HCV – hepatitis C virus; NM – not mentioned; OS – overall survival.

Regorafenib compared to nivolumab after sorafenib failure

Objective response

The objective response rate included complete response and partial response. We found a statistically significant difference in the patients’ objective response rate between the regorafenib and nivolumab groups, with regorafenib having a better response. The pooled OR was 0.296 (95% CI: 0.161–0.544, $p = 0.000$; Fig. 2). The heterogeneity of the included articles was low ($\chi^2 = 0.10$, $T^2 = 0.000$, $df = 2$, $I^2 = 0.00\%$, $p = 0.951$).

Disease control rate

Disease control rate included complete response, partial response and stable disease. No statistically significant difference in the patients’ disease control rate

between the regorafenib and nivolumab groups was found. The pooled OR was 1.111 (95% CI: 0.793–1.557, $p = 0.541$; Fig. 3). The heterogeneity of the included articles was low ($\chi^2 = 2.70$, $T^2 = 0.041$, $df = 2$, $I^2 = 26.04\%$, $p = 0.259$).

Progressive disease

No statistically significant difference between the groups based on the number of progressive disease events was found; the pooled OR was 0.972 (95% CI: 0.693–1.362, $p = 0.867$; Fig. 4). The heterogeneity of the included articles was low ($\chi^2 = 1.47$, $T^2 = 0.000$, $df = 2$, $I^2 = 0.00\%$, $p = 0.478$).

Study quality

Due to the nature of included studies (retrospective cohort studies), none of these publications were randomized or blinded. Allocation concealment was not employed

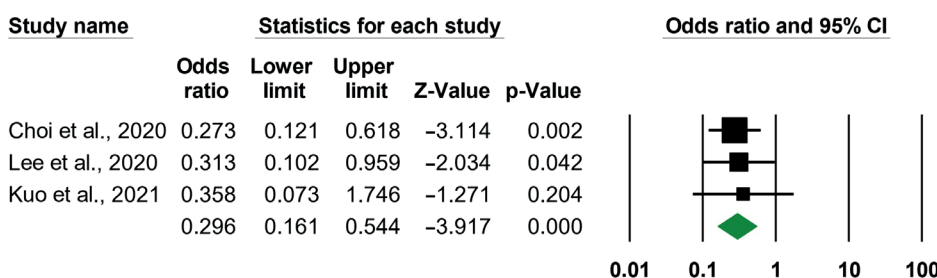


Fig. 2. Forest plot of standardized mean difference (SMD) for the objective response for regorafenib therapy compared to nivolumab therapy in patients with advanced hepatocellular carcinoma (HCC). The green diamond shows the overall pooled effect. Black squares indicate the SMD in each study. Horizontal lines represent 95% confidence interval (95% CI)

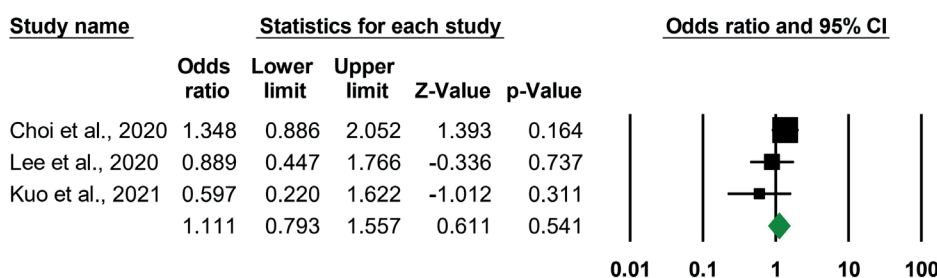


Fig. 3. Forest plot of standardized mean difference (SMD) for the disease control rate for regorafenib therapy compared to nivolumab therapy in patients with advanced hepatocellular carcinoma (HCC). The green diamond shows the overall pooled effect. Black squares indicate the SMD in each study. Horizontal lines represent 95% confidence interval (95% CI)

Study name	Statistics for each study					Odds ratio and 95% CI
	Odds ratio	Lower limit	Upper limit	Z-Value	p-Value	
Choi et al., 2020	0.865	0.571	1.310	-0.685	0.493	
Lee et al., 2020	1.038	0.507	2.124	0.102	0.919	
Kuo et al., 2021	1.676	0.617	4.556	1.012	0.311	
	0.972	0.693	1.362	-0.167	0.867	

Fig. 4. Forest plot of standardized mean difference (SMD) for progressive disease for regorafenib therapy compared to nivolumab therapy in patients with advanced hepatocellular carcinoma (HCC). The green diamond shows the overall pooled effect. Black squares indicate the SMD in each study. Horizontal lines represent 95% confidence interval (95% CI)

	Random sequence generation (selection bias)	Allocation concealment (selection bias)	Blinding of participants and personnel (performance bias)	Blinding of outcome assessment (detection bias)	Incomplete outcome data (attrition bias)	Selective reporting (reporting bias)	Other bias
Choi et al., 2020	⊖	⊖	⊖	⊖	⊕	⊕	
Kuo et al., 2021	⊖	⊖	⊖	⊖	⊕	⊕	
Lee et al., 2020	⊖	⊖	⊖	⊖	⊕	⊕	

Fig. 5. Different levels of risk of bias for each item in included studies. The risk of bias (RoB) was evaluated using the Cochrane Collaboration tool for assessing risk of bias in randomized trials

in any of the analyzed papers. There was no evidence of attrition nor reporting bias in this set of articles (Fig. 5).

Discussion

This meta-analysis found that nivolumab monotherapy had an objective response rate superior to regorafenib monotherapy after sorafenib failure in patients with advanced HCC. However, we failed to find a difference in disease control rate between the 2 groups. Safety analysis of these medications could not be performed due to incomplete data.

Hepatocellular carcinoma has a poor prognosis because most patients are diagnosed in the advanced stages of the disease. These late diagnoses limit the efficacy

of locoregional therapies such as transarterial chemoembolization (TACE), radiofrequency ablation (RFA) or hepatic resection. Accordingly, systemic therapy is the main therapeutic strategy in this set of patients.¹⁹

The first agent that was approved for systemic therapy in patients with advanced HCC was sorafenib, based on the results from 2 randomized, double-blind, phase III clinical trials.^{20,21} Sorafenib is a multi-targeted tyrosine kinase inhibitor (mTKI) that largely acts against vascular angiogenesis by inhibiting platelet-derived growth factor receptor (PDGFR) and vascular endothelial growth factor receptor (VEGFR). Tumor proliferation is also prohibited by sorafenib through inhibition of Raf-1, B-Raf and kinase activity in the Ras/Raf/MEK/ERK signaling pathways.²² In 2017, 2 second-line medications, namely regorafenib (RESORCE trial) and nivolumab (CheckMate 040), were approved for the treatment of patients who fail to respond to sorafenib as a first-line medication.^{12,16} Based on the RESORCE trial, in which 567 patients were randomized to regorafenib (n = 374) or placebo (n = 193) groups, sequential treatment with regorafenib after sorafenib failure improved OS (hazard ratio (HR) of 0.63 (95% CI: 0.50–0.79; one-sided p < 0.001)), and increased both median survival (26.0 months compared to 19.6 months) and progression-free survival (PFS) (3.1 months compared to 1.5 months, p < 0.001). The most common treatment-related adverse events were hypertension, hand-foot skin reaction (HFSR), fatigue, and diarrhea.¹⁶ The CheckMate 040 trial showed that sequential administration of nivolumab after sorafenib failure in patients with advanced HCC improved PFS by 4.1 months. In the CheckMate 040 trial, the objective response rate was 20% and the disease control rate was 64%.¹² These results were further replicated for other anti-PD-1 agents, namely pembrolizumab and tislelizumab. Patients with advanced HCC who had previously been treated with sorafenib both responded well to and tolerated pembrolizumab.²³ Single-agent tislelizumab also provided a clinically meaningful OS benefit over sorafenib, with a favorable safety profile as a first-line treatment option for patients with unresectable HCC.²⁴ Thus, both regorafenib and nivolumab have shown to be superior to placebo in HCC patients after sorafenib failure. When the results from the RESORCE and CheckMate 040 studies were compared, it was found that the objective response in the regorafenib group (11%) was lower than in the nivolumab group (19%). Further, the disease

control rate for both medications in these 2 studies was almost the same (64% for nivolumab compared to 65% for regorafenib).^{12,16} These previous findings are in line with the results of our study. However, a question remains unanswered: Which treatment should be sequentially administered in patients with sorafenib failure?

According to current guidelines, both regorafenib and nivolumab are approved only for HCC patients with Child–Pugh B class. Presently, after sorafenib failure, the only systemic therapy that provides efficacy and has an acceptable safety profile for patients with compromised liver function (Child–Pugh B class) is metronomic capecitabine.^{25,26}

In a recent retrospective study by Choi et al., 373 patients with advanced HCC were enrolled, and the efficacy of regorafenib ($n = 223$) or nivolumab ($n = 150$) monotherapy was evaluated after sorafenib failure. That study found no significant difference in PFS, time to progression (TTP) and OS between these 2 treatment modalities. However, the objective response rate was significantly higher in patients treated with nivolumab than in those treated with regorafenib (13.3% compared to 4.0%; $p = 0.002$). Progression-free survival ($p = 0.001$), TTP ($p < 0.001$) and OS ($p = 0.013$) were significantly longer in the 59 nonprogressors (patients who achieved complete response, partial response or stable disease after first response evaluation) following nivolumab administration than in the 104 nonprogressors to regorafenib.²⁷

In another recent study by Lee et al., performed on 150 patients (102 received regorafenib and 48 received nivolumab), it was found that nivolumab monotherapy was associated with a higher objective response rate compared with regorafenib monotherapy (16.7% and 5.9%, respectively) in advanced HCC patients. Median OS and TTP were not significantly different between the treatment groups.²⁸ Another study by Kuo et al., in which 90 patients were recruited (32 patients in the nivolumab group and 58 patients in the regorafenib group), no difference was found in the objective response rate, disease control rate, OS, and TTP between treatments. Improvements in OS in patients with advanced HCC was similarly observed in treatment modalities.²⁹ The regorafenib group had significantly higher rates of treatment-related adverse events than the nivolumab group (68% compared to 37.5%, $p = 0.006$). The rate of adverse events did not significantly differ between treatment modalities in the study by Lee et al. ($p = 0.34$).²⁸ The most common adverse events observed in patients who received regorafenib were HFSR (in 23.8% of the patients), diarrhea, fatigue, and elevated alkaline aminotransferase (ALT) level, while 37.5% of patients who received nivolumab experienced a treatment-related adverse events, including fatigue in 12.1%, dermatitis in 9.3% and hyperbilirubinaemia in 6.2%.²⁹ It is unknown if prophylactic/therapeutic measures had been applied to prevent or treat these adverse reactions.

Limitations


This meta-analysis was not previously registered and has no previously published protocols. It has several shortcomings that should be addressed in future studies. First, this meta-analysis was only hypothesis-generating, meaning that it was based on the existing data. The main issue with the data used in this meta-analysis is that they are from retrospective cohort studies. Due to this, several vital statistics could not be determined in the included studies, leading to significant bias in the selection of controls. The retrospective nature of these studies predisposes them also to selection bias. Furthermore, there is an absence of common information on potential confounding factors in the included studies. Thus, well-designed randomized clinical trials (RCTs) should be conducted to assess and compare the effects of regorafenib with nivolumab in patients with advanced HCC. Second, only a limited number of studies were included in this meta-analysis. With the completion of more research, future meta-analyses should include a higher number of publications to address this important issue. Third, the included papers were from Taiwan and South Korea (Eastern Asian race) and from a single center each. This limits the generalizability of the results. Fourth, the results of this study may not be generalizable to etiologies other than HBV and HCV, as most of the patients in these studies had HCC due to these viruses. This may also worsen the prognosis of the disease and response to medications. Fifth, due to the lack of data, it was impossible to obtain accurate information about adverse events that occurred during the study period and perform safety analysis. Sixth, if both treatments are available for particular patients, regorafenib is more likely to be used after sorafenib failure in patients with advanced HCC; this introduces an important bias that should be addressed in future studies.


Conclusions

Both regorafenib and nivolumab have been shown to exhibit significant therapeutic efficacy compared with a placebo in patients with HCC. However, which systemic therapy should be administered following sorafenib failure for patients with advanced HCC is still unknown. This study showed that nivolumab is superior to regorafenib in terms of objective response rate after sorafenib failure in patients with advanced HCC. However, both treatments achieved similar disease control rate. Due to the retrospective nature of the studies and the limited number of studies included in this meta-analysis, future RCTs should be designed to directly determine which treatment is superior.

ORCID iDs

Shuheng Yang  <https://orcid.org/0000-0003-1257-6165>

Yadong Zhou  <https://orcid.org/0000-0003-3610-5499>

Lei Zeng  <https://orcid.org/0000-0002-6220-7205>

References

- Kudo M, Finn RS, Qin S, et al. Lenvatinib versus sorafenib in first-line treatment of patients with unresectable hepatocellular carcinoma: A randomised phase 3 non-inferiority trial. *Lancet*. 2018; 391(10126):1163–1173. doi:10.1016/S0140-6736(18)30207-1
- Yi SW, Choi JS, Yi JJ, Lee YH, Han KJ. Risk factors for hepatocellular carcinoma by age, sex, and liver disorder status: A prospective cohort study in Korea. *Cancer*. 2018;124(13):2748–2757. doi:10.1002/cncr.31406
- Turati F, Galeone C, Rota M, et al. Alcohol and liver cancer: A systematic review and meta-analysis of prospective studies. *Ann Oncol*. 2014;25(8):1526–1535. doi:10.1093/annonc/mdu020
- Finn R. Emerging targeted strategies in advanced hepatocellular carcinoma. *Semin Liver Dis*. 2013;33(Suppl 1):S11–S19. doi:10.1055/s-0033-1333632
- Yang JD, Hainaut P, Gores GJ, Amadou A, Plymoth A, Roberts LR. A global view of hepatocellular carcinoma: Trends, risk, prevention and management. *Nat Rev Gastroenterol Hepatol*. 2019;16(10):589–604. doi:10.1038/s41575-019-0186-y
- Roayaie S, Jibara G, Tabrizian P, et al. The role of hepatic resection in the treatment of hepatocellular cancer. *Hepatology*. 2015;62(2): 440–451. doi:10.1002/hep.27745
- Daher S, Massarwa M, Benson AA, Khoury T. Current and future treatment of hepatocellular carcinoma: An updated comprehensive review. *J Clin Transl Hepatol*. 2018;6(1):69–78. doi:10.14218/JCTH. 2017.00031
- Kondo M, Numata K, Hara K, et al. Treatment of advanced hepatocellular carcinoma after failure of sorafenib treatment: Subsequent or additional treatment interventions contribute to prolonged survival postprogression. *Gastroenterol Res Pract*. 2017;2017:5728946. doi:10.1155/2017/5728946
- Harding JJ, El Dika I, Abou-Alfa GK. Immunotherapy in hepatocellular carcinoma: Primed to make a difference? *Cancer*. 2016;122(3): 367–377. doi:10.1002/cncr.29769
- Chiew Woon L, Joycelyn Jie Xin L, Su Pin C. Nivolumab for the treatment of hepatocellular carcinoma. *Exp Opin Biol Ther*. 2020;20(7): 687–693. doi:10.1080/14712598.2020.1749593
- El-Khoueiry AB, Melero I, Crocenzi TS, et al. Phase I/II safety and anti-tumor activity of nivolumab in patients with advanced hepatocellular carcinoma (HCC): CA209-040. *J Clin Oncol*. 2015;33(18 Suppl): LBA101. doi:10.1200/jco.2015.33.18_suppl.lba101
- El-Khoueiry AB, Sangro B, Yau T, et al. Nivolumab in patients with advanced hepatocellular carcinoma (CheckMate 040): An open-label, non-comparative, phase 1/2 dose escalation and expansion trial. *Lancet*. 2017;389(10088):2492–2502. doi:10.1016/S0140-6736(17)31046-2
- Morse MA, Sun W, Kim R, et al. The role of angiogenesis in hepatocellular carcinoma. *Clin Cancer Res*. 2019;25(3):912–920. doi:10.1158/1078-0432.CCR-18-1254
- Wilhelm SM, Dumas J, Adnane L, et al. Regorafenib (BAY 73-4506): A new oral multikinase inhibitor of angiogenic, stromal and oncogenic receptor tyrosine kinases with potent preclinical antitumor activity. *Int J Cancer*. 2011;129(1):245–255. doi:10.1002/ijc.25864
- Granito A, Forgione A, Marinelli S, et al. Experience with regorafenib in the treatment of hepatocellular carcinoma. *Therap Adv Gastroenterol*. 2021;14:175628482110169. doi:10.1177/17562848211016959
- Bruix J, Qin S, Merle P, et al. Regorafenib for patients with hepatocellular carcinoma who progressed on sorafenib treatment (RESORCE): A randomised, double-blind, placebo-controlled, phase 3 trial. *Lancet*. 2017;389(10064):56–66. doi:10.1016/S0140-6736(16)32453-9
- Liberati A, Altman DG, Tetzlaff J, et al. The PRISMA statement for reporting systematic reviews and meta-analyses of studies that evaluate health care interventions: Explanation and elaboration. *PLoS Med*. 2009;6(7):e1000100. doi:10.1371/journal.pmed.1000100
- Higgins JPT, Altman DG, Gotzsche PC, et al. The Cochrane Collaboration's tool for assessing risk of bias in randomised trials. *BMJ*. 2011;343:d5928. doi:10.1136/bmj.d5928
- Galle PR, Forner A, Llovet JM, et al. EASL Clinical Practice Guidelines: Management of hepatocellular carcinoma. *J Hepatol*. 2018;69(1): 182–236. doi:10.1016/j.jhep.2018.03.019
- Llovet JM, Ricci S, Mazzaferro V, et al. Sorafenib in advanced hepatocellular carcinoma. *N Engl J Med*. 2008;359(4):378–390. doi:10.1056/NEJMoa0708857
- Cheng AL, Kang YK, Chen Z, et al. Efficacy and safety of sorafenib in patients in the Asia-Pacific region with advanced hepatocellular carcinoma: A phase III randomised, double-blind, placebo-controlled trial. *Lancet Oncol*. 2009;10(1):25–34. doi:10.1016/S1470-2045(08)70285-7
- Lamarca A, Mendiola M, Barriuso J. Hepatocellular carcinoma: Exploring the impact of ethnicity on molecular biology. *Crit Rev Oncol Hematol*. 2016;105:65–72. doi:10.1016/j.critrevonc.2016.06.007
- Zhu AX, Finn RS, Edeline J, et al. Pembrolizumab in patients with advanced hepatocellular carcinoma previously treated with sorafenib (KEYNOTE-224): A non-randomised, open-label phase 2 trial. *Lancet Oncol*. 2018;19(7):940–952. doi:10.1016/S1470-2045(18)30351-6
- Qin S, Finn RS, Kudo M, et al. RATIONALE 301 study: Tislelizumab versus sorafenib as first-line treatment for unresectable hepatocellular carcinoma. *Future Oncol*. 2019;15(16):1811–1822. doi:10.2217/fon-2019-0097
- Granito A, Marinelli S, Terzi E, et al. Metronomic capecitabine as second-line treatment in hepatocellular carcinoma after sorafenib failure. *Digest Liver Dis*. 2015;47(6):518–522. doi:10.1016/j.dld.2015.03.010
- Trevisani F, Brandi G, Garuti F, et al. Metronomic capecitabine as second-line treatment for hepatocellular carcinoma after sorafenib discontinuation. *J Cancer Res Clin Oncol*. 2018;144(2):403–414. doi:10.1007/s00432-017-2556-6
- Choi W, Choi J, Lee D, et al. Regorafenib versus nivolumab after sorafenib failure: Real-world data in patients with hepatocellular carcinoma. *Hepatol Commun*. 2020;4(7):1073–1086. doi:10.1002/hep4.1523
- Lee CH, Lee YB, Kim MA, et al. Effectiveness of nivolumab versus regorafenib in hepatocellular carcinoma patients who failed sorafenib treatment. *Clin Mol Hepatol*. 2020;26(3):328–339. doi:10.3350/cmh.2019.0049n
- Kuo YH, Yen YH, Chen YY, et al. Nivolumab versus regorafenib in patients with hepatocellular carcinoma after sorafenib failure. *Front Oncol*. 2021;11:683341. doi:10.3389/fonc.2021.683341

The prognostic value of tumor-infiltrating lymphocytes in non-small cell lung cancer patients who received neoadjuvant chemotherapy followed by surgery

Zexin Hou^{1,A,C,D}, Lili Zhao^{1,E,F}, Lingjun Zou^{1,B,C}, Benlan Li^{2,B,C}

¹ Department of Oncology, The Second Affiliated Hospital, Guizhou Medical University, Kaili, China

² Department of Pathology, The Second Affiliated Hospital, Guizhou Medical University, Kaili, China

A – research concept and design; B – collection and/or assembly of data; C – data analysis and interpretation;

D – writing the article; E – critical revision of the article; F – final approval of the article

Advances in Clinical and Experimental Medicine, ISSN 1899–5276 (print), ISSN 2451–2680 (online)

Adv Clin Exp Med. 2023;32(8):847–853

Address for correspondence

Lili Zhao

E-mail: 934848847@qq.com

Funding sources

None declared

Conflict of interest

None declared

Acknowledgements

We thank Bullet Edits Limited for the linguistic editing and proofreading of the manuscript.

Received on July 13, 2022

Reviewed on October 1, 2022

Accepted on January 12, 2023

Published online on March 7, 2023

Cite as

Hou Z, Zhao L, Zou L, Li B. The prognostic value of tumor-infiltrating lymphocytes in non-small cell lung cancer patients who received neoadjuvant chemotherapy followed by surgery. *Adv Clin Exp Med.* 2023;32(8):847–853. doi:10.17219/acem/159242

DOI

10.17219/acem/159242

Copyright

Copyright by Author(s)

This is an article distributed under the terms of the Creative Commons Attribution 3.0 Unported (CC BY 3.0) (<https://creativecommons.org/licenses/by/3.0/>)

Abstract

Background. The relationship between tumor-infiltrating lymphocyte (TIL) levels and the prognosis of patients with non-small cell lung cancer (NSCLC) who receive neoadjuvant chemotherapy followed by surgery is a problem that requires more research.

Objectives. To evaluate the prognostic value of TIL levels in patients with NSCLC who received neoadjuvant chemotherapy followed by surgery.

Materials and methods. Patients with NSCLC who received neoadjuvant chemotherapy followed by surgery in our hospital from December 2014 to December 2020 were selected for a retrospective analysis. Sections were stained with hematoxylin and eosin (H&E) to evaluate TIL levels in surgically-resected tumor tissues. Patients were divided into TIL– (low-level infiltration) and TIL+ (medium- to high-level infiltration) groups according to the recommended TIL evaluation criteria. Univariate (Kaplan–Meier) and multivariate (Cox) survival analyses were used to analyze the impact of clinicopathological features and TIL levels on prognosis.

Results. The study involved 137 patients, including 45 who were TIL– and 92 who were TIL+. The median overall survival (OS) and disease-free survival (DFS) of the TIL+ group were higher than those of the TIL– group. The univariate analysis showed that smoking, clinical and pathological stages, and TIL levels, were the factors influencing OS and DFS. The multivariate analysis showed that smoking (OS, hazard ratio (HR): 1.881, 95% confidence interval (95% CI): 1.135–3.115, $p = 0.014$; DFS, HR: 1.820, 95% CI: 1.181–2.804, $p = 0.007$) and clinical stage III (DFS, HR: 2.316, 95% CI: 1.350–3.972, $p = 0.002$) were adverse factors affecting the prognosis of patients with NSCLC who received neoadjuvant chemotherapy followed by surgery. At the same time, TIL+ status was an independent factor for a good prognosis in OS (HR: 0.547, 95% CI: 0.335–0.894, $p = 0.016$) and DFS (HR: 0.445, 95% CI: 0.284–0.698, $p = 0.001$).

Conclusions. Medium to high levels of TILs were associated with a good prognosis in NSCLC patients who received neoadjuvant chemotherapy followed by surgery. The levels of TILs are of prognostic value in this population of patients.

Key words: non-small cell lung cancer, overall survival, neoadjuvant chemotherapy, disease-free survival, tumor-infiltrating lymphocyte

Background

Lung cancer is one of the most common malignant tumors in the world and the leading cause of cancer-related death.¹ Non-small cell lung cancer (NSCLC) is the main form of lung cancer. If there are no contraindications and the prognosis is good, tumors in patients with stage I or II disease can be removed surgically.² However, due to the low popularity of lung cancer screening, most patients with NSCLC are diagnosed with locally advanced or metastatic disease and lose the opportunity for radical surgery.³

Some studies have shown that preoperative neoadjuvant chemotherapy can reduce the staging of some stage III NSCLC patients with surgical indications, which increases the possibility of complete resection of tumor tissue.^{4–6} Chemotherapy changes the tumor immune microenvironment. Cancer patients who receive preoperative neoadjuvant chemotherapy usually have a high level of T cells, which participate in the antitumor processes through a specific immune response. Indeed, the immune response has been shown to play an important role in the invasion, progression and metastasis of cancer.⁷ Previous studies have shown that the level of tumor-infiltrating lymphocytes (TILs), such as CD8⁺ T cells, is considered to be an expression of an immune response. Such responses are related to survival rate and response to treatment in patients with a variety of solid tumors, and have an impact on the overall survival (OS) and disease-free survival (DFS) of these patients.^{8–11} Recent studies have demonstrated that patients with NSCLC who underwent early surgery had high levels of TILs in tumors, which were associated with an improvement in relapse-free survival rate and a decreased risk of systemic recurrence.⁸ Additionally, Gataa et al. reported an association between TILs and the prognosis of patients with advanced NSCLC who were receiving immunotherapy.¹²

Objectives

This study aimed to evaluate the correlation between TIL levels and the prognosis of patients with NSCLC who received neoadjuvant chemotherapy followed by surgery.

Materials and methods

Patients

The clinical and pathological data of patients with NSCLC who underwent surgery after neoadjuvant chemotherapy in the Second Affiliated Hospital of Guizhou Medical University (Guizhou, China) from December 2014 to December 2020 were retrospectively analyzed. The following inclusion criteria were used: 1) patients diagnosed with NSCLC through pathological biopsy before neoadjuvant therapy; 2) patients who had stage I–III NSCLC

according to the American Joint Committee on Cancer Eighth Edition TNM Staging Manual Classifications for T2b and T3 NSCLC¹³; 3) patients whose operations were R0 resected; and 4) patients whose resected specimens were well preserved and could be stained with hematoxylin and eosin (H&E). The following exclusion criteria were used: 1) patients who received neoadjuvant chemotherapy combined with immunotherapy; 2) patients who received neoadjuvant immunotherapy.

This research complied with the Declaration of Helsinki. The approval was granted by the Ethics Committee of the Second Affiliated Hospital of Guizhou Medical University (approval No. 2020-Ethical Review-03). The risks, benefits and goals of the study were briefly explained to each participant. In addition, all of the individuals gave signed informed consent. A total of 164 patients were included in the study, though 10 samples could not be used. Additionally, there were 8 cases of R1 resection, 4 cases of mixed large and small cell types, and 5 cases lost on follow-up. Therefore, 137 cases were included in the analysis. Age of the patients ranged from 33 to 79 years, with a median age of 62 years. The last follow-up was in January 2022, with a median follow-up of 32 months, a median DFS of 23 months and an unmet median OS. There were 45 patients assessed as TIL– (low-level infiltration) and 92 patients assessed as TIL+ (medium- and high-level infiltration).

Tumor-infiltrating lymphocyte assessment

Two pathologists evaluated the TIL level of hematoxylin and eosin (H&E)-stained postoperative tumor tissue sections. The levels of TIL assessed on each slide were used to divide patients into TIL– and TIL+ groups. It has been reported that low-level infiltration is indicated by a scattered distribution of lymphocytes in the stroma, and high-level infiltration by the presence of a large number of stromal lymphocytes and lymphocytes infiltrating between tumor cells.⁸ Medium-level infiltration is indicated by a small number of stromal lymphocytes in the absence of tumor nest infiltration.

Response assessment

The primary endpoints included OS and DFS. Overall survival was defined as the time from diagnosis until death from any cause, and DFS was defined as the time from radical surgery to disease recurrence or death from any cause.

Statistical analyses

The data were statistically analyzed using IBM SPSS v. 22.0 software (IBM Corp., Armonk, USA). The general data were analyzed using descriptive analysis, and the baseline data of patients with various levels of TIL were compared using the χ^2 test. The Kaplan–Meier curves and log-rank tests

were used for the survival analysis. Multivariate Cox proportional hazards (PH) regression modeling was used to analyze the risk factors associated with survival. In Cox regression analysis, the univariate Cox analysis was initially performed on the variables, and then the variables with $p < 0.05$ were further analyzed with multifactor Cox analysis. The survival plot output (log of negative log), in which the abscissa is the log of time and the ordinate is the log of the survival function, was visually inspected. The judgment method was as follows: if the survival curves were roughly parallel, then the PH condition of Cox regression was considered valid; if the curves were not parallel and there was a crossover phenomenon, the PH condition was considered not valid. It was found that the survival curves of all variables were roughly parallel. The evaluation indicators were hazard ratio (HR) and 95% confidence interval (95% CI). The value of $p < 0.05$ was considered statistically significant.

Results

There was a relationship between levels of TILs and clinicopathological features in patients with NSCLC.

Table 1 lists the baseline characteristics of the 137 patients. Forty-five patients were classified as TIL⁻ and the remaining 92 patients were defined as TIL⁺. Compared with TIL⁻, more TIL⁺ patients had a lower pathological stage.

Univariate analysis of OS and DFS in patients with NSCLC

The univariate analysis showed that lower clinical and pathological stages, being TIL⁺ and never smoking were associated with better OS and DFS, as shown in Table 2 and Fig. 1.

Multivariate analysis of OS and DFS in patients with NSCLC

Figure 2 presents the results of multivariate analysis on the relationship between clinicopathological variables and OS and DFS in patients with NSCLC. In the multivariate survival analysis, being a current or ex-smoker was associated with poor OS and DFS, and clinical stage III was associated with poor DFS. However, TIL⁺ was a potentially positive prognostic factor for OS and DFS.

Discussion

Previous studies have confirmed that neoadjuvant chemotherapy is beneficial to patients with NSCLC (stage IIIA). To some extent, neoadjuvant chemotherapy can change the tumor immune microenvironment and the local infiltration of tumor cells to effectively achieve pathological decline, improve R0 resection rate, inhibit disease progression, improve patient survival rate, and improve prognosis.^{14,15} Mounting evidence shows that there are dynamic and complex interactions between TILs and other immune and tumor cells, and that these interactions closely controls tumor progression.¹⁶

Tumor-infiltrating lymphocyte level is a prognostic factor in patients with cancer. Indeed, the correlation between TIL levels and prognosis has been demonstrated in various cancers.^{8–11} A large-scale study conducted by Feng et al. showed that TIL⁺ patients had better postoperative survival results compared with TIL⁻ patients with pathological stage IIIA (N2) NSCLC who underwent complete cancer resection (5-year OS of 35.6% compared to 34%).¹⁷ However, there are few reports on the relationship between TILs and the prognosis of patients with NSCLC after neoadjuvant chemotherapy. Therefore, the current

Table 1. Relationship between TIL levels and clinicopathologic features of NSCLC patients evaluated using the χ^2 test

Characteristics		Number of patients	TIL ⁻ , n (%)	TIL ⁺ , n (%)	χ^2	p-value
All patients		137	45 (32.8)	92 (67.2)	–	–
Gender	male	86	24 (27.9)	62 (72.1)	2.537	0.111
	female	51	21 (41.2)	30 (58.8)		
Age [years]	<60	54	17 (31.5)	37 (68.5)	0.075	0.784
	≥60	83	28 (33.7)	55 (66.3)		
Smoking status	never smoking	59	23 (39.0)	36 (61.0)	1.756	0.185
	current or ex-smoker	78	22 (28.2)	56 (71.8)		
Pathological pattern	adenocarcinoma	78	24 (30.8)	54 (69.2)	0.352	0.553
	squamous carcinoma	59	21 (35.6)	38 (64.4)		
Clinical stages	I–II	40	12 (30.0)	28 (70.0)	0.206	0.649
	III	97	33 (34.0)	64 (66.0)		
Pathological stages	I–II	82	20 (24.4)	62 (77.6)	6.574	0.010
	III	55	25 (45.5)	30 (54.5)		
Regimens	PP	62	17 (27.4)	45 (72.6)	1.594	0.451
	GP	44	17 (38.6)	27 (61.4)		
	TP	31	11 (35.5)	20 (64.5)		

NSCLC – non-small cell lung cancer; PP – pemetrexed + platinum; TP – paclitaxel + platinum; GP – gemcitabine + platinum; TIL – tumor-infiltrating lymphocyte.

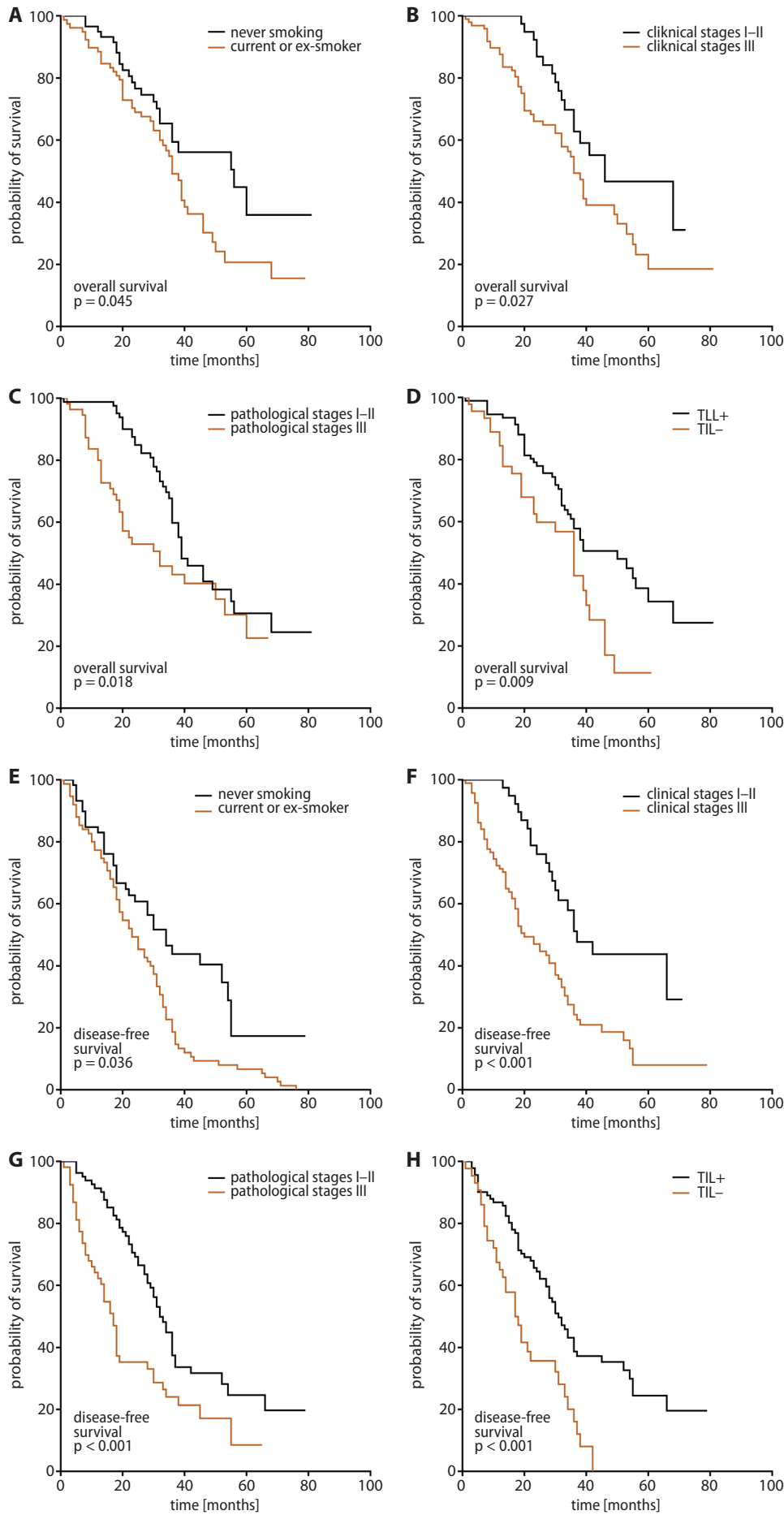


Fig. 1. Kaplan–Meier analysis of overall survival and disease-free survival in patients with non-small cell lung cancer

Table 2. Univariate analysis of OS and DFS in patients with NSCLC using the log-rank test

Characteristics		OS				DFS			
		MST [months]	5-year [%]	χ^2	p-value	MST [months]	5-year [%]	χ^2	p-value
Gender	male	39	28.6	0.215	0.643	27	22.2	0.211	0.646
	female	38	23.2			28	10.8		
Age [years]	<60	50	30.5	1.550	0.213	29	21.8	1.059	0.303
	≥60	36	26.8			27	15.0		
Smoking status	never smoking	56	35.9	4.018	0.045	34	17.3	4.378	0.036
	current or ex-smoker	36	20.7			23	16.4		
Pathological pattern	adenocarcinoma	38	30.9	0.003	0.952	25	17.3	0.419	0.517
	squamous carcinoma	39	26.0			30	18.7		
Clinical stages	I–II	46	46.7	4.864	0.027	37	43.7	15.098	<0.001
	III	36	18.5			19	7.75		
Pathological stages	I–II	39	30.6	5.587	0.018	32	24.3	13.389	<0.001
	III	32	22.6			16	8.24		
Regimens	PP	36	32.7	0.924	0.630	23	12.3	1.778	0.411
	GP	50	30.9			25	25.3		
	TP	39	29.6			32	20.2		
TIL levels	TIL–	36	11.4	6.747	0.009	17	0.00	15.414	<0.001
	TIL+	50	34.3			31	24.2		

NSCLC – non-small cell lung cancer; OS – overall survival; DFS – disease-free survival; MST – median survival time; TIL – tumor-infiltrating lymphocyte.

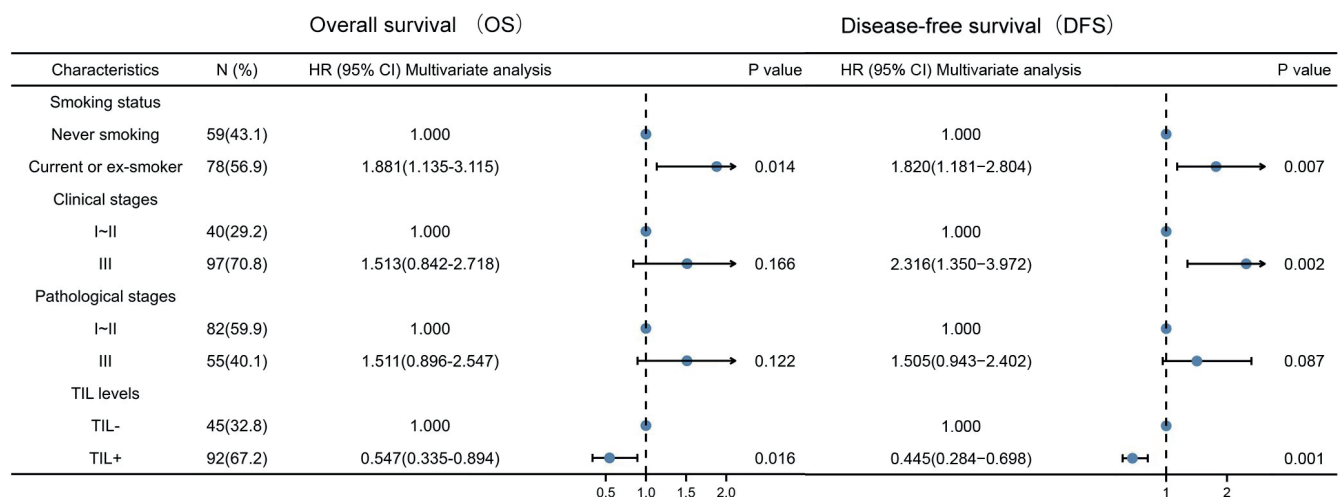


Fig. 2. Multivariate Cox regression analysis represented by a forest plot

TIL – tumor-infiltrating lymphocyte; HR – hazard ratio; 95% CI – 95% confidence interval.

study evaluated TIL levels in the tumor stroma of patients with NSCLC who were diagnosed and treated in a single medical institution to determine its effectiveness as a prognostic factor for patients with NSCLC undergoing surgery after neoadjuvant chemotherapy.

An intense spectrum of TIL staining was observed in the tumor samples of patients with NSCLC who had received surgery after neoadjuvant chemotherapy. More than 60% of the samples were considered TIL+, suggesting that high levels of TILs may be more common in patients with NSCLC who received surgery after neoadjuvant chemotherapy. However, the proportion of TIL+ patients in our cohort was higher than that found in NSCLC studies conducted by Horne et al., who used the same TIL evaluation method.⁸ This could be attributed to the fact that

neoadjuvant chemotherapy improves the tumor immune microenvironment, thereby increasing the density of TILs. Nonetheless, despite the possibility that the proportion of TIL+ patients and the neoadjuvant chemotherapy may be related, it is important to note that there was no significant relationship between the TIL+ ratio and the neoadjuvant chemotherapy regimen. Studies have shown that there is a lower proportion of TIL+ patients in the cancer population with higher stages of the disease.¹⁶

The results of this study showed that the proportion of TIL+ patients in pathological stage I–II (77.6%) was significantly higher than it was for pathological stage III (54.5%), while TIL+ status was not related to gender, age stratification, smoking status, or clinical stage, as has been reported by others.^{16–18} A study on NSCLC reported

that TILs had a higher infiltration frequency in squamous cell carcinoma due to the heterogeneity of tumor types.¹⁹ Notably, we observed that TIL+ results were not related to the histological type of NSCLC. This may be due to the large number of adenocarcinomas included in the study or the different genetic backgrounds of the patients. However, these findings should be considered and validated in future TIL studies.

Our data showed that a TIL+ status improved the survival rate of patients with NSCLC who received surgery after neoadjuvant chemotherapy. This indicates that patients with high TIL levels may have a strong immune response to the tumor, resulting in a better prognosis. A study that evaluated the TIL levels in tumor tissues surgically removed from 537 patients with stage I–III NSCLC found that the TIL level in tumor tissues was closely related to OS (HR: 0.51, 95% CI: 0.32–0.82) and DFS (HR: 0.34, 95% CI: 0.19–0.64), and a higher TIL level was an independent indicator of a good prognosis.²⁰ A similar result was obtained from the multivariate analysis in our study. In addition, higher levels of TIL in NSCLC are related to a better prognosis, which was confirmed in another comparative study.²¹ However, in our study, variables in the multivariate analysis were derived from the univariate analysis. Therefore, whether gender, pathological type or other variables play a role in prognosis in multivariate analysis is still unknown and should be given attention in future studies.

The antitumor mechanisms of TILs described by recent studies may include the following: 1) lymphocytes mediate cell lysis and apoptosis by inhibiting the proliferation of regulatory T cells, increasing interferon gamma (IFN- γ) secretion and reducing the secretion of transforming growth factor beta (TGF- β), interleukin 10 (IL-10) and IL-17. This pathway can kill target cells by releasing particles or through a direct cell contact²²; 2) lymphocytes bind to suicide-related factors on target cells, which mediates apoptosis²³; 3) perforin or granzyme-mediated apoptosis.²⁴ Although this study demonstrated that high levels of TILs improved the prognosis of patients with NSCLC who underwent surgery after neoadjuvant chemotherapy, the challenges in the analysis of prognoses,^{25,26} such as the activation status of TILs and their location and density in the tumor, still remain. Previous studies found that CD8⁺ T cells were more likely to play an antitumor role in tumors than in the matrix.²⁶ Also, when CD8⁺ T cells are in a state of inhibition, focusing only on the number of cells may result in different conclusions.

In addition to the TIL level, the multivariate analysis suggests that a history of smoking and a higher clinical stage may indicate a poor prognosis for patients with NSCLC who received surgery after neoadjuvant chemotherapy. Recent studies have also shown that NSCLC patients with higher smoking rates and those at advanced stages of disease have lower OS.²⁷ The results of a large prospective cohort study by Fujiyoshi et al. showed that for TIL– cancers,

the correlation between smoking status and colorectal cancer mortality was stronger when diagnosing colorectal cancer, indicating that there may be an interaction between smoking and the lymphocyte response in the colorectal cancer microenvironment.²⁸ However, whether this relationship exists in NSCLC patients who received surgery after neoadjuvant chemotherapy remains unclear and further studies are required.

Limitations

There were certain limitations to the present study. First of all, this was a single-center study. Similar studies should be conducted in the future to further verify the accuracy of the findings. In addition, because this was a retrospective study of outcomes related to a subjective assessment of pathological variables, we cannot be fully confident about the effects of TILs in patients with early-stage NSCLC.


Conclusions


This study confirmed that TILs in surgical specimens from NSCLC patients treated with neoadjuvant chemotherapy may be associated with prognosis. Therefore, low levels of TILs in tumor tissue sections after an operation indicate a poor prognosis, and the number of postoperative adjuvant chemotherapy should be strengthened, to improve the therapeutic effect and prolong patients survival.

ORCID iDs

Zexin Hou  <https://orcid.org/0000-0001-7154-0424>

Lili Zhao  <https://orcid.org/0000-0003-3471-5840>

Lingjun Zou  <https://orcid.org/0000-0003-4247-1022>

Benlan Li  <https://orcid.org/0000-0003-3383-8806>

References

1. Sung H, Ferlay J, Siegel RL, et al. Global Cancer Statistics 2020: GLOBOCAN estimates of incidence and mortality worldwide for 36 cancers in 185 countries. *CA A Cancer J Clin*. 2021;71(3):209–249. doi:10.3322/caac.21660
2. Duma N, Santana-Davila R, Molina JR. Non-small cell lung cancer: Epidemiology, screening, diagnosis, and treatment. *Mayo Clin Proc*. 2019;94(8):1623–1640. doi:10.1016/j.mayocp.2019.01.013
3. Kocher F, Hilbe W, Seeber A, et al. Longitudinal analysis of 2293 NSCLC patients: A comprehensive study from the TYROL registry. *Lung Cancer*. 2015;87(2):193–200. doi:10.1016/j.lungcan.2014.12.006
4. Sinn K, Mosleh B, Steindl A, et al. Neoadjuvant chemoradiotherapy is superior to chemotherapy alone in surgically treated stage III/N2 non-small-cell lung cancer: A retrospective single-center cohort study. *ESMO Open*. 2022;7(2):100466. doi:10.1016/j.esmoop.2022.100466
5. Montemuiño S, de Dios NR, Martín M, et al. High-dose neoadjuvant chemoradiotherapy versus chemotherapy alone followed by surgery in potentially-resectable stage IIIA-N2 NSCLC: A multi-institutional retrospective study by the Oncologic Group for the Study of Lung Cancer (Spanish Radiation Oncology Society). *Rep Pract Oncol Radiother*. 2020;25(3):447–455. doi:10.1016/j.rpor.2020.03.006
6. Darling GE, Li F, Patsios D, et al. Neoadjuvant chemoradiation and surgery improves survival outcomes compared with definitive chemoradiation in the treatment of stage IIIA N2 non-small-cell lung cancer. *Eur J Cardiothorac Surg*. 2015;48(5):684–690. doi:10.1093/ejcts/ezu504

7. Pardoll DM. The blockade of immune checkpoints in cancer immunotherapy. *Nat Rev Cancer*. 2012;12(4):252–264. doi:10.1038/nrc3239
8. Horne ZD, Jack R, Gray ZT, et al. Increased levels of tumor-infiltrating lymphocytes are associated with improved recurrence-free survival in stage 1A non-small-cell lung cancer. *J Surg Res*. 2011;171(1):1–5. doi:10.1016/j.jss.2011.03.068
9. Ku BM, Kim Y, Lee KY, et al. Tumor infiltrated immune cell types support distinct immune checkpoint inhibitor outcomes in patients with advanced non-small cell lung cancer. *Eur J Immunol*. 2021;51(4):956–964. doi:10.1002/eji.202048966
10. Caparica R, Bruzzone M, Agostinetti E, et al. Tumour-infiltrating lymphocytes in non-invasive breast cancer: A systematic review and meta-analysis. *Breast*. 2021;59:183–192. doi:10.1016/j.breast.2021.07.007
11. Casanova JM, Almeida JS, Reith JD, et al. Tumor-infiltrating lymphocytes and cancer markers in osteosarcoma: Influence on patient survival. *Cancers*. 2021;13(23):6075. doi:10.3390/cancers13236075
12. Gataa I, Mezquita L, Rossoni C, et al. Tumour-infiltrating lymphocyte density is associated with favourable outcome in patients with advanced non-small cell lung cancer treated with immunotherapy. *Eur J Cancer*. 2021;145:221–229. doi:10.1016/j.ejca.2020.10.017
13. Kumar A, Kumar S, Gilja S, et al. Reconsidering the American Joint Committee on Cancer Eighth Edition TNM Staging Manual Classifications for T2b and T3 NSCLC. *J Thorac Oncol*. 2021;16(10):1672–1683. doi:10.1016/j.jtho.2021.06.016
14. Zhao L, Zhang L, Gong F, Xu J. Thoracoscopic radical resection in the treatment of NSCLC patients (stage IIIA) after neoadjuvant chemotherapy. *J BUON*. 2021;26(2):313–319. PMID:34076974.
15. Yu WD, Sun G, Li J, Xu J, Wang X. Mechanisms and therapeutic potentials of cancer immunotherapy in combination with radiotherapy and/or chemotherapy. *Cancer Lett*. 2019;452:66–70. doi:10.1016/j.canlet.2019.02.048
16. Xie QK, He WZ, Hu WM, et al. Tumor-infiltrating lymphocyte as a prognostic biomarker in stage IV colorectal cancer should take into account the metastatic status and operation modality. *Cancer Manag Res*. 2018;10:1365–1375. doi:10.2147/CMAR.S162147
17. Feng W, Li Y, Shen L, et al. Prognostic value of tumor-infiltrating lymphocytes for patients with completely resected stage IIIA(N2) non-small cell lung cancer. *Oncotarget*. 2016;7(6):7227–7240. doi:10.18632/oncotarget.6979
18. Gataa I, Mezquita L, Rossoni C, et al. Tumour-infiltrating lymphocyte density is associated with favourable outcome in patients with advanced non-small cell lung cancer treated with immunotherapy. *Eur J Cancer*. 2021;145:221–229. doi:10.1016/j.ejca.2020.10.017
19. Lee TK, Horner RD, Silverman JF, Chen YH, Jenny C, Scarantino CW. Morphometric and morphologic evaluations in stage III non-small cell lung cancers: Prognostic significance of quantitative assessment of infiltrating lymphoid cells. *Cancer*. 1989;63(2):309–316. doi:10.1002/1097-0142(19890115)63:2<309::aid-cnrcr2820630218>3.0.co;2-n
20. Rakaee M, Kilvaer TK, Dalen SM, et al. Evaluation of tumor-infiltrating lymphocytes using routine H&E slides predicts patient survival in resected non-small cell lung cancer. *Hum Pathol*. 2018;79:188–198. doi:10.1016/j.humpath.2018.05.017
21. Devarakonda S, Rotolo F, Tsao MS, et al. Tumor mutation burden as a biomarker in resected non-small-cell lung cancer. *J Clin Oncol*. 2018;36(30):2995–3006. doi:10.1200/JCO.2018.78.1963
22. Wang WC, Zhang ZQ, Li PP, et al. Anti-tumor activity and mechanism of oligoclonal hepatocellular carcinoma tumor-infiltrating lymphocytes in vivo and in vitro. *Cancer Biol Ther*. 2019;20(9):1187–1194. doi:10.1080/15384047.2019.1599663
23. Cullen SP, Martin SJ. Fas and TRAIL 'death receptors' as initiators of inflammation: Implications for cancer. *Semin Cell Dev Biol*. 2015;39:26–34. doi:10.1016/j.semcd.2015.01.012
24. Voskoboinik I, Whisstock JC, Trapani JA. Perforin and granzymes: Function, dysfunction and human pathology. *Nat Rev Immunol*. 2015;15(6):388–400. doi:10.1038/nri3839
25. Trojan A, Urošević M, Dummer R, Giger R, Weder W, Stahel RA. Immune activation status of CD8⁺ T cells infiltrating non-small cell lung cancer. *Lung Cancer*. 2004;44(2):143–147. doi:10.1016/j.lungcan.2003.11.004
26. Zhuang X, Xia X, Wang C, et al. A high number of CD8⁺ T cells infiltrated in NSCLC tissues is associated with a favorable prognosis. *Appl Immunohistochem Mol Morphol*. 2010;18(1):24–28. doi:10.1097/PAI.0b013e3181b6a741
27. Steuer CE, Jegede OA, Dahlberg SE, et al. Smoking behavior in patients with early-stage NSCLC: A report from ECOG-ACRIN 1505 Trial. *J Thorac Oncol*. 2021;16(6):960–967. doi:10.1016/j.jtho.2020.12.017
28. Fujiyoshi K, Chen Y, Haruki K, et al. Smoking status at diagnosis and colorectal cancer prognosis according to tumor lymphocytic reaction. *JNCI Cancer Spectr*. 2020;4(5):pkaa040. doi:10.1093/jncics/pkaa040

The outcome of ibrutinib-based regimens in relapsed/refractory central nervous system lymphoma and the potential impact of genomic variants

Shu Wang^{1,A-D}, YuQi Zhu^{2,B,C}, Xiaohan Qian^{1,B,C}, Tianling Ding^{1,C,E}, Yan Yuan^{1,C,E}, Yuan Li^{2,C,E}, Hanfeng Wu^{3,A,B,F}, Tong Chen^{1,A,E,F}

¹ Department of Hematology, Huashan Hospital, Fudan University, Shanghai, China

² Department of Radiology, Huashan Hospital, Fudan University, Shanghai, China

³ Department of Neurosurgery, Shanghai Gamma Hospital, China

A – research concept and design; B – collection and/or assembly of data; C – data analysis and interpretation;

D – writing the article; E – critical revision of the article; F – final approval of the article

Advances in Clinical and Experimental Medicine, ISSN 1899–5276 (print), ISSN 2451–2680 (online)

Adv Clin Exp Med. 2023;32(8):855–863

Address for correspondence

Tong Chen

E-mail: chentong@fudan.edu.cn

Funding sources

None declared

Conflict of interest

None declared

Acknowledgements

This work was supported by the National Natural Science Foundation of China (grant No. 81870081), Program for Outstanding Medical Academic Leader of Shanghai (grant No. 2019LJ05), Shanghai Collaborative Innovation Program on Regenerative Medicine and Stem Cell Research (grant No. 2019CXJQ01), and Translational Research Grant of the National Clinical Research Center for Hematologic Diseases (No. 2020ZKMB03), all awarded to Dr. Tong Chen. Additionally, we thank Professor Xiaolei Lin (Fudan University) for her kind help on statistical analysis.

Received on October 15, 2022

Reviewed on January 9, 2023

Accepted on January 13, 2023

Published online on March 7, 2023

Cite as

Wang S, Zhu YQ, Qian XH, et al. The outcome of ibrutinib-based regimens in relapsed/refractory central nervous system lymphoma and the potential impact of genomic variants. *Adv Clin Exp Med.* 2023;32(8):855–863. doi:10.17219/acem/159288

DOI

10.17219/acem/159288

Copyright

Copyright by Author(s)

This is an article distributed under the terms of the Creative Commons Attribution 3.0 Unported (CC BY 3.0) (<https://creativecommons.org/licenses/by/3.0/>)

Abstract

Background. Relapsed/refractory (r/r) central nervous system lymphoma (CNSL) exhibits aggressive behavior and poor outcomes. As an effective bruton tyrosine kinase (BTK) inhibitor, ibrutinib yields benefits in B-cell malignancies.

Objectives. We aimed to explore the efficacy of ibrutinib in treating r/r CNSL patients, and whether genomic variants impact treatment outcomes.

Materials and methods. The ibrutinib-based regimens in 12 r/r primary CNSL (PCNSL) and 2 secondary CNSL (SCNSL) patients were analyzed retrospectively. The impact of genetic variants on the effects of treatments was examined using whole-exome sequencing (WES) technology.

Results. In PCNSL, the overall response rate was 75%, with median overall survival (OS) not reached (NR) and progression-free survival (PFS) of 4 months. Both SCNSL patients responded to ibrutinib, with median OS NR and PFS of 0.5–1.5 months. Infections were common during ibrutinib therapy (42.86%). The PCNSL patients harboring gene mutations in *PIM1*, *MYD88* and *CD79B*, and the proximal BCR and nuclear factor kappa B (NF- κ B) pathways responded to ibrutinib. Patients who harbored simple genetic variants and those with a low tumor mutation burden (TMB; 2.39–5.56/Mb) responded swiftly and maintained remission for more than 10 months. A patient with a TMB of 11/Mb responded to ibrutinib but continued to experience disease progression. In contrast, patients with complex genomic features, especially extremely high TMB (58.39/Mb), responded poorly to ibrutinib.

Conclusions. Our study demonstrates that ibrutinib-based therapy is effective and relatively safe for the treatment of r/r CNSL. Patients with less genomic complexity, especially with regard to TMB, might benefit more from ibrutinib regimens.

Key words: ibrutinib, tumor mutation burden, central nervous system lymphoma, relapsed/refractory, genomic variants

Background

Central nervous system lymphoma (CNSL) is a type of extra-nodal lymphoma that most commonly manifests as primary CNSL (PCNSL) and secondary CNSL (SCNSL). Primary CNSL is a rare and aggressive type of lymphoma, 95% of which are diffuse large B cell lymphoma (DLBCL),¹ while SCNSL refers to systematic DLBCL that has spread to the CNS. The backbone of PCNSL treatment is high-dose methotrexate (HD-MTX) in combination with other agents.² However, due to the blood–brain barrier and the special immune microenvironment of the CNS, CNSL tends to show more aggressive behavior than systematic DLBCL, resulting in a poorer prognosis for relapsed/refractory (r/r) patients under standard treatments.³

Bruton tyrosine kinase (BTK), which mediates signals from the B-cell antigen receptor (BCR), toll-like receptor (TLR) and downstream pathways, plays an irreplaceable role in the survival of B cells.⁴ In recent years, the first-generation BTK inhibitor ibrutinib has been used to treat CNSL,⁵ yielding promising results with an acceptable safety profile across its combination regimens and single-agent-targeted therapy for r/r CNSL. For patients who fail to respond to traditional treatments,^{6–9} this offers a great alternative treatment option.

Although mutations of *MYD88* and *CD79B* are widely accepted as hallmarks of DLBCL in immune-privileged sites due to their key roles in the BCR and TLR signaling pathways, there has been no consensus regarding their effects on ibrutinib treatment.^{10,11} Some studies have claimed that *CD79B* mutations weaken the response to BTK inhibitors,⁹ while others have reported that *MYD88*, *CD79B* or BCR pathway mutations have no effects on the tumor response to ibrutinib.^{7,8}

Based on the distinct molecular subtypes of DLBCL,¹² a massive prospective study has recently demonstrated that 100% of MCD or N1 subtype DLBCL cases responded to R-CHOP regimes combined with ibrutinib rather than placebo.¹³ This highlights the significant likelihood of a potential relationship between genome variants and BTK inhibitor response.

Objectives

In this single-center retrospective study of a CNSL cohort, we aimed to evaluate the effectiveness and side effects of ibrutinib-based regimens, and uncover relationships between clinical outcomes and genomic variants.

Materials and methods

Patients

The r/r CNSL patients who started ibrutinib-based regimens at Huashan Hospital (Shanghai, China) from 2018 to 2020 were enrolled in this single-center retrospective

study. The study included 12 r/r PCNSL and 2 r/r SCNSL patients. All patients received enhanced brain magnetic resonance imaging (MRI), whole-body positron emission tomography (PET) or computed tomography (CT) scans, cerebral spinal fluid evaluation, and bone marrow aspiration to determine whether they had primary or secondary CNSL. The responses to treatments were evaluated according to the International PCNSL Collaborative Group (IPCG) guidelines.¹⁴ The National Cancer Institute Common Terminology Criteria for Adverse Events (v. 5.0) were used to assess adverse events (AEs) during ibrutinib therapy. This retrospective cohort study was approved by the Institutional Review Board of Huashan Hospital (Shanghai, China; approval No. KY2020-879). The study complies with the Declaration of Helsinki (as revised in 2013). Informed consent was obtained individually from the included patients.

Whole-exome sequencing and data processing

Exon regions were captured using SureSelect Exome arrays (Agilent Technologies, Santa Clara, USA) and sequenced with HiSeq System (Illumina, San Diego, USA). Paired-end fastq reads were mapped to University of California Santa Cruz (UCSC) human genome hg19 using BWA software (<https://hpc.nih.gov/apps/bwa.html>).¹⁵ Mutations were called by the Genome Analysis Toolkit (GATK v. 4.1.2) and Mutect (v. 2) workflow (Broad Institute, Cambridge, USA).¹⁶ All mutations were annotated by ANNOVAR software (<http://annovar.openbioinformatics.org>).¹⁷ Facets software was used to calculate somatic copy number variation (CNV).¹⁸ The R package “sigminer” (R Foundation for Statistical Computing, Vienna, Austria) was applied to analyze mutation signature.¹⁹

Pipeline filtering paired tumor samples had the following characteristics: 1) at least $\times 10$ coverage, variant allele frequency (VAF) $\geq 5\%$ and altered reads ≥ 3 ; 2) all variants had less than 0.0025 VAF in a matched normal sample; 3) variants located in exon or splice were retained; 4) nonsynonymous somatic nucleotide variant (SNV) was required; 5) variants with a frequency over 1% in 1000G in the East Asian or East Asian of Genome Aggregation Database (gnomAD_EAS) sites^{20,21} and not listed in the COSMIC v. 92 database were excluded.²²

The criteria for formalin-fixed paraffin-embedded (FFPE) samples were: 1) variants with at least $\times 20$ coverage, VAF $\geq 5\%$ and altered reads ≥ 3 ; 2) for variants reads ranging $\times 10$ – 20 , VAF must be higher than 0.2; 3) variants located in exon or splice were retained and nonsynonymous SNV was required; 4) germline variants were filtered including a) variants with a frequency over 1% in both 1000G East Asian or gnomAD_EAS sites, and b) sites not included in COSMIC v. 92 but in the single nucleotide polymorphism database (dbSNP)150 or with VAF $\geq 80\%$; and 5) C > T and G > T base substitution with VAF < 15% were filtered out to avoid artifacts brought by formalin.^{23,24}

Statistical analyses

To reflect the general survival and disease improvement, overall survival (OS) and progression-free survival (PFS) were both calculated. Overall survival was measured from the initiation of ibrutinib therapy until discontinuation or death. Progression-free survival was defined as the time elapsed from the initiation of ibrutinib therapy until disease progression, according to MRI assessment. Since the sample size was small in this cohort, the 95% confidence interval (95% CI) of overall response rate (ORR) was estimated using the Clopper–Pearson method, which works when $np > 5$ or $n(1-p) > 5$ (where n – number, p – probability).^{25,26} The OS and PFS rates with 95% CIs were calculated using the Kaplan–Meier method.^{8,9}

Results

Characteristics of r/r patients treated with ibrutinib-based therapy

To investigate the clinical benefits of the BTK inhibitor, 14 r/r CNSL patients treated with ibrutinib-based regimens were enrolled in this single-center study (12 PCNSL and 2 SCNSL patients). The basic characteristics of these patients are listed in Table 1. The median age was 58 years at diagnosis (37–80 years), with 6 patients (42.86%) aged over 60 years. In the PCNSL cohort, 66.67% were refractory patients. Both SCNSL patients experienced recurrent disease. All patients received a median of 3 lines of therapy (range: 2–4) before being prescribed ibrutinib (Fig. 1A). In the PCNSL cohort, HD-MTX was administered to all 12 patients, rituximab to 10 patients and radiotherapy to 5 patients. Both SCNSL patients received prior R-CHOP treatment. Combined with ibrutinib, 11 PCNSL and both SCNSL patients were treated with HD-MTX-based chemotherapy. One PCNSL patient (PCNSL #11) was not eligible for HD-MTX-based chemotherapy due to MTX-related myelosuppression, and was given ibrutinib combined with cytarabine. In the PCNSL cohort, the median time from the last treatment to ibrutinib initiation was 1.5 months (range: 0.5–5 months). For the 2 SCNSL patients, the interval was 2.5 months and 3.5 months, respectively.

Response to ibrutinib-based treatment

The initial dose of ibrutinib was 420 mg/day, and for 4 patients this was later increased to 560 mg/day to address progressive disease. Sulfamethoxazole was administered to prevent infections during ibrutinib treatment. Therapeutic responses were evaluated at a median follow-up time of 6.5 months (range: 2.5–21 months). Among the 12 PCNSL cases, 6 patients achieved complete remission/unconfirmed complete remission (CR/CR(u); 50%) and 3 patients achieved partial remission (PR; 25%) at their best

Table 1. Baseline characteristics of relapsed/refractory (r/r) patients before ibrutinib treatment

Characteristics		Values
Age [years]	median	58
	range	37–80
	≥60	6 (42.86%)
Gender, n (%)	male	10 (71.43)
	female	4 (28.57)
ECOG (range)		1 (1–2)
Status from previous treatment, n (%)	primary CNS lymphoma	12 (85.71)
	refractory	8 (66.67)
	recurrent	4 (33.33)
	secondary CNS lymphoma	2 (14.28)
	refractory	0
	recurrent	2 (100)
CNS involvement, n (%)	brain	14 (100)
	eye	1 (7.14)
	cerebrospinal fluid	1 (7.14)
	spinal cord	1 (7.14)
Previous regimens, n (%)	primary CNS lymphoma	12
	HD-MTX	12 (100)
	rituximab	10 (83.33)
	radiation	5 (41.67)
	WBRT	4 (80)
	stem cell transplant	3 (25)
	secondary CNS lymphoma	2
	R-CHOP	2 (100)
	stem cell transplant	1 (50)
	radiation	1 (50)
Median number of prior treatments (range)		3 (2–4)
Ibrutinib-based treatments, n (%)	primary CNS lymphoma	12
	HD-MTX	11 (91.67)
	rituximab	3 (25)
	chemotherapy	4 (33.33)
	secondary CNS lymphoma	2
	HD-MTX	2 (100)
rituximab	1 (50)	
chemotherapy	1 (50)	

ECOG – Eastern Cooperative Oncology Group; HD-MTX – high-dose methotrexate; CNS – central nervous system; WBRT – whole-brain radiotherapy.

responses (Fig. 1A), yielding an ORR of 75% (9/12; 95% CI: 42.81–94.51%). Both SCNSL patients achieved CR/CR(u) during ibrutinib-based therapy, but the possibility of caustic information brought by 2 cases only cannot be excluded. Median OS was reached neither in PCNSL nor in SCNSL, as no death occurred during ibrutinib treatment. Median PFS was 4 months (range: 1–17 months, 95% CI, 1.5 months – not reached) in PCNSL. Progression-free survival for the 2 SCNSL patients was 1.5 months and

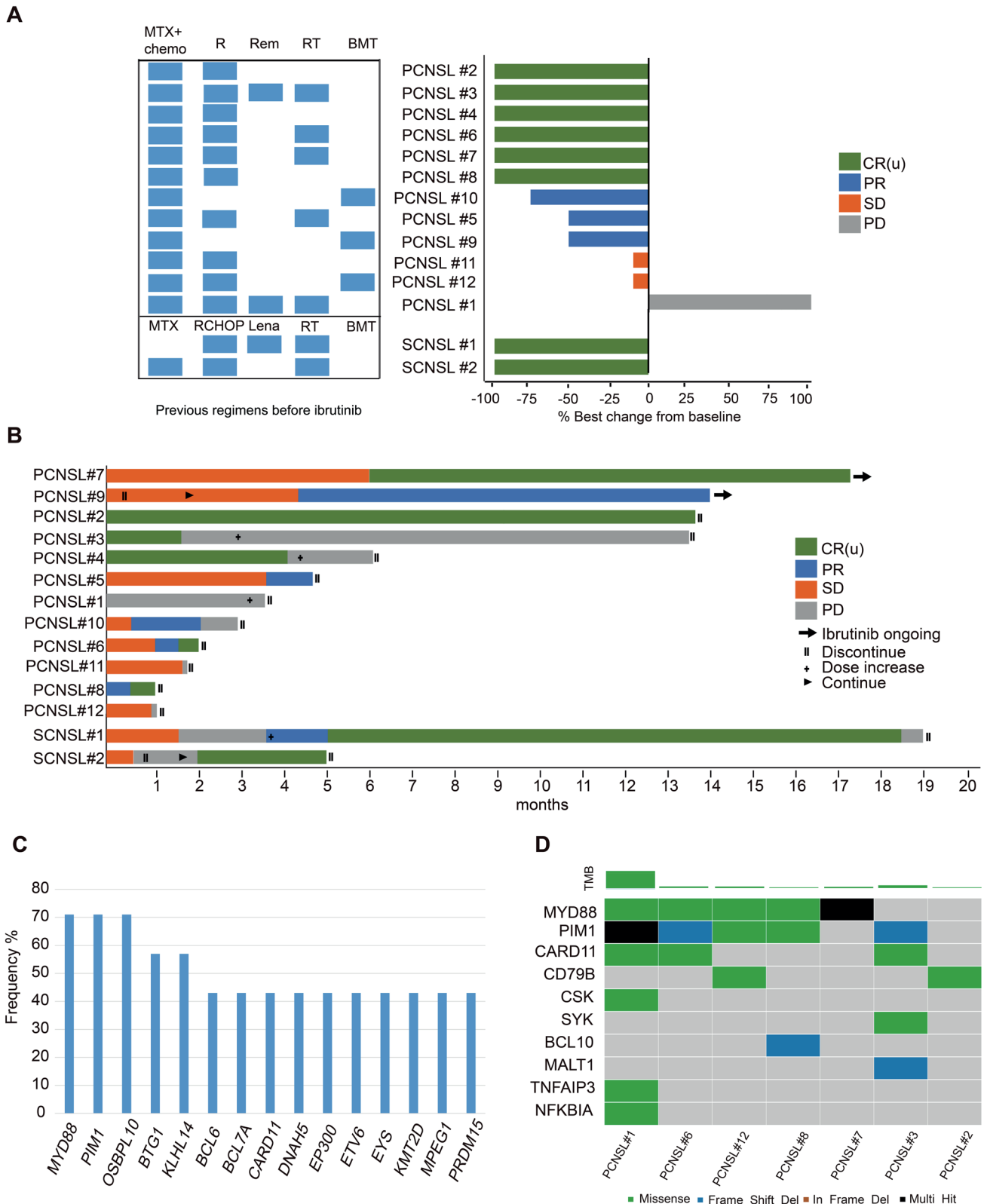


Fig. 1. Response to ibrutinib-based treatment in relapsed/refractory (r/r) primary central nervous system lymphoma (PCNSL) patients. **A.** Previous regimens before ibrutinib and best responses to ibrutinib-based treatments. Blue diamonds of each column in the light panel indicated therapies experienced (the corresponding column name). Negative bars represent tumor volume shrinkage; **B.** Response to and duration of ibrutinib-based treatment in a r/r CNSL cohort (n = 14) based on first disease evaluation. The colors of the bars represent the results of tumor assessment. The symbols represent different ibrutinib usage; **C.** Top gene mutations (over 30%) in PCNSL; **D.** Mutation profile of the B-cell antigen receptor (BCR) and nuclear factor kappa B (NF- κ B) pathways. Each row represents 1 gene and each column represents 1 sample. Types of variants are indicated by different colors of each diamond

SCNSL – secondary central nervous system lymphoma; MTX – methotrexate; chemo – chemotherapy; R – rituximab; Rem – surgical removal; RT – radiation therapy; BMT – bone marrow transplantation; Lena – lenalidomide; CR – complete remission; CR(u) – complete remission unconfirmed; PR – partial remission; SD – stable disease; PD – progressive disease; TMB – tumor mutation burden.

Table 2. Adverse events during ibrutinib treatment (CTCAE v. 5.0)

Adverse events	Number of events (%)			
	grade 1–2	grade 3	grade 4	total
Anemia	7 (50)	1 (7.14)	N/O	8 (57.14)
Platelet count decreased	6 (42.86)	3 (21.43)	N/O	8 (57.14)
Lung infection	N/O	6 (42.86)	N/O	6 (42.86)
White blood cell decreased	3 (21.43)	2 (14.29)	N/O	4 (28.57)
Hypocalcemia	4 (28.57)	N/O	N/O	4 (28.57)
Hyperglycemia	4 (28.57)	N/O	N/O	4 (28.57)
Lymphocyte count decreased	4 (28.57)	N/O	N/O	4 (28.57)
Hypokalemia	3 (21.43)	1 (7.14)	N/O	4 (28.57)
GGT increased	3 (21.43)	N/O	N/O	3 (21.43)
ALP increased	3 (21.43)	N/O	N/O	3 (21.43)
Hematoma	2 (13.33)	N/O	N/O	2 (14.29)
Neutrophil count decreased	2 (14.29)	N/O	N/O	2 (14.29)
Hypoalbuminemia	2 (14.29)	N/O	N/O	2 (14.29)
Headache	1 (7.14)	N/O	N/O	1 (7.14)
Nausea	1 (7.14)	N/O	N/O	1 (7.14)
Diarrhea	1 (7.14)	N/O	N/O	1 (7.14)
Aspartate aminotransferase increased	1 (7.14)	N/O	N/O	1 (7.14)
Abdominal pain	1 (7.14)	N/O	N/O	1 (7.14)
Infectious enterocolitis	N/O	1 (7.14)	N/O	1 (7.14)
Sinus tachycardia	1 (7.14)	N/O	N/O	1 (7.14)
Hearing impaired	1 (7.14)	N/O	N/O	1 (7.14)

CTCAE – Common Terminology Criteria for Adverse Events; GGT – gamma-glutamyl transpeptidase; ALP – alkaline phosphatase; N/O – no occurrence.

0.5 months, respectively. In the PCNSL cohort, the median time to achieve response was 1.5 months (range: 1–6.5 months). For the 2 SCNSLs, it took 4 and 5 months to respond, respectively. During the entire follow-up period, 1/3 of the PCNSL cases and 1 SCNSL case experienced progressive disease (PD) after achieving response. Ibrutinib therapy for the 2 PCNSL cases was continued until the end of follow-up. No influence of previous regimens on the effects of ibrutinib were observed after combining the clinical information before and after the BTK inhibitor for each patient (Fig. 1A). Causes that warranted ibrutinib discontinuation included infections (PCNSL #1, #4, #10), economic reasons (PCNSL #2, #6, #8) and disease progression (PCNSL #3, #10, #11, #12; SCNSL #1, #2). The evaluation of every patient's response during follow-up is presented in Fig. 1B.

Adverse events after ibrutinib-based treatments

As PCNSL is more commonly found in elderly patients, special attention was paid to AEs related to ibrutinib in clinical practice. All AEs that happened in this cohort are listed in Table 2. A total of 14 episodes of grade 3 events were observed. Anemia and low platelet count were the most common AEs (57.14%). Six patients experienced lung infection, 4 of whom were diagnosed with a fungal infection.

Three patients discontinued ibrutinib due to persistent infections. One patient withdrew from ibrutinib therapy due to pancytopenia. Other events that occurred in over 20% of patients included a decreased blood cell count (white blood cells and lymphocytes), metabolic disorders (Ca^{2+} , K^+ and glycemia) and liver insufficiency (increased gamma-glutamyl transpeptidase (GGT) and alkaline phosphatase (ALP)). Neither grade 4 AEs nor atrial fibrillation events were observed during ibrutinib treatment.

Effects of genetic alterations on ibrutinib therapy

Available whole-exome sequencing (WES) data of 7 r/r PCNSL patients at diagnosis were analyzed. Mutations of *MYD88* (71%), *PIM1* (71%), *OSBPL10* (71%), *BTG1* (57%), and *KLHL14* (57%) were most frequently found in this PCNSL cohort (Fig. 1C). Consistent with the key roles of the BCR pathway and the downstream nuclear factor kappa B (NF- κ B) pathway in the survival of DLBCL tumor cells,¹¹ mutations of the proximal BCR pathway and downstream NF- κ B pathway were also identified in these 7 PCNSL patients (Fig. 1D). The LymphGen algorithm was then applied to classify the individuals.¹² Molecular subsets of MCD (subtype with *MYD88* L265P and *CD79B* mutations; 2 cases), BN2 (subtype with *BCL6* translocations and

Table 3. Molecular features of relapsed/refractory (r/r) patients treated with ibrutinib-based therapy

Patient	PCNSL #2	PCNSL #7	PCNSL #3	PCNSL #6	PCNSL #8	PCNSL #12	PCNSL #1
Age	69	56	38	66	69	54	51
Ibrutinib duration [months]	15.5	17.5	15	2.5	3	3	5.5
Best response	CR	CR(u)	CR(u)	CR(u)	CR(u)	SD	PD
Response duration [months]	13.5	11	1.5	1	1	–	–
COO	non-GCB	non-GCB	N/O	non-GCB	non-GCB	GCB	non-GCB
TMB [/Mb]	2.39	5.56	11.19	5.90	2.53	5.64	58.39
LymphGen	unclassified	MCD	BN2	MCD/N1	BN2	MCD/EZB	MCD
<i>PIM1</i>	WT	WT	MT	MT	MT	MT	MT
<i>MYD88</i>	WT	L265P P258T	WT	L265P	L142F D148V	L265P	L265P
<i>CD79B</i>	G135A	WT	WT	WT	WT	Y197C	WT
Proximal BCR pathway	WT	WT	SYK	WT	WT	WT	CSK
NF-κB pathway	WT	WT	<i>CARD11</i> (C49Y) <i>MALT1</i>	<i>CARD11</i> (E588K)	<i>BCL10</i>	WT	<i>CARD11</i> (S879L) <i>TNFAIP3</i> <i>NFKBIA</i>

PCNSL – primary central nervous system lymphoma; CR – complete remission; CR(u) – complete remission unconfirmed; SD – stable disease; PD – progressive disease; COO – cell of origin; GCB – germinal center B-cell like; N/O – no occurrence; TMB – tumor mutation burden; MT – mutation; WT – wild type; BCR – B-cell antigen receptor; NF-κB – nuclear factor kappa B; MCD – subtype with MYD88L265P and CD79B mutations; BN2 – subtype with BCL6 translocations and NOTCH2 mutations; EZB – subtype with EZH2 mutations and BCL2 translocations; N1 – subtype with NOTCH1 mutations.

NOTCH2 mutations; 2 cases), complex phenotype (MCD/N1 (subtype with *NOTCH1* mutations), MCD/EZB (subtype with *EZH2* mutations and *BCL2* translocations)), and 1 unclassified case were obtained using this algorithm (Table 3).

In addition, the relationships between the ibrutinib response and genomic variants in these 7 r/r PCNSL patients were analyzed (Table 3). Patients who harbored mutations in *PIM1*, *MYD88* and *CD79B* responded to ibrutinib-based therapy. Patients with mutations in other genes in the proximal BCR pathway and the NF-κB pathway (such as *CARD11*, *SYK*, *MALT1*, and *BCL10*) also responded to ibrutinib. Based on the LymphGen classification, patients with MCD, BN2, composite (MCD/N1), and unclassified subtypes were all observed to respond to ibrutinib treatment.

Other than gene mutations, the impact of genomic complexity on BTK inhibition was also analyzed, especially in patients with particularly favorable (Fig. 2A,B) and poor (Fig. 2C,D) outcomes. The PCNSL #2 achieved CR(u) soon after 7 weeks of ibrutinib initiation and maintained remission for the entire follow-up (13.5 months; Fig. 2A). Although ibrutinib therapy was discontinued due to economic reasons, the remission of the disease was maintained for another 16 months. The analysis of genomic variants showed a low tumor mutation burden (TMB, 2.39/Mb; Fig. 3). Furthermore, high copy gains of epidermal growth factor receptor (*EGFR*) residing on 7p11.2 were also identified (Fig. 2B). Similarly, PCNSL #7 with a TMB of 5.56/Mb maintained CR(u) for more than 10 months, but required a longer duration to achieve this response (Fig. 3). The PCNSL #6 and #8 harbored a low TMB (5.90/Mb and 2.53/Mb, respectively), and achieved CR(u) to ibrutinib which was maintained for 1 month only. This might have

been due to the limited duration of the ibrutinib treatments (2.5 months and 3 months, respectively). For PCNSL #3, who harbored a TMB of 11.19/Mb, the CR response was only maintained for 1.5 months despite ibrutinib treatment being continued for 15 months (Fig. 3). The PCNSL #1, who received surgical resection at diagnosis, relapsed after being administered a rituximab combined with the HD-MTX regimen, and continued to experience PD despite several lines of treatments, including whole-brain radiotherapy (WBRT). Unfortunately, ibrutinib-based therapy (420 mg/day and 560 mg/day) yielded no improvements in his outcome. During the 5.5 months of ibrutinib treatment, a few new lesions emerged, while the original tumors shrank or persisted. Finally, ibrutinib was discontinued due to a fungal lung infection (Fig. 2C). Whole-exome sequencing showed that this patient harbored a high genomic complexity with an extra high TMB of 58.39/Mb (Fig. 3). In addition to multiple alternations in the BCR and NF-κB pathways, this patient also presented a unique genomic signature, exhibiting ultra-hypermutations, similar to the error-prone polymerase *POLE* cancer signatures from the COSMIC database (<https://cancer.sanger.ac.uk/cosmic/signatures>; Fig. 2D). The mutations of genes involved in DNA repair (*MSH4*, *MSH6* and *POLE*) were also identified in PCNSL #1.

Discussion

This is a retrospective single-center study examining ibrutinib-based regimens in CNSL and exploring the impact of genomic variantson the outcomes of the treatment. In previous reports, the ORR for ibrutinib-based regimens

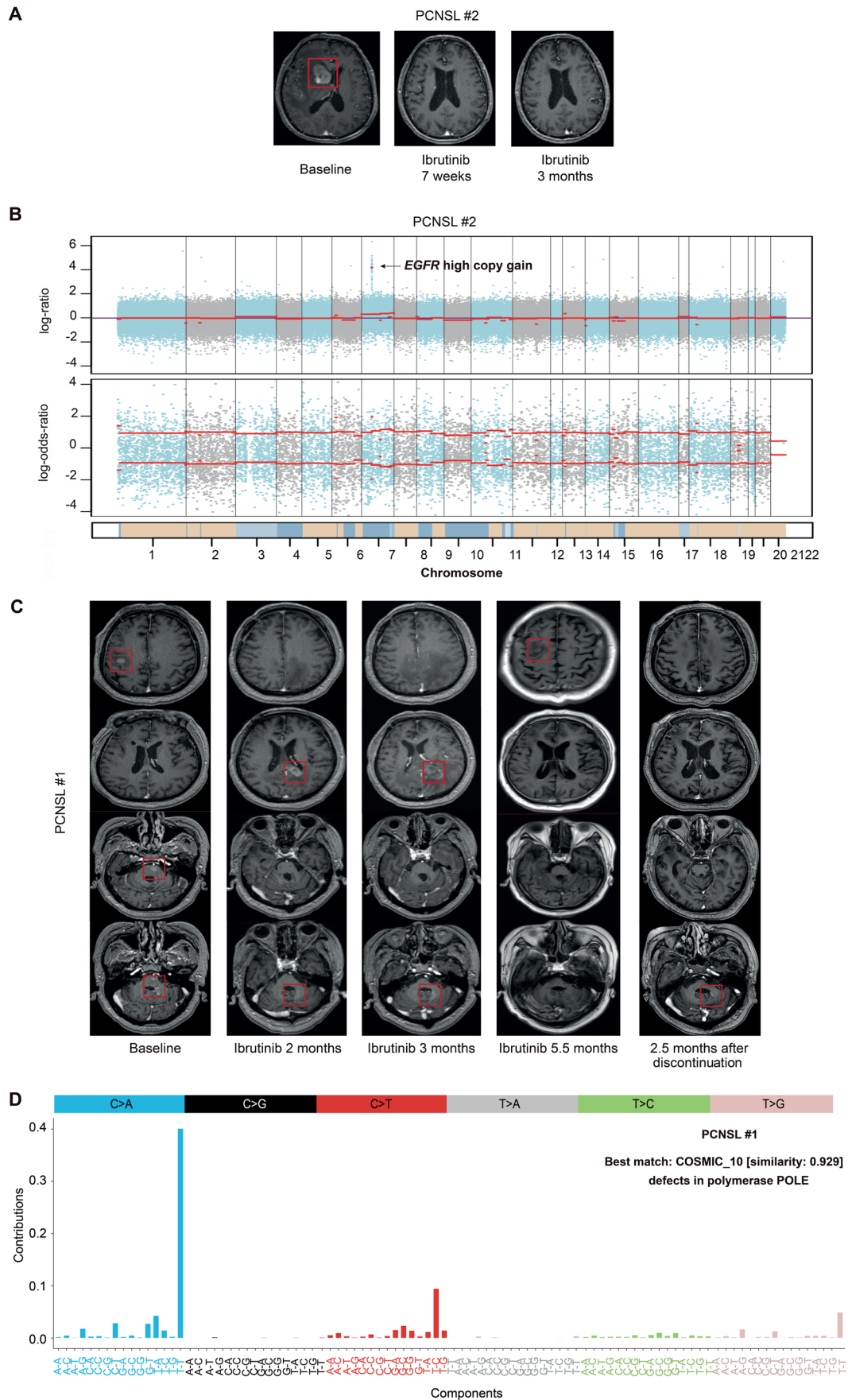


Fig. 2. Response to ibrutinib and genetic events in 2 primary central nervous system lymphoma (PCNSL) patients. **A.** Response to ibrutinib treatment was assessed using magnetic resonance imaging (MRI) in PCNSL patient #2; **B.** Log ratio of each chromosome of PCNSL #2. Chromosome numbers are labeled in chromosome cytoband at the bottom. Arrows indicate the location of epidermal growth factor receptor (EGFR). Tumor was assessed by enhanced MRI and is marked with red diamonds; **C.** Dynamic changes in the tumor lesion at different time points along with ibrutinib treatment in PCNSL #1; **D.** Mutational signature of PCNSL #1 according to 96 trinucleotide mutational patterns. The similarities with the COSMIC-defined signature are labeled. Base substitutions are labeled in different colors. Tumor was assessed using enhanced MRI and is marked with red diamonds. The MRI images obtained at different time points and at the same scanned level during ibrutinib therapy were piled together, including the centrum semiovale, periventricular, mesencephalon, and fourth ventricle from the top to bottom

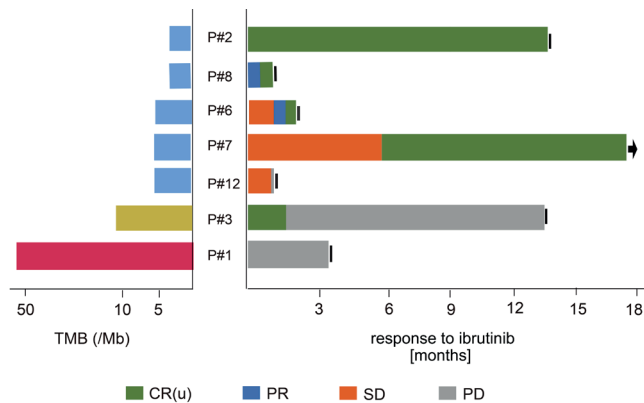


Fig. 3. Relationship between response to ibrutinib and tumor mutation burden (TMB). The height of each bar in the upper panel represents TMB (/Mb) and in the lower panel represents the response to ibrutinib (months) in 7 primary central nervous system lymphoma (PCNSL) patients with whole-exome sequencing (WES) data. Barcodes of samples are labeled at bottom. The distinct colors of the bars in the upper panel represent different levels of TMB. Different colors in the lower panel represent various disease stages. The symbols represent different ibrutinib usages: ongoing treatment (→); discontinued (I). In the left panel, TMB is illustrated by bars with different lengths and colors (red indicates TMB > 50/Mb, yellow indicates TMB > 10/Mb, blue indicates TMB < 10/Mb)

CR – complete remission; CR(u) – complete remission unconfirmed; PR – partial remission; SD – stable disease; PD – progressive disease.

in r/r PCNSL ranged from 45% to 89%, and for ibrutinib monotherapy from 50% to 59%.^{6–8,27–30} Consistent with previous reports, the current response rate for the PCNSL cohort (75%) confirmed the effectiveness of ibrutinib for r/r cases in a real-world clinical setting. However, no relationship was found between the responses to ibrutinib and previous regimens, possibly due to the limited sample size.

Although encouraging remission was achieved by ibrutinib, the PD after remission revealed in this study (45%) and in prior reports (25–71%) indicates persisting challenges.^{7–9} The newest regimens that have been explored in B-cell malignancies, such as combining a BTK inhibitor with CAR-T immunology therapy, may provide a promising potential for targeted therapy resistance patients.³¹

In line with previous reports, the safety profile of ibrutinib-based regimens was confirmed to be of low toxicity to organs.^{7,9,32} However, incidences of infection and the need to discontinue ibrutinib were observed in nearly half of the cohort, consistent with previous reports,^{6,8} indicating significant problems during the therapy process. A previous study suggests that the inhibition of BTK or interleukin 2-inducible T-cell kinase (ITK) can result in immune suppression, especially when corticosteroids are applied.^{33,34} According to the findings by Lionakis et al., in clinical cases and murine models, ibrutinib as a BTK inhibitor might also block macrophage activation in the immune system during, especially fungal, infections.⁶ Hence, studies targeting optimized regimens and infection prevention during ibrutinib therapy are needed.

Based on our limited patient sample, a preliminary relationship between genomic alternations and the response to BTK

inhibitors was indicated, which requires future validation. The effects of ibrutinib were found to be independent of mutations in *MYD88*, *PIM1*, *CD79B*, and in the BCR or NF- κ B pathways, which is in accordance with findings by Grommes et al. and Soussain et al. stating that the ibrutinib response would not be impacted by mutation.^{7,8} Wilson et al. indicated that both MCD and N1 subtypes could respond to ibrutinib-based regimens.¹³ However, in this study, we observed that 1 MCD case resisted ibrutinib due to complex genomic alterations (PCNSL #1). This case harbored highly complex genomic alterations and showed multiple recurrent intracranial tumors as well as multiresistance to therapeutic regimens, suggesting that the genomic features of ultra-hypermutations and mismatch repair deficiency may contribute to the efficacy of ibrutinib more than molecular classification.³⁵

In contrast, another unclassified patient under the LymphGen system with low TMB and high copy gains of *EGFR* responded quickly to ibrutinib, and his CR status was maintained for more than 2 years. Even though the off-target effects of ibrutinib on *EGFR* and *ITK* are recognized as disadvantages in clinical applications,^{36,37} they might have played a role in suppressing the overexpression of *EGFR* to control the tumor in this patient. Although more cases and explorations are warranted to confirm this association, all of the above findings indicate that comprehensive genetic factors need to be considered for BTK inhibitor effects.

Overall, in this retrospective single-center study, we summarized the clinical benefits, safety profile and the impact of genetic variants on ibrutinib-based regimens in r/r CNSL patients in a clinical setting.

Limitations

The empirical results reported here should be considered in the light of some limitations. As only 2 SCNSL patients were included in this study, the current results may deviate from real-world practice. More SCNSL cases need to be evaluated in future studies.^{7,27,28} The influences of genetic variants on ibrutinib therapies were examined in only 7 patients, thus the negative influences of genetic complexity need to be validated and further examined in a larger cohort. Additionally, as a retrospective study, heterogeneity in treatment regimens was unavoidable. Hence, a well-designed prospective study is needed in the future.

Conclusions

In this study, we verified the low organ toxicity of ibrutinib-based regimens, and expounded the relationship between genomic alterations and responses to a BTK inhibitor. High genomic complexity (especially TMB) may negatively impact responses toward ibrutinib, suggesting that patients harboring less genetic events may benefit more from an ibrutinib regimen.

Our results are consistent with previous studies, indicating low organ toxicity and a high effectiveness for ibrutinib in r/r cases. Our results cast a new light on the response to ibrutinib-based regimens in patients possessing a low genomic complexity.

ORCID iDs

Shu Wang  <https://orcid.org/0000-0002-8873-1603>
 YuQi Zhu  <https://orcid.org/0000-0001-5315-7210>
 Xiaohan Qian  <https://orcid.org/0000-0003-4873-5359>
 Tianling Ding  <https://orcid.org/0000-0002-2876-3435>
 Yan Yuan  <https://orcid.org/0000-0002-2981-8418>
 Yuan Li  <https://orcid.org/0000-0002-4256-0706>
 Hanfeng Wu  <https://orcid.org/0000-0001-8427-2756>
 Tong Chen  <https://orcid.org/0000-0001-7895-2077>

References

- Grommes C, DeAngelis LM. Primary CNS lymphoma. *J Clin Oncol*. 2017;35(21):2410–2418. doi:10.1200/JCO.2017.72.7602
- Ferreri AJM, Assanelli A, Crocchiolo R, Ciceri F. Central nervous system dissemination in immunocompetent patients with aggressive lymphomas: Incidence, risk factors and therapeutic options. *Hematol Oncol*. 2009;27(2):61–70. doi:10.1002/hon.881
- Carnevale J, Rubenstein JL. The challenge of primary central nervous system lymphoma. *Hematol Oncol Clin North Am*. 2016;30(6):1293–1316. doi:10.1016/j.hoc.2016.07.013
- Myers DR, Zikherman J, Roose JP. Tonic signals: Why do lymphocytes bother? *Trends Immunol*. 2017;38(11):844–857. doi:10.1016/j.it.2017.06.010
- Hendriks RW, Yuvaraj S, Kil LP. Targeting Bruton's tyrosine kinase in B cell malignancies. *Nat Rev Cancer*. 2014;14(4):219–232. doi:10.1038/nrc3702
- Lionakis MS, Dunleavy K, Roschewski M, et al. Inhibition of B cell receptor signaling by ibrutinib in primary CNS lymphoma. *Cancer Cell*. 2017;31(6):833–843.e5. doi:10.1016/j.ccell.2017.04.012
- Grommes C, Tang SS, Wolfe J, et al. Phase 1b trial of an ibrutinib-based combination therapy in recurrent/refractory CNS lymphoma. *Blood*. 2019;133(5):436–445. doi:10.1182/blood-2018-09-875732
- Soussain C, Choquet S, Blonski M, et al. Ibrutinib monotherapy for relapse or refractory primary CNS lymphoma and primary vitreoretinal lymphoma: Final analysis of the phase II 'proof-of-concept' iLOC study by the LYmphoma Study Association (LYSA) and the French Oculo-Cerebral Lymphoma (LOC) network. *Eur J Cancer*. 2019;117:121–130. doi:10.1016/j.ejca.2019.05.024
- Grommes C, Pastore A, Palaskas N, et al. Ibrutinib unmasks critical role of Bruton tyrosine kinase in primary CNS lymphoma. *Cancer Discov*. 2017;7(9):1018–1029. doi:10.1158/2159-8290.CD-17-0613
- Chapuy B, Roemer MGM, Stewart C, et al. Targetable genetic features of primary testicular and primary central nervous system lymphomas. *Blood*. 2016;127(7):869–881. doi:10.1182/blood-2015-10-673236
- Phelan JD, Young RM, Webster DE, et al. A multiprotein supercomplex controlling oncogenic signalling in lymphoma. *Nature*. 2018;560(7718):387–391. doi:10.1038/s41586-018-0290-0
- Wright GW, Huang DW, Phelan JD, et al. A probabilistic classification tool for genetic subtypes of diffuse large B cell lymphoma with therapeutic implications. *Cancer Cell*. 2020;37(4):551–568.e14. doi:10.1016/j.ccell.2020.03.015
- Wilson WH, Wright GW, Huang DW, et al. Effect of ibrutinib with R-CHOP chemotherapy in genetic subtypes of DLBCL. *Cancer Cell*. 2021;39(12):1643–1653.e3. doi:10.1016/j.ccell.2021.10.006
- Abrey LE, Batchelor TT, Ferreri AJM, et al. Report of an International Workshop to Standardize Baseline Evaluation and Response Criteria for Primary CNS Lymphoma. *J Clin Oncol*. 2005;23(22):5034–5043. doi:10.1200/JCO.2005.13.524
- Li H, Durbin R. Fast and accurate short read alignment with Burrows–Wheeler transform. *Bioinformatics*. 2009;25(14):1754–1760. doi:10.1093/bioinformatics/btp324
- McKenna A, Hanna M, Banks E, et al. The Genome Analysis Toolkit: A MapReduce framework for analyzing next-generation DNA sequencing data. *Genome Res*. 2010;20(9):1297–1303. doi:10.1101/gr.107524.110
- Wang K, Li M, Hakonarson H. ANNOVAR: Functional annotation of genetic variants from high-throughput sequencing data. *Nucleic Acids Res*. 2010;38(16):e164. doi:10.1093/nar/gkq603
- Shen R, Seshan VE. FACETS: Allele-specific copy number and clonal heterogeneity analysis tool for high-throughput DNA sequencing. *Nucleic Acids Res*. 2016;44(16):e131. doi:10.1093/nar/gkw520
- Wang S, Li H, Song M, et al. Copy number signature analysis tool and its application in prostate cancer reveals distinct mutational processes and clinical outcomes. *PLoS Genet*. 2021;17(5):e1009557. doi:10.1371/journal.pgen.1009557
- Abecasis G, Auton A, Brooks L, et al. An integrated map of genetic variation from 1,092 human genomes. *Nature*. 2012;491(7422):56–65. doi:10.1038/nature11632
- Zou J, Valiant G, Valiant P, et al. Quantifying unobserved protein-coding variants in human populations provides a roadmap for large-scale sequencing projects. *Nat Commun*. 2016;7(1):13293. doi:10.1038/ncomms13293
- Forbes SA, Beare D, Boutselakis H, et al. COSMIC: Somatic cancer genetics at high-resolution. *Nucleic Acids Res*. 2017;45(D1):D777–D783. doi:10.1093/nar/gkw1121
- Devarakonda S, Rotolo F, Tsao MS, et al. Tumor mutation burden as a biomarker in resected non-small-cell lung cancer. *J Clin Oncol*. 2018;36(30):2995–3006. doi:10.1200/JCO.2018.78.1963
- Wong SQ, Li J, Tan AYC, et al. Sequence artefacts in a prospective series of formalin-fixed tumours tested for mutations in hotspot regions by massively parallel sequencing. *BMC Med Genomics*. 2014;7(1):23. doi:10.1186/1755-8794-7-23
- Brown LD, Cai TT, DasGupta A. Interval estimation for a binomial proportion. *Statist Sci*. 2001;16(2):101–133. doi:10.1214/ss/1009213286
- Antonia SJ, Villegas A, Daniel D, et al. Overall survival with durvalumab after chemoradiotherapy in stage III NSCLC. *N Engl J Med*. 2018;379(24):2342–2350. doi:10.1056/NEJMoa1809697
- Lewis KL, Chin CK, Manos K, et al. Ibrutinib for central nervous system lymphoma: The Australasian Lymphoma Alliance/MD Anderson Cancer Center experience. *Br J Haematol*. 2021;192(6):1049–1053. doi:10.1111/bjh.16946
- Lauer EM, Waterhouse M, Braig M, et al. Ibrutinib in patients with relapsed/refractory central nervous system lymphoma: A retrospective single-centre analysis. *Br J Haematol*. 2020;190(2):e110–e114. doi:10.1111/bjh.16759
- Chamoun K, Choquet S, Boyle E, et al. Ibrutinib monotherapy in relapsed/refractory CNS lymphoma: A retrospective case series. *Neurology*. 2017;88(1):101–102. doi:10.1212/WNL.0000000000003420
- Chen F, Pang D, Guo H, et al. Clinical outcomes of newly diagnosed primary CNS lymphoma treated with ibrutinib-based combination therapy: A real-world experience of off-label ibrutinib use. *Cancer Med*. 2020;9(22):8676–8684. doi:10.1002/cam4.3499
- Fan F, Yoo HJ, Stock S, et al. Ibrutinib for improved chimeric antigen receptor T-cell production for chronic lymphocytic leukemia patients. *Int J Cancer*. 2021;148(2):419–428. doi:10.1002/ijc.33212
- Lv L, Sun X, Wu Y, Cui Q, Chen Y, Liu Y. Efficacy and safety of ibrutinib in central nervous system lymphoma: A PRISMA-compliant single-arm meta-analysis. *Front Oncol*. 2021;11:707285. doi:10.3389/fonc.2021.707285
- Ghez D, Calleja A, Protin C, et al. Early-onset invasive aspergillosis and other fungal infections in patients treated with ibrutinib. *Blood*. 2018;131(17):1955–1959. doi:10.1182/blood-2017-11-818286
- Tillman BF, Pauff JM, Satyanarayana G, Talbott M, Warner JL. Systematic review of infectious events with the Bruton tyrosine kinase inhibitor ibrutinib in the treatment of hematologic malignancies. *Eur J Haematol*. 2018;100(4):325–334. doi:10.1111/ejh.13020
- Kandoth C, Schultz N, Cherniack AD, et al. The Cancer Genome Atlas Research Network. Integrated genomic characterization of endometrial carcinoma. *Nature*. 2013;497(7447):67–73. doi:10.1038/nature12113
- Wu J, Liu C, Tsui ST, Liu D. Second-generation inhibitors of Bruton tyrosine kinase. *J Hematol Oncol*. 2016;9(1):80. doi:10.1186/s13045-016-0313-y
- Dubovsky JA, Beckwith KA, Natarajan G, et al. Ibrutinib is an irreversible molecular inhibitor of ITK driving a Th1-selective pressure in T lymphocytes. *Blood*. 2013;122(15):2539–2549. doi:10.1182/blood-2013-06-507947

Allogeneic platelet gel therapy for refractory abdominal wound healing: A preliminary study

Shujun Wang^{1,2,A–F}, Weiwei Ding^{3,A,E}, Ying Du^{1,4,B–D}, Qing Qi^{2,B}, Kaiyun Luo^{2,B}, Jianfeng Luan^{2,A}, Yanfei Shen^{4,A}, Baoan Chen^{1,A,F}

¹ Department of Hematology and Oncology, School of Medicine, Zhongda Hospital, Southeast University, Nanjing, China

² Department of Blood Transfusion, School of Medicine, Jinling Hospital, Nanjing University, China

³ Division of Trauma and Surgical Intensive Care Unit, School of Medicine, Jinling Hospital, Nanjing University, China

⁴ School of Medicine, Southeast University, Nanjing, China

A – research concept and design; B – collection and/or assembly of data; C – data analysis and interpretation;

D – writing the article; E – critical revision of the article; F – final approval of the article

Advances in Clinical and Experimental Medicine, ISSN 1899–5276 (print), ISSN 2451–2680 (online)

Adv Clin Exp Med. 2023;32(8):865–872

Address for correspondence

Baoan Chen

E-mail: cba8888@hotmail.com

Funding sources

The study was funded by the Scientific Research Project of Jiangsu Health Commission (grant No. H2019110), Hospital Project (grant No. YYMS2021019) and the Key Medicine of Jiangsu Province (grant No. ZDXKB2016020).

Conflict of interest

None declared

Received on August 5, 2022

Reviewed on December 21, 2022

Accepted on January 8, 2023

Published online on February 8, 2023

Cite as

Wang S, Ding W, Du Y, et al. Allogeneic platelet gel therapy for refractory abdominal wound healing: A preliminary study.

Adv Clin Exp Med. 2023;32(8):865–872.

doi:10.17219/acem/159088

DOI

10.17219/acem/159088

Copyright

Copyright by Author(s)

This is an article distributed under the terms of the Creative Commons Attribution 3.0 Unported (CC BY 3.0)

(<https://creativecommons.org/licenses/by/3.0/>)

Abstract

Background. Refractory abdominal wounds are commonly complicated by surgical site infections, which prolong hospital stays and increase medical costs. There is little clinical data on the use of allogeneic platelet gel (PG) therapy for refractory infected wounds.

Objectives. This study aimed to evaluate the efficacy and safety of allogeneic PGs in the treatment of refractory abdominal wounds.

Materials and methods. A prospective single-center study was performed in a national abdominal trauma referral center between June 2019 and June 2021. A total of 11 patients with refractory abdominal wounds were treated with allogeneic PGs after the failure of standard medical treatments. The PGs were derived from platelets collected from healthy donors using apheresis, and each PG was tested for platelet count, transfusion-related diseases, aerobic and anaerobic bacteria, and growth factor concentration. Clinical efficacy was evaluated by assessing the wound surface and observing the condition of the wound, including wound area and percentage of granulation.

Results. The median age of the patients was 37 years (1st quartile, 3rd quartile (Q1, Q3): 31–55 years), median (Q1, Q3) hemoglobin level was 95 g/L (78–120 g/L) and median (Q1, Q3) serum albumin level was 39.9 g/L (34.9–42.7 g/L). The PG platelet count was $976.5 \pm 174.9 \times 10^9/L$. Results of transfusion-associated contagion tests for aerobic and anaerobic bacteria were negative. Growth factor contents (pg/mL) were: for transforming growth factor beta 1 (TGF- β 1); 2542.39 ± 430.60 , for platelet-derived growth factor BB (PDGF-BB); 23230.03 ± 4236.14 and FOR vascular endothelial growth factor (VEGF); 91.41 ± 23.31 . The rate of wound healing was 100%, and the median (Q1, Q3) healing time was 30 days (18–40 days). The follow-up period was 5–27 months, during which no recurrence of the wounds was found.

Conclusions. The present study demonstrated that allogeneic PGs are a safe and effective treatment for refractory abdominal wounds.

Key words: wound healing, growth factor, surgical site infection, allogeneic platelet gel, refractory abdominal wound

Background

Surgical site infection (SSI) is a wound infection that occurs within 30 days of an operative procedure, or within 1 year if an implant is left in place and the infection is thought to be related to the operative procedure.¹ Surgical site infections increase the burden on the health-care system and prolong the hospital stay by 7–10 days.² The SSIs occur after 1–3% of all surgical procedures³ and are categorized as superficial, deep or organ/space, based on the depth of infection involvement.⁴ Abdominal surgeries are related to a high incidence of SSIs and are an independent risk factor for SSIs.⁵ Indeed, the incidence of organ/intra-abdominal SSIs ranges from 2.9% to 22.1%,^{5–9} which is much higher than for other types of surgery. Furthermore, data indicate that 77% of deaths in patients with an SSI are directly related to the SSI.¹⁰ Currently, the management strategies for refractory wounds include the treatment of primary disease, wound treatment, negative-pressure wound therapy, and wound dressing.^{11,12} However, such therapies usually take a long time and the effects seem to be unsatisfactory, with many patients still suffering from wounds after SSI therapy. Thus, there is a growing need to develop new therapeutic options that can achieve better clinical outcomes.

Platelet-rich plasma (PRP) is a platelet derivative that contains a higher concentration of platelets than baseline and is capable of promoting wound healing.¹³ A platelet gel (PG) takes on a colloidal shape and is produced after PRP is activated by adding bovine thrombin or calcium.^{14,15} The PG contents are released from α -granules¹⁶ and other granules, and they include various classes of bioactive mediators such as growth and clotting factors, chemokines, adhesion molecules, and integral membrane proteins, as well as immune mediators that are primed to respond to tissue injury.¹⁷ Once tissue injury occurs, all of the above contents are ready to respond. At present, PGs have been used in a variety of clinical conditions including dental applications,¹⁸ sports injuries¹⁹ and wound healing.¹⁵

Platelet-rich plasma is either autologous or allogeneic, the former of which makes up the majority. However, autologous PRP use may be limited for some patients (e.g., patients in this study), for whom harvesting or administering derivatives is difficult or even dangerous. This includes patients from whom large quantities of platelets cannot be collected (such as those with thrombocytopenia, severe anemia or hypoproteinemia), the elderly, neonates, and severe trauma patients. Fortunately, PRP from allogeneic sources may help overcome the above problems.

Objectives

There is currently little experience with PG therapy for refractory abdominal wounds in SSI. Also, the patient's condition often does not meet the requirements for

extracting autologous PG of sufficient quality and quantity. Therefore, this study aimed to investigate the efficacy and safety of allogeneic PGs in the treatment of refractory abdominal wounds.

Materials and methods

Study design and setting

A single-arm pilot study was performed on patients with refractory abdominal wounds from June 2019 to June 2021 at Jinling Hospital, a national abdominal trauma referral center in Nanjing, China. This study was approved by the local Institutional Review Board (Ethics Committee of Jinling Hospital, approval No. 2019(KY)-008). The study adhered to the Declaration of Helsinki.

Participants

Patient inclusion,^{20,21} exclusion and withdrawal criteria are reported in Table 1. After obtaining written informed consent, 11 patients were included. The number of participants included reflected the preliminary nature of the study.

Table 1. Inclusion, exclusion and withdrawal criteria

Criteria	Details
Inclusion criteria	refractory infectious wounds caused by SSIS, resistant to traditional treatment
	duration > 6weeks
Exclusion criteria	reached 1 or more of the following: spontaneous wound dehiscence necrotizing fasciitis necrotic tissue with/without formation of purulent secretion
	patient's age <18 years
	cachectic or terminal patient
	metastatic tumor, lesions with evidence or high risk of neoplastic degeneration
Withdrawal criteria	pregnant patient
	patient with mental illness and unable to cooperate with treatment
	patient's condition turning for the worse
	serious treatment-related adverse events

SSIS – surgical site infections.

Data sources and measurement

Preparation of allogeneic platelet-rich plasma

To prepare allogeneic PRP, platelets were obtained from healthy donors using apheresis (Jiangsu Province Blood Center, Nanjing, China). Each 250–300 mL donor unit had at least 2.5×10^{11} platelets suspended in donor plasma

containing approx. 30 mL of anticoagulant citrate dextrose solution (formula A (ACD-A)) and was qualified by testing for hepatitis B surface antigen (HBsAg), hepatitis C virus (HCV), human immunodeficiency virus (HIV), treponema pallidum (TP), and alanine transaminase (ALT). Each unit was subdivided into 10–20-milliliter portions using a 4-bag system (Fresenius Kabi, Guangzhou, China). Next, all aliquots of PRP were frozen at -80°C ^{22,23} until further use.

Platelet-rich plasma characterization

After PRP preparation, 0.5 mL of them was collected within 30 min and a platelet count was taken for each unit of PRP before cryopreservation, using the XE2100™ automatic hematology analyzer (Sysmex Corporation, Hyogo, Japan). Each unit of PRP was tested for the presence of aerobic and anaerobic bacteria using Plus Aerobic/F and Lytic/10 Anaerobic/F (9184994 and 0301023; BD Biosciences, Franklin Lakes, USA), respectively. Calcium gluconate (10%) was added to each PRP sample at a ratio of 1:4 in a 37°C water bath. The PG formed within a few minutes. To isolate platelet growth factors (GFs), PG was ultracentrifuged at $10,000 \times g$ for 15 min to eliminate fibrous protein and platelet debris,²⁴ and the GF concentration in the supernatant was measured. The following 3 GFs were evaluated: transforming growth factor beta 1 (TGF- β 1), platelet-derived growth factor BB (PDGF-BB) and vascular endothelial growth factor (VEGF).¹⁵ To change the latent form into an immune-reactive form, the content of TGF- β 1 was tested after acidic activation and neutralization of the sample. The GF concentrations were measured using Human VEGF enzyme-linked immunosorbent assay (ELISA) Kit (A18310135; Multi Sciences, Hangzhou, China), Human/Mouse/Rat TGF- β 1 ELISA Kit (A98110121; Multi Sciences), and Human/Rat PDGF-BB ELISA Kit (A913700823; Multi Sciences), and were tested using Hamilton Microlab FAME (M8; Hamilton Corporation, Bonaduz, Switzerland). All of the above tests were performed before PG treatment.

Treatment procedure

To minimize the residual infection risk, a single unit of platelets was used to treat just 1 patient. A frozen PRP aliquot was thawed at 37°C for 15 min before use. The refractory wounds were first debrided to remove the necrotic and infected tissues. Then, the wound area was thoroughly cleaned with iodine solution and 3% perhydrol liquid. After that, the wound was rewashed with normal saline and dried with sterile gauze. Wound volume was calculated as lesion area \times depth. Based on the wound size, the appropriate volume of PRP was added to 10% calcium gluconate (PRP:calcium gluconate ratio of 4:1) with sufficient mixing, and the mixture was sprayed onto the wound. A PG was formed on the wound within 1–3 min, exploiting the contact with body heat,²⁵ and a vaseline gauze was

used to cover the wound followed by a dry sterile gauze. The dressing was changed every day and wound healing was observed.

During the PRP therapy, the patient's wounds were not treated with therapeutic agents containing basic fibroblast GFs or with negative pressure wound therapy.

At least 3 months after the last treatment, patient blood samples were tested for transfusion-related diseases. In addition, wounds were photographed before each treatment and during the follow-up visit using a digital camera, and examined for abnormalities such as bleeding, exudation, infection, and poor wound healing. These observational indexes were used to evaluate the safety of allogeneic PG therapy.

Several parameters were selected to evaluate the efficacy of PG therapy, including the presence of infection, granulation growth in wounds, wound healing rate, and healing time. If the patient had a skin graft after PRP therapy, graft survival and graft edema were assessed after the transplantation. The following formula was used to calculate the wound healing rate:

$$\text{wound healing rate (\%)} = \left(\frac{\text{the original wound size} - \text{wound size}}{\text{the original wound size}} \right) \times 100.$$

Statistical analyses

The IBM SPSS v. 25.0 software (IBM Corp., Armonk, USA) was used for statistical analysis. Data of patients are expressed as median (Q1–Q3), and PRP data ($p > 0.09$ in the Kolmogorov–Smirnov normality test of the variables) are expressed as mean \pm standard deviation ($M \pm SD$). The statistical analysis of differences was not conducted because of the small number of patients enrolled.

Results

Patients

Eleven patients, having 1 or more wounds caused by SSI that had not healed after extensive conventional wound management, were included and treated with topical administration of an allogeneic PG. Their mean age was 37 years (range: 31–55 years), with mean hemoglobin of 95 g/L (78–120 g/L) and serum albumin of 39.9 g/L (34.9–42.7 g/L). The characteristics of patients are presented in Table 2.

Platelet-rich plasma characterization

The $M \pm SD$ platelet count of the PRP was $976.5 \pm 174.9 \times 10^9/\text{L}$, and $M \pm SD$ ALT was 19.00 ± 5.60 U, while the results of aerobic and anaerobic bacteria tests were negative. At the same time, testing for HBsAg, HCV, HIV, and TP also yielded negative results. The GF concentrations of PRP samples are shown in Table 3.

Table 2. Characteristics of the study population (n = 11)

Parameter	Number of patients (n)	Percentage
Age [years]		
18–30	2	18.18
31–40	4	36.36
41–50	2	18.18
51–60	2	18.18
61–70	1	9.09
Gender		
Male	8	72.73
Female	3	27.27
Nutritional condition		
Serum albumin >30 g/L	9	81.82
Serum albumin ≤30 g/L	2	18.18
Anemia		
No	3	27.27
Yes	8	72.73
Wound infection		
No	4	36.36
Yes	7	63.64

Clinical efficacy and healing rate analysis

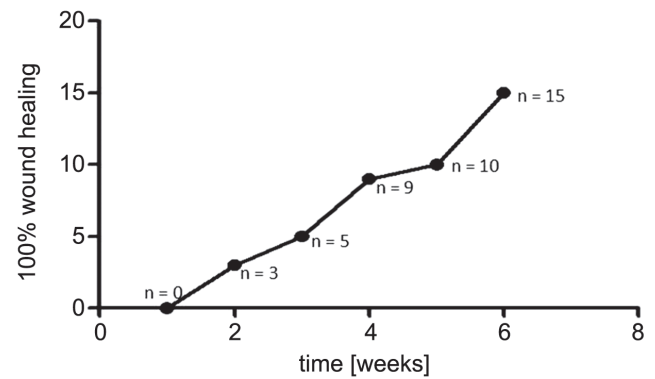
During the study period, no patients were found to have treatment-related adverse reactions or immune responses. Before the first treatment and after the last (the exact time was 4 (3–8) months after the last treatment), patients' blood samples tested negative for HBsAg, HCV, HIV, and TP. Each patient's data and wound characteristics are reported in Table 4. The mean number of PG treatments was 8 (5–11), and the mean healing time was 30 (18–40) days (Fig. 1); the healing was observed as early as 10 days after PG application. One week after the PG treatment, small islands of granulation tissue appeared over the wound, and tissue granulation increased from 90% (33.84–95.00%) to 100% (98–100%). At the same time, the wound size was reduced by 67.82% (54.20–74.51%). Only 1 patient (patient number 2) underwent skin grafting after the last PG treatment. The follow-up period was 5–27 months, during which no recurrence of the wound was found.

Overall, the wound size was reduced and the wound healing rate was 100% in all of the treated patients. To depict the reduction in wound size with time after PG administration, Fig. 2–4 show pre-treatment and follow-up pictures of 3 patients (patients 1, 2 and 8).

Table 3. Platelet growth factor concentrations of PRP samples (M ±SD; n = 11)

Measure unit	TGF-β1	VEGF	PDGF-BB
pg/mL	2452.39 ±430.60	91.41 ±23.31	23230.03 ±4236.14
pg/10 ⁹ platelets	2537.58 ±393.26	94.87 ±22.97	24495.91 ±6186.57

PRP – platelet-rich plasma; M ±SD – mean ± standard deviation; TGF-β1 – transforming growth factor-β1; VEGF – vascular endothelial growth factor; PDGF-BB – platelet-derived growth factor BB.

**Fig. 1.** Distribution of cumulative wound healing following platelet gel treatment

Discussion

The current study is the first to characterize the safety and efficacy of allogeneic PGs in the treatment of refractory abdominal wounds after SSI. All patients achieved a 100% healing rate in a short time, and no treatment-related adverse reactions or immune responses occurred during the treatment. This indicates that allogeneic PRP has low immunogenicity.

Refractory wounds are one of the outcomes of SSIs and are challenging to treat. Conventional treatment for refractory wounds includes control of infection, adequate debridement, avoidance of excessive pressure, revascularization of ischemic tissue, changing the wound environment, and medical management of comorbidities.^{26,27} However, these treatments are ineffective. Wound healing involves the phasic production of GFs and cytokines to progress the wound to a scar.²⁷ In vitro and in vivo studies analyzing refractory wounds have demonstrated the deregulation of several GFs and indicated them as potential targets for therapy.²⁸ Exogenous GFs and cytokines are used in a clinical setting to promote refractory wound healing. They have become a promising approach for the treatment of intractable wounds.

Platelet gels are colloidal in shape, and form after PRP is activated by calcium. This delays the loss of platelets and makes platelets secrete GFs on the wound surface over a long period at a high concentration. With the deepening of PG research, PGs have been used as a new application to promote favorable wound healing.

The benefit of allogeneic PRP is that it can be collected from voluntary blood donors, and be ready to use at any time without having to collect any samples from the patient.^{17,29} Moreover, it has been demonstrated that the potential

Table 4. Individual patient data, number of PG treatments, follow-up time, and wound conditions at enrollment and after 1 week of treatment

Patient (wound) No.	Age, gender	Number of PG treatments	Timepoint	Wound size [cm]	Tissue type	Percentage of granulation (%)	Healing rate (%)	Healing time [days]	Follow-up time [months]
1 (1)		6	before treatment after 1 week of treatment	8.1x6.1x0.2 5.7x2.7	granulation + slough + necrotic tissue granulation tissue	33.84 90.65	– 72.13	30	27
1 (2)	47, M	5	before treatment after 1 week of treatment	3.8x3.7 2.8x2.3	granulation + necrotic tissue granulation tissue	16 100	– 54.20	21	27
1 (3)		5	before treatment after 1 week of treatment	4.7x3.6 2.8x2	granulation + necrotic tissue granulation tissue	20 100	– 66.90	18	27
2	31, M	18	before treatment after 1 week of treatment after 4 weeks of treatment	18x8x1.8 11.7x5.6x1.27 skin grafting	granulation + slough + necrotic tissue granulation + slough + necrotic tissue granulation tissue + skin graft	17.25 68.26 –	– 67.82 –	42	26
3	56, M	4	before treatment after 1 week of treatment	6x7x0.4 3.6x3x0.2	granulation + necrotic tissue granulation tissue	45 100	– 87.14	28	24
4	37, M	10	before treatment after 1 week of treatment	5.5x5 5.5x3	granulation + necrotic tissue granulation tissue	95 98	– 40	42	23
5	43, M	8	before treatment after 1 week of treatment	8.8x3.2x3.3 5.9x2.4x2.4	granulation + necrotic tissue granulation + necrotic tissue	90 98	– 63.43	40	15
6 (1)		10	before treatment after 1 week of treatment	2x1x0.3 1.4x0.4x0.2	granulation + necrotic tissue granulation tissue	75 100	– 81.33	10	13
6 (2)	32, F	11	before treatment after 1 week of treatment	1.8x0.5x0.3 1.5x0.5x0.2	granulation + necrotic tissue granulation tissue	90 100	– 44.44	14	13
6 (3)		16	before treatment after 1 week of treatment	1.7x0.8x0.3 1.3x0.4x0.2	granulation + necrotic tissue granulation tissue	90 100	– 74.51	28	13
7	67, M	15	before treatment after 1 week of treatment	4.5x2x1.4 6.5x2x0.8	granulation tissue + slough granulation tissue	95 100	– 17.46	40	11
8	27, M	10	before treatment after 1 week of treatment	10x7x4.6 7x5x2.6	granulation + necrotic tissue granulation + necrotic tissue	78.26 87	– 71.74	30	10
9	19, F	7	before treatment after 1 week of treatment	3x1.5x1.2 2.3x1x0.8	granulation + necrotic tissue granulation tissue	90 100	– 65.93	38	9
10	55, F	5	before treatment after 1 week of treatment	1.7x0.5x1.3 0.8x0.5x0.8	granulation tissue granulation tissue	100 100	– 71.45	35	8
11	33, M	6	before treatment after 1 week of treatment	13.5x1.8x1.2 10x1.3x0.3	granulation tissue granulation tissue	100 100	– 86.63	14	5

PG – platelet gel.

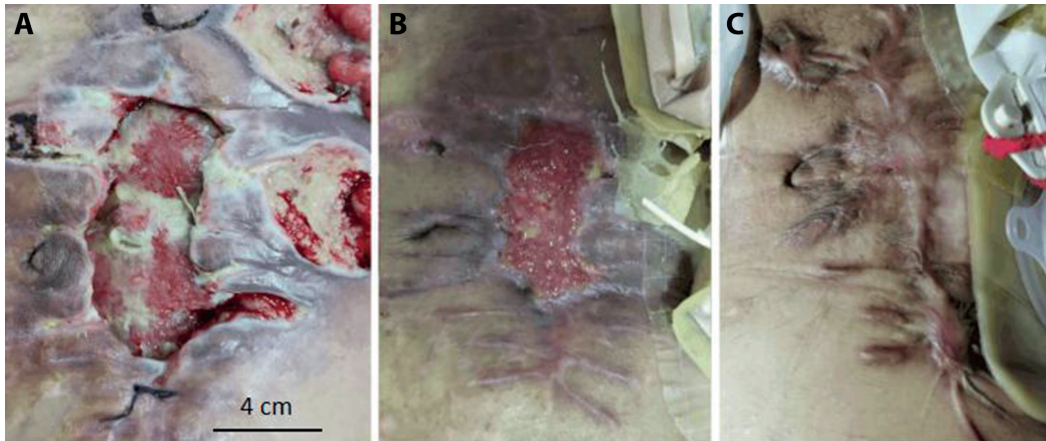


Fig. 2. Wound of patient No. 1. A. The wound size before treatment was 8.1x6.1x0.2 cm; B. After 1 week of treatment with platelet gel (PG), and also after the last treatment, the wound size was 5.7x2.7 cm; C. After 53 weeks of PG treatment, the wound exhibited no ulceration or exudation

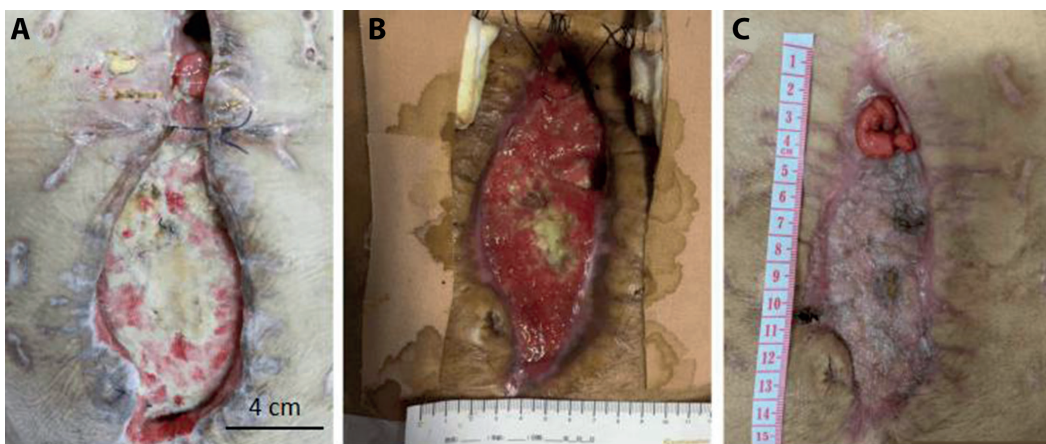


Fig. 3. Wound of patient No. 2. A. The wound size before treatment was 18x8x1.8 cm; B. After 4 weeks of treatment with platelet gel (PG), and also after the last treatment, the wound size was 10.5x4.3x0.5 cm, after which the patient underwent skin grafting; C. After 7 weeks of PG treatment, the wound exhibited no ulceration or exudation

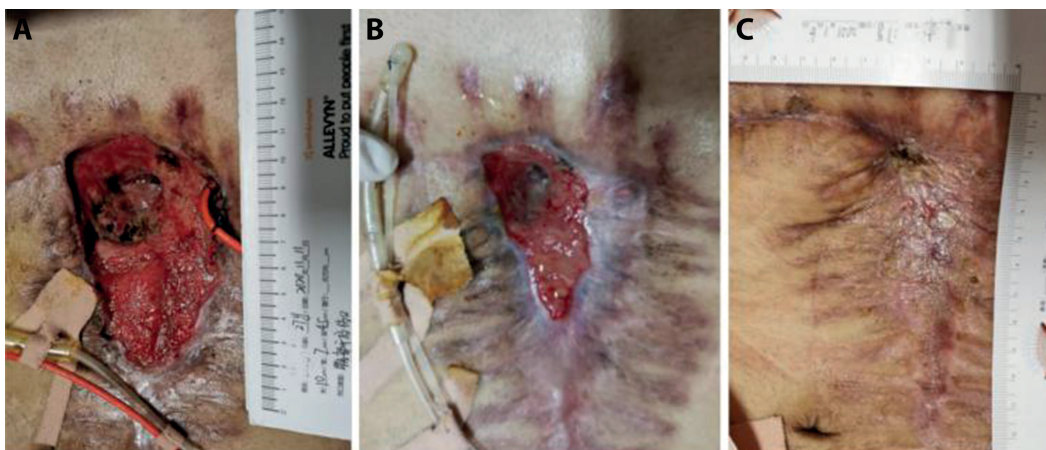


Fig. 4. Wound of patient No. 8. A. The wound size before treatment was 10x7x4.6 cm. B. After 2 weeks of platelet gel (PG) treatment, and also after the last treatment, the wound size was 7.0x3.5x2.2 cm. C. After 8 weeks of treatment with PG, the wound exhibited no ulceration or exudation

immunogenicity of allogeneic PRP is not a significant risk.³⁰ There is a non-systematic review that discusses allogeneic PRP for wound treatment,¹⁷ including 3 case series and 5 randomized controlled trials. The refractory wound types included pressure sores,³¹ venous ulcers,³² diabetic lower limb ulcers,^{33,34} lower extremity ulcers,³⁵ and ulcers of various etiologies.^{36–38} All of these studies, with or without a control group, showed improvement in hard-to-heal wounds when treated with allogeneic PRP. There is scant literature on PRP as a treatment for refractory abdominal wounds after SSI, although in 1 case report, cord blood PG

(CBPG) was used to enhance the healing of deep surgical site dehiscence.³⁹ The CBPG was applied twice a week for 4 weeks and then once a week for 4 weeks, which resulted in the cavities being completely filled.

In this study, 8 out of the 11 patients were anemic, 2 had hypoproteinemia, 7 had a wound infection, and 5 had suffered from surgical wound dehiscence resulting from wound infection. Repeated blood sampling (approx. 50 mL of whole blood is required for each 5 mL of PRP preparation) may have caused harm to these patients. The primary goal of any treatment is to achieve wound

closure expeditiously. Herein, blood bank platelet concentrate was used as a source of allogeneic PRP. The advantages are as follows: 1) the characteristics of platelet concentrates from the blood bank are well specified, and residual white and red blood cell content is highly standardized³⁸; 2) the entire process of platelet collection is performed using a closed system and aseptic; 3) they are obtained without the need for a platelet separation system, and the concentrations of GFs are within the range of clinical efficacy⁴⁰; and 4) they are suitable for the repeated treatment of large-sized wounds.

To avoid blood-borne diseases and after tests for transfusion-related diseases, the platelet concentrate from 1 donor was divided into several portions and used for 1 patient. Tests for transfusion-related diseases showed negative results for all patients after the last treatment of PRP.

To explore the mechanisms of wound healing promoted by PGs, 3 representative GFs were selected for detection, and the results were comparable to those reported in the literature.^{41–45} However, the contents of GFs differed between various voluntary blood donors and blood biomaterials. As such, the relative amount of each factor may vary depending on donor characteristics, platelet count enrichment, production methods, and thrombin preparation.⁴⁶

In recent years, PRP has emerged as a potential option for the prevention and treatment of acute and chronic postoperative wound infections.⁴⁷ In 7 patients with local infection, the results of bacterial culture were *Staphylococcus epidermidis* and/or *Staphylococcus aureus*. In the patients for whom conventional treatment was ineffective, necrotizing fasciitis may have been aggravated by the nonhealing wound. Therefore, to enhance wound healing, PG therapy was offered and the frequency varied from twice a week³⁹ to once a day. This provided adequate PRP and allowed for wounds to be cleaned every day, as well as gave the opportunity for the close inspection of the wounds.

Although our results showed that allogeneic PG exhibited positive effects in refractory abdominal wounds, the following aspects of this product still need to be considered: 1) to avoid the spread of blood-borne diseases, the allogeneic PGs from donor blood must undergo the same tests as platelets used for intravenous infusion; 2) the process of PG extraction must follow the standard operating procedures of the institution; 3) the PG process must adhere to the principles of sterility; 4) if the wound is accompanied by a suppurative infection, anti-infection therapy should be applied initially; and 5) PGs may be combined with vacuum suction and wound skin grafting.


Limitations

In this study, it was difficult to recruit a large enough number of patients with comparable lesions that would have allowed for a classic case-control study. Therefore, this single-arm study was designed.

Conclusions

In this study, the treatment of refractory abdominal wounds with allogeneic PGs achieved significant results in a short time. Allogeneic PGs are a feasible, effective and safe therapy for refractory abdominal wounds. More randomized controlled clinical trials should be conducted to bring more evidence of the value of allogeneic PGs in treating refractory abdominal wounds.

ORCID iDs

Shujun Wang  <https://orcid.org/0000-0001-9718-101X>
 Weiwei Ding  <https://orcid.org/0000-0002-5026-689X>
 Ying Du  <https://orcid.org/0000-0003-0467-4494>
 Qing Qi  <https://orcid.org/0000-0002-4984-0874>
 Kaiyun Luo  <https://orcid.org/0000-0002-0908-6766>
 Jianfeng Luan  <https://orcid.org/0000-0002-6759-3678>
 Yanfei Shen  <https://orcid.org/0000-0003-0369-5920>
 Baoan Chen  <https://orcid.org/0000-0003-3978-7886>

References

- Horan TC, Andrus M, Dudeck MA. CDC/NHSN surveillance definition of health care-associated infection and criteria for specific types of infections in the acute care setting. *Am J Infect Control*. 2008;36(5):309–332. doi:10.1016/j.ajic.2008.03.002
- Waltz PK, Zuckerbraun BS. Surgical site infections and associated operative characteristics. *Surg Infect*. 2017;18(4):447–450. doi:10.1089/sur.2017.062
- Durbin S, DeAngelis R, Peschman J, Milia D, Carver T, Dodgion C. Superficial surgical infections in operative abdominal trauma patients: A Trauma Quality Improvement Database analysis. *J Surg Res*. 2019;243:496–502. doi:10.1016/j.jss.2019.06.101
- Alkaaki A, Al-Radi OO, Khoja A, et al. Surgical site infection following abdominal surgery: A prospective cohort study. *Can J Surg*. 2019;62(2):111–117. doi:10.1503/cjs.004818
- Aga E, Keinan-Boker L, Eithan A, Mais T, Rabinovich A, Nassar F. Surgical site infections after abdominal surgery: Incidence and risk factors. A prospective cohort study. *Infect Dis*. 2015;47(11):761–767. doi:10.3109/23744235.2015.1055587
- Morales CH. Intra-abdominal infection in patients with abdominal trauma. *Arch Surg*. 2004;139(12):1278. doi:10.1001/archsurg.139.12.1278
- Zhang XF, Chen J, Wang PG, et al. Surgical site infection after abdominal surgery in China: A multicenter cross-sectional study [in Chinese]. *Zhonghua Wei Chang Wai Ke Za Zhi*. 2020;23(11):1036–1042. doi:10.3760/cma.j.cn.441530-20200810-00470
- Morales C. Surgical site infection in abdominal trauma patients: Risk prediction and performance of the NNIS and SENIC indexes. *Can J Surg*. 2011;54(1):17–24. doi:10.1503/cjs.022109
- Tabiri S, Yenli E, Kyere M, Anyomih TTK. Surgical site infections in emergency abdominal surgery at Tamale Teaching Hospital, Ghana. *World J Surg*. 2018;42(4):916–922. doi:10.1007/s00268-017-4241-y
- Anderson DJ, Podgorny K, Berríos-Torres SI, et al. Strategies to prevent surgical site infections in acute care hospitals: 2014 update. *Infect Control Hosp Epidemiol*. 2014;35(6):605–627. doi:10.1086/676022
- Liu P, Liu Y, Ke CN, Li WS, Liu YM, Xu S. Therapeutic effect of autologous concentrated growth factor on lower-extremity chronic refractory wounds: A case report. *World J Clin Cases*. 2021;9(18):4797–4802. doi:10.12998/wjcc.v9.i18.4797
- Lu Q, Yin Z, Shen X, et al. Clinical effects of high-intensity laser therapy on patients with chronic refractory wounds: A randomised controlled trial. *BMJ Open*. 2021;11(7):e045866. doi:10.1136/bmjopen-2020-045866
- Alves R, Grimalt R. A review of platelet-rich plasma: History, biology, mechanism of action, and classification. *Skin Appendage Disord*. 2018;4(1):18–24. doi:10.1159/000477353
- Piccin A, Di Pierro AM, Canzian L, et al. Platelet gel: A new therapeutic tool with great potential. *Blood Transfus*. 2016;15(4):333–340. doi:10.2450/2016.0038-16

15. Wang S, Yang J, Zhao G, et al. Current applications of platelet gels in wound healing: A review. *Wound Rep Reg*. 2021;29(3):370–379. doi:10.1111/wrr.12896
16. Blair P, Flaumenhaft R. Platelet α -granules: Basic biology and clinical correlates. *Blood Rev*. 2009;23(4):177–189. doi:10.1016/j.blre.2009.04.001
17. Akbarzadeh S, McKenzie MB, Rahman MM, Cleland H. Allogeneic platelet-rich plasma: Is it safe and effective for wound repair? *Eur Surg Res*. 2021;62(1):1–9. doi:10.1159/000514223
18. Anitua E, Fernández-de-Retana S, Alkhraisat MH. Platelet rich plasma in oral and maxillofacial surgery from the perspective of composition. *Platelets*. 2021;32(2):174–182. doi:10.1080/09537104.2020.1856361
19. Bava ED, Barber FA. Platelet-rich plasma products in sports medicine. *Phys Sportsmed*. 2011;39(3):94–99. doi:10.3810/psm.2011.09.1925
20. Gupta P, Singh HS, Shukla VK, Nath G, Bhartiya SK. Bacteriophage therapy of chronic nonhealing wound: Clinical study. *Int J Low Extrem Wounds*. 2019;18(2):171–175. doi:10.1177/1534734619835115
21. Chen X, Liu L, Nie W, et al. Vacuum sealing drainage therapy for refractory infectious wound on 16 renal transplant recipients. *Transplant Proc*. 2018;50(8):2479–2484. doi:10.1016/j.transproceed.2018.04.014
22. Huber SC, de Moraes Martinelli B, Quintero M, et al. A case series of platelet rich plasma in chronic venous ulcers. *Regen Ther*. 2021;18:51–58. doi:10.1016/j.reth.2021.03.005
23. Massara M, Pucci G, Stilo G, et al. The role of cord blood platelet gel in the management of a diabetic foot with tendon exposure. *Regen Med*. 2021;16(12):1051–1056. doi:10.2217/rme-2021-0044
24. Weibrich G, Kleis WKG, Hitzler WE, Hafner G. Comparison of the platelet concentrate collection system with the plasma-rich-in-growth-factors kit to produce platelet-rich plasma: A technical report. *Int J Oral Maxillofac Implants*. 2005;20(1):118–123. PMID:15747683.
25. Napolitano M, Matera S. Autologous platelet gel for tissue regeneration in degenerative disorders of the knee. *Blood Transfus*. 2012;10(1):72–77. doi:10.2450/2011.0026-11
26. Suthar M, Gupta S, Bukhari S, Ponemone V. Treatment of chronic non-healing ulcers using autologous platelet rich plasma: A case series. *J Biomed Sci*. 2017;24(1):16. doi:10.1186/s12929-017-0324-1
27. Berry-Kilgour C, Cabral J, Wise L. Advancements in the delivery of growth factors and cytokines for the treatment of cutaneous wound indications. *Adv Wound Care*. 2021;10(11):596–622. doi:10.1089/wound.2020.1183
28. Yamakawa S, Hayashida K. Advances in surgical applications of growth factors for wound healing. *Burns Trauma*. 2019;7:10. doi:10.1186/s41038-019-0148-1
29. He M, Chen T, Lv Y, et al. The role of allogeneic platelet-rich plasma in patients with diabetic foot ulcer: Current perspectives and future challenges. *Front Bioeng Biotechnol*. 2022;10:993436. doi:10.3389/fbioe.2022.993436.
30. Zhang ZY, Huang AW, Fan JJ, et al. The potential use of allogeneic platelet-rich plasma for large bone defect treatment: Immunogenicity and defect healing efficacy. *Cell Transplant*. 2013;22(1):175–187. doi:10.3727/096368912X653183
31. Scevola S, Nicoletti G, Brenta F, Isernia P, Maestri M, Faga A. Allogeneic platelet gel in the treatment of pressure sores: A pilot study. *Int Wound J*. 2010;7(3):184–190. doi:10.1111/j.1742-481X.2010.00671.x
32. de Oliveira MG, Abbade LPF, Miot HA, Ferreira RR, Deffune E. Pilot study of homologous platelet gel in venous ulcers. *An Bras Dermatol*. 2017;92(4):499–504. doi:10.1590/abd1806-4841.20175496
33. Jeong SH, Han SK, Kim WK. Treatment of diabetic foot ulcers using a blood bank platelet concentrate. *Plast Reconstr Surg*. 2010;125(3):944–952. doi:10.1097/PRS.0b013e3181cb6589
34. Shan GQ, Zhang YN, Ma J, et al. Evaluation of the effects of homologous platelet gel on healing lower extremity wounds in patients with diabetes. *Int J Low Extrem Wounds*. 2013;12(1):22–29. doi:10.1177/1534734613477113
35. Chen TM, Tsai JC, Burnouf T. A novel technique combining platelet gel, skin graft, and fibrin glue for healing recalcitrant lower extremity ulcers. *Dermatol Surg*. 2010;36(4):453–460. doi:10.1111/j.1524-4725.2010.01480.x
36. Greppi N, Mazzucco L, Galetti G, et al. Treatment of recalcitrant ulcers with allogeneic platelet gel from pooled platelets in aged hypomobile patients. *Biologicals*. 2011;39(2):73–80. doi:10.1016/j.biologicals.2011.01.002
37. Liao X, Liang JX, Li SH, et al. Allogeneic platelet-rich plasma therapy as an effective and safe adjuvant method for chronic wounds. *J Surg Res*. 2020;246:284–291. doi:10.1016/j.jss.2019.09.019
38. Semenič D. Regeneration of chronic wounds with allogeneic platelet gel versus hydrogel treatment: A prospective study. *Acta Clin Croat*. 2018;57(3):434–442. doi:10.20471/acc.2018.57.03.05
39. Volpe P, Pucci G, Stilo G, et al. Use of cord blood platelet gel to enhance healing of deep surgical site dehiscences after peripheral bypass. *Regen Med*. 2020;15(8):1951–1956. doi:10.2217/rme-2020-0034
40. Crovetti G, Martinelli G, Issi M, et al. Platelet gel for healing cutaneous chronic wounds. *Transfus Apher Sci*. 2004;30(2):145–151. doi:10.1016/j.transci.2004.01.004
41. Dohan Ehrenfest DM, Bielecki T, Jimbo R, et al. Do the fibrin architecture and leukocyte content influence the growth factor release of platelet concentrates? An evidence-based answer comparing a pure platelet-rich plasma (P-PRP) gel and a leukocyte- and platelet-rich fibrin (L-PRF). *Curr Pharm Biotechnol*. 2012;13(7):1145–1152. doi:10.2174/138920112800624382
42. Castillo TN, Pouliot MA, Kim HJ, Dragoo JL. Comparison of growth factor and platelet concentration from commercial platelet-rich plasma separation systems. *Am J Sports Med*. 2011;39(2):266–271. doi:10.1177/0363546510387517
43. Eppley BL, Woodell JE, Higgins J. Platelet quantification and growth factor analysis from platelet-rich plasma: Implications for wound healing. *Plast Reconstr Surg*. 2004;114(6):1502–1508. doi:10.1097/01.PRS.0000138251.07040.51
44. Everts PA, Brown Mahoney C, Hoffmann JJ, et al. Platelet-rich plasma preparation using three devices: Implications for platelet activation and platelet growth factor release. *Growth Factors*. 2006;24(3):165–171. doi:10.1080/08977190600821327
45. Jeong SH, Han SK, Kim WK. Treatment of diabetic foot ulcers using a blood bank platelet concentrate. *Plast Reconstr Surg*. 2010;125(3):944–952. doi:10.1097/PRS.0b013e3181cb6589
46. Burnouf T, Goubran HA, Chen TM, Ou KL, El-Ekiaby M, Radosevic M. Blood-derived biomaterials and platelet growth factors in regenerative medicine. *Blood Rev*. 2013;27(2):77–89. doi:10.1016/j.blre.2013.02.001
47. Sethi D, Martin KE, Shrotriya S, Brown BL. Systematic literature review evaluating evidence and mechanisms of action for platelet-rich plasma as an antibacterial agent. *J Cardiothorac Surg*. 2021;16(1):277. doi:10.1186/s13019-021-01652-2

Serum levels of SOCS6 are decreased in diabetic retinopathy and are related to severity of the disease

Lan Li^{1,A–D}, Xiaoyan Wu^{2,E}, Lemin He^{3,E}, Rong Luo^{1,E}, LiQiong Lou^{4,F}

¹ Department of Ophthalmology, Jiangxi Provincial People's Hospital, The First Affiliated Hospital of Nanchang Medical College, China

² Department of Ophthalmology, Yihuang County People's Hospital, Fuzhou, China

³ Department of Ophthalmology, Poyang County Traditional Chinese Medicine Hospital, Shangrao, China

⁴ Sterilization and Supply Center, Jiangxi Provincial People's Hospital, The First Affiliated Hospital of Nanchang Medical College, China

A – research concept and design; B – collection and/or assembly of data; C – data analysis and interpretation;

D – writing the article; E – critical revision of the article; F – final approval of the article

Advances in Clinical and Experimental Medicine, ISSN 1899–5276 (print), ISSN 2451–2680 (online)

Adv Clin Exp Med. 2023;32(8):873–880

Address for correspondence

LiQiong Lou

E-mail: louliqiong@163.com

Funding sources

None declared

Conflict of interest

None declared

Received on April 20, 2022

Reviewed on August 30, 2022

Accepted on January 11, 2023

Published online on August 17, 2023

Abstract

Background. Diabetic retinopathy (DR) is one of the most common microvascular complications of diabetes mellitus (DM). A recent in vitro study found that the suppressor of cytokine signaling 6 (SOCS6) plays a protective role in DR and DM. However, to date, no clinical studies have focused on the role of SOCS6 in DR development.

Objectives. The present study aimed to investigate the expression and clinical significance of serum SOCS6 in DR.

Materials and methods. A total of 159 DR patients were enrolled in the study. Additionally, 156 type 2 DM (T2DM) patients without DR were recruited as controls. Serum levels of SOCS6, C-reactive protein (CRP), interleukin-6 (IL-6), tumor necrosis factor alpha (TNF- α), interleukin-1 β (IL-1 β), vascular endothelial growth factor (VEGF), and angiopoietin-2 (ANG-2) were measured using enzyme-linked immunosorbent assay (ELISA). Demographic and clinical data were collected.

Results. Age, the course of DM, systolic blood pressure (SBP), diastolic blood pressure (DBP), and the levels of low-density lipoprotein cholesterol (LDL-C) and total cholesterol (TC) were significantly higher in proliferative DR (PDR) patients. Serum SOCS6 levels in PDR patients were remarkably lower than in non-PDR patients or non-DR T2DM patients. The Pearson's analysis showed that SOCS6 was negatively correlated with CRP, IL-6, TNF- α , IL-1 β , VEGF, and ANG-2. The serum levels of CRP, IL-6, TNF- α , IL-1 β , VEGF, and ANG-2 in the SOCS6 low expression group were significantly increased compared to patients with high SOCS6 levels. Receiver operating characteristic (ROC) curves showed that SOCS6 could be a potential diagnostic biomarker for DR. For logistic regression, 3 models were used. It was found that SOCS6, the course of DM, SBP and DBP in model 1, IL-1 β and TNF- α in model 2, and VEGF and ANG-2 in model 3 were risk factors for DR.

Conclusions. The SOCS6 is decreased in DR patients and is related to severity and clinical outcomes, including inflammatory and angiogenic factors.

Key words: inflammatory factors, angiogenic factors, SOCS6, diabetic retinopathy

Cite as

Li L, Wu X, He L, Luo R, Lou L. Serum levels of SOCS6 are decreased in diabetic retinopathy and are related to severity of the disease. *Adv Clin Exp Med.* 2023;32(8):873–880. doi:10.17219/acem/159215

DOI

10.17219/acem/159215

Copyright

Copyright by Author(s)

This is an article distributed under the terms of the Creative Commons Attribution 3.0 Unported (CC BY 3.0) (<https://creativecommons.org/licenses/by/3.0/>)

Background

Diabetes mellitus (DM) is a metabolic disease characterized by hyperglycemia. Type 2 DM (T2DM) is currently the most common type of the disease, accounting for 95% of total DM cases.^{1,2} In 2021, DM was estimated to affect 10.5% (536.6 million) of individuals aged 20–79 years old, worldwide.³ China is the country with the greatest number of DM cases in the world. Over the past 30 years, the prevalence of DM in China has increased by about 10 times.^{4,5}

Diabetic retinopathy (DR) is one of the most common microvascular complications of DM, with a global prevalence rate of about 27%.⁶ Diabetic retinopathy is divided into 2 types, namely nonproliferative DR (NPDR) and proliferative DR (PDR), which are classified from low to high, according to severity.⁷ Diabetic retinopathy is one of the main causes of visual impairment and blindness in adults, with studies reporting that DR accounts for 4.8% of cases of blindness around the world.⁸ Many risk factors are reported to be associated with DR, including DM, increased blood pressure, elevated blood glucose levels, and impaired kidney function.⁹ However, deeper insights are still needed to predict DR onset and clinical outcomes.

As a member of the suppressor of cytokine family of proteins, suppressor of cytokine signaling 6 (SOCS6) is generally considered to regulate bacterial infection-induced inflammation.¹⁰ Studies have suggested that SOCS6 can regulate a variety of physiological and pathological processes, including inflammation, cell proliferation, apoptosis, and angiogenesis.^{11–13} In the pathogenesis of DR, it is thought that neuroinflammation, oxidative stress and vascular-related risk factors play central roles.^{14–16} A recent *in vitro* study found that SOCS6 plays a protective role in DR and DM.¹² However, to date, no clinical studies have focused on the role of SOCS6 in the development of DR.

Objectives

In this prospective observational study, we aimed to explore the expression of SOCS6 in DR patients and to examine its correlation with clinical results. The study may reveal the clinical significance of SOCS6 in patients with DR and provide novel targets for DR treatment.

Materials and methods

Patients

A total of 159 DR patients who were admitted to Jiangxi Provincial People's Hospital between March 2019 and December 2021 were enrolled in the study. The diagnosis of T2DM was in line with the guidelines for the prevention and treatment of T2DM in China (2017 edition),¹⁷ including 1) typical diabetes symptoms (polydipsia, polyuria,

hyperphagia, unexplained weight loss) and 2) fasting plasma glucose concentration higher than 7.0 mmol/L, plasma glucose concentration higher than 11.1 mmol/L, or oral glucose tolerance test 2-hour plasma glucose concentration higher than 11.1 mmol/L. Diabetic retinopathy was diagnosed with fundus photography with dilated pupils using a retinograph (CR-2 AF Digital Retinal Camera; Canon Inc., Tokyo, Japan), and all patients were diagnosed and classified according to the international clinical DR severity scales.¹⁸

The criteria for inclusion were as follows: 1) patients diagnosed with DR according to the above guidelines; and 2) patients ≥ 18 years old. The exclusion criteria were: 1) diagnosis of type 1 DM, gestational DM or another special type of DM; 2) presence of diabetic ketoacidosis, hyperosmolar nonketotic diabetic coma or other acute DM complications; 3) presence of cataracts, glaucoma, uveitis, retinal detachment, optic nerve disease, high myopia, and other diseases significantly affecting the fundus examination; and 4) presence of serious infection, malignancy, or severe liver, renal or cardiovascular dysfunction. All patients who met the above criteria were consecutively enrolled.

The DR patients were further divided into: 1) patients with no fundus abnormalities; 2) NPDR patients, including patients with microaneurysms, hard exudates, retinal hemorrhages, and intraretinal microvascular abnormalities; and 3) PDR patients, including patients with neovascularization, fibrous tissue or hemorrhages in the vitreous body. Additionally, 156 T2DM patients without retinopathy were recruited during the same period. The inclusion and exclusion criteria for T2DM patients were the same as the diagnostic criteria for T2DM listed above.

For sample size calculations, the following formula² was used^{1,2} (Equation 1):

$$n = \frac{(Z_{\alpha} + Z_{\beta})^2 \times \sigma^2}{d^2} \quad (1)$$

According to previous studies, $\delta = 2$, $\sigma = 7$ and $Z_{1-\alpha/2} = 1.96$ (δ – tolerance error; σ – standard deviation, $1-\alpha$ – confidence level), and the minimal sample size was 48. All patients signed a written informed consent form. The study was approved by the Ethical Committee of Jiangxi Provincial People's Hospital (approval No. 2021007).

Blood sampling and ELISA

Serum levels of SOCS6, C-reactive protein (CRP), interleukin-6 (IL-6), tumor necrosis factor alpha (TNF- α), interleukin-1 β (IL-1 β), vascular endothelial growth factor (VEGF), and angiopoietin-2 (ANG-2) were measured using enzyme-linked immunosorbent assay (ELISA). Briefly, fasting cubital venous blood (5 mL) was collected from all patients within 24 h of admission. The blood samples were centrifuged at 2000 g for 15 min. After centrifugation, the levels of SOCS6, CRP, IL-6, TNF- α , IL-1 β , VEGF,

and ANG-2 were measured using commercially available ELISA kits (SOCS6: MBS2610988 (MyBioSource, San Diego, USA), detection range 0.156–10 ng/mL; CRP: EK1316, detection range 312–20000 pg/mL; IL-6: EK0410, detection range 4.69–300 pg/mL; TNF- α : EK0525, detection range 15.6–1000 pg/mL; IL-1 β : EK0392, detection range 3.9–250 pg/mL; VEGF: EK0539, detection range 31.2–2000 pg/mL; ANG-2: EK0657, detection range 156–10000 pg/mL), according to the manufacturer's (unless stated otherwise: Boster Bio-Engineering, Wuhan, China) instructions.

Patient data collection

Demographic and clinical data were collected from all patients, including age, body mass index (BMI), sex, the course of DM, systolic blood pressure (SBP), diastolic blood pressure (DBP), use of tobacco, etc. Whole blood testing was performed using an automatic biochemical analyzer (Hitachi 7600; Hitachi Corp., Tokyo, Japan), and the levels of fasting plasma glucose (FPG), total cholesterol (TC), triglycerides (TG), high-density lipoprotein cholesterol (HDL-C), and low-density lipoprotein cholesterol (LDL-C) were recorded.

Statistical analyses

Continuous data are presented as mean \pm standard deviation (M \pm SD) for normally-distributed data or median (minimum to maximum) for non-normally-distributed data (confirmed with Kolmogorov–Smirnov test). For non-normally distributed data, Mann–Whitney U test was used for comparisons between the 2 groups. For normally distributed data, comparisons between the 2 groups were conducted using Student's t-test. The χ^2 test was used to analyze the rates. The correlations among SOCS6, inflammatory factors and angiogenic factors were determined with Pearson's rank correlation analysis. Receiver operating characteristic (ROC) curves were used for the analysis of SOCS6 in DR patients. The logistic regression was conducted for DR risk factors. The Hosmer–Lemeshow test and the Nagelkerke's R^2 were used for the goodness-of-fit analysis. A value of $p < 0.05$ was considered statistically significant. The SPSS v. 18.0 software (SPSS Inc., Chicago, USA) was used for all statistical analyses.

Results

Basic patient characteristics

This study included 159 DR patients – 81 NPDR patients and 78 PDR patients. The course of DM was significantly longer, and the age, SBP, DBP, and the levels of LDL-C and TC were significantly higher in PDR patients compared

to the NPDR patients ($p < 0.05$). Compared to the T2DM patients without retinopathy ($n = 156$), the course of DM was significantly longer, and the age, SBP, DBP, ratio of smokers, and the levels of LDL-C and TC were markedly higher in the DR patients (Table 1). No other significant differences were found.

Expression of SOCS6

Next, the expression levels of serum SOCS6 were determined. The DR patients showed significantly lower SOCS6 levels compared to the T2DM patients without retinopathy (Fig. 1). In addition, the serum SOCS6 levels in PDR patients were remarkably lower than in NPDR patients, suggesting that SOCS6 is associated with the severity of DR.

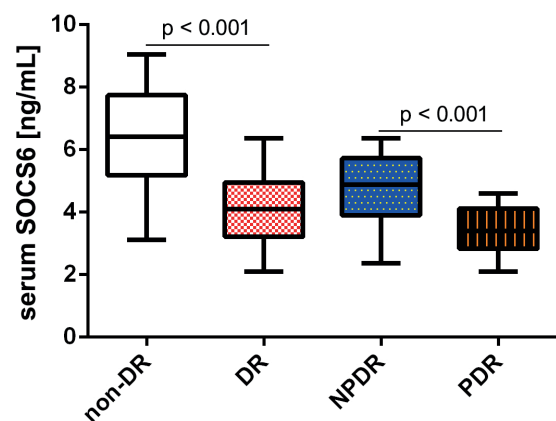


Fig. 1. Serum levels of suppressor of cytokine signaling 6 (SOCS6) in all patients. In the boxplots, the data are expressed as medians (minimum to maximum). The continuous data were compared using Student's t-test. All data are normally distributed

DR – diabetic retinopathy; NPDR – nonproliferative DR; PDR – proliferative DR.

Correlations between SOCS6 and angiogenic and inflammatory factors

The IL-6, TNF- α , IL-1 β , VEGF, and ANG-2 levels in PDR patients were remarkably higher than in NPDR patients (Fig. 2). Comparisons with T2DM patients without retinopathy showed that the CRP, IL-6, TNF- α , IL-1 β , VEGF, and ANG-2 levels in DR patients were also pronouncedly higher. The Pearson's analyses showed that SOCS6 levels correlated negatively with CRP, IL-6, TNF- α , IL-1 β , VEGF, and ANG-2 (Table 2).

Correlations between serum SOCS6 levels and T2DM patients' clinical outcomes

Next, all patients were divided into SOCS6 high-expression and low-expression groups according to the mean value (4.15 ng/mL), and the clinical characteristics between these groups were compared. As summarized

Table 1. Basic clinical characteristics of all patients

Variables	Non-retinopathy T2DM (n = 156)	All DR (n = 165)	NPDR (n = 87)	PDR (n = 78)	U/ χ^2	p ₁	U/ χ^2	p ₂
Age [years]	58 (44–74)	62 (46–75)	62 (46–75)	62 (51–73)	10228.00	0.010	3296.00	0.751
Female, n (%)	70 (44.87)	72 (43.63)	38 (43.68)	34 (43.59)	0.031	0.999	<0.001	0.999
BMI	25.24 (21.02–29.32)	25.12 (20.95–29.23)	25.39 (20.95–29.21)	24.42 (20.96–29.23)	12485.00	0.643	2885.00	0.097
Current smoker, n (%)	31 (19.87)	70 (42.42)	37 (42.53)	33 (42.31)	13.816	0.010	0.001	0.999
Course of DM [years]	8 (1–15)	15 (7–22)	14 (7–20)	16 (10–22)	3958.00	<0.001	2029.00	<0.001
Complications								
Serum uric acid, n (%)	18 (11.54)	21 (12.74)	9 (10.34)	13 (16.67)	0.068	0.999	1.715	0.214
Diabetic nephropathy, n (%)	35 (22.44)	52 (31.52)	24 (27.59)	28 (35.90)	2.092	0.151	1.594	0.289
Coronary disease, n (%)	41 (26.28)	57 (35.55)	27 (31.03)	30 (38.46)	2.012	0.219	1.217	0.372
SBP [mm Hg]	127.45 (107.12–144.96)	139.15 (117.88–157.90)	135.12 (117.88–148.47)	143.86 (124.61–157.90)	5616.00	<0.001	1583.00	<0.001
DBP [mm Hg]	83.86 (71.41–94.21)	95.43 (82.98–103.45)	91.66 (82.98–99.69)	97.52 (89.74–103.45)	2549.00	<0.001	1236.00	<0.001
FBG [mmol/L]	8.31 (7.23–9.33)	8.28 (7.22–9.33)	8.38 (7.23–9.33)	8.23 (7.22–9.33)	12541.50	0.693	3259.00	0.662
TC [mmol/L]	4.86 (3.36–6.09)	5.13 (3.34–7.65)	4.63 (3.34–6.09)	5.83 (3.49–7.65)	10425.50	0.030	1473.50	<0.001
TG [mmol/L]	1.49 (0.68–2.35)	1.62 (0.71–2.36)	1.57 (0.71–2.35)	1.74 (0.78–2.36)	11159.50	0.400	2938.50	0.138
HDL-C [mmol/L]	1.02 (0.48–1.52)	1.00 (0.50–1.52)	1.03 (0.50–1.52)	0.99 (0.50–1.52)	12694.00	0.832	3207.50	0.545
LDL-C [mmol/L]	3.00 (1.89–3.75)	3.30 (1.85–4.98)	2.93 (1.85–3.75)	3.90 (2.53–4.98)	9227.00	<0.001	897.50	<0.001

DR – diabetic retinopathy; NPDR – nonproliferative DR; PDR – proliferative DR; BMI – body mass index; T2DM – type 2 diabetes mellitus; SBP – systolic blood pressure; DBP – diastolic blood pressure; FBG – fasting plasma glucose; TC – total cholesterol; TG – triglycerides; HDL-C – high-density lipoprotein cholesterol; LDL-C – low-density lipoprotein cholesterol; p₁ – comparison between non-retinopathy T2DM patients and all DR patients; p₂ – comparison between NPDR patients and PDR patients. All continuous data were non-normally distributed (age, BMI, course of DM, SBP, DBP, FBG, TC, TG, HDL-C, and LDL-C), and were expressed as median (minimum to maximum). The comparisons between the 2 groups were analyzed using the Mann–Whitney U test. The χ^2 test was used for comparing rates (sex, current smoker, serum uric acid, diabetic nephropathy, coronary artery disease (CAD)). U/ χ^2 – levels of U in Mann–Whitney U test or χ^2 in χ^2 test.

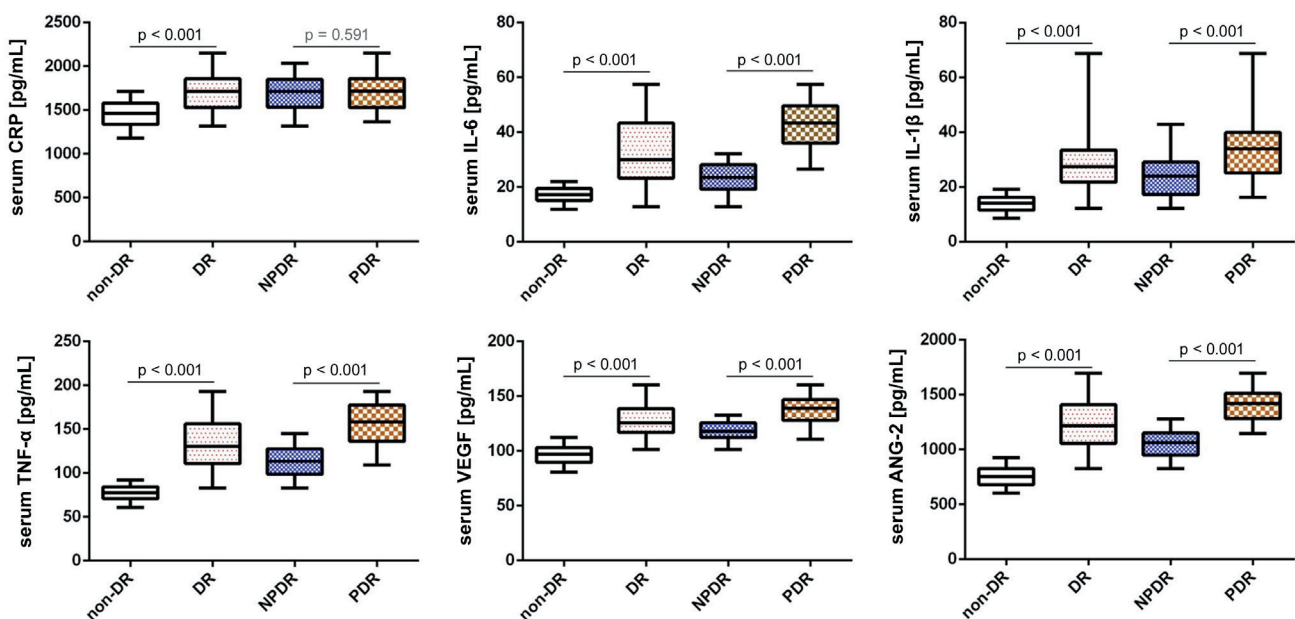


Fig. 2. Serum levels of C-reactive protein (CRP), interleukin-6 (IL-6), tumor necrosis factor alpha (TNF- α), interleukin-1 β (IL-1 β), vascular endothelial growth factor (VEGF), and angiopoietin-2 (ANG-2) in all patients. In the boxplots, data are expressed as medians (minimum to maximum). The continuous data were compared using Student's t-test. All data are normally distributed

DR – diabetic retinopathy; NPDR – nonproliferative DR; PDR – proliferative DR.

Table 2. Correlation analysis of SOCS6, angiogenic factors and inflammatory factors

Variables and Pearson's correlation		SOCS6	CRP	IL-6	TNF-α	IL-1β	VEGF	ANG-2
SOCS6	Pearson's correlation	1	-0.373	-0.592	-0.627	-0.561	-0.597	-0.646
	p-value	-	<0.001	<0.001	<0.001	<0.001	<0.001	<0.001
CRP	Pearson's correlation	-0.373	1	0.378	0.454	0.401	0.491	0.459
	p-value	<0.001	-	<0.001	<0.001	<0.001	<0.001	<0.001
IL-6	Pearson's correlation	-0.592	0.378	1	0.781	0.682	0.754	0.820
	p-value	<0.001	<0.001	-	<0.001	<0.001	<0.001	<0.001
TNF-α	Pearson's correlation	-0.627	0.454	0.781	1	0.729	0.758	0.818
	p-value	<0.001	<0.001	<0.001	-	<0.001	<0.001	<0.001
IL-1β	Pearson's correlation	-0.561	0.401	0.682	0.729	1	0.658	0.749
	p-value	<0.001	<0.001	<0.001	<0.001	-	<0.001	<0.001
VEGF	Pearson's correlation	-0.597	0.491	0.754	0.758	0.658	1	0.794
	p-value	<0.001	<0.001	<0.001	<0.001	<0.001	-	<0.001
ANG-2	Pearson's correlation	-0.646	0.459	0.820	0.818	0.749	0.794	1
	p-value	<0.001	<0.001	<0.001	<0.001	<0.001	<0.001	-

SOCS6 – suppressor of cytokine signaling 6; CRP – C-reactive protein; IL-6 – interleukin-6; TNF-α – tumor necrosis factor alpha; IL-1β – interleukin-1β; VEGF – vascular endothelial growth factor; ANG-2 – angiotensin-2.

Table 3. Comparison of clinical outcomes between patients with high and low expression of SOCS6

Variables	High SOCS6 (n = 79)	Low SOCS6 (n = 86)	U/t/χ ²	p-value
Age [years]	62 (46–75)	62 (48–75)	3272.50	0.684
Female, n (%)	31 (39.24)	41 (47.67)	1.436	0.254
Course of DM [years]	14 (7–22)	15 (7–22)	2608.00	0.010
Current smoker, n (%)	35 (40.70)	35 (44.30)	0.270	0.775
BMI	25.72 (20.95–29.21)	24.48 (20.96–29.23)	2852.50	0.076
FBG [mmol/L]	8.29 (7.22–9.33)	8.26 (7.23–9.33)	3218.00	0.559
SBP [mm Hg]	136.30 (117.88–154.50)	142.66 (120.08–157.90)	2436.00	0.002
DBP [mm Hg]	93.62 (82.98–102.99)	96.06 (84.63–103.45)	2333.50	0.001
TC [mmol/L]	4.90 (3.34–7.55)	5.48 (3.38–7.65)	2500.50	0.003
TG [mmol/L]	1.60 (0.71–2.35)	1.65 (0.78–2.36)	3299.50	0.750
HDL-C [mmol/L]	1.03 (0.52–1.52)	0.99 (0.50–1.52)	3028.50	0.229
LDL-C [mmol/L]	3.11 (1.85–4.85)	3.60 (1.85–4.98)	2206.00	<0.001
CRP [pg/mL]	1692.76 ±193.27	1707.83 ±212.66	0.475	0.635
IL-6 [pg/mL]	27.96 ±10.32	37.11 ±11.51	5.382	<0.001
TNF-α [pg/mL]	123.34 ±28.82	142.69 ±27.76	4.391	<0.001
IL-1β [pg/mL]	25.19 ±8.53	30.86 ±9.22	4.094	<0.001
VEGF [pg/mL]	120.84 ±12.03	132.88 ±13.86	5.968	<0.001
ANG-2 [pg/mL]	1117.45 ±210.79	1319.58 ±195.02	6.398	<0.001

SOCS6 – suppressor of cytokine signaling 6; BMI – body mass index; DM – diabetes mellitus; SBP – systolic blood pressure; DBP – diastolic blood pressure; FBG – fasting plasma glucose; TC – total cholesterol; TG – triglycerides; HDL-C – high-density lipoprotein cholesterol; LDL-C – low-density lipoprotein cholesterol; CRP – C-reactive protein; IL-6 – interleukin-6; TNF-α – tumor necrosis factor alpha; IL-1β – interleukin-1β; VEGF – vascular endothelial growth factor; ANG-2 – angiotensin-2. The comparison between high and low SOCS6 groups is expressed by p-values. Continuous data that were non-normally distributed (age, BMI, course of DM, SBP, DBP, FBG, TC, TG, HDL-C, and LDL-C) are expressed as median (minimum to maximum) and analyzed with Mann-Whitney U test. Continuous data that were normally distributed (CRP, IL-6, TNF-α, IL-1β, VEGF, and ANG-2) are expressed as mean ± standard deviation (M ±SD) and analyzed using Student's t-test. The χ² test was used for rates (gender and current smoker). U/χ² – levels of U in Mann-Whitney U test or χ² in χ² test.

in Table 3, the serum levels of IL-6, TNF-α, IL-1β, VEGF, and ANG-2 in the SOCS6 low-expression group were significantly higher compared to those in the SOCS6 high-expression group (p < 0.05). In addition, compared

to the SOCS6 high-expression group, the course of DM was significantly prolonged, and the age SBP, DBP, as well as the levels of LDL-C and TC were significantly increased in the SOCS6 low-expression group. These results suggest

that SOCS6 is associated with clinical outcomes and severity in T2DM patients.

Diagnostic value of SOCS6 and angiogenic and inflammatory factors for DR

The ROC curves were constructed to evaluate the diagnostic value of SOCS6 in DR patients. The results showed that SOCS6 could be a potential diagnostic biomarker for DR (Fig. 3). The area under the curve (AUC) for SOCS6 was 0.871 and the cutoff value was 4.61 ng/mL, with a sensitivity of 85% and a specificity of 69%. The SOCS6 could

also be used as a biomarker for NPDR or PDR patients. As shown in Fig. 3, the AUC for SOCS6 was 0.825, with a cutoff value of 3.66 ng/mL, a sensitivity of 79%, and a specificity of 64%.

Logistic regression for risk factors for DR

Finally, we used the logistic regression to identify the risk factors for DR. For logistic regression, we used 3 models for the entry method. In model 1 (age, BMI, course of DM, SBP, DBP, TC, TG, HDL-C, LDL-C, and SOCS6), the results of the Hosmer–Lemeshow test ($p = 0.139$) and

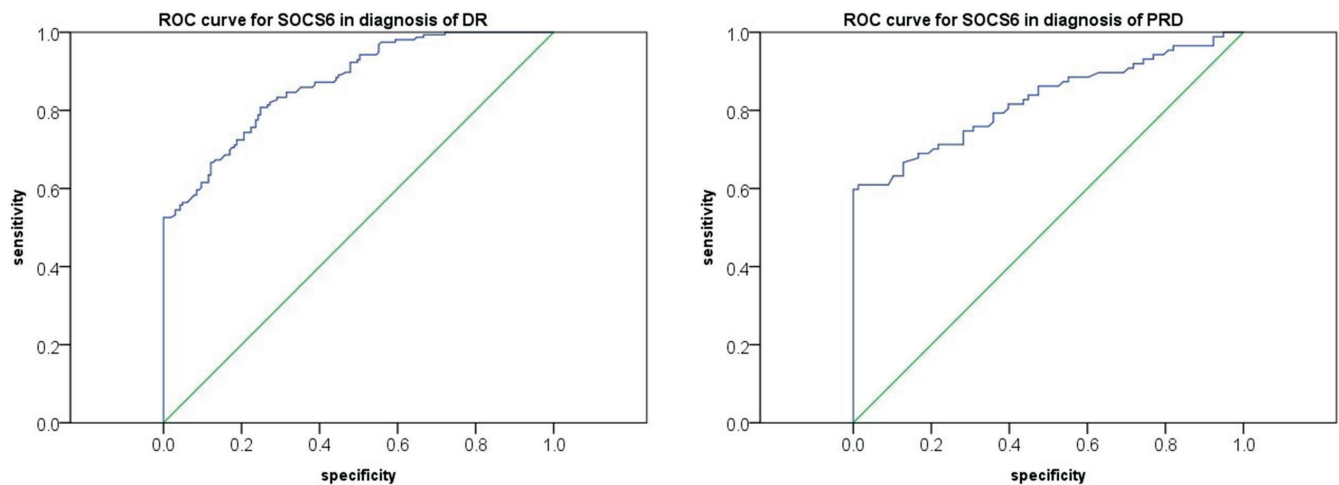


Fig. 3. Receiver operating characteristic (ROC) curves for the diagnostic value of suppressor of cytokine signaling 6 (SOCS6) for diabetic retinopathy (DR) or proliferative DR (PDR)

NPDR – nonproliferative DR.

Table 4. Logistic regression for risk factors of DR

Model	Variables	H–L test	Nagelkerke R ²	Wald	OR	95% CI	p-value
Model 1	age	0.139	0.844	2.926	1.051	0.993–1.113	0.087
	BMI			0.372	1.066	0.869–1.308	0.542
	course of DM			23.433	1.387	1.215–1.584	<0.001
	SBP			12.756	1.098	1.043–1.156	<0.001
	DBP			27.846	1.316	1.189–1.458	<0.001
	TC			5.416	0.508	0.287–0.899	<0.001
	TG			1.645	1.983	0.696–5.645	0.200
	LDL-C			0.123	1.155	0.516–2.586	0.726
	HDL-C			0.005	0.945	0.179–4.971	0.945
	SOCS6			19.253	0.410	0.275–0.610	<0.001
Model 2	CRP	0.999	0.981	1.714	1.008	0.996–1.102	0.190
	IL-6			2.721	1.479	0.929–2.355	0.099
	TNF- α			5.216	1.548	1.064–2.253	0.022
	IL-1 β			5.003	2.238	1.105–4.532	0.025
Model 3	VEGF	1.000	0.981	8.112	1.725	1.185–2.510	0.004
	ANG-2			7.438	1.049	1.014–1.086	0.006

DR – diabetic retinopathy; H–L – Hosmer–Lemeshow test; OR – odds ratio; 95% CI – 95% confidence interval; BMI – body mass index; DM – diabetes mellitus; SBP – systolic blood pressure; DBP – diastolic blood pressure; TC – total cholesterol; TG – triglycerides; LDL-C – low-density lipoprotein cholesterol; HDL-C – high-density lipoprotein cholesterol; SOCS6 – suppressor of cytokine signaling 6; CRP – C-reactive protein; IL-6 – interleukin-6; TNF- α – tumor necrosis factor alpha; IL-1 β – interleukin-1 β ; VEGF – vascular endothelial growth factor; ANG-2 – angiotensin-2.

the Nagelkerke's R^2 (0.844) showed adequate goodness-of-fit, with SOCS6, the course of DM, SBP, and DBP identified as risk factors for DR (Table 4). In model 2 (inflammatory factors CRP, IL-6, TNF- α , and IL-1 β), the Hosmer–Lemeshow test ($p = 0.999$) and the Nagelkerke's R^2 (0.981) showed adequate goodness-of-fit, and IL-1 β and TNF- α were identified as risk factors for DR. In model 3 (angiogenesis factors VEGF and ANG-2), the Hosmer–Lemeshow test ($p = 1.000$) and the Nagelkerke's R^2 (0.981) showed adequate goodness-of-fit, with both VEGF and ANG-2 identified as risk factors for DR.

Discussion

Globally, it is estimated that the number of DR cases will grow to 191 million by 2030, with vision-threatening DR patients numbering over 56 million.¹⁹ Despite the development of DR diagnostic and treatment strategies, DR is still the leading cause of blindness in working-age population. However, at present, DR is diagnosed using fundus photography with dilated pupils²⁰ and lacks specific biomarkers. Thus, it is urgent to develop new biomarkers and comprehensive approaches to reduce the risk of vision loss by prompt diagnosis and early treatment of DR. In the present study, we showed that serum SOCS6 levels were decreased in DR patients and were associated with clinical outcomes and severity.

A number of studies have indicated that cytokines, angiogenic markers and some clinical biomarker changes may cause DR. For example, a prospective study by Muni et al. found that serum high-sensitivity CRP is significantly correlated with the risk for DR.²¹ In addition, a case-control study by Churchill et al. confirmed that VEGF is associated with the severity of DR.²² In the current study, we found that the inflammatory factors CRP, IL-6, IL-1 β , and TNF- α were elevated in DR patients. These results are consistent with several previous studies.^{23–25} Changes in several clinical biomarkers are also associated with DR. For example, a 3-year prospective study in Taiwan showed that serum uric acid levels are associated with DR.⁹ Gao et al. reported that there may be a significant correlation between serum thyroglobulin antibody levels and the severity of DR.²⁶ However, at present, there are no specific biomarkers for the diagnosis of DR.

The SOCS6 is an anti-inflammatory factor in many diseases, including DM. It has been previously reported that the inhibition of SOCS6 causes a significant increase in cell permeability and inflammation, and that overexpressing SOCS6 reverses cell permeability and the inflammatory response.²⁷ Chen et al. found that the upregulation of lncRNA FGD5-AS1 could protect against periodontitis through enhancing the levels of SOCS6.¹¹ Meng et al. showed that the knockdown of miR-16-5p could suppress cell proliferation and accelerate the apoptosis of fibroblast-like synoviocytes through targeting SOCS6.²⁸ In addition,

Xue et al. reported that miR-494-3p facilitated high glucose-induced renal fibrosis through the promotion of cell apoptosis and epithelial–mesenchymal transformation via targeting SOCS6.²⁹ The SOCS6 is also correlated with angiogenic markers. Yuan et al. confirmed that the upregulation of SOCS6 inhibits angiogenesis and tumor xenograft growth, and is significantly associated with the prognosis of human prostate cancer.³⁰

The SOCS proteins improve glucose metabolism, reduce the deleterious effects of inflammation and promote neuroprotection. Most of the known SOCS proteins are involved in the regulation of insulin resistance, β -cell failure and the eventual development of DM.³¹ Several studies have also focused on the molecular mechanistic effects of SOCS6 in DM. Luo et al. confirmed that SOCS6 could regulate inflammation, oxidative stress and apoptosis in retinal epithelial cells, and attenuate DR in a rat model.³² In addition, Liu et al. suggested that the constitutive expression of the SOCS6 protein in retinal neurons improves glucose metabolism in vivo and in vitro.³³ Xiao et al. confirmed that MEG3 targets the miR-19b/SOCS6 axis in order to inhibit high glucose-induced human retinal microvascular endothelial cells apoptosis, while increasing the expression of SOCS6 and benefiting DR.¹²

As inflammation and vascular risk factors play important roles in the pathogenesis of DR, we inferred that SOCS6 may also influence DR development through the regulation of inflammation and angiogenesis. However, there is a lack of relevant reports regarding the role of SOCS6 in DR. In the present study, we found that the expression of serum SOCS6 is decreased in DR and DM patients, and is correlated with the severity of multiple clinical features, including inflammatory and angiogenic factors.

Limitations

The present study has some limitations. First, we only included a small sample of the study population. In addition, we examined a relatively small number of inflammatory and angiogenic factors. Finally, the molecular mechanisms of SOCS6 that influence DR development were not examined.

Conclusions

This study showed that the serum levels of SOCS6 are decreased in DR patients. Serum SOCS6 levels were also related to DR severity and clinical outcomes, including inflammatory and angiogenic factors. Thus, this study provides more evidence for the role of SOCS6 in DR.

Data availability

All data can be obtained from the corresponding author by reasonable request.

ORCID iDs

Lan Li  <https://orcid.org/0000-0002-9842-2601>
 Xiaoyan Wu  <https://orcid.org/0000-0001-7405-3082>
 Lemin He  <https://orcid.org/0000-0001-6194-7554>
 Rong Luo  <https://orcid.org/0000-0001-9151-9905>
 LiQiong Lou  <https://orcid.org/0000-0002-4639-2105>

References

- Saeedi P, Petersohn I, Salpea P, et al. Global and regional diabetes prevalence estimates for 2019 and projections for 2030 and 2045: Results from the International Diabetes Federation Diabetes Atlas, 9th edition. *Diabetes Res Clin Pract.* 2019;157:107843. doi:10.1016/j.diabres.2019.107843
- American Diabetes Association. Classification and diagnosis of diabetes: Standards of Medical Care in Diabetes 2021. *Diabetes Care.* 2021;44(Suppl 1):S15–S33. doi:10.2337/dc21-S002
- Sun H, Saeedi P, Karuranga S, et al. IDF Diabetes Atlas: Global, regional and country-level diabetes prevalence estimates for 2021 and projections for 2045. *Diabetes Res Clin Pract.* 2022;183:109119. doi:10.1016/j.diabres.2021.109119
- Xu Y, Wang L, He J, et al. Prevalence and control of diabetes in Chinese adults. *JAMA.* 2013;310(9):948. doi:10.1001/jama.2013.168118
- Weng JP, Bi Y. Epidemiological status of chronic diabetic complications in China. *Chin Med J (Engl).* 2015;128(24):3267–3269. doi:10.4103/0366-6999.171350
- Thomas RL, Halim S, Gurudas S, Sivaprasad S, Owens DR. IDF Diabetes Atlas: A review of studies utilising retinal photography on the global prevalence of diabetes related retinopathy between 2015 and 2018. *Diabetes Res Clin Pract.* 2019;157:107840. doi:10.1016/j.diabres.2019.107840
- Hartnett ME, Baehr W, Le YZ. Diabetic retinopathy, an overview. *Vision Res.* 2017;139:1–6. doi:10.1016/j.visres.2017.07.006
- Al-Turki YA. Blood sugar control, ophthalmology referral and creatinine level among adult diabetic patients in primary health care, Riyadh, Saudi Arabia. *Saudi Med J.* 2002;23(11):1332–1334. PMID:12506290.
- Lee JJ, Yang IH, Kuo HK, et al. Serum uric acid concentration is associated with worsening in severity of diabetic retinopathy among type 2 diabetic patients in Taiwan: A 3-year prospective study. *Diabetes Res Clin Pract.* 2014;106(2):366–372. doi:10.1016/j.diabres.2014.07.027
- Duncan SA, Baganizi DR, Sahu R, Singh SR, Dennis VA. SOCS proteins as regulators of inflammatory responses induced by bacterial infections: A review. *Front Microbiol.* 2017;8:2431. doi:10.3389/fmicb.2017.02431
- Chen H, Lan Z, Li Q, Li Y. Abnormal expression of long noncoding RNA FGD5-AS1 affects the development of periodontitis through regulating miR-142-3p/SOCS6/NF- κ B pathway. *Artif Cells Nanomed Biotechnol.* 2019;47(1):2098–2106. doi:10.1080/21691401.2019.1620256
- Xiao F, Li L, Fu JS, Hu YX, Luo R. Regulation of the miR-19b-mediated SOCS6-JAK2/STAT3 pathway by lncRNA MEG3 is involved in high glucose-induced apoptosis in hRMECs. *Biosci Rep.* 2020;40(7):BSR20194370. doi:10.1042/BSR20194370
- Yuan D, Wang W, Su J, et al. SOCS6 functions as a tumor suppressor by inducing apoptosis and inhibiting angiogenesis in human prostate cancer. *Curr Cancer Drug Targets.* 2018;18(9):894–904. doi:10.2174/1568009618666180102101442
- Spijkerman AMW, Gall MA, Tarnow L, et al. Endothelial dysfunction and low-grade inflammation and the progression of retinopathy in type 2 diabetes: Original article. *Diabetes Med.* 2007;24(9):969–976. doi:10.1111/j.1464-5491.2007.02217.x
- Rodríguez-Carrizalez AD, Castellanos-González JA, Martínez-Romero EC, et al. The effect of ubiquinone and combined antioxidant therapy on oxidative stress markers in non-proliferative diabetic retinopathy: A phase IIa, randomized, double-blind, and placebo-controlled study. *Redox Rep.* 2016;21(4):155–163. doi:10.1179/1351000215Y.0000000040
- Aljundi W, Suffo S, Munteanu C, Langenbacher A, Seitz B, Abdin A. Intravitreal injection for diabetic macular edema as adjunctive therapy for proliferative diabetic retinopathy: A retrospective study. *Clin Ophthalmol.* 2022;16:135–143. doi:10.2147/OPHT.346065
- Chinese Elderly Type 2 Diabetes Prevention and Treatment of Clinical Guidelines Writing Group, Geriatric Endocrinology and Metabolism Branch of Chinese Geriatric Society, Geriatric Endocrinology and Metabolism Branch of Chinese Geriatric Health Care Society, Geriatric Professional Committee of Beijing Medical Award Foundation, National Clinical Medical Research Center for Geriatric Diseases (PLA General Hospital). Clinical guidelines for prevention and treatment of type 2 diabetes mellitus in the elderly in China (2022 edition) [in Chinese]. *Zhonghua Nei Ke Za Zhi.* 2022;61(1):12–50. doi:10.3760/cma.j.cn112138-20211027-00751
- Wilkinson CP, Ferris FL, Klein RE, et al. Proposed international clinical diabetic retinopathy and diabetic macular edema disease severity scales. *Ophthalmology.* 2003;110(9):1677–1682. doi:10.1016/S0161-6420(03)00475-5
- Zheng Y, He M, Congdon N. The worldwide epidemic of diabetic retinopathy. *Indian J Ophthalmol.* 2012;60(5):428. doi:10.4103/0301-4738.100542
- Mookiah MRK, Acharya UR, Chua CK, Lim CM, Ng EYK, Laude A. Computer-aided diagnosis of diabetic retinopathy: A review. *Comput Biol Med.* 2013;43(12):2136–2155. doi:10.1016/j.combiomed.2013.10.007
- Muni RH, Kohly RP, Lee EQ, Manson JE, Semba RD, Schaumberg DA. Prospective study of inflammatory biomarkers and risk of diabetic retinopathy in the diabetes control and complications trial. *JAMA Ophthalmol.* 2013;131(4):514. doi:10.1001/jamaophthalmol.2013.2299
- Churchill AJ, Carter JG, Ramsden C, et al. VEGF polymorphisms are associated with severity of diabetic retinopathy. *Invest Ophthalmol Vis Sci.* 2008;49(8):3611. doi:10.1167/iiov.07-1383
- Nowak M, Wielkoszyński T, Marek B, et al. Antioxidant potential, paraoxonase 1, ceruloplasmin activity and C-reactive protein concentration in diabetic retinopathy. *Clin Exp Med.* 2010;10(3):185–192. doi:10.1007/s10238-009-0084-7
- Gustavsson C, Agardh E, Bengtsson B, Agardh CD. TNF- α is an independent serum marker for proliferative retinopathy in type 1 diabetic patients. *J Diabetes Complications.* 2008;22(5):309–316. doi:10.1016/j.jdiacomp.2007.03.001
- Khalaf N, Helmy H, Labib H, Fahmy I, Abd El Hamid M, Moemen L. Role of angiopoietins and Tie-2 in diabetic retinopathy. *Electron Physician.* 2017;9(8):5031–5035. doi:10.19082/5031
- Gao X, Wang X, Zhong Y, Liu L, Teng W, Shan Z. Serum antithyroglobulin antibody levels are associated with diabetic retinopathy among euthyroid type 2 diabetes patients: A hospital-based, retrospective study. *J Diabetes Res.* 2022;2022:2552186. doi:10.1155/2022/2552186
- Ma J, Xu LY, Sun QH, Wan XY, Li B. Inhibition of miR-1298-5p attenuates sepsis lung injury by targeting SOCS6. *Mol Cell Biochem.* 2021;476(10):3745–3756. doi:10.1007/s11010-021-04170-w
- Meng D, Pan W, Li J. MicroRNA-16-5p promoted fibroblast-like synovioyte proliferation and suppressed apoptosis via targeting suppressor of cytokine signaling 6 (SOCS6) in human rheumatoid arthritis. *J Biomater Tissue Eng.* 2021;11(9):1744–1751. doi:10.1166/jbt.2021.2600
- Xue X, Liu M, Wang Y, et al. MicroRNA-494-3p exacerbates renal epithelial cell dysfunction by targeting SOCS6 under high glucose treatment. *Kidney Blood Press Res.* 2022;47(4):247–255. doi:10.1159/000521647
- Yuan D, Wang W, Su J, et al. SOCS6 functions as a tumor suppressor by inducing apoptosis and inhibiting angiogenesis in human prostate cancer. *Curr Cancer Drug Targets.* 2018;18(9):894–904. doi:10.2174/1568009618666180102101442
- Suchy D, Łabuzek K, Machnik G, Kozłowski M, Okopień B. SOCS and diabetes: Ups and downs of a turbulent relationship. *Cell Biochem Funct.* 2013;31(3):181–195. doi:10.1002/cbf.2940
- Luo R, Li L, Xiao F, Fu J. LncRNA FLG-AS1 mitigates diabetic retinopathy by regulating retinal epithelial cell inflammation, oxidative stress, and apoptosis via miR-380-3p/SOCS6 axis. *Inflammation.* 2022;45(5):1936–1949. doi:10.1007/s10753-022-01665-6
- Liu X, Mameza MG, Lee YS, et al. Suppressors of cytokine-signaling proteins induce insulin resistance in the retina and promote survival of retinal cells. *Diabetes.* 2008;57(6):1651–1658. doi:10.2337/db07-1761

Favipiravir-induced inflammatory and hydropic degenerative liver injury in rats

Sami Bilici^{1,D,F}, Durdu Altuner^{2,C}, Zeynep Suleyman^{3,C}, Seval Bulut^{3,C}, Cengiz Sarigul^{4,B,C}, Mine Gulaboglu^{5,B,C}, Fikret Altindag^{6,A,C}, Adalet Ozcicek^{7,E}, Cebrail Gursul^{8,E}, Halis Suleyman^{2,D,F}

¹ Department of General Surgery, Faculty of Medicine, Erzincan Binali Yildirim University, Turkey

² Department of Pharmacology, Faculty of Medicine, Erzincan Binali Yildirim University, Turkey

³ Department of Pharmacology, Institute of Health Sciences, Erzincan Binali Yildirim University, Turkey

⁴ Department of Medical Biochemistry, Faculty of Medicine, Atatürk University, Erzurum, Turkey

⁵ Department of Biochemistry, Faculty of Pharmacy, Atatürk University, Erzurum, Turkey

⁶ Department of Histology and Embryology, Faculty of Medicine, Van Yüzüncü Yıl University, Turkey

⁷ Department of Internal Medicine, Faculty of Medicine, Erzincan Binali Yildirim University, Turkey

⁸ Department of Physiology, Faculty of Medicine, Erzincan Binali Yildirim University, Turkey

A – research concept and design; B – collection and/or assembly of data; C – data analysis and interpretation; D – writing the article; E – critical revision of the article; F – final approval of the article

Advances in Clinical and Experimental Medicine, ISSN 1899–5276 (print), ISSN 2451–2680 (online)

Adv Clin Exp Med. 2023;32(8):881–887

Address for correspondence

Halis Suleyman
E-mail: halis.suleyman@gmail.com

Funding sources

None declared

Conflict of interest

None declared

Received on October 19, 2022

Reviewed on November 16, 2022

Accepted on January 8, 2023

Published online on February 8, 2023

Cite as

Bilici S, Altuner D, Suleyman Z, et al. Favipiravir-induced inflammatory and hydropic degenerative liver injury in rats. *Adv Clin Exp Med*. 2023;32(8):881–887. doi:10.17219/acem/159089

DOI

10.17219/acem/159089

Copyright

Copyright by Author(s)

This is an article distributed under the terms of the Creative Commons Attribution 3.0 Unported (CC BY 3.0) (<https://creativecommons.org/licenses/by/3.0/>)

Abstract

Background. Favipiravir is very effective in the treatment of many viral infections, especially at high doses. It was used at such doses to treat coronavirus disease 2019 (COVID-19) during the pandemic. However, liver damage was reported in patients undergoing such treatment.

Objectives. This study aimed to investigate the effects of low and high doses of favipiravir on the liver of rats, using biochemical and histopathological methods.

Materials and methods. Wistar albino rats were allocated to one of 3 groups, namely a healthy group (HG), a 100 mg/kg favipiravir (FAV-100) group and a 400 mg/kg favipiravir (FAV-400) group. Favipiravir was administered orally at 100 mg/kg and 400 mg/kg doses to the FAV-100 (n = 6) and FAV-400 (n = 6) groups, respectively. Distilled water was administered orally (1 mL) using the same method to the HG (n = 6). This procedure was repeated twice a day for 1 week. At the end of this period, the animals were euthanized with a high dose of thiopental anesthesia (50 mg/kg) and their liver tissues were removed.

Results. Favipiravir caused an increase in malondialdehyde (MDA), nuclear factor kappa B (NF-κB) and interleukin 6 (IL-6) levels in the liver tissue, as well as elevated alanine aminotransaminase (ALT) and aspartate aminotransferase (AST) levels in the blood. Moreover, favipiravir caused a decrease in total glutathione (tGSH), superoxide dismutase (SOD) and catalase (CAT) levels. In addition, severe edema, lymphocyte infiltration and hydropic degeneration were observed in the liver tissue of the FAV-400.

Conclusions. High-dose favipiravir caused more significant oxidative and inflammatory damage in the liver tissue of rats than low-dose favipiravir.

Key words: inflammation, rat, hydropic degeneration, favipiravir

Background

Favipiravir is an antiviral drug that has been tested for use against coronavirus disease 2019 (COVID-19).¹ It has also been found to be effective in treating influenza and severe acute respiratory syndrome coronavirus 2 (SARS-CoV-2).² Favipiravir is effective against RNA viruses such as human rhinovirus, respiratory syncytial virus, metapneumovirus, and parainfluenza, and has been considered a candidate for the treatment of hantavirus-induced infections.³ The drug is converted to the active favipiravir-ribofuranosyl-50-triphosphate metabolite through phosphorylation and ribosylation in tissues.⁴ The antiviral effects of favipiravir depend on blocking the inward and outward movements of viruses by the drug.⁵ The action is achieved through the inhibition of RNA-dependent RNA polymerase (RdRp).⁶ Favipiravir has been found to be effective against these infections at high doses.⁷ Two doses of 2400–3000 mg every 12 h have been recommended for the treatment of COVID-19, followed by 1200–1800 mg every 12 h.^{8,9} However, favipiravir can cause toxic effects at high doses.¹⁰

The most frequent toxic effects of favipiravir are diarrhea, nephrotoxicity, increased serum uric acid and transaminase levels, decreased white blood cell count and neutrophil level, nausea, vomiting, abdominal pain, skin rash, itching, delirium, hallucinations, and convulsions.^{11,12} Moreover, liver damage has been reported in patients undergoing favipiravir treatment.¹³ This was also shown experimentally, with favipiravir causing hepatic dysfunction and vacuolization in hepatocytes.^{13,14} Furthermore, favipiravir treatment was shown to cause an increase in liver enzymes and oxidative and histopathological damage in rats. Recent study reported that endogenous oxidants and antioxidants such as superoxide dismutase (SOD), catalase (CAT), malondialdehyde (MDA), and total glutathione (tGSH) played a critical role in the pathogenesis of favipiravir hepatotoxicity.¹⁵ These data indicated that oxidative stress was responsible for favipiravir-induced hepatotoxicity. However, no studies investigated the effects of favipiravir on the liver of animals treated with low and high doses of this drug.

Objectives

The purpose of the study was to examine the biochemical and histopathological effects of different doses of favipiravir on rat liver.

Materials and methods

Animals

Rats were obtained from Medical Experimental Application and Research Center (Erzincan Binali Yıldırım

University, Erzincan, Turkey). In total, 18 albino male Wistar rats weighing 280–290 g were included in the study. Before the commencement of the study, the rats were housed at room temperature (22°C) in a 12-hour light/dark cycle. The animals were fed with normal tap water and pellet food. The procedures were approved by the Animal Experiments Local Ethics Committee (September 29, 2022, meeting No. 09/46, approval No. E-85748827-050.01.04-204261)

Chemicals

The thiopental sodium was procured from a commercial supplier (IE Ulagay, Istanbul, Turkey), and the favipiravir was obtained from the Education and Research Hospital (Erzincan, Turkey) affiliated with the Ministry of Health.

Animal groups

The rats were randomly assigned to one of 3 groups (n = 6/group), namely a healthy group (HG), a 100 mg/kg favipiravir (FAV-100) group and a 400 mg/kg favipiravir (FAV-400) group.

Experimental procedure

Favipiravir was given orally at doses of 100 mg/kg or 400 mg/kg to the FAV-100 and FAV-400 animal groups, respectively. Distilled water was administered orally (1 mL) to the HG using the same method. This practice was continued twice a day for 1 week. At the end of the 1st week, the rats were euthanized with a high dose of thiopental anesthesia (50 mg/kg), and their liver tissues were excised. The MDA, tGSH, SOD, and CAT levels in liver tissues were measured. In addition, serum alanine aminotransferase (ALT) and aspartate aminotransferase (AST) activities were determined in blood samples taken from the rats before they were euthanized. The liver tissues were assessed biochemically and histopathologically. All experimental results were analyzed by comparing the groups.

Biochemical analyses

Malondialdehyde, glutathione, superoxide dismutase, catalase, and protein determination in tissue

The concentration of SOD, tGSH and MDA in liver tissues of the experimental animals was evaluated using commercially available enzyme-linked immunosorbent assay (ELISA) kits (cat. No. 706002, 703002 and 10009055, respectively) according to the kit instructions (Cayman Chemical Company, Ann Arbor, USA). The determination of CAT was performed according to the method described by Góth.¹⁶ The protein analysis was performed according to the Bradford method.¹⁷

Nuclear factor kappa B and interleukin 6 analysis in tissues

The samples were weighed and all tissues was separated, snap-frozen using liquid nitrogen, and homogenized with a mortar. After the samples were melted, they were stored at 2–8°C as a standard. Phosphate-buffered saline (PBS) (pH 7.4, 1/10 w/v) was added to the samples, which were then vortexed for 10 s and centrifuged for 20 min at 10,000 × g. Nuclear factor kappa B (NF-κB; pg/L) was assayed using a rat NF-κB ELISA immunoassay kit (Shanghai Sunred Biological Technology Co., Ltd., Shanghai, China) and the levels of interleukin 6 (IL-6; ng/L) were assayed using a commercial ELISA kit (Hangzhou Eastbiopharm Co., Ltd., Hangzhou, China).

Alanine aminotransferase and aspartate aminotransferase analysis in tissues

Serum AST and ALT activities were measured with commercially available kits (Roche Diagnostics GmbH, Mannheim, Germany) to assess liver function. Samples were analyzed spectrophotometrically using a cobas® 8000 auto-analyzer (Roche Diagnostics GmbH).

Histopathological analyses

Sections of liver tissue were stained with hematoxylin and eosin (H&E) and examined using an Olympus BX51 fluorescence microscope (Olympus Corp., Tokyo, Japan). Histopathological severity of damage was evaluated as normal (0), mild injury (1), moderate injury (2), or severe injury (3).

Statistical analyses

The experimental results are presented as mean ± standard deviation ($M \pm SD$) and 95% confidence interval (95% CI) of the mean. The Shapiro–Wilk test was used to determine whether the data were distributed normally, and the homogeneity of variances was determined with

the Levene's test. Since the data were normally distributed, one-way analysis of variance (ANOVA) was chosen for statistical analysis. Subsequently, the Tukey's honest significant difference (HSD) and Games–Howell post hoc tests were performed after ANOVA. GraphPad Prism v. 8 software (GraphPad Software, San Diego, USA) was used to create the images. Biochemical findings were analyzed with IBM SPSS v. 25.0 software (IBM Corp., Armonk, USA). A value of $p < 0.05$ was considered statistically significant.

Results

Biochemical findings

Oxidative and antioxidant findings in liver tissue

Favipiravir increased MDA levels more significantly at a dose of 400 mg/kg and decreased tGSH levels more significantly at a dose of 100 mg/kg (Fig. 1). Also, favipiravir decreased SOD and CAT activity more significantly at a dose of 400 mg/kg compared to a dose of 100 mg/kg (Fig. 2).

Nuclear factor kappa B and interleukin 6 findings in liver tissues

We found that levels of NF-κB and IL-6 in liver tissue were significantly increased at a favipiravir dose of 400 mg/kg compared to the 100 mg/kg dose (Fig. 3).

Alanine aminotransferase and aspartate aminotransferase findings in the blood

Favipiravir significantly increased ALT and AST activity in comparison to the HG ($p < 0.001$). The ALT and AST activities were higher in the FAV-400 group than in the FAV-100 group ($p < 0.001$; Fig. 4). Biochemical parameters are presented in Table 1.

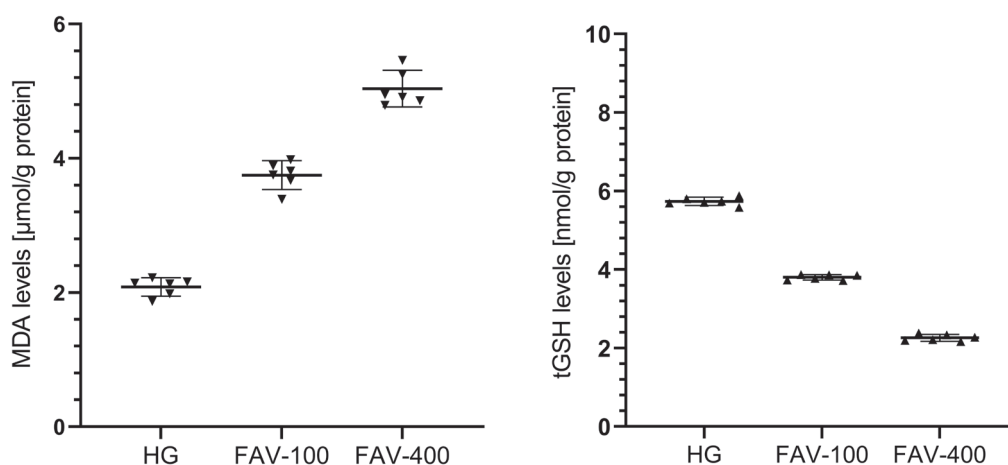


Fig. 1. Malondialdehyde (MDA) and total glutathione (tGSH) analysis of liver tissue

HG – healthy group; FAV-100 – favipiravir 100 mg/kg group; FAV-400 – favipiravir 400 mg/kg group. Mean values and 95% confidence intervals (95% CIs) are presented.

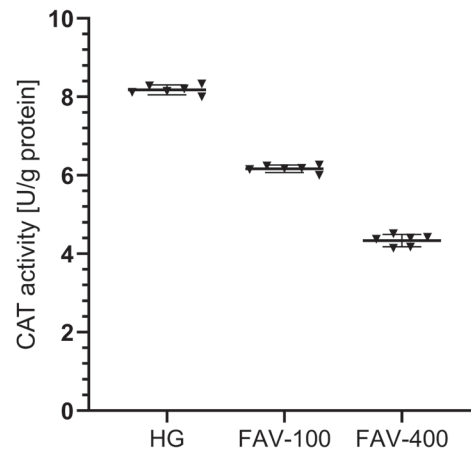
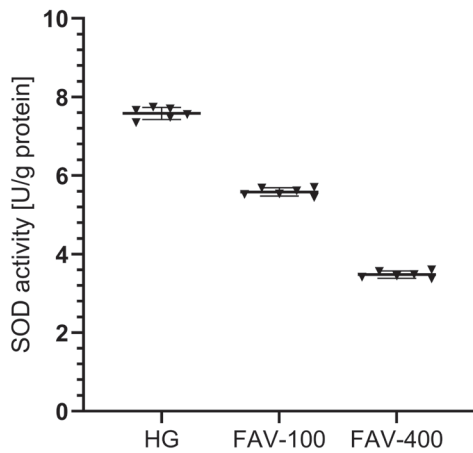


Fig. 2. Superoxide dismutase (SOD) and catalase (CAT) analysis of liver tissue

HG – healthy group; FAV-100 – favipiravir 100 mg/kg group; FAV-400 – favipiravir 400 mg/kg group. Mean values and 95% confidence intervals (95% CIs) are presented.

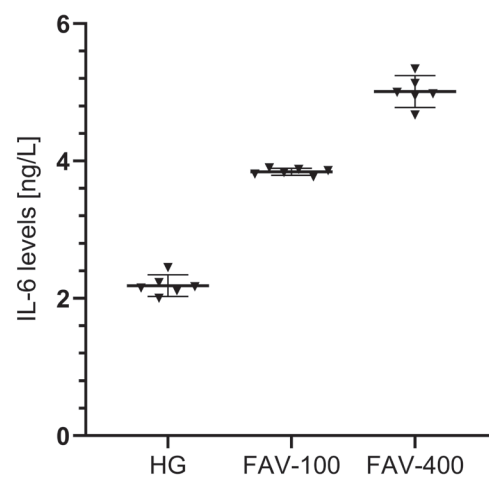
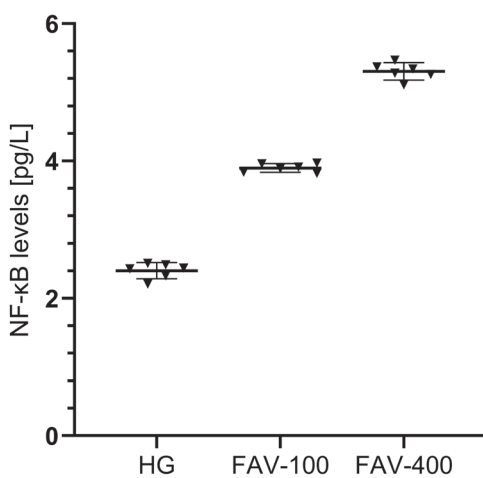


Fig. 3. Nuclear factor kappa-B (NF-κB) and interleukin 6 (IL-6) analysis of liver tissue

HG – healthy group; FAV-100 – favipiravir 100 mg/kg group; FAV-400 – favipiravir 400 mg/kg group. Mean values and 95% confidence intervals (95% CIs) are presented.

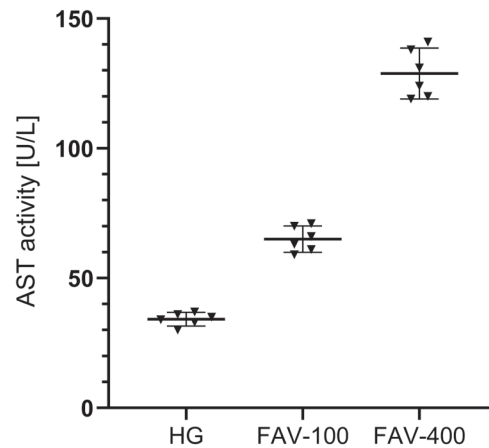
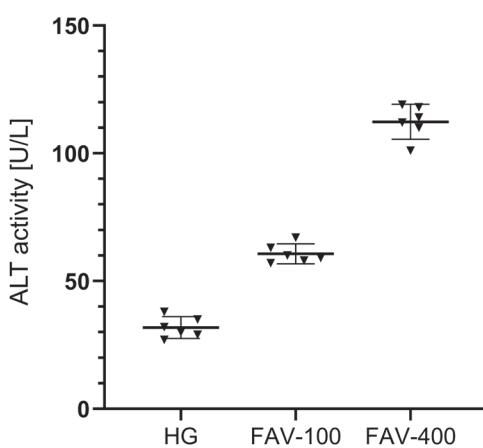


Fig. 4. Alanine aminotransferase (ALT) and aspartate aminotransferase (AST) analysis of blood

HG – healthy group; FAV-100 – favipiravir 100 mg/kg group; FAV-400 – favipiravir 400 mg/kg group. Mean values and 95% confidence intervals (95% CIs) are presented.

Histopathological findings

As shown in Fig. 5A, no microscopic pathological findings were found in the HG. However, moderate edema and lymphocyte infiltration were found in the FAV-100 group (Fig. 5B). Moreover, severe edema, lymphocyte infiltration and hydropic degeneration were observed in the FAV-400 group (Fig. 5C).

Discussion

Favipiravir has been used at high doses for the treatment of COVID-19 as its antiviral efficacy is known to be greater at such doses.¹⁸ In this study, the effects of low and high doses of favipiravir on the liver were analyzed biochemically and histopathologically. The biochemical tests revealed that a high dose of favipiravir significantly increased MDA, NF-κB, IL-6, ALT, and AST levels when compared to the low dose. A high dose also decreased the levels of antioxidants,

Table 1. Results and analysis of biochemical parameters

Variables		MDA [μmol/g protein]	tGSH [nmol/g protein]	SOD [U/g protein]	CAT [U/g protein]	NF-κB [pg/L]	IL-6 [ng/L]	ALT [U/L]	AST [U/L]	
Groups (M ±SD)	HG	2.08 ±0.05	5.73 ±0.42	7.58 ±0.06	8.18 ±0.05	2.40 ±0.05	2.19 ±0.06	31.83 ±1.66	34.17 ±1.01	
	FAV-100	3.75 ±0.08	3.80 ±0.03	5.58 ±0.04	6.17 ±0.04	3.90 ±0.03	3.84 ±0.02	60.67 ±1.52	65.00 ±1.98	
	FAV-400	5.04 ±0.11	2.26 ±0.04	3.48 ±0.04	4.34 ±0.06	5.31 ±0.05	5.01 ±0.09	112.33 ±2.67	128.83 ±3.81	
95% CI for the mean change	HG	lower	1.9456	5.6264	7.4242	8.0537	2.2832	2.0269	27.5619	31.5606
		upper	2.2211	5.8403	7.7358	8.3029	2.5201	2.3431	36.1048	36.7727
	FAV-100	lower	3.5322	3.7285	5.4740	6.0701	3.8342	3.7914	56.7588	59.9019
		upper	3.9645	3.8715	5.6860	6.2632	3.9625	3.8920	64.5746	70.0981
	FAV-400	lower	4.7629	2.1667	3.3836	4.1804	5.1779	4.7821	105.4784	119.0467
		upper	5.3105	3.3466	3.5697	4.4896	5.4321	5.2432	119.1882	138.6199
p-values	HG vs. FAV-100	<0.001	<0.001	<0.001	<0.001	<0.001	<0.001	<0.001	<0.001	
	HG vs. FAV-400	<0.001	<0.001	<0.001	<0.001	<0.001	<0.001	<0.001	<0.001	
	FAV-100 vs. FAV-400	<0.001	<0.001	<0.001	<0.001	<0.001	<0.001	<0.001	<0.001	
F value		309.002	2441.326	1889.563	1502.463	1218.373	492.657	409.619	359.465	
df (df1/df2)		2/15	2/15	2/15	2/15	2/15	2/15	2/15	2/15	

HG – healthy group; FAV-100 – 100 mg/kg favipiravir group; FAV-400 – 400 mg/kg favipiravir group; MDA – malondialdehyde; tGSH – total glutathione; SOD – superoxide dismutase; CAT – catalase; NF-κB – nuclear factor kappa B; IL-6 – interleukin 6; ALT – alanine aminotransferase; AST – aspartate aminotransferase; M ±SD – mean ± standard deviation. The Tukey’s honest significant difference and the Games–Howell post hoc tests were performed following analysis of variance (ANOVA) (F (2,15)).

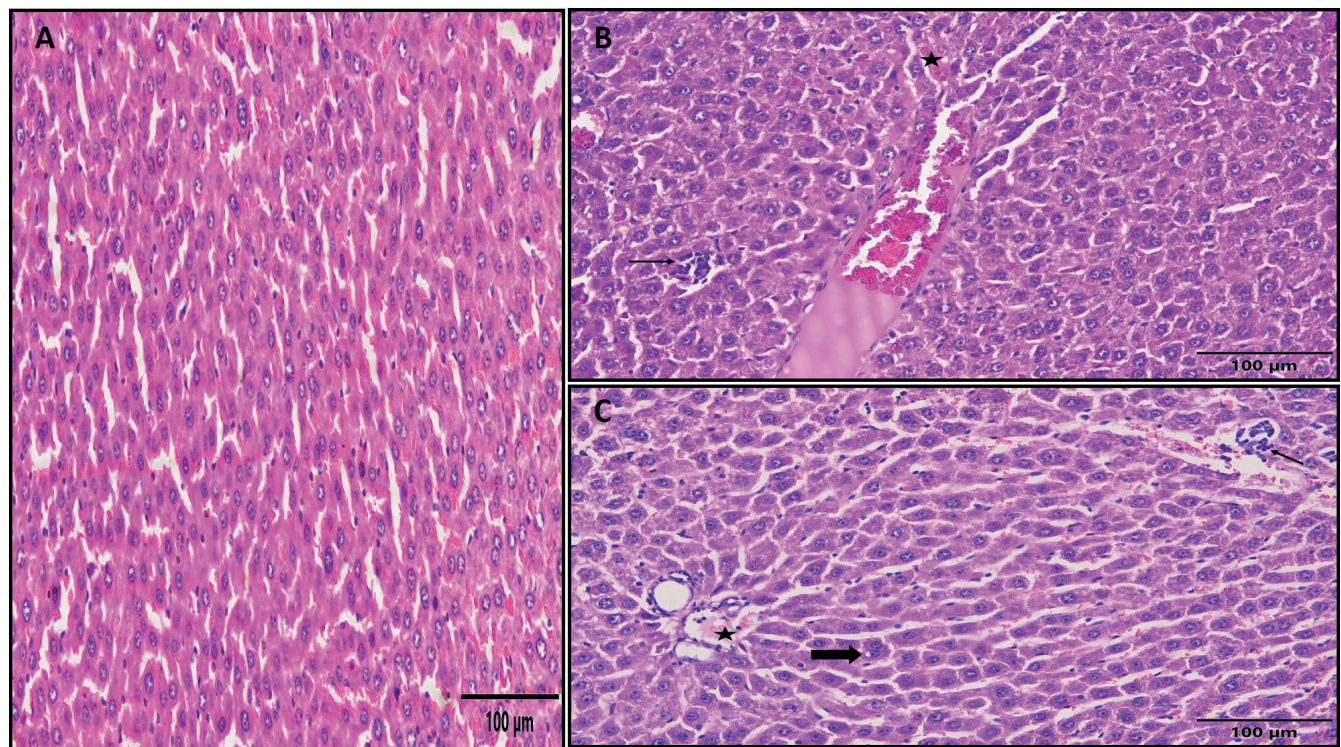


Fig. 5. A. Liver tissue of a healthy rat. No microscopic pathological changes were found in the liver tissue of the animals in the healthy group (HG); B. Liver tissue of the favipiravir 100 mg/kg (FAV-100) group. Moderate-level edema and lymphocyte infiltration were observed in the liver tissue of the FAV-100 group; C. Liver tissue of the favipiravir 400 mg/kg (FAV-400) group. Severe edema, lymphocyte infiltration and hydropic degeneration were observed in the liver tissue of the FAV-400 group

including tGSH, SOD and CAT. The MDA is known to be one of the most important indicators of oxidative damage and is the final product of lipid peroxidation (LPO),¹⁹ a process that is associated with tissue damage.²⁰

In healthy tissues, a small portion of oxygen is converted to reactive oxygen species (ROS) during metabolism in the mitochondria and other cellular compartments. The primary ROS include hydrogen peroxide (H₂O₂),

superoxide radical ($O_2^{\cdot-}$) and hydroxyl radical ($OH\cdot$).¹⁹ Excessive ROS formation causes inflammatory diseases,²¹ oxidative stress, and damage at a molecular and cellular level.²² Results of this study, as well as information derived from other studies, indicate that favipiravir causes oxidative damage at low and high doses. Indeed, recent study showed that favipiravir caused oxidative damage by increasing MDA levels in liver tissue.¹⁵ Another study demonstrated that side effects increased as the dose of favipiravir increased, which is in agreement with our biochemical findings.¹⁰

Antioxidants are known to protect liver tissue from oxidative damage.²³ Therefore, we performed antioxidant measurements to analyze liver injury. The tGSH levels in the liver tissue of animals treated with a 400 mg/kg dose of favipiravir were found to be significantly lower than in those treated with a 100 mg/kg dose. The GSH is a tripeptide that includes L-glutamate, L-cysteine and glycine, and it is one of the most remarkable antioxidants.²⁴ Indeed, in living tissues, GSH detoxifies ROS reactions and protects cells from ROS toxicity.²⁵ The decrease in tGSH levels in the liver tissue of animals administered favipiravir indicated that the oxidant/antioxidant balance had changed in favor of oxidants, which was determined to be oxidative stress.²⁶ Similar results were found in another study, in which it was observed that the GSH levels of cells decreased after favipiravir treatment.²⁷

Other parameters used to evaluate oxidative stress included SOD and CAT levels.²⁸ Normal levels of SOD and CAT help maintain tissue integrity and function by neutralizing overproduced ROS.²⁹ Our experimental results showed a decrease in the levels of the enzymatic antioxidants SOD and CAT in groups treated with favipiravir. Similarly, Kara et al. showed that SOD and CAT levels decreased in lung and liver tissue groups treated with favipiravir compared to healthy tissues,¹⁵ which is consistent with our experimental results.

The levels of the pro-inflammatory cytokines NF- κ B and IL-6 were found to be increased in the liver tissue of animals treated with favipiravir. The NF- κ B plays an important role in mediating the cellular response to damage, stress and inflammation.³⁰ According to previous studies, favipiravir increased NF- κ B and IL-6 levels in the liver,¹⁵ and increased NF- κ B in primary intervertebral disc tissue cell cultures.³¹ At the same time, Zhao et al. also reported that favipiravir increased levels of IL-6.³² In other words, favipiravir plays an important role in inflammation by causing an increase in pro-inflammatory cytokine production.

Increased serum transaminase, an important indicator of hepatocellular damage, occurs in 8% of the population.³³ In this study, favipiravir significantly increased ALT and AST levels at a dose of 100 mg/kg and 400 mg/kg. Bayram et al. found that serum ALT and AST levels were elevated in patients treated with favipiravir.³⁴ Another study showed that ALT and AST levels increased in patients

administered favipiravir for the treatment of COVID-19, which caused hepatotoxicity.¹³ Furthermore, a study by Izci Cetinkaya et al. showed a significant increase in ALT and AST levels in patients treated with favipiravir.³⁵

The biochemical results obtained from the liver tissues of animals in this study aligned with the histopathological findings. Severe edema (grade 3), lymphocyte infiltration and hydropic degeneration were observed in the liver tissues of the FAV-400 group, which also had high oxidant and low antioxidant levels. However, only moderate edema (grade 2) and lymphocyte infiltration were observed in the FAV-100 group. These results indicate that increasing the dose of favipiravir increased hepatic edema, lymphocyte infiltration and hydropic degeneration. It has been reported that hydropic degeneration is associated with oxidative liver injury.³⁶ In addition, it was shown that increased inflammatory cells and pro-inflammatory mediators were associated with ROS production.³⁷







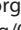

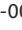
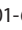
Limitations

The study did not investigate the effects of favipiravir in combination with other drugs in the treatment of COVID-19 or other infections. This should be clarified in future studies. Due to a very small sample size used, it is impossible to reliably verify the statistical test assumptions; therefore, the calculated p-values need to be interpreted with caution.

Conclusions

In conclusion, high dose of favipiravir caused significantly more oxidative and inflammatory injury in liver tissue compared to the low dose. Indeed, animals administered a high dose (400 mg/kg) of favipiravir had higher levels of oxidants and pro-inflammatory cytokines, as well as hydropic degeneration of the liver. This is the first study to show hydropic degeneration of the liver with the use of favipiravir. Therefore, hydropic degeneration may be associated with the excessive production of oxidants and pro-inflammatory cytokines. Due to its adverse effects on the liver, close and frequent follow-up of liver bioparameters during favipiravir therapy would be beneficial for predicting the occurrence of complications.

ORCID iDs

Sami Bilici  <https://orcid.org/0000-0003-1076-1447>
 Durdu Altuner  <https://orcid.org/0000-0002-5756-3459>
 Zeynep Suleyman  <https://orcid.org/0000-0003-0128-7990>
 Seval Bulut  <https://orcid.org/0000-0003-4992-1241>
 Cengiz Sarigul  <https://orcid.org/0000-0001-8826-5502>
 Mine Gulaboglu  <https://orcid.org/0000-0002-3248-1502>
 Fikret Altindag  <https://orcid.org/0000-0002-7085-623X>
 Adalet Ozcicek  <https://orcid.org/0000-0003-3029-4524>
 Cebrail Gursul  <https://orcid.org/0000-0001-6521-6169>
 Halis Suleyman  <https://orcid.org/0000-0002-9239-4099>

References

- Drugs and Lactation Database (LactMed). Favipiravir. CAS:259793-96-9. 2022. <https://www.ncbi.nlm.nih.gov/books/NBK556878/>. Accessed September 21, 2022.
- García-Lledó A, Gómez-Pavón J, González del Castillo J, et al. Pharmacological treatment of COVID-19: An opinion paper. *Rev Esp Quimioter.* 2022;35(2):115–130. doi:10.37201/req/158.2021
- Smyk JM, Majewska A. Favipiravir in the battle with respiratory viruses. *Mini Rev Med Chem.* 2022;22(17):2224–2236. doi:10.2174/1389557522666220218122744
- Furuta Y, Gowen BB, Takahashi K, Shiraki K, Smeed DF, Barnard DL. Favipiravir (T-705), a novel viral RNA polymerase inhibitor. *Antiviral Res.* 2013;100(2):446–454. doi:10.1016/j.antiviral.2013.09.015
- Batiha GES, Moubarak M, Shaheen HM, et al. Favipiravir in SARS-CoV-2 infection: Is it worth it? *Comb Chem High Throughput Screen.* 2022;25(14):2413–2428. doi:10.2174/1386207325666220414111840
- Łagocka R, Dziedziejko V, Kłos P, Pawlik A. Favipiravir in therapy of viral infections. *J Clin Med.* 2021;10(2):273. doi:10.3390/jcm10020273
- Beigel JH, Tomashek KM, Dodd LE, et al. Remdesivir for the treatment of Covid-19: Final report. *N Engl J Med.* 2020;383(19):1813–1826. doi:10.1056/NEJMoa2007764
- Mentré F, Taburet AM, Guedj J, et al. Dose regimen of favipiravir for Ebola virus disease. *Lancet Infect Dis.* 2015;15(2):150–151. doi:10.1016/S1473-3099(14)71047-3
- Sissoko D, Laouenan C, Folkesson E, et al. Experimental treatment with favipiravir for Ebola virus disease (the JIKI Trial): A historically controlled, single-arm proof-of-concept trial in Guinea. *PLoS Med.* 2016;13(3):e1001967. doi:10.1371/journal.pmed.1001967
- Pilkington V, Pepperrell T, Hill A. A review of the safety of favipiravir: A potential treatment in the COVID-19 pandemic? *J Virus Erad.* 2020;6(2):45–51. doi:10.1016/S2055-6640(20)30016-9
- Chen C, Zhang Y, Huang J, et al. Favipiravir versus arbidol for clinical recovery rate in moderate and severe adult COVID-19 patients: A prospective, multicenter, open-label, randomized controlled clinical trial. *Front Pharmacol.* 2021;12:683296. doi:10.3389/fphar.2021.683296
- Dogan E, Alkan-Çeviker S, Vurucu S, et al. Investigation of the frequency of adverse effects in patients treated with favipiravir as SARS-CoV-2 treatment. *Klimik Derg.* 2021;34(2):95–98. doi:10.36519/kd.2021.3563
- Kumar P, Kulkarni A, Sharma M, Rao PN, Reddy DN. Favipiravir-induced liver injury in patients with coronavirus disease 2019. *J Clin Transl Hepatol.* 2021;9(2):276–278. doi:10.14218/JCTH.2021.00011
- Japanese Ministry of Health, Labour and Welfare. Director of Evaluation and Licensing Division, Pharmaceutical and Food Safety Bureau. Handling of marketing application for combination products. October 24, 2014. <https://www.pmda.go.jp/files/000153158.pdf>. Accessed October 10, 2021.
- Kara A, Yakut S, Caglayan C, Atçalı T, Ulucan A, Kandemir FM. Evaluation of the toxicological effects of favipiravir (T-705) on liver and kidney in rats: Biochemical and histopathological approach [published online as ahead of print on April 21, 2022]. *Drug Chem Toxicol.* 2022. doi:10.1080/01480545.2022.2066116
- Góth L. A simple method for determination of serum catalase activity and revision of reference range. *Clin Chim Acta.* 1991;196(2–3):143–151. doi:10.1016/0009-8981(91)90067-M
- Bradford MM. A rapid and sensitive method for the quantitation of microgram quantities of protein utilizing the principle of protein-dye binding. *Anal Biochem.* 1976;72(1–2):248–254. doi:10.1016/0003-2697(76)90527-3
- Hassanipour S, Arab-Zozani M, Amani B, Heidarzad F, Fathalipour M, Martinez-de-Hoyo R. Addendum: The efficacy and safety of favipiravir in treatment of COVID-19: A systematic review and meta-analysis of clinical trials. *Sci Rep.* 2022;12(1):1996. doi:10.1038/s41598-022-05835-2
- Özcan O, Erdal H, Çakırca G, Yönden Z. Oxidative stress and its impacts on intracellular lipids, proteins and DNA [in Turkish]. *J Clin Exp Invest.* 2015;6(3):383–389. doi:10.5799/ahinjs.01.2015.03.0545
- Niki E, Yoshida Y, Saito Y, Noguchi N. Lipid peroxidation: Mechanisms, inhibition, and biological effects. *Biochem Biophys Res Commun.* 2005;338(1):668–676. doi:10.1016/j.bbrc.2005.08.072
- Mittal M, Siddiqui MR, Tran K, Reddy SP, Malik AB. Reactive oxygen species in inflammation and tissue injury. *Antioxid Redox Signal.* 2014;20(7):1126–1167. doi:10.1089/ars.2012.5149
- Jakubczyk K, Dec K, Kałduńska J, Kawczuga D, Kochman J, Janda K. Reactive oxygen species: Sources, functions, oxidative damage. *Pol Merkur Lek.* 2020;48(284):124–127. PMID:32352946.
- Poli G, Albano E, Dianzani MU. The role of lipid peroxidation in liver damage. *Chem Phys Lipids.* 1987;45(2–4):117–142. doi:10.1016/0009-3084(87)90063-6
- Kurt N, Gunes O, Suleyman B, Bakan N. The effect of taxifolin on high-dose-cisplatin-induced oxidative liver injury in rats. *Adv Clin Exp Med.* 2021;30(10):1025–1030. doi:10.17219/acem/138318
- Owen JB, Butterfield DA. Measurement of oxidized/reduced glutathione ratio. *Methods Mol Biol.* 2010;648:269–277. doi:10.1007/978-1-60761-756-3_18
- Kisaoglu A, Borekci B, Yapca OE, Bilen H, Suleyman H. Tissue damage and oxidant/antioxidant balance. *Eurasian J Med.* 2013;45(1):47–49. doi:10.5152/eajm.2013.08
- Gunaydin-Akyildiz A, Aksoy N, Boran T, İlhan EN, Özhan G. Favipiravir induces oxidative stress and genotoxicity in cardiac and skin cells. *Toxicol Lett.* 2022;371:9–16. doi:10.1016/j.toxlet.2022.09.011
- Ji Y, Gao Y, Chen H, Yin Y, Zhang W. Indole-3-acetic acid alleviates nonalcoholic fatty liver disease in mice via attenuation of hepatic lipogenesis, and oxidative and inflammatory stress. *Nutrients.* 2019;11(9):2062. doi:10.3390/nu11092062
- Urso ML, Clarkson PM. Oxidative stress, exercise, and antioxidant supplementation. *Toxicology.* 2003;189(1–2):41–54. doi:10.1016/S0300-483X(03)00151-3
- Zhongyi S, Sai Z, Chao L, Jiwei T. Effects of nuclear factor kappa B signaling pathway in human intervertebral disc degeneration. *Spine (Phila Pa 1976).* 2015;40(4):224–232. doi:10.1097/BRS.0000000000000733
- Yılmaz I, Akalan H, Sirin Yasar D, Karaarslan N, Ozbek H, Ates O. Is favipiravir a potential therapeutic agent in the treatment of intervertebral disc degeneration by suppressing autophagy and apoptosis? *Turk Neurosurg.* 2022;32(4):680–687. doi:10.5137/1019-5149.JTN.38252-22.3
- Zhao H, Zhu Q, Zhang C, et al. Tocilizumab combined with favipiravir in the treatment of COVID-19: A multicenter trial in a small sample size. *Biomed Pharmacother.* 2021;133:110825. doi:10.1016/j.biopha.2020.110825
- Lala V, Goyal A, Bansal P, Minter D. Liver function tests. In: *StatPearls*. Treasure Island, USA: StatPearls Publishing; 2021. <https://www.ncbi.nlm.nih.gov/books/NBK482489/>
- Bayram M, Yildirim O, Ozmen RS, et al. Elevation of serum transaminase levels due to favipiravir use in the treatment of COVID-19. *Cureus.* 2021;13(9):e18166. doi:10.7759/cureus.18166
- Izci Cetinkaya F, Karagoz H, Yildiz O. Comparison of liver safety of favipiravir and hydroxychloroquine in COVID-19 treatment. *Klimik Dergisi.* 2020;33(3):235–240. doi:10.5152/kd.2020.49
- Farzanegi P, Dana A, Ebrahimpoor Z, Asadi M, Azarbayjani MA. Mechanisms of beneficial effects of exercise training on non-alcoholic fatty liver disease (NAFLD): Roles of oxidative stress and inflammation. *Eur J Sport Sci.* 2019;19(7):994–1003. doi:10.1080/17461391.2019.1571114
- Gursul C, Ozcicek A, Ozkaraca M, et al. Amelioration of oxidative damage parameters by carvacrol on methanol-induced liver injury in rats. *Exp Anim.* 2022;71(2):224–230. doi:10.1538/expanim.21-0143

The time-dependent adverse effects of a high-fat diet on sperm parameters

Xiangyu Qi^{D,1–4}, Qingbo Guan^{E,1–4}, Wenjing Zhang^{B,1–4}, Xinshuang Huang^{C,1–5}, Chunxiao Yu^{F,1–4}

¹ Department of Endocrinology, Shandong Provincial Hospital Affiliated to Shandong First Medical University, Jinan, China

² Shandong Key Laboratory of Endocrinology and Lipid Metabolism, Jinan, China

³ Shandong Institute of Endocrine and Metabolic Diseases, Jinan, China

⁴ Shandong Engineering Laboratory of Prevention and Control for Endocrine and Metabolic Diseases, Jinan, China

⁵ Shandong University of Traditional Chinese Medicine, Jinan, China

A – research concept and design; B – collection and/or assembly of data; C – data analysis and interpretation;

D – writing the article; E – critical revision of the article; F – final approval of the article

Advances in Clinical and Experimental Medicine, ISSN 1899–5276 (print), ISSN 2451–2680 (online)

Adv Clin Exp Med. 2023;32(8):889–900

Address for correspondence

Qingbo Guan

E-mail: doctorguanqingbo@163.com

Funding sources

This work was supported by the National Natural Science Foundation of China (grants No. 82270839, 81770860 and 81641030) and the Key Research and Development Plan of Shandong Province (grant No. 2017CXGC1214).

Conflict of interest

None declared

Received on July 22, 2022

Reviewed on October 24, 2022

Accepted on January 8, 2023

Published online on March 30, 2023

Cite as

Qi X, Guan Q, Zhang W, Huang X, Yu C. The time-dependent adverse effects of a high-fat diet on sperm parameters.

Adv Clin Exp Med. 2023;32(8):889–900.

doi:10.17219/acem/159090

DOI

10.17219/acem/159090

Copyright

Copyright by Author(s)

This is an article distributed under the terms of the Creative Commons Attribution 3.0 Unported (CC BY 3.0)

(<https://creativecommons.org/licenses/by/3.0/>)

Abstract

Background. Studies indicate a relationship between a high-fat diet (HFD) and sperm quality. However, the time-dependent adverse effects of a HFD on sperm parameters and the underlying mechanisms remain unclear.

Objectives. The present study was designed to determine the effects of a HFD on sperm quality at various time points in order to assess whether a HFD causes cumulative damage to sperm.

Materials and methods. Male C57BL/6 mice were fed a normal diet (the ND group) or a HFD (the HFD group) for 16, 30 or 42 weeks ($n = 6$ for each group). Body weight, lipid profile, sperm parameters, testicular morphology, and testicular oxidative stress levels were evaluated alongside the proliferation, DNA damage and rate of germ cell apoptosis.

Results. Sperm quality was reduced in HFD-fed animals in a time-dependent manner, which was demonstrated by a decline in sperm density, motility and progressive motility. Further analysis showed a progressive deterioration of the testicular histoarchitecture of HFD-fed mice, which was accompanied by a decrease in DEAD-box helicase 4 (*DDX4*) expression and superoxide dismutase (SOD) levels, increased malondialdehyde (MDA) levels and gamma-H2A histone family member X (*γ-H2AX*) expression, and increased apoptosis of germ cells.

Conclusions. These findings demonstrate that a HFD exerted adverse effects on sperm quality, and the deteriorating effect was progressive with long-term feeding. The inhibited proliferation and apoptosis of germ cells, and the increased oxidative stress levels and DNA damage may be the underlying mechanisms.

Key words: adverse effects, high-fat diet, sperm parameters, time-dependent manner

Background

With the rapid development of society, an unhealthy high-fat diet (HFD) has become a common dietary problem.¹ In both clinical and animal studies, HFD leads to the occurrence and development of obesity and a series of diseases, including diabetes and cardiovascular disease (CVD).^{2–4} Moreover, the adverse effects of a HFD on the quality of male sperm are gradually being recognized.^{5–7} Numerous studies have demonstrated that HFD results in a reduced sperm quality.⁸ Furthermore, a clinical study showed that a diet containing palmitic acid (PA) may contribute to asthenozoospermia in males.⁹ Animal studies have reported a decreasing trend in sperm motility in animals fed a HFD.^{10,11} However, whether the HFD has time-dependent adverse effects on sperm quality remains controversial. Fernandez et al. found that consuming a HFD for 16 or 45 weeks did not impair sperm quality, but only reduced the number of ejaculations.¹² Moreover, recent studies found an increase in sperm concentration in mice treated with a HFD for 30 weeks.^{11,12} These conflicting findings suggest that a dynamic analysis of the cumulative effects of a HFD is required to understand the impact of a HFD on sperm quality.

The molecular mechanisms of HFD-induced sperm alterations remain uncharted to a large extent. Numerous studies have demonstrated a link between the inhibition of the proliferation of germ cells and the cessation of spermatogenesis. It has also been reported that DEAD-box helicase 4 (*DDX4*) has a vital role in the proliferation of germ cells and that the expression of *DDX4* decreased in the testes of mice and rats.^{13,14} In addition, a previous report provided evidence that a HFD may decrease fertility through oxidative stress.¹³ A recent study reported that oxidative stress led to DNA double-strand breaks (DSBs), which can be detected as a phosphorylation of gamma-H2A histone family member X (γ -*H2AX*) foci in cells.^{15,16} If DSBs are not correctly repaired, γ -*H2AX* will be expressed continuously and germ cells will gradually undergo apoptosis.^{17,18} However, the effects of a HFD on the expression of γ -*H2AX* and the proliferation of germ cells remain unclear.

Objectives

The aim of the study was to assess whether a HFD alters sperm quality, and whether a HFD could be the cause of cumulative sperm damage, as well as to pinpoint the underlying mechanisms. The present study investigated alterations in murine sperm quality induced by a HFD over various timeframes.

Materials and methods

Animals and diets

This study was approved by the Animal Ethics Committee of Shandong Provincial Hospital (Jinan, China; approval No. NSFC: NO.2019-243 issued on February 22, 2019). Male 8-week-old C57BL/6 mice ($n = 32$) were purchased from the Vital River Laboratory Animal Technology Co. Ltd. (Beijing, China). The animals were adapted to a 12-hour light/dark cycle at 22–25°C. They were randomly split into 2 groups ($n = 24$ per group) and were fed a normal diet (ND) containing 10 kcal% fat (D12450B; Research Diets, New Brunswick, USA)¹⁹ or a HFD containing 60 kcal% fat (D12492; Research Diets)²⁰ for 16, 30 or 42 weeks ($n = 6$ for each group at each different time). Mice from each group were euthanized at the end of 16, 30 and 42 weeks of diet intervention.

After 8-hour fasting, all mice were anesthetized with pentobarbital sodium and weighed. Then, sperm was collected immediately from the epididymal cauda. Blood samples were drawn from the retro-orbital vein and stored at –80°C, and the testes and epididymal fat were separated and weighed. The testis coefficient was calculated by dividing the weight of the testis by body weight. The testes were rapidly preserved in liquid nitrogen for Oil Red O staining and protein analysis, or in modified Davidson's fluid (mDF) for morphological analysis.^{21,22}

Measurement of lipid profile

The serum levels of glucose (GLU), low-density lipoprotein cholesterol (LDL-C), total cholesterol (TC), and triglycerides (TG) were evaluated using Mindray Automatic biochemical analyzer BS-830 (Mindray Bio-Medical Electronics Co., Ltd., Shenzhen, China).^{21,22}

Detection of sperm parameters

The epididymal cauda of the mice were transferred to a Petri dish containing HyClone™ Medium 199 (Cytiva, Marlborough, USA) and 0.5% bovine serum albumin (BSA). Using sharp surgical scissors, multiple incisions were made in the epididymal cauda to facilitate sperm suspension in the culture medium. Suspensions were then placed in an incubator (37°C, 5% CO₂) for 5 min to maximize sperm drainage. Subsequently, 10 μ L of diluted sperm suspension (1:20) was transferred to a sperm counting plate of the computer-assisted semen analyzer (CASA) IVOS II (Hamilton-Thorne Bioscience, Beverly, USA) for the automated analysis.²² This analysis included sperm concentration and progressive and nonprogressive motility, as well as characterizing movement as rapid, moderate or static. Sperm velocity was also assessed, including average path velocity (VAP), linear velocity (VSL) and curvilinear velocity (VCL).

Hematoxylin and eosin staining

Testis samples that had been fixed in mDF for 24 h were embedded in paraffin, and then sectioned at a thickness of 5 μm . Sections were deparaffinized, rehydrated, stained with hematoxylin and eosin (H&E), and then scanned with the Aperio VERSA light microscopy scanning system (Leica Biosystems, Richmond, USA).²² Damage to seminiferous tubules and spermatogenesis were evaluated according to the Cosentino's scoring system: 1. Normal testicular architecture with an orderly arrangement of germinal cells; 2. Injury showed less orderly, non-cohesive germinal cells and closely packed seminiferous tubules; 3. Injury exhibited disordered sloughed germinal cells, with reduced size of pyknotic nuclei and less distinct seminiferous tubule borders; 4. Injury exhibited seminiferous tubules that were closely packed with coagulative necrosis of the germinal cells.

Oil Red O staining

Frozen testis sections (7- μm thick) were sunk in 95% alcohol for 15 s, stained with Oil Red O (Beyotime Biotechnology, Shanghai, China) for 15 min in the dark, and counterstained with hematoxylin for 3 min.²² The specimens were then imaged using the Aperio VERSA light microscopy scanning system (Leica Biosystems).

Malondialdehyde and superoxide dismutase measurements

The malondialdehyde (MDA) content (STA-330; Cell Biolabs Inc., San Diego, USA) and superoxide dismutase (SOD) levels (S0087; Beyotime Biotechnology) of testes were evaluated using commercially available kits (MDA: STA-330; Cell Biolabs Inc.; SOD: S0087; Beyotime Biotechnology) according to the manufacturer's instructions.

Immunofluorescence

Paraffin-embedded testis sections (5- μm thick) were deparaffinized, immersed in citrate buffer antigen retrieval solution and heated in a microwave oven for 20 min. Then, they were cooled for 60 min and incubated in 5% BSA for 60 min at room temperature. Afterward, sections were incubated overnight at 4°C with rabbit polyclonal anti-*DDX4* (ab13840, 1:200) or recombinant anti- γ -*H2AX* (ab81299, 1:200) primary antibodies (Abcam, Cambridge, UK). The negative control was incubated without a primary antibody. On the next day, sections were incubated with a secondary antibody (1:1000; Thermo Fisher Scientific, Waltham, USA). The nuclei were then stained with 4',6-diamidino-2-phenylindole (DAPI).²¹ Images were acquired with a Nikon AX confocal microscope (Nikon Corp., Tokyo, Japan), equipped with a $\times 40$ objective. Images were

merged and processed using Nikon confocal analysis software. For descriptive analyses, each sample was examined at least 3 times.

Terminal deoxynucleotidyl transferase dUTP nick end labeling

Paraffin-embedded testis sections (5- μm thick) were stained using a terminal deoxynucleotidyl transferase dUTP nick end labeling (TUNEL) assay kit (KGA704-1; Keygen Biotech Co., Ltd., Nanjing, China) according to the manufacturer's protocol. The cell nuclei were stained with DAPI and the sections were observed using the Aperio VERSA light microscopy scanning system (Leica Biosystems). Using ImageJ software (National Institutes of Health, Bethesda, USA), the number of TUNEL-positive (TUNEL+) cells/high power field (HPF) was calculated. Each sample was assessed at least 3 times.

Statistical analyses

Outliers were removed by the robust regression followed by outlier identification (ROUT) method, using GraphPad Prism 9 (GraphPad Software Inc., San Diego, USA). Data were analyzed using two-way analysis of variance (ANOVA) followed by the Tukey's post hoc test for the between-diet per period and between-period per diet. A value of $p < 0.05$ was considered statistically significant.

Results

Characterization of mice fed a high-fat diet

To evaluate the effect of a HFD on body weight and metabolic parameters, the relevant values were examined. Throughout the course of the study, body weight, testis weight, testis coefficient, epididymal adipose weight, and TC were significantly higher in the mice fed a HFD compared to the mice fed a ND, at all timepoints (16 weeks (w): $p < 0.05$; 30 w: $p < 0.05$; 42 w: $p < 0.05$). Glucose levels were similar at 16 and 42 weeks and increased at 30 weeks ($p < 0.05$; Fig. 1). Total TG and LDL-C levels were similar between the groups at 16 weeks but increased at 30 weeks ($p < 0.05$) and 42 weeks ($p < 0.05$). Furthermore, the body weight (16 w compared to 42 w: $p < 0.05$), testis coefficient (16 w compared to 42 w: $p < 0.05$), GLU (16 w compared to 30 w: $p < 0.05$; 16 w compared to 42 w: $p < 0.05$; 30 w compared to 42 w: $p < 0.05$), TC (16 w compared to 30 w: $p < 0.05$; 16 w compared to 42 w: $p < 0.05$), and LDL-C (16 w compared to 42 w: $p < 0.05$; 30 w compared to 42 w: $p < 0.05$) were elevated significantly in a time-dependent manner in mice fed a HFD, while only GLU (16 w compared to 42 w: $p < 0.05$; 30 w compared to 42 w: $p < 0.05$) and TC (30 w compared to 42 w: $p < 0.05$) were elevated over time in mice fed ND. These results indicated that

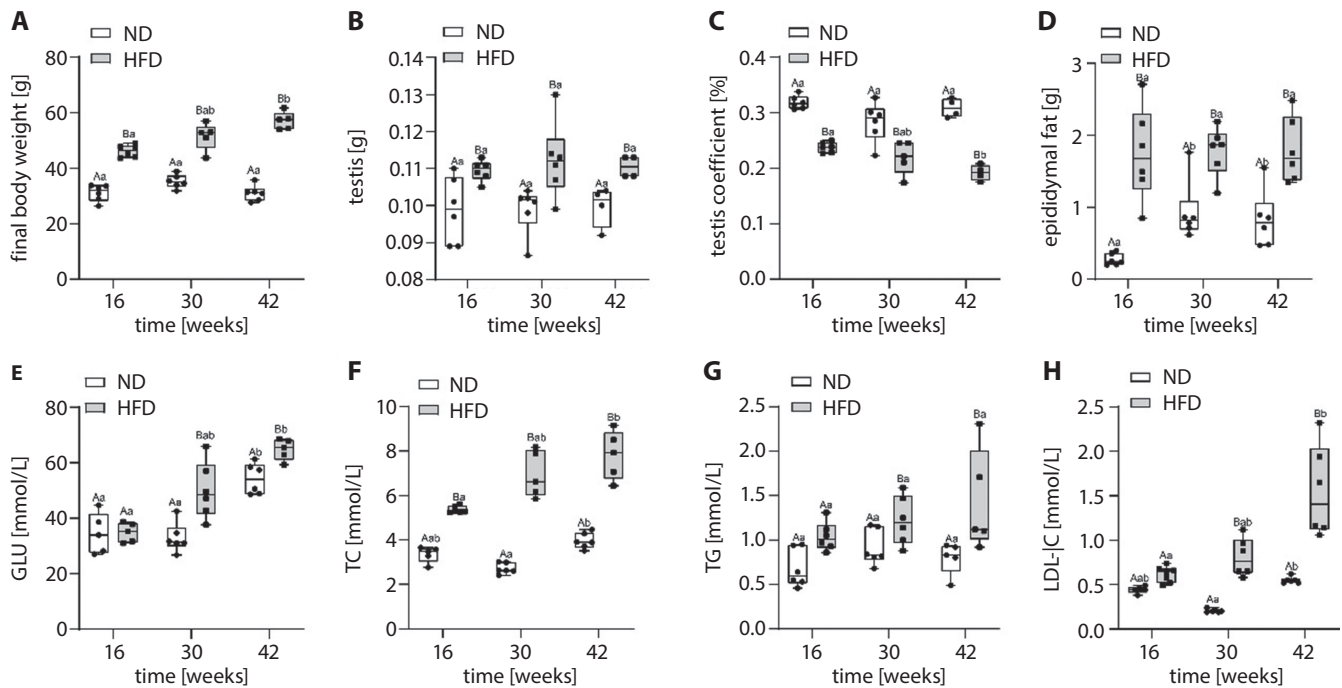


Fig. 1. General conditions induced by a high-fat diet (HFD). Comparison of body weight between the normal diet (ND) and HFD groups (A). Testicular weight (B), testis coefficient (C) and epididymal fat (D) in the ND group and the HFD group ($n=6$ for each group). Comparison of the levels of serum glucose (GLU) (E), total serum cholesterol (TC) (F), triglycerides (TG) (G), and low-density lipoprotein cholesterol (LDL-C) (H), between the ND and HFD groups ($n=6$ for each group). The capital letters refer to the comparison between the ND and HFD groups at the same feeding time, while lowercase letters refer to the comparisons between different feeding times. Different letters indicate a significant difference ($p < 0.05$)

the high-fat model was successfully established. The high-fat model tended to have more metabolic disorders the longer the mice were fed a HFD.

Alteration of sperm parameters induced by a high-fat diet

To confirm the effects of a HFD on sperm quality, sperm parameters in the epididymal cauda were evaluated with a CASA after different feeding intervals. The CASA evaluation revealed that striking changes occurred in the sperm of all of the HFD groups compared to the control groups (Fig. 2). It was found that 16 weeks on a HFD did not cause any significant change in the sperm parameters, although sperm concentration was reduced by approx. 20%. Continuous feeding with a HFD for 30 and 42 weeks caused increasing sperm dysfunction, including a lowered sperm concentration and decreased motility. Indeed, there was a significant decrease in the progressive motility of sperm at 42 weeks ($p < 0.05$). Furthermore, when animals fed the HFD for different periods were compared, a time-dependent impairment was found for all parameters except for VAP, VSL and VCL, and all of the damaging changes were statistically significant (sperm density: 16 w compared to 42 w: $p < 0.05$; static sperm: 30 w compared to 42 w: $p < 0.05$; sperm motility, rapid sperm and moderate sperm: 16 w compared to 42 w: $p < 0.05$; sperm progressive motility: 16 w compared to 30 w: $p < 0.05$, and 16 w

compared to 42 w: $p < 0.05$). Conversely, there was only a time-dependent difference in sperm concentration in the ND groups (16 w compared to 42 w: $p < 0.05$; 30 w compared to 42 w: $p < 0.05$), and there were no differences in sperm parameters related to motility. These results demonstrate that sperm parameters were adversely affected by a HFD and these adverse effects were most severe in the mice fed a HFD for 42 weeks.

Alterations of testicular histoarchitecture induced by a high-fat diet

To investigate changes in the seminiferous tubules after HFD exposure, testicular morphology was analyzed using H&E staining for the 3 feeding intervals (Fig. 3A). Normal histological features were observed in all 3 ND groups (Fig. 3A). Conversely, seminiferous tubules were loosely arranged in the mice fed a HFD for 16 weeks. The changes in histoarchitecture were more evident in the 30-week group, with distinct structural disorganization and increased vacuolization in both seminiferous tubules and interstitial spaces. Drastic structural alterations, characterized by obvious tubular degeneration and prominent vacuolization, were noticed after 42 weeks. Figure 3B shows the Cosentino's scores obtained after the histopathological examination of each group. There were significant increases in both scores in the HFD mice after 30 and 42 weeks compared to the ND group (30 w: $p < 0.05$; 42 w: $p < 0.05$). Furthermore, the scores

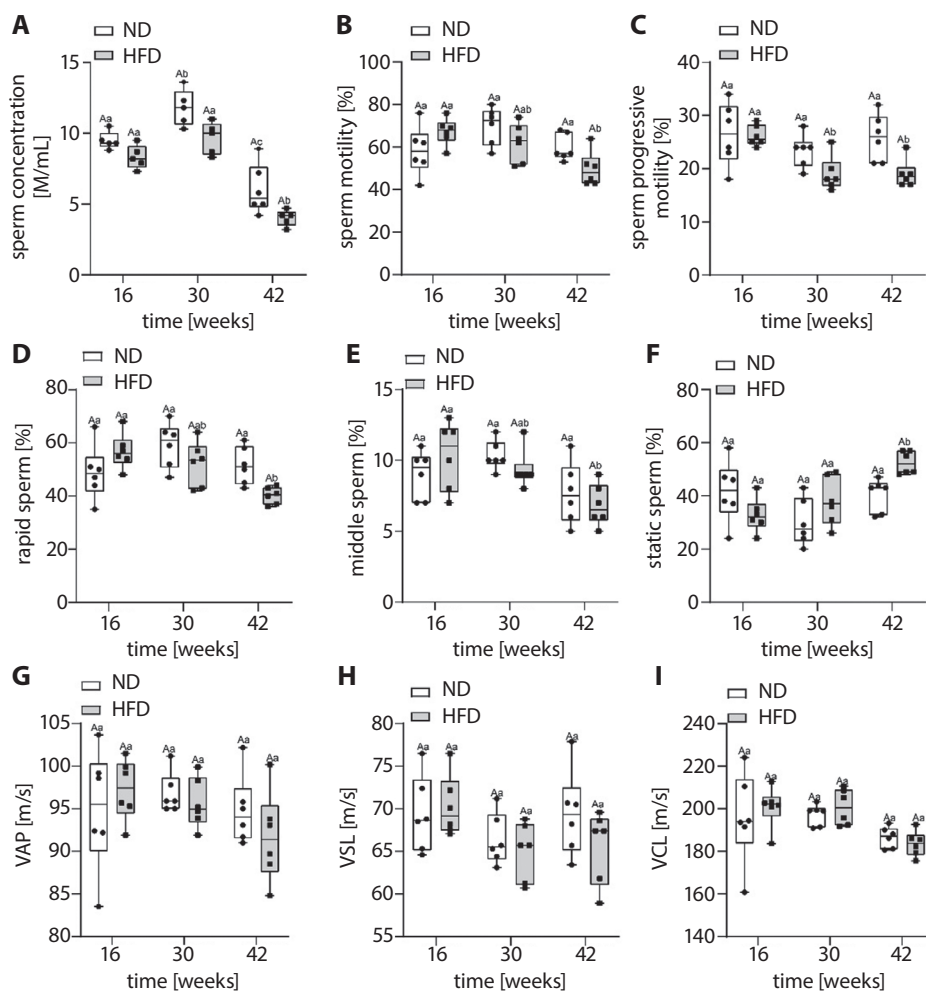


Fig. 2. Sperm parameter changes induced by a high-fat diet (HFD). Comparison of sperm concentration (A), sperm motility (B), sperm progressive motility (C), rapid sperm (D), moderate sperm (E), static sperm (F), average path velocity (VAP) (G), linear velocity (VSL) (H), and curvilinear velocity (VCL) (I) between the normal diet (ND) and HFD groups (n = 6 for each group). The capital letters refer to comparisons between ND and HFD groups at the same feeding time, while lowercase letters refer to comparisons between different feeding times. Different letters indicate a significant difference ($p < 0.05$)

increased in a time-dependent manner in mice fed a HFD (16 w compared to 30 w: $p < 0.05$; 16 w compared to 42 w: $p < 0.05$).

To evaluate ectopic lipid deposition in the testes of mice fed a HFD, testicular morphology was analyzed using Oil Red O staining at 16, 30 and 42 weeks (Fig. 3C). Ectopic lipid deposition was increased in all HFD groups compared with the ND groups (Fig. 3B). Interestingly, while frozen sections from the group fed a ND exhibited progressive ectopic lipid deposition in the testes with time, a more obvious progressive deposition was observed with prolonged time in the testes of the mice fed a HFD. These results indicate that the short-term influence of a HFD on testicular histoarchitecture may not be obvious; however, long-term effects may mean distinct damage.

High-fat diet inhibited the proliferation of germ cells

While conventional sperm analysis can determine the sperm quality to a certain extent, it may not display potential defects such as the inhibition of proliferation. To evaluate the proliferation of germ cells, *DDX4* was

detected in mouse testes by means of immunofluorescent staining (Fig. 4). Compared with the corresponding ND groups, a considerable decrease in the number of *DDX4*-positive cells was observed in all of the HFD groups. Interestingly, in the HFD groups, *DDX4* decreased with time and reached a minimum expression at 42 weeks. These findings highlight the deleterious role a HFD has in testicular injury, which most likely occurred through the inhibition of the proliferation of germ cells, and this inhibition worsened with time.

High-fat diet exposure induced oxidative stress in testes

To evaluate whether a HFD influences sperm quality by aggravating oxidative stress, the testicular oxidative stress-related index was assessed, and the levels of the antioxidative enzyme SOD and pro-oxidative by-product MDA were determined (Fig. 5A,B). At the end of the experimental procedure, the MDA concentration tended to increase while the SOD concentration tended to decrease in all HFD groups. However, none of the changes were significantly different, except for the MDA concentration at 42 weeks ($p < 0.05$). The MDA concentration

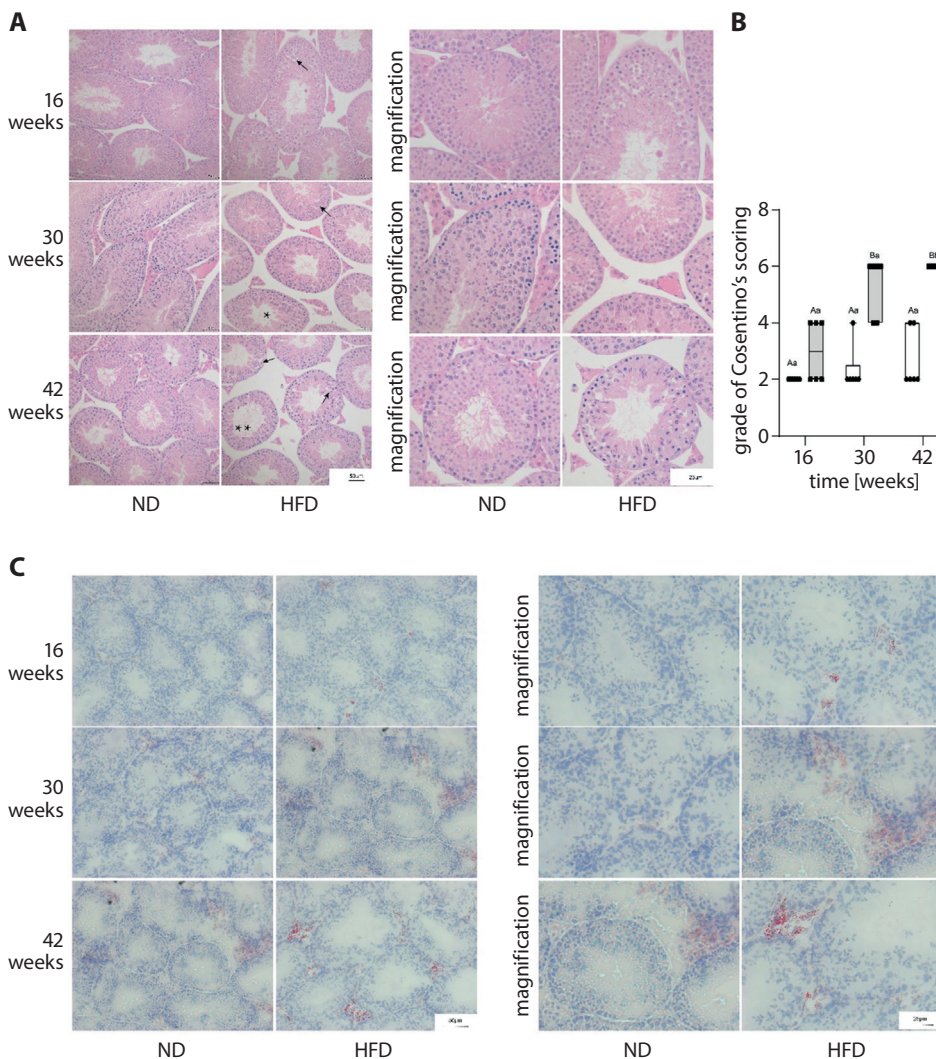


Fig. 3. Testicular morphological changes and lipid deposition induced by a high-fat diet (HFD). A. Representative pictures of testicular hematoxylin and eosin (H&E) staining ($n=3$ for each group); B. Grade of Cosentino's scoring ($n=3$ for each group, each sample was assessed at least 2 times); C. Representative pictures of testicular Oil Red O staining ($n=3$ for each group). The capital letters refer to comparisons between normal diet (ND) and HFD groups at the same feeding time, while lowercase letters refer to comparisons between different feeding times. Different letters indicate a significant difference ($p < 0.05$)

* partial atrophy; ** complete atrophy; ← vacuolization.

increased significantly with time (16 w compared to 42 w: $p < 0.05$), and the SOD concentration tended to decrease over time in the HFD group. The results indicate that the level of testicular oxidative stress in obese mice increased, which may result in a reduced sperm quality.

High-fat diet exposure induced the apoptosis of germ cells

To further assess whether the decreased epididymal sperm quality was a result of germ cell apoptosis, TUNEL staining was performed on the mouse testes (Fig. 5C,D). A considerable increase in the number of TUNEL+ cells was observed at 30 and 42 weeks (30 w: $p < 0.05$; 42 w: $p < 0.05$). When animals fed the HFD for different periods were compared, a time-dependent increase in the number of TUNEL+ cells was found (16 w compared to 30 w: $p < 0.05$; 16 w compared to 42 w: $p < 0.05$). These findings demonstrate the deleterious role of a HFD in inducing injury to the testes through the initiation of apoptosis in germ cells, and this activation increases with time.

High-fat diet exposure induced DNA damage in mouse testes

To detect DNA damage in the testes, the expression of γ -H2AX was evaluated using immunofluorescence. As shown in Fig. 6, the HFD groups had a significantly higher γ -H2AX expression in comparison with the ND groups. More interestingly, the expression of γ -H2AX increased in a time-dependent manner for both the ND groups and the HFD groups. These results indicate that DNA damage was induced by the HFD, which may be an underlying mechanism of the decreased sperm parameters.

Discussion

The relationship between a HFD and HFD-related disorders such as obesity, CVD and cancers has been recognized for a long time.¹⁴ Recently, a great deal of evidence has come to light showing that a HFD can also exert a profound impact on sperm quality. However, the cumulative effects

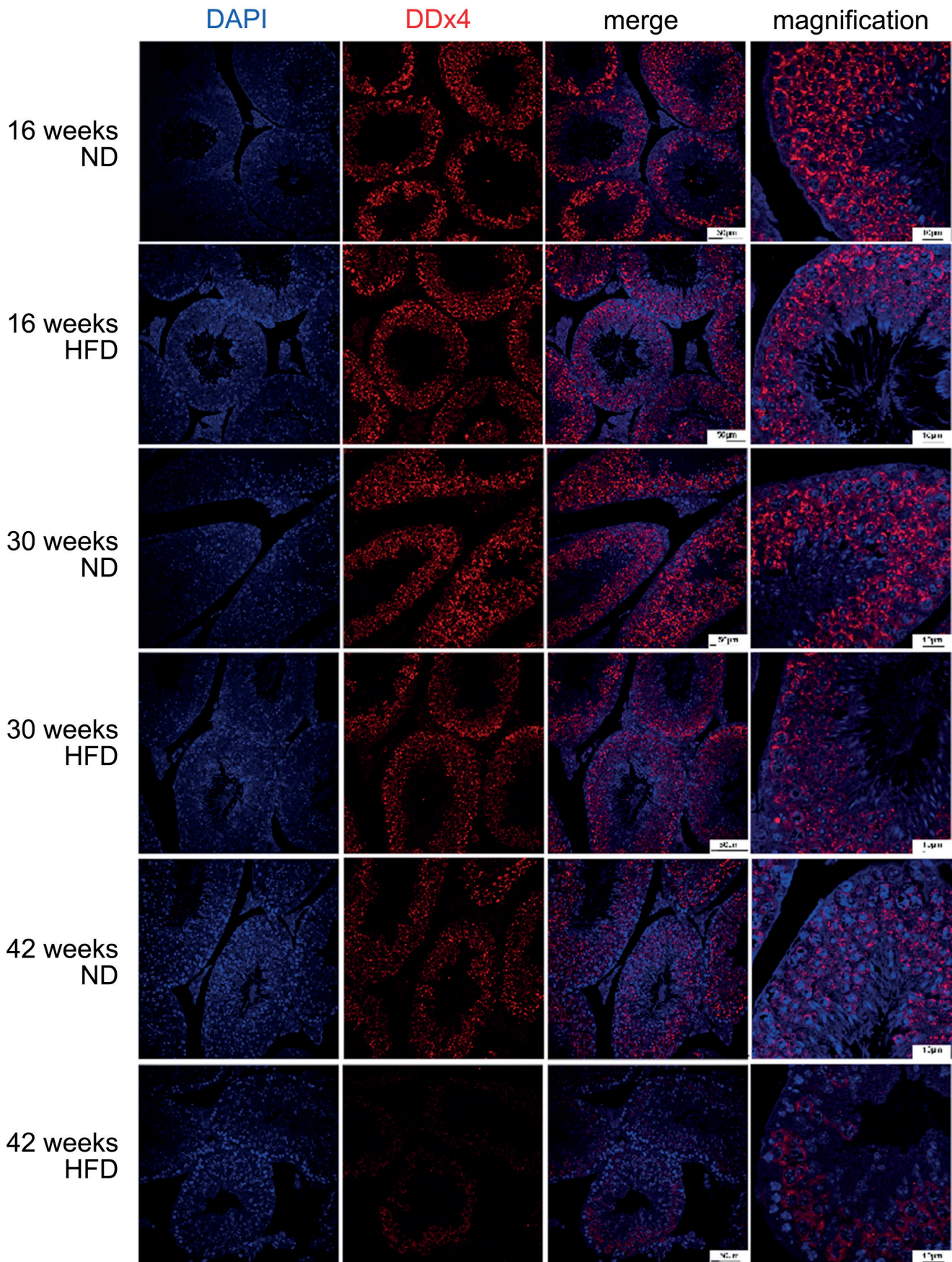


Fig. 4. Inhibition of germ cell proliferation induced with a HFD. Representative images of DEAD-box helicase 4 (*DDX4*) staining in the testes of mice fed a HFD for 8, 16 or 42 weeks (n = 3 for each group)

ND – normal diet; HFD – high-fat diet.

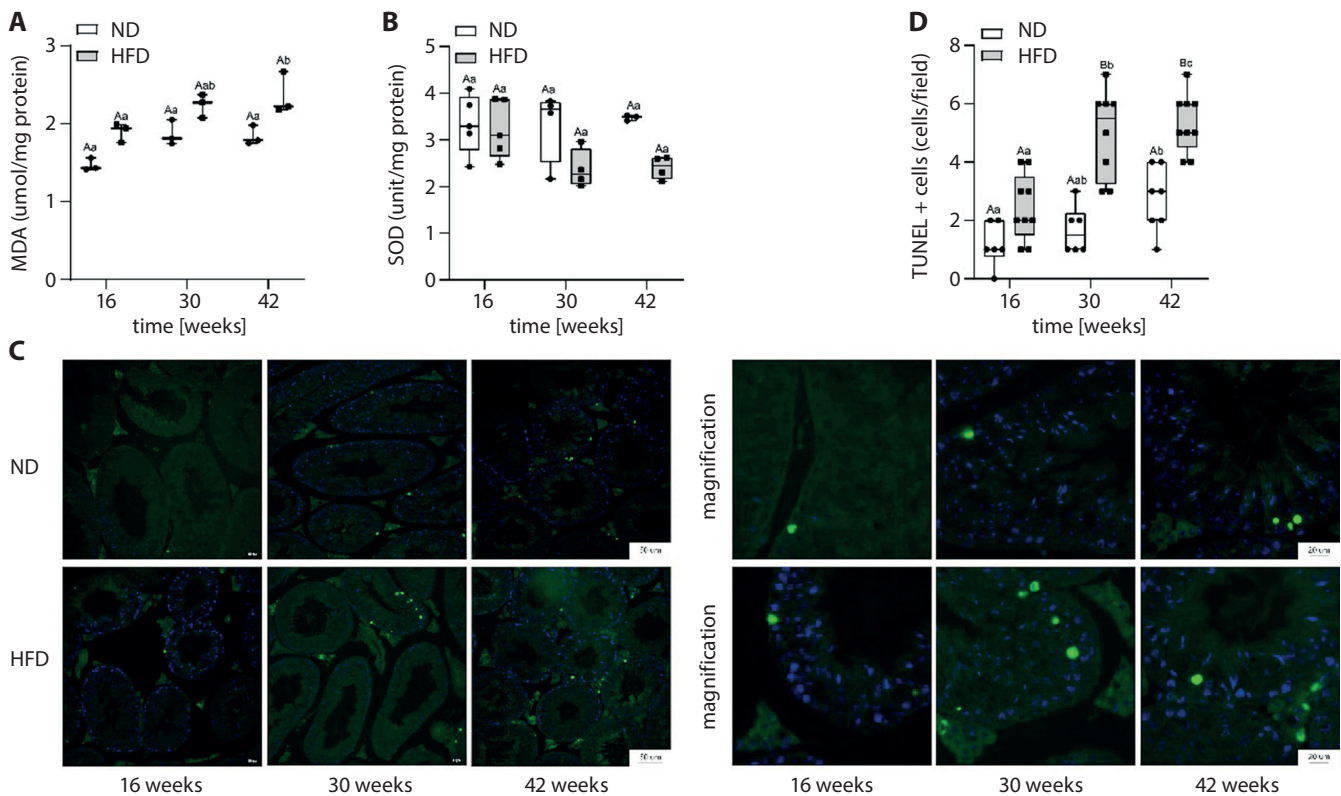


Fig. 5. Oxidative stress and apoptosis induced with a high-fat diet (HFD). Malondialdehyde (MDA) concentration (A) and testicular superoxide dismutase (SOD) concentration (B) ($n=3/4$ for each group); C. Representative pictures of terminal deoxynucleotidyl transferase dUTP nick end labeling (TUNEL) staining; D. TUNEL-positive germ cells/high power field ($n=3$ for each group, each sample was assessed at least 2 times). The capital letters refer to comparisons between normal diet (ND) and HFD groups at the same feeding time, while lowercase letters refer to comparisons between different feeding times. Different letters indicate a significant difference ($p < 0.05$)

of a HFD on sperm quality are controversial and there is currently a lack of in-depth investigations in this area. In this study, by developing a HFD-related model, it was demonstrated that a HFD reduced sperm quality. Also, HFD-induced sperm damage may be cumulative and occur in a time-dependent manner. The inhibited proliferation of germ cells, increased oxidative stress levels in the testes, increased DNA damage, and the promotion of apoptosis may be the underlying mechanisms.

In this study, mice exposed to a HFD for 16, 30 or 42 weeks experienced weight gain, testicular weight gain and epididymal adipose weight gain. Abnormal lipid and GLU metabolism were also observed at different intervals in the HFD group, including increased GLU, TC, TG, and LDL-C. These results demonstrate that the HFD-related model was successfully established. Moreover, body weight, GLU, TC, and LDL-C increased in a time-dependent manner in the HFD groups, while only epididymal fat deposits and GLU increased in a time-dependent manner in the ND groups.

The ability of sperm to fertilize the ovum partly depends on its concentration and kinematics, both of which affect the fertility of males from a wide range of animals, such as fish, birds and mammals.^{23,24} Therefore, the concentration of sperm present and the kinematic parameters, including sperm motility, sperm progressive motility, and

the VCL, VSL and VAP in the epididymal cauda are vital indicators of sperm quality. Furthermore, a series of studies have shown that sperm motility and sperm progressive motility signify the function of mitochondria and energy status, which have been associated with fertility.^{25,26} Studies have also shown that the VCL reflects the high-energy state of sperm and hyperactivated motility, which are essential for successful fertilization.^{27,28} However, to a large extent, the short-term and cumulative effects of a HFD on these sperm parameters are controversial. A previous study found that sperm concentration tended to reduce after 8 weeks of a HFD,²⁹ while another study reported that sperm quality was not impaired in mice fed a HFD for 16 or 45 weeks. Furthermore, a recent study demonstrated that feeding a HFD from 12 to 24 weeks did not influence any of the motility parameters or the concentration of sperm in the epididymal cauda.³⁰

The current study aimed to reveal the short-term and cumulative effects of a HFD on sperm parameters. There was a trend of decreased sperm concentration after 42 weeks of exposure to a HFD, which is consistent with our previous work. When sperm motility parameters were compared between different time points, the differences were found in the mice fed a HFD but not in the mice fed a ND. This may not only be due to the aging process but also due to the reproductive toxicity induced by the HFD. These

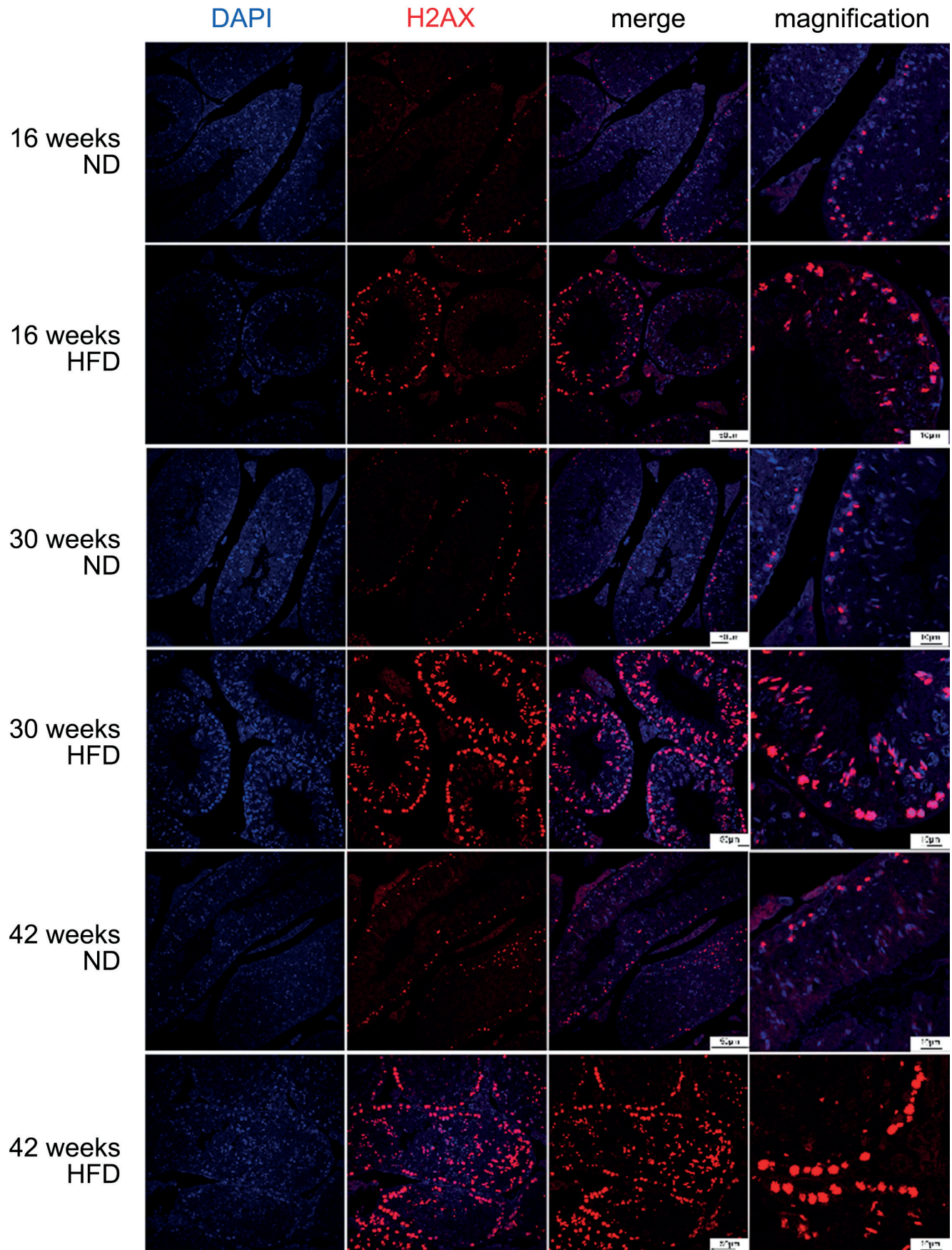


Fig. 6. Increased DNA damage induced with HFD. Representative images of gamma-H2A histone family member X (γ -H2AX) staining in the testes of mice fed a HFD for 8, 16 or 42 weeks (n=3 for each group)

ND – normal diet; HFD – high-fat diet.

results showed that sperm parameters were adversely affected by a HFD and tended to be more severe over time.

Spermatogenesis is a complex process that produces sperm in the seminiferous tubules of the mammalian testes. When the structure of the seminiferous tubules is damaged, spermatogenesis is impaired.^{31–33} Numerous studies, including those by Fan et al.³⁴ and Hammami et al.¹¹ have shown that the seminiferous epithelia become atrophied in mice fed a HFD. In contrast, Gómez-Eliás et al. showed normal histological results in mice fed a HFD.³⁵ Although the histological results were varied, the histological analysis could explain the variations in the sperm parameters in all cases. In this study, the alterations in the relative sperm parameters in mice fed a HFD were also supported by histological changes. Indeed, distinct structural disorganization, loose seminiferous tubules and a decreased number of mature sperm provide distinct evidence that spermatogenesis was impaired and restricted in mice fed a HFD. Furthermore, the tissue damage induced by a HFD was shown to occur in a time-dependent manner, and included partial to complete atrophy of tubules and increased vacuolization within tubules.

Apart from the distinct structural disorganization of the testes of male mice, ectopic deposition of lipids was found. In the testes of animals fed a HFD, a large volume of lipid accumulation was deposited in the testicular interstitium, compared with the control animals, and this accumulation reached its maximum with a prolonged HFD. These results suggest that the testes and seminiferous tubules were damaged after the intervention of a HFD, which led to impaired spermatogenesis.

Spermatogenesis is responsible for producing sperm and passing genetic information to the next generation. The germ cell-specific gene, *DDX4*, is crucial for the proliferation and survival of germ cells, both of which play a critical role in spermatogenesis.¹³ The expression of *DDX4* has been reported in undifferentiated seminiferous tubule cells (spermatogonia and spermatocytes), while no *DDX4* expression was detected in the sperm.³⁶ In the present study, immunofluorescence results indicated that the expression of *DDX4* was positive in spermatogonia and spermatocytes, which is consistent with previous studies. Further analysis showed that the level of *DDX4* was higher in mice fed a HFD than in those fed a ND. This indicates that the damaging role of a HFD on the quality of sperm most likely occurred through the inhibition of the germ cell proliferation. Similarly, Khanlarkhani et al. reported that there was a link between the inhibition of the proliferation of germ cells and the cessation of spermatogenesis. There was also a relationship between the arrest of proliferation and sterility.³⁷ Notably, the inhibition worsened with time in groups consuming a HFD. This indicates that a long-term and continuous HFD has a more serious effect on sperm quality.

Oxidative stress is highly correlated with a wide range of metabolic disease states, including metabolic disorders

induced by a HFD.^{38,39} Oxidative stress is a process in which free radicals, which are inadequately neutralized by antioxidants, cause cumulative damage, and this damage is aggravated by the reduced activity of antioxidative enzymes, such as SOD.⁴⁰ Numerous studies have reported that there are many sources of oxidative stress in animals fed a HFD. Furthermore, strong evidence showing that increased levels of oxidative stress in testes may impact sperm quality was demonstrated in previous studies.^{10,41,42} In the present study, the testicular levels of SOD and MDA were evaluated to determine the effects of a HFD on the levels of oxidative stress. It was found that the HFD downregulated SOD and upregulated MDA in testicular tissues, which suggests that the HFD leads to increased levels of oxidative stress in the testes. These results indicate that oxidative stress may be an underlying mechanism responsible for the reduced sperm quality induced by a HFD.

Numerous recent studies have reported that increased oxidative stress along with decreased antioxidant defense may result in sperm DNA damage. One study reported that fluoride exposure generated reactive oxygen species (ROS) followed by H2AX phosphorylation (γ -H2AX), which is a marker of DSB and can be used to monitor DNA repair.¹⁵ Another recent study reported that significant negative correlations were found between γ -H2AX, sperm concentration and kinematic parameters, such as sperm motility and sperm progressive motility.¹⁶ Consequently, in this study, the number of γ -H2AX-positive cells was assessed using immunofluorescence. A higher number of γ -H2AX-positive germ cells was observed in the testes of mice fed a HFD, compared with those fed a ND. In the HFD groups, the number of γ -H2AX-positive germ cells was higher at 30 and 42 weeks than at 16 weeks. The results demonstrate that γ -H2AX is negatively correlated with sperm quality, which is in agreement with the aforementioned study.

It has been demonstrated that the accumulation of γ -H2AX indicates that the incidence of unrepaired DNA breaks has increased. Without repair of these DSBs, this condition would be accompanied by the apoptosis of the germ cell.^{17,18} In this study, apoptosis was evaluated in testis sections from various groups using TUNEL staining. There was an increase in the number of apoptotic germ cells in all HFD groups compared with the ND groups. A further analysis revealed that there was also a time-dependent increase in TUNEL+ nuclei and seminiferous tubules. Additionally, an obvious increase in the number of γ -H2AX-positive germ cells was paralleled by a strong increase in the number of TUNEL+ cells, suggesting that DNA DSBs did not repair appropriately, which resulted in the apoptosis of the germ cells. Studies have shown that apoptosis under physiological conditions can maintain the number of germ cells in a balanced state to ensure adequate production of sperm.^{43–45} However, an increased number of apoptotic germ cells is one of the most vital

mechanisms underlying the decreased number of sperm in mice fed a HFD.^{46–48} Therefore, the combination of elevated oxidative stress in the testes increased DNA damage, and the initiation of apoptosis of germ cells may have led to a significant decline in sperm quality.




Limitations

Several limitations of the present study should be mentioned. No information was obtained about sex hormones that can affect sperm quality, such as testosterone levels.^{49,50} At the same time, conclusions could only be drawn on the association between a HFD and sperm quality, but not the association between a HFD and fertility.^{51,52} Further studies are needed to validate this relationship. Moreover, some details, such as data on food and water intake, were not measured. Furthermore, even though the distribution of the data cannot be convincingly determined for very small samples, the authors assume that the observations came from a normal distribution, and agree that if this assumption is not true, the reported p-values and confidence intervals are unreliable, and must be interpreted with caution. Additional research will be carried out to add more details, which will make future studies more rigorous and accurate.

Conclusions

In summary, the results reported in the study demonstrate that not only did a HFD have short-term deteriorative impact on sperm quality but also resulted in a progressive deterioration of sperm quality over an extended period. Mice fed a HFD had histological changes, inhibited proliferation of germ cells, increased testicular oxidative stress levels, increased DNA damage, and an increased number of apoptotic germ cells. These findings reinforce the need for maintaining vigilance against high-fat diets and underscore the importance of improving dietetic habits as soon as possible. As obesity is a growing health problem, more research is needed to investigate the relationship between obesity and male fertility in a greater depth.

ORCID iDs

Xiangyu Qi  <https://orcid.org/0000-0002-9874-8599>
 Qingbo Guan  <https://orcid.org/0000-0002-1549-5304>
 Wenjing Zhang  <https://orcid.org/0000-0001-6336-8636>
 Xinshuang Huang  <https://orcid.org/0000-0003-1021-0020>
 Chunxiao Yu  <https://orcid.org/0000-0003-4605-6010>

References

- Hohos NM, Skaznik-Wikiel ME. High-fat diet and female fertility. *Endocrinology*. 2017;158(8):2407–2419. doi:10.1210/en.2017-00371
- Zimmerman B, Kundu P, Rooney WD, Raber J. The effect of high fat diet on cerebrovascular health and pathology: A species comparative review. *Molecules*. 2021;26(11):3406. doi:10.3390/molecules26113406
- Rabinovich-Nikitin I, Dhingra R, Kirshenbaum LA. Activation of mitophagy in high-fat diet-induced diabetic cardiomyopathy. *Circ Res*. 2019;124(9):1288–1290. doi:10.1161/CIRCRESAHA.119.314967
- Tong Y, Gao H, Qi Q, et al. High fat diet, gut microbiome and gastrointestinal cancer. *Theranostics*. 2021;11(12):5889–5910. doi:10.7150/thno.56157
- Schjenken JE, Moldenhauer LM, Sharkey DJ, et al. High-fat diet alters male seminal plasma composition to impair female immune adaptation for pregnancy in mice. *Endocrinology*. 2021;162(10):bqab123. doi:10.1210/endocr/bqab123
- Akbarian F, Rahmani M, Tavalaee M, et al. Effect of different high-fat and advanced glycation end-products diets in obesity and diabetes-prone C57BL/6 mice on sperm function. *Int J Fertil Steril*. 2021;15(3):226–233. doi:10.22074/ijfs.2021.137231.1022
- Xiong YW, Tan LL, Zhang J, et al. Combination of high-fat diet and cadmium impairs testicular spermatogenesis in an m6A-YTHDF2-dependent manner. *Environ Pollut*. 2022;313:120112. doi:10.1016/j.envpol.2022.120112
- Ding N, Zhang X, Zhang XD, et al. Impairment of spermatogenesis and sperm motility by the high-fat diet-induced dysbiosis of gut microbes. *Gut*. 2020;69(9):1608–1619. doi:10.1136/gutjnl-2019-319127
- Eslamian G, Amirjannati N, Rashidkhani B, Sadeghi MR, Baghestani AR, Hekmatdoost A. Dietary fatty acid intakes and asthenozoospermia: A case-control study. *Fertil Steril*. 2015;103(1):190–198. doi:10.1016/j.fertnstert.2014.10.010
- Vieira HR, Gonçalves GD, Alves VS, et al. Neonatal metformin short exposure inhibits male reproductive dysfunction caused by a high-fat diet in adult rats. *Toxicol Appl Pharmacol*. 2021;429:115712. doi:10.1016/j.taap.2021.115712
- Hammami I, Ben Ali R, Nahdi A, et al. Kefir milk consumption decreases sperm alterations due to the high-fat diet in adult male rats. *Andrologia*. 2022;54(7):1631–1642. doi:10.1111/and.14428
- Fernandez CD, Bellentani FF, Fernandes GS, et al. Diet-induced obesity in rats leads to a decrease in sperm motility. *Reprod Biol Endocrinol*. 2011;9(1):32. doi:10.1186/1477-7827-9-32
- Abdallah W, Hashad D, Abdelmaksoud R, Hashad MM. Does detection of *DDX4* mRNA in cell-free seminal plasma represents a reliable noninvasive germ cell marker in patients with nonobstructive azoospermia? *Andrologia*. 2017;49(8):e12739. doi:10.1111/and.12739
- Lu M, Mu Y, Liu Y. Triphenyltin disrupts the testicular microenvironment and reduces sperm quality in adult male rats. *Chemosphere*. 2022;301:134726. doi:10.1016/j.chemosphere.2022.134726
- Llavanera M, Delgado-Bermúdez A, Ribas-Maynou J, Salas-Huetos A, Yeste M. A systematic review identifying fertility biomarkers in semen: A clinical approach through omics to diagnose male infertility. *Fertil Steril*. 2022;118(2):291–313. doi:10.1016/j.fertnstert.2022.04.028
- Zhang XY, Wang B, Xu S, et al. Reactive oxygen species-evoked genotoxic stress mediates arsenic-induced suppression of male germ cell proliferation and decline in sperm quality. *J Hazard Mater*. 2021;406:124768. doi:10.1016/j.jhazmat.2020.124768
- Park HJ, Lee WY, Zhang M, et al. Evaluation of resmethrin toxicity to neonatal testes in organ culture. *Toxicol Sci*. 2020;173(1):53–64. doi:10.1093/toxsci/kfz212
- Onn L, Portillo M, Ilic S, et al. SIRT6 is a DNA double-strand break sensor. *eLife*. 2020;9:e51636. doi:10.7554/eLife.51636
- Research Diets. D12450B. Rodent diet with 10 kcal% fat. <https://researchdiets.com/en/formulas/d12450b>. Accessed April 1, 2022.
- Research Diets. D12492. Rodent diet with 60 kcal% fat. <https://researchdiets.com/en/formulas/d12492>. Accessed April 1, 2022.
- Su Y, Tian Z, Qi X, et al. Effects of increasing intake of soybean oil on synthesis of testosterone in Leydig cells. *Nutr Metab (Lond)*. 2021;18(1):53. doi:10.1186/s12986-021-00580-1
- Qi X, Zhang M, Sun M, Luo D, Guan Q, Yu C. Restoring impaired fertility through diet: Observations of switching from high-fat diet during puberty to normal diet in adulthood among obese male mice. *Front Endocrinol*. 2022;13:839034. doi:10.3389/fendo.2022.839034
- Hook KA, Fisher HS. Methodological considerations for examining the relationship between sperm morphology and motility. *Mol Reprod Dev*. 2020;87(6):633–649. doi:10.1002/mrd.23346
- Barquero V, Roldan ERS, Soler C, et al. Relationship between fertility traits and kinematics in clusters of boar ejaculates. *Biology*. 2021;10(7):595. doi:10.3390/biology10070595
- Chen G, Ren L, Chang Z, et al. Lysine acetylation participates in boar spermatozoa motility and acrosome status regulation under different glucose conditions. *Theriogenology*. 2021;159:140–146. doi:10.1016/j.theriogenology.2020.10.027

26. Johnson C, Dance A, Kovalchuk I, Kastelic J, Thundathil J. Enhanced pre-pubertal nutrition upregulates mitochondrial function in testes and sperm of post-pubertal Holstein bulls. *Sci Rep*. 2020;10(1):2235. doi:10.1038/s41598-020-59067-3
27. Farooq U, Malecki IA, Mahmood M, Martin GB. Correlation between objective semen analysis and fertility in Japanese quail. *Theriogenology*. 2018;115:23–29. doi:10.1016/j.theriogenology.2018.04.012
28. Benon M, Linet T. Sperm hyperactivated motility: Influence of the capacitation medium [in French]. *Journal de Gynécologie Obstétrique et Biologie de la Reproduction*. 2005;34(5):488–492. doi:10.1016/S0368-2315(05)82857-1
29. Yan WJ, Mu Y, Yu N, et al. Protective effects of metformin on reproductive function in obese male rats induced by high-fat diet. *J Assist Reprod Genet*. 2015;32(7):1097–1104. doi:10.1007/s10815-015-0506-2
30. Skovmand A, Erdely A, Antonini JM, et al. Inhalation of welding fumes reduced sperm counts and high fat diet reduced testosterone levels: Differential effects in Sprague Dawley and Brown Norway rats. *Part Fibre Toxicol*. 2020;17(1):2. doi:10.1186/s12989-019-0334-0
31. Neto FTL, Bach PV, Najari BB, Li PS, Goldstein M. Spermatogenesis in humans and its affecting factors. *Semin Cell Dev Biol*. 2016;59:10–26. doi:10.1016/j.semcdb.2016.04.009
32. Iqbal T, Cao M, Zhao Z, et al. Damage to the testicular structure of rats by acute oral exposure of cadmium. *Int J Environ Res Public Health*. 2021;18(11):6038. doi:10.3390/ijerph18116038
33. Hu Z, Zhang Y, Zhang L, Tian Y. Respiratory exposure to carbon black nanoparticles may induce testicular structure damage and lead to decreased sperm quality in mice. *Reprod Toxicol*. 2021;106:32–41. doi:10.1016/j.reprotox.2021.10.001
34. Fan Y, Liu Y, Xue K, et al. Diet-induced obesity in male C57BL/6 mice decreases fertility as a consequence of disrupted blood–testis barrier. *PLoS One*. 2015;10(4):e0120775. doi:10.1371/journal.pone.0120775
35. Gómez-Elías MD, Rainero Cáceres TS, Giaccagli MM, et al. Association between high-fat diet feeding and male fertility in high reproductive performance mice. *Sci Rep*. 2019;9(1):18546. doi:10.1038/s41598-019-54799-3
36. Zhu W, Wang T, Zhao C, et al. Evolutionary conservation and divergence of Vasa, Dazl and Nanos1 during embryogenesis and gametogenesis in dark sleeper (*Odontobutis potamophila*). *Gene*. 2018;672:21–33. doi:10.1016/j.gene.2018.06.016
37. Khanlarkhani N, Mortezaee K, Amidi F, et al. Role of stromal derived factor-1a (SDF-1a) for spermatogenesis of busulfan-injured rats. *Reprod Toxicol*. 2017;73:142–148. doi:10.1016/j.reprotox.2017.08.006
38. Rius-Pérez S, Torres-Cuevas I, Millán I, Ortega ÁL, Pérez S. PGC-1 α , inflammation, and oxidative stress: An integrative view in metabolism. *Oxid Med Cell Longev*. 2020;2020:1452696. doi:10.1155/2020/1452696
39. Oladele CA, Akintayo CO, Badejogbin OC, et al. Melatonin ameliorates endocrine dysfunction and defective sperm integrity associated with high-fat diet-induced obesity in male Wistar rats. *Andrologia*. 2022;54(1):e14242. doi:10.1111/and.14242
40. Billah MM, Khatiwada S, Lecomte V, Morris MJ, Maloney CA. Ameliorating high-fat diet-induced sperm and testicular oxidative damage by micronutrient-based antioxidant intervention in rats. *Eur J Nutr*. 2022;61(7):3741–3753. doi:10.1007/s00394-022-02917-9
41. Sertorio MN, César H, de Souza EA, et al. Parental high-fat high-sugar diet intake programming inflammatory and oxidative parameters of reproductive health in male offspring. *Front Cell Dev Biol*. 2022;10:867127. doi:10.3389/fcell.2022.867127
42. Naghibi M, Tayefi Nasrabadi H, Soleimani Rad J, Gholami Farashah MS, Mohammadnejad D. The effects of metformin and forskolin on sperm quality parameters and sexual hormones in type II diabetic male rats. *Andrologia*. 2022;54(7):1605–1617. doi:10.1111/and.14426
43. Jeng HA, Pan CH, Chao MR, Lin WY. Sperm DNA oxidative damage and DNA adducts. *Mutation Res Genet Toxicol Environ Mutagen*. 2015;794:75–82. doi:10.1016/j.mrgentox.2015.09.002
44. Henkel R, Hoogendijk CF, Bouic PJD, Kruger TF. TUNEL assay and SCSA determine different aspects of sperm DNA damage: Different tests for the determination of sperm DNA damage. *Andrologia*. 2010;42(5):305–313. doi:10.1111/j.1439-0272.2009.01002.x
45. Takeda K, Uchiyama K, Kinukawa M, Tagami T, Kaneda M, Watanabe S. Evaluation of sperm DNA damage in bulls by TUNEL assay as a parameter of semen quality. *J Reprod Dev*. 2015;61(3):185–190. doi:10.1262/jrd.2014-140
46. Nejatbakhsh R, Riyahi S, Farrokhi A, et al. Ameliorating effects of fenel and cumint extracts on sperm quality and spermatogenic cells apoptosis by inducing weight loss and reducing leptin concentration in diet-induced obese rats. *Andrologia*. 2017;49(8):e12748. doi:10.1111/and.12748
47. Mu Y, Yin TL, Huang XX, Hu X, Yin L, Yang J. Sulforaphane ameliorates high-fat diet-induced spermatogenic deficiency in mice. *Biol Reprod*. 2019;101(1):223–234. doi:10.1093/biolre/iox067
48. Mu Y, Yin TL, Yin L, Hu X, Yang J. CTRP3 attenuates high-fat diet-induced male reproductive dysfunction in mice. *Clin Sci (Lond)*. 2018;132(8):883–899. doi:10.1042/CS20180179
49. Erthal RP, Staurengo-Ferrari L, Fattori V, et al. Exposure to low doses of malathion during juvenile and peripubertal periods impairs testicular and sperm parameters in rats: Role of oxidative stress and testosterone. *Reprod Toxicol*. 2020;96:17–26. doi:10.1016/j.reprotox.2020.05.013
50. López-Trinidad BP, Viguera-Villaseñor RM, Königsberg M, et al. Alterations in epididymal sperm maturation caused by ageing. *Reprod Fertil Dev*. 2021;33(18):855. doi:10.1071/RD21081
51. Farahani L, Tharakan T, Yap T, Ramsay JW, Jayasena CN, Minhas S. The semen microbiome and its impact on sperm function and male fertility: A systematic review and meta-analysis. *Andrology*. 2021;9(1):115–144. doi:10.1111/andr.12886
52. Almeida S, Rato L, Sousa M, Alves MG, Oliveira PF. Fertility and sperm quality in the aging male. *Curr Pharm Des*. 2017;23(30):4429–4437. doi:10.2174/1381612823666170503150313

The contribution of donated human embryos suitable for the production of embryonic stem cells to increase the quality of life: Selection and preparation of embryos in the Czech Republic

Tomáš Ventruba^{1,C,D,F}, Pavel Ventruba^{1,A,D–F}, Michal Jeřeta^{1,A,B,D}, Jana Žáková^{1,A,C,E},
Eva Lousová^{1,B,C}, Igor Crha^{1,C,E}, Tereza Souralová^{2,3,B,C,E}, Irena Koutná^{2,3,A,E}, Aleš Hampel^{2,A,E}

¹ Department of Obstetrics and Gynecology, University Hospital Brno and Masaryk University, Czech Republic

² Department of Histology and Embryology, Faculty of Medicine, Masaryk University, Brno, Czech Republic

³ Cell and Tissue Engineering Facility, International Clinical Research Centre, St. Anne's University Hospital, Brno, Czech Republic

A – research concept and design; B – collection and/or assembly of data; C – data analysis and interpretation;

D – writing the article; E – critical revision of the article; F – final approval of the article

Advances in Clinical and Experimental Medicine, ISSN 1899–5276 (print), ISSN 2451–2680 (online)

Adv Clin Exp Med. 2023;32(8):901–907

Address for correspondence

Tomáš Ventruba

E-mail: tventruba@gmail.com

Funding sources

None declared

Conflict of interest

None declared

Acknowledgements

This research was funded by the Czech Health Research Council (grants No. NV18-01-00412 and No. NV18-08-00291; MH CZ – DRO (FNBr, 65269705)). The work was carried out with institutional support of Masaryk University, Brno, Czech Republic.

Received on October 31, 2022

Reviewed on November 30, 2022

Accepted on December 28, 2022

Published online on February 8, 2023

Cite as

Ventruba T, Ventruba P, Jeřeta M, et al. The contribution of donated human embryos suitable for the production of embryonic stem cells to increase the quality of life: Selection and preparation of embryos in the Czech Republic. *Adv Clin Exp Med.* 2023;32(8):901–907. doi:10.17219/acem/158777

DOI

10.17219/acem/158777

Copyright

Copyright by Author(s)

This is an article distributed under the terms of the Creative Commons Attribution 3.0 Unported (CC BY 3.0) (<https://creativecommons.org/licenses/by/3.0/>)

Abstract

Background. Human embryonic stem cells (hESCs) have the unique ability to differentiate into any cell type in the human body and to proliferate indefinitely. Cell therapies involving hESC have shown very promising results for the treatment of certain diseases and confirmed the safety of hESC-derived cells for humans. They are used in cell therapy, mainly in targeted therapy of diseases that are currently incurable.

Objectives. The aim of this study was the derivation of clinical-grade hESCs usable in drug development, non-native medicine and cell therapy.

Materials and methods. Embryos were thawed, cultivated to the blastocyst stage if necessary, and assisted hatching was subsequently performed. Embryoblasts were mechanically isolated using narrow needles. Each line was kept as a separate batch. The derived hESCs were cultured under hypoxic culture conditions (5% O₂, 5% CO₂, 37°C) in a NutriStem® hPSC XF Medium with a daily medium change.

Results. From January 2018 to July 2020, 138 selected clients were asked for consent to donate embryos, of whom 52 did not respond, 19 terminated the storage of their embryos and 29 extended the storage. Only 38 clients (27.5%) agreed to donate embryos for the derivation of hESCs. At the same time, personal communication with clients took place and another 17 embryo donors were recruited. A total of 160 embryos from 55 donors aged 26–42 years were collected. The embryos were frozen at the blastocyst (33.1%) or morula (46.3%) stage. After the preparation of 64 embryos, embryoblasts were isolated and cultured. Finally, 7 hESC lines were obtained, 4 research-grade and 3 clinical-grade, the first in the Czech Republic.

Conclusions. We established a current good manufacturing practice (cGMP)-defined xeno-free and feeder-free system for the derivation, culture and banking of clinical-grade hESC lines that are suitable for preclinical and clinical trials. The quality control testing with criteria concerning sterility, safety and characterization according to cGMP ensured the clinical-grade quality of hESC lines.

Key words: stem cells, IVF, human, embryo, hESC

Background

Stem cell research is a promising field of medical science. Contemporary medicine is increasingly dealing with the problems of chronic diseases or diseases for which there is no permanent cure. The potential of stem cells is enormous because the replacement of damaged cells with newly created ones would provide solutions to a whole range of diseases and economic issues associated with healthcare in the 21st century.

Freedom of research, protection of life, new treatment methods, economic disputes, and ethics are the topics colliding in the discussion. Due to different cultural backgrounds and the level of research, nearly every country has a different approach to the topic. This is demonstrated by the differences in legislation regulating the acquisition of stem cells and research concerning them.¹

Human embryonic stem cells (hESCs), contrary to somatic stem cells, have a unique ability to differentiate into every cell type of the human body. This ability makes them a tremendous cell source for regenerative medicine. Moreover, pluripotent hESCs have an unlimited self-renewal capacity. These features are used in cell therapy to replace missing or damaged cells in the human body. The goal is to enable targeted therapy for currently incurable diseases such as diabetes mellitus,² spinal cord injury or Parkinson's disease.³ Therapeutic approaches using hESCs bring promising results, especially in age-related macular degeneration.⁴ However, there are several technical problems. One of the most important issues is to avoid possible teratoma/tumor formation that can arise from all redundant undifferentiated stem cells.⁵ For prevention of differentiation to tumor cells, the residual ESCs need to be eliminated using magnetic or fluorescence-activated cell sorting (MACS or FACS)⁶ or with antibodies against undifferentiated hESCs.⁷ Another problem with the clinical application of ESCs is the allogenic immune rejection of the hESC cells by the recipient. Current immune suppression systems effectively prevent allogenic immune rejection but persistent use of immune suppressants is toxic for patients and increases the risk of infection or cancer, mainly in patients with cytomegalovirus or herpes virus.⁸ Despite these shortcomings, treatments using ESC cells are promising for the therapy of a wide range of diseases. The derivation of clinical-grade quality hESC lines enables their application in preclinical and clinical studies.

Objectives

The aim of this study was the derivation of clinical-grade hESCs, usable in drug development, non-native medicine and cell therapy. The use of these methods will increase the quality of life of treated individuals.^{9–11}

The task of the clinical part of the project was to select and ensure a sufficient number of donated embryos.

Research activities using human embryos in the Czech Republic are regulated by Act No. 227/2006 Coll. on Research on Human Embryonic Stem Cells and Related Activities and Act No. 373/2011 Coll. on Specific Health Services.^{12,13}

The methods of isolation and cultivation of hESCs are subject to strict regulations issued by the Ministry of Education, Youth and Sports of the Czech Republic (Ministerstvo školství, mládeže a tělovýchovy České republiky (MŠMT)), and its approval (No. MŠMT-2922/2020-14) was a precondition for initiating our project. A condition for the successful implementation of the project was an interdisciplinary team managing the medical, technological, and instrumental procedures and protocols necessary for the proposed research.

The study was conducted in accordance with the Declaration of Helsinki, and approved by the Ethical Committee of the University Hospital Brno, Czech Republic, on June 26, 2017 (approval No. 16/2017). Written informed consent was obtained from all participants included in the study.

Materials and methods

The derivation of hESCs must be performed in accordance to the legislation of the Czech Republic and the European Union. An informed consent form was developed by us for the donors regarding the donation of discarded embryos that are not suitable for in vitro fertilization treatment according to Directive 2004/23/EC. Center of Assisted Reproduction (CAR) of the University Hospital Brno was involved in oocyte collection; culture and cryopreservation of embryos; communication with clients; and ensuring informed consent of embryo donors. A handover protocol and transfer of the thawed embryos with the original numerical code were developed in cooperation with the Cell and Tissue Engineering Facility (CTEF) of St. Anne's University Hospital Brno. Before the embryos were handed over to the CTEF, they were thawed and cultivated to the blastocyst stage if necessary. Subsequently, assisted hatching was performed.

Embryo selection aspects

Embryo selection began by reviewing CAR laboratory protocols for the cryopreservation of embryos. It was necessary to check the addresses of the clients, including a relatively complex tracing of the storage fee, and the current number and stage of the embryos. A basic database of potential donors was created and included contact details of patients, patient age, date of freezing, number and stage of embryos, number of embryos in each tube, and information on genetic testing.

Creation of the informed consent form required cooperation with a lawyer and approval by the Ethical

Committee of the University Hospital Brno and the Faculty of Medicine of Masaryk University, Brno. Then, the Czech and English versions were prepared. A letter with basic information and a request for a decision on how to handle the cryopreserved embryos was sent together with a return envelope. Subsequent communication took place through telephone calls, e-mails, letters, and personal meetings.

Under Act No. 373/2011 Coll. on Specific Health Services, embryos can be treated as follows:

- 1) stored for further use by the recipient, i.e., the storage of embryos is extended at the request of both partners;
- 2) used for research on human embryonic stem cells with a granted informed consent to their usage;
- 3) destroyed with written consent (upon consent, the embryos are subsequently thawed and destroyed).

Embryo preparation

Embryos intended for the specified date of transfer to CTEF were thawed using Warm Cleave or Warm Blast media (Vitrolife, Västra Frölunda, Sweden) depending on the stages at which they had been frozen.¹⁴ For the earlier stages, we performed cultivation to the blastocyst stage in medium (Blastocyst Medium; Cook Medical, Bloomington, USA) on the premises of the CAR of the University Hospital Brno embryological laboratory. After reaching the blastocyst stage, assisted hatching was performed using a laser (OCTAX NaviLase; Vitrolife) (Fig. 1).

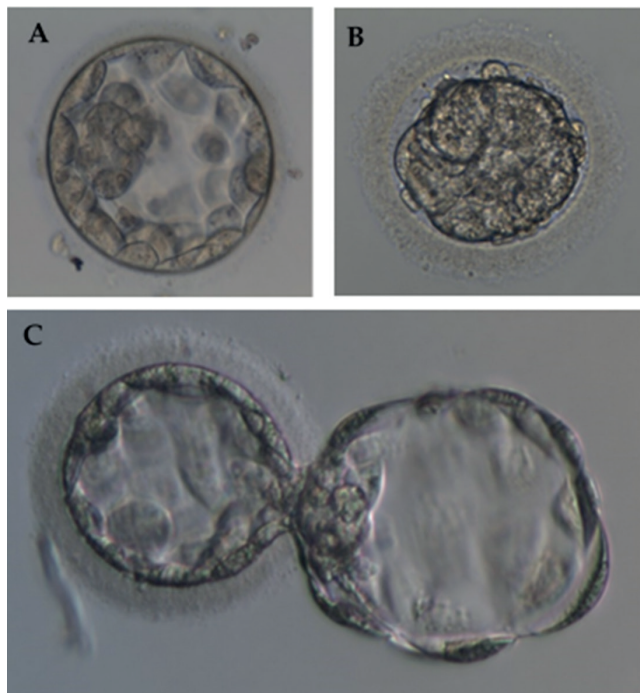


Fig. 1. Preparation of the donated embryos prior to isolation of embryoblasts and cultivation of human embryonic stem cells (hESC) lines. A. A morula stage embryo after thawing; B. A blastocyst after cultivation; C. A blastocyst after assisted hatching

Embryo transfer and embryoblast isolation at CTEF

The prepared embryos in the hatched blastocyst stage were placed in the transport medium and transferred to the CTEF laboratory using a temperature-controlled transport incubator at 37°C (ICT-P portable incubator; Falc Instruments, Treviglio, Italy).¹⁵ Immediately afterwards, the embryoblast was isolated, followed by cultivation of the hESC line 8.

The embryoblast was mechanically isolated using a microscope (Nikon Eclipse Ti; Nikon Corp., Tokyo, Japan) with attached micromanipulators (Eppendorf, Hamburg, Germany) and an oil and air microinjector (CellTram[®] 4r Air/Oil; Eppendorf). Prior to the isolation of the embryoblast, the blastocyst was placed in medium (Sydney IVF Gamete Buffer; Cook Medical) covered with culture oil (Sydney IVF Culture Oil; Cook Medical) using denudation micropipettes (Microtech IVF, Brno, Czech Republic). A biopsy and fixation micropipette (Microtech IVF) was used for subsequent isolation. Each embryoblast was isolated separately and aseptically, and detailed records were kept describing the derivation and all subsequent preparation steps.

Derivation of hESCs

The derivation of hESCs was carried out in the cleanrooms of the CTEF department in purity class A against the background of purity class B, according to current good manufacturing practice (cGMP). The manufacturing process was undertaken according to standard operating procedures; microbiological and particle monitoring was performed in cleanrooms. Each line was kept as a separate batch, which was controlled during production and as a final product by quality control staff for sterility, quality, safety, and other critical parameters. An analytical certificate was created for each final product, i.e., the hESC line in clinical-grade quality.

Embryoblast was mechanically isolated using narrow needles. The derived hESCs were cultured under hypoxic culture conditions (5% O₂, 5% CO₂, 37°C) in NutriStem[®] hPSC XF Medium (Biological Industries, Kibbutz Beit-Haemek, Israel) with a daily medium change.

Results

Between January 2018 and July 2020, 138 suitable clients whose embryos were frozen in the years 2014–2017 were asked for consent to donate embryos. Of those, 52 (37.7%) did not respond, 19 (13.8%) terminated the embryo storage and 29 (21.0%) extended the storage (Table 1, column n1). Only 38 clients (27.5%) agreed for the use of their embryos for the derivation of hESCs.

At the same time, personal communication with suitable CAR clients took place. Out of 22 personally contacted couples at CAR, with embryos frozen between January 2018 and

Table 1. Composition of embryo donors contacted between January 2018 and July 2020

Embryo donors	Contacted						Personal communication			
	n1	2013	2014	2015	2016	2017	n2	2018	2019	2020
Number of donors	138	3	27	29	34	45	22	8	9	5
No reply	52	2	13	10	12	15	–	–	–	–
Terminated storage	19	1	4	7	5	2	–	–	–	–
Extended storage	29	0	4	3	8	14	–	–	–	–
Embryos donated for research	38	0	6	9	9	14	17	6	7	4
Frozen embryos/year										
Total number of embryos	107	0	15	27	20	45	53	16	26	11
Embryos/patient	2.8	0	2.5	3.0	2.2	3.2	3.1	2.7	3.7	2.8

Table 2. Composition of the stages of the frozen donated embryos in 2014–2020

Stage of frozen embryos	n	%
Blastocyst	53	33.1
Morula	74	46.3
10-cell	6	3.8
8-cell	13	8.1
6-cell	6	3.8
5-cell	1	0.6
4-cell	5	3.1
3-cell	1	0.6
Pronuclei	1	0.6
Total	160	100.0

July 2020, another 17 embryo donors were recruited (77.3%) (Table 1, column n2). A significantly higher proportion of donors from directly contacted clients compared to the group contacted by mail (27.5%) were influenced in their decision by a personal discussion with the selected group of couples, especially in cases with genetically examined embryos unsuitable for transfer (6 pairs, 27.3%). The remaining donors were recruited from clients who did not consider cryopreservation of all embryos (6 pairs, 27.3%) or wanted to terminate their embryos (10 pairs, 45.4%). The time lag, and the development of an opinion on the need for medical research can also have a significant impact on the total number of recruited embryos. Following personal communication with 22 couples, cryopreservation was terminated in 5 cases (22.7%) by thawing and disposal of embryos. A total of 160 embryos were obtained from 55 donors aged 26–42 years. Most often, the embryos were frozen at blastocyst (53 embryos (33.1%)) or morula (74 embryos (46.3%)) stages. The composition of embryo stages is presented in Table 2. The number of frozen embryos in each tube was 1 or 2 according to the patient's wishes. Our recommended standard is 1 embryo per tube and 61.2% of embryos (98 tubes) were frozen individually in our group. The other 62 (38.8%) embryos were frozen in pairs (31 patients).

Of the 29 genetically examined embryos, there were 5 euploid embryos (17.2%), 2 mosaic embryos (7.9%),

Table 3. Genetic testing results of donated embryos

Genetic state	n	%
Euploid embryo	5	17.2
Mosaic	2	6.9
Aneuploid embryo	16	55.2
Translocation	4	13.8
PGT-M (<i>SURF1</i> gene)	2	6.9
Total	29	100.0

PGT-M – preimplantation genetic testing for monogenic disorders.

16 aneuploid embryos (55.2%), and 6 embryos with a translocation or carrying a monogenic defect (20.7%) (Table 3). The relatively small number of genetically examined embryos from the whole group (18.1%) is due to predominance of healthy embryos in the whole group of donated embryos. Even so, this share is higher than the average at the CAR of the University Hospital Brno. In 2021, 64 embryos were transferred to the CTEF for further processing, from which 7 hESC lines were obtained: 3 clinical-grade lines (MUCG01, MUCG02 and MUCG03) and 4 research-grade lines (MUES 10, MUES 11, MUES 12, and MUES 13) (Fig. 2). Laminin 521 (Bio-Lamina AB, Sundbyberg, Sweden) was used in combination with NutriStem hPSC XF Medium (Biological Industries), human serum albumin and E-cadherin for mechanical derivation. The hESCs were cultured on Laminin 521 in the NutriStem hPSC XF Medium. The isolated lines were frozen according to the procedure described by Souralova et al.¹⁶

After thawing, the cell lines were tested using a cell viability test. Cell attachment was examined 2 days after thawing by counting the number of colonies. Growth was assessed by a change in confluency between days 2 and 5 after thawing. The cells were counted, and viability was measured during the first passage after thawing using cell counter Countess III (Thermo Fisher Scientific, Waltham, USA). The isolated hESC lines underwent mycoplasma examination, karyotype determination and genetic analyses, and the pluripotency markers were established using flow cytometry and immunocytochemistry.¹⁶

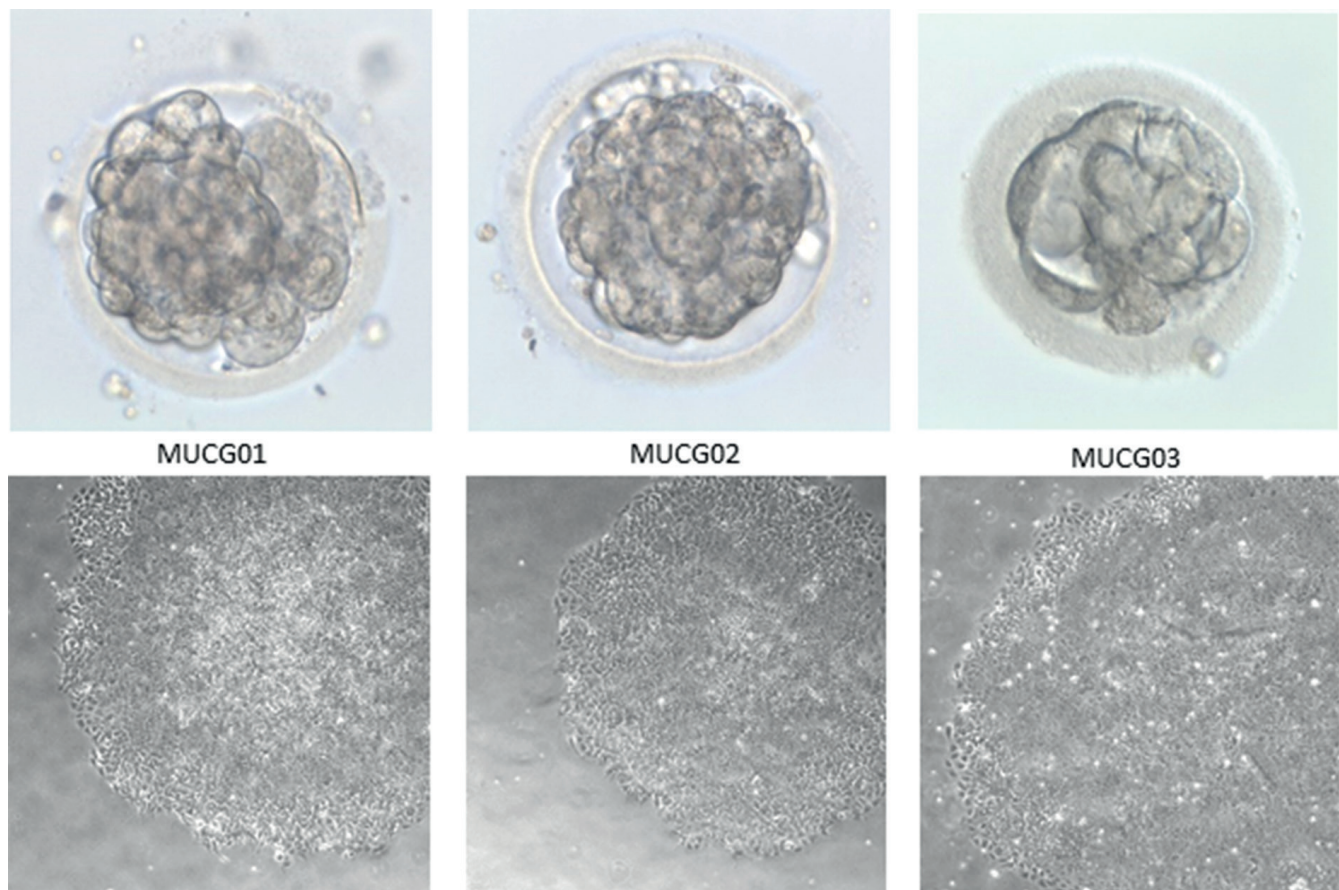


Fig. 2. Isolated embryos and corresponding derived human embryonic stem cells (hESC) clinical-grade lines MUCG01-03

Discussion

Research on stem cells of an adult organism usually does not raise ethical problems. Use of fetal tissues is mostly acceptable, or even completely legal in countries where abortion is permitted. A problem arises with the acquisition of stem cells from human embryos, which brings several questions based mainly on moral and religious principles. International Consortium on Stem Cells, Ethics and Law divides countries into 4 groups according to the extent to which their national legislation restricts stem cell research. The groups are 1) countries with a liberal policy; 2) countries with a compromise liberal policy; 3) countries with a compromise restrictive policy; and 4) countries with a restrictive policy.¹ The Czech Republic is among the states with a compromise liberal policy.

Research on hESC is controversial in some countries because it involves the destruction of human early embryos. Several people believe that human life begins at conception and that an embryo is a person.¹⁷ On the other hand, many excess early human embryos are unnecessarily stored or discarded without further use. Senator Hatch says: “I believe that human life begins in the womb, not in a Petri dish or refrigerator... To me, the morality of the situation dictates that these embryos, which are routinely discarded, be used to improve and save lives. The tragedy would be

in not using these embryos to save lives when the alternative is that they would be discarded”.¹⁸ We agree with this opinion and do not see a problem with the use of hESCs for research purposes to bring more effective therapeutic methods for incurable diseases. In these cases, we talk about embryos that are on the verge of being either discarded or used for research, i.e., about isolation of embryonic cells in vitro conditions. This means a continuous monolayer of embryonic cells, which does not resemble a human embryo or a person. In this study, we worked only with unwanted embryos and these embryos were primarily produced for infertility therapy and are not desired anymore, perhaps because the reproductive wish of the parents has been either fulfilled or abandoned.

A condition for the successful implementation of our project was the creation of a fully operational team, covering medical, technological and instrumental aspects that are necessary for the proposed research and development. These include: 1) proven expertise in hESCs derivation; 2) direct access to cGMP facilities with relevant expertise in advanced therapy medicinal products (ATMP) medical application development; and 3) CAR involvement with expertise in human embryo handling and access to potential donors.^{19,20}

Czech Act 227/2006 Coll. on Research on Human Embryonic Stem Cells and Related Activities states that:

- only research carried out on hESC lines is allowed (§2a);
- hESC lines are all hESCs that are stored in cultures or are subsequently stored in cryopreserved form (§2c);
- hESCs are all pluripotent stem cells derived from human preimplantation embryos created extracorporeally (§2b);
- only embryos that are not older than 7 days (without cryopreservation period) can be used (§8/3).

Convention on Human Rights and Biomedicine (In vitro embryo research: Article 18/1 “If the law allows for in vitro embryo research, adequate embryo protection must be provided by law.”) does not distinguish between embryos and hESCs; it only requires legal embryo protection within the permitted research. The Explanatory Memorandum to the Human Embryonic Stem Cell Research Act states that “the draft law does not concern embryo stem cell research but only human embryonic stem cell research, in line with the principles of the Convention on Human Rights and Biomedicine”.¹³

In previous studies, we have dealt with the issue of thawing embryos in different culture conditions according to stages at which they were frozen.^{13,21,22} The oldest embryos suitable for donation for basic research we have are from 1997. The problem is that most donors from this period have ceased communicating with CAR and do not pay for embryo storage. However, not all ethical aspects have been resolved so far, and the Ethical Committee of the University Hospital Brno has not approved the termination of storage for these embryos.

Almost 38% of respondents did not reply to the letter. Approximately 20% of clients responded positively, did not want to lose the embryos and wanted to arrange a transfer date. A relatively large proportion of the contacted clients (14%) wanted to end storage without participating in a research project. For some couples, this information has provoked conflicting reactions and conflicts of opinion between the partners on which option to choose.

In personal communication, the 2 most important reasons for donating embryos for research purposes were mentioned. The 1st was the view that it was better to use the embryos for research than to destroy or waste them. Many respondents were in favor and made positive general statements about the research. The 2nd reason was altruism, expressed as a desire to help other infertile couples and to contribute to the development of scientific and medical knowledge.

There are many reasons for refusing to use stem cells and embryos for research purposes.¹² The use of stem cells is increasing in clinical therapy, from chronic diseases to plastic and esthetic surgery.^{23–25} The most common view is that of the embryo as a potential child. Some patients had a strong emotional reaction to the idea of embryo donation for medical research, and others referred to the children that the embryos can become. These reasons are common and similar to those reported by patients

in previous studies.²⁶ In an Australian study, parents of 5-year-old children conceived after in vitro fertilization (IVF), who were asked about the use of frozen embryos for research purposes, often referred to these embryos as siblings of the children born and commented on the psychological implications of manipulating embryos under a microscope.²⁷




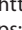


Limitations of the study

First, we are limited by the number of infertile couples willing to donate redundant embryos for research purposes. Second, due to the ongoing COVID-19 pandemic, personal contact with clients was minimized, with a negative impact on the number of embryos donated for research purposes.

Conclusions

Based on the signed informed consent, a total of 160 donated embryos were obtained from patients. A transfer protocol and embryo transfer methodology were developed. The delivery plan for thawed anonymized embryos included approx. 5 thawed blastocysts per week with assisted hatching. Subsequently, embryos were prepared and 64 embryos were transferred. After their transfer, embryoblasts were isolated and subsequently cultured. Finally, 3 clinical-grade quality hESC lines were obtained, the first created in the Czech Republic, respecting the requirements for ATMP.

ORCID iDs

Tomáš Ventruba  <https://orcid.org/0000-0002-7334-7131>
 Pavel Ventruba  <https://orcid.org/0000-0001-9264-0336>
 Michal Jeřeta  <https://orcid.org/0000-0003-1778-3454>
 Jana Žáková  <https://orcid.org/0000-0002-7079-2977>
 Igor Crha  <https://orcid.org/0000-0002-7217-4902>
 Tereza Souralová  <https://orcid.org/0000-0002-7175-9327>
 Irena Koutná  <https://orcid.org/0000-0002-1680-5052>
 Aleš Hampl  <https://orcid.org/0000-0002-8963-9235>

Reference

1. Djakoualno LH, Truong TT, eds. Stem Cells Research. Prague Student Summit UNESCO. [in Czech]. Prague, Czech Republic: Association for International Affairs; 2011. <https://www.amo.cz/wp-content/uploads/2016/01/PSS-V%C3%BDzkum-kmenov%C3%BDch-bun%C4%9Bk-UNESCO.pdf>.
2. Agulnick AD, Ambruzs DM, Moorman MA, et al. Insulin-producing endocrine cells differentiated in vitro from human embryonic stem cells function in macroencapsulation devices in vivo. *Stem Cell Transl Med.* 2015;4(10):1214–1222. doi:10.5966/sctm.2015-0079
3. Li JY, Christophersen NS, Hall V, Soulet D, Brundin P. Critical issues of clinical human embryonic stem cell therapy for brain repair. *Trends Neurosci.* 2008;31(3):146–153. doi:10.1016/j.tins.2007.12.001
4. Mehat MS, Sundaram V, Ripamonti C, et al. Transplantation of human embryonic stem cell-derived retinal pigment epithelial cells in macular degeneration. *Ophthalmology.* 2018;125(11):1765–1775. doi:10.1016/j.ophtha.2018.04.037
5. Blum B, Benvenisty N. The tumorigenicity of human embryonic stem cells. *Adv Cancer Res.* 2008;100:133–158. doi:10.1016/S0065-230X(08)00005-5

6. Fong CY, Peh GSL, Gauthaman K, Bongso A. Separation of SSEA-4 and TRA-1–60 labelled undifferentiated human embryonic stem cells from a heterogeneous cell population using magnetic-activated cell sorting (MACS) and fluorescence-activated cell sorting (FACS). *Stem Cell Rev Rep*. 2009;5(1):72–80. doi:10.1007/s12015-009-9054-4
7. Choo AB, Tan HL, Ang SN, et al. Selection against undifferentiated human embryonic stem cells by a cytotoxic antibody recognizing podocalyxin-like protein-1. *Stem Cells*. 2008;26(6):1454–1463. doi:10.1634/stemcells.2007-0576
8. Fishman JA. Overview: Cytomegalovirus and the herpesviruses in transplantation. *Am J Transplant*. 2013;13(Suppl 3):1–8. doi:10.1111/ajt.12002
9. Liang Y, Wang H, Niu M, Zhu X, Cai J, Wang X. Health-related quality of life before and after hematopoietic stem cell transplant: Evidence from a survey in Suzhou, China. *Hematology*. 2018;23(9):626–632. doi:10.1080/10245332.2018.1457199
10. Ovayolu Ö, Ovayolu N, Kaplan E, Pehlivan M, Karadağ G. Symptoms and quality of life before and after stem cell transplantation in cancer. *Pak J Med Sci*. 2013;29(3):803–808. doi:10.12669/pjms.293.3290
11. Palmer J, Kosiorek HE, Wolschke C, et al. Assessment of quality of life following allogeneic stem cell transplant for myelofibrosis. *Biol Blood Marrow Transplant*. 2019;25(11):2267–2273. doi:10.1016/j.bbmt.2019.07.001
12. Czech Act No. 227/2006 Coll. Act of April 26, 2006 on Research on Human Embryonic Stem Cells and Related Activities and on Amendment to Some Related Acts. Collection of Laws of the Czech Republic No. 227/2006. https://www.msmt.cz/file/38373_1_1/
13. Czech act No. 373/2011 Coll. Act of 6 November 2011 on Specific Health Services. Collection of Laws of the Czech Republic No. 373/2011. https://www.sujb.cz/fileadmin/sujb/docs/legislativa/zakony/373_2011_Coll.pdf.
14. Jeřeta M, Celá A, Žáková J, et al. Metabolic activity of human embryos after thawing differs in atmosphere with different oxygen concentrations. *J Clin Med*. 2020;9(8):2609. doi:10.3390/jcm9082609
15. Souralová T, Hampl A, Koutná I, Ventruba P. Clinical-grade human embryonic stem cells: Derivation and characterization [in Czech]. Proceedings of the 29th Symposium of Assisted Reproduction SAR ČGPS ČLS JEP and the 18th Czech-Slovak Conference of Reproductive Gynecology 2019. Brno, Czech Republic, November 12–13, 2019. 2019:35–36. ISBN:978-80-905578-9-5.
16. Souralova T, Rehakova D, Jeseta M, et al. The manufacture of xeno- and feeder-free clinical-grade human embryonic stem cell lines: First step for cell therapy. *Int J Mol Sci*. 2022;23(20):12500. doi:10.3390/ijms232012500
17. Verginer L, Riccaboni M. Stem cell legislation and its impact on the geographic preferences of stem cell researchers. *Eurasian Bus Rev*. 2021;11(1):163–189. doi:10.1007/s40821-021-00182-0
18. Lo B, Parham L. Ethical issues in stem cell research. *Endocrine Rev*. 2009;30(3):204–213. doi:10.1210/er.2008-0031
19. Hampl A, Jeřeta M, Koutná I, Ventruba P, Žáková P. The first ever effort to establish clinical grade human embryonic stem cells in the Czech Republic [in Czech]. Proceedings of the 17th Czech-Slovak Conference on Reproductive Gynecology and 28th Symposium on Assisted Reproduction SAR ČGPS ČLS JEP, 2018. Brno, Czech Republic, November 13–14, 2018:24–25. ISBN:978-80-905578-6-4.
20. Ventruba P, Žáková J, Jeřeta M, et al. Aspects of embryo selection and their preparation for the formation of human embryonic stem cells intended for human therapy. *Ceska Gynekol*. 2021;86(1):5–10. doi:10.48095/cccg20215
21. Celá A, Mádr A, Jeřeta M, Žáková J, Crha I, Glatz Z. Study of metabolic activity of human embryos focused on amino acids by capillary electrophoresis with light-emitting diode-induced fluorescence detection. *Electrophoresis*. 2018;39(23):3040–3048. doi:10.1002/elps.201800265
22. Wang H, Ou Z, Chen Z, Yang L, Sun L. Influence of different post-thaw culture time on the clinical outcomes of different quality embryos. *Adv Clin Exp Med*. 2019;28(4):523–527. doi:10.17219/acem/91010
23. Žok A, Wiertelowska-Bielarz J, Ewa B. Determinants of moral attitudes toward stem cells. *Adv Clin Exp Med*. 2020;29(12):1379–1387. doi:10.17219/acem/127678
24. Kožlik M, Wójcicki P. The use of stem cells in plastic and reconstructive surgery. *Adv Clin Exp Med*. 2014;23(6):1011–1017. doi:10.17219/acem/37360
25. Ventruba T, Brančíková D, Ventruba P, Minář L, Felsing M, Vomela J. Breast reconstruction in patients with BRCA mutation and breast cancer: Our approach. *Ceska Gynekol*. 2021;86(6):374–380. doi:10.48095/cccg2021374
26. McMahon CA. Embryo donation for medical research: Attitudes and concerns of potential donors. *Hum Reprod*. 2003;18(4):871–877. doi:10.1093/humrep/deg167
27. McMahon C, Gibson F, Cohen J, Leslie G, Tennant C, Saunders D. Mothers conceiving through in vitro fertilization: Siblings, setbacks, and embryo dilemmas after five years. *Reprod Technol*. 2000;10(3):131–135. <http://www.scopus.com/inward/record.url?scp=0033789324&partnerID=8YFLogxK>

Alpha-solanine inhibits endothelial inflammation via nuclear factor kappa B signaling pathway

Nan Wang^{1,A,C,D,F}, Daquan Jiang^{2,B,C,E,F}, Chunxiu Zhou^{3,B,E,F}, Xi Han^{4,A,E,F}

¹ Department of Orthopaedics, Zhejiang Chinese Medical University Affiliated Jiangnan Hospital, Hangzhou, China

² Outpatient Department of Surgery, Zhejiang Chinese Medical University Affiliated Jiangnan Hospital, Hangzhou, China

³ Department of Nursing, Zhejiang Chinese Medical University Affiliated Jiangnan Hospital, Hangzhou, China

⁴ School of Pharmacy, Zhejiang Chinese Medical University, Hangzhou, China

A – research concept and design; B – collection and/or assembly of data; C – data analysis and interpretation;

D – writing the article; E – critical revision of the article; F – final approval of the article

Advances in Clinical and Experimental Medicine, ISSN 1899–5276 (print), ISSN 2451–2680 (online)

Adv Clin Exp Med. 2023;32(8):909–920

Address for correspondence

Nan Wang

E-mail: wangnan1105@126.com

Funding sources

The study was supported by Planning Project of Health Science and Technology Project of Hangzhou City (grant No. 0020190874).

Conflict of interest

None declared

Received on March 14, 2022

Reviewed on November 17, 2022

Accepted on December 28, 2022

Published online on February 8, 2023

Cite as

Wang N, Jiang D, Zhou C, Han X. Alpha-solanine inhibits endothelial inflammation via nuclear factor kappa B signaling pathway. *Adv Clin Exp Med*. 2023;32(8):909–920. doi:10.17219/acem/158781

DOI

10.17219/acem/158781

Copyright

Copyright by Author(s)

This is an article distributed under the terms of the Creative Commons Attribution 3.0 Unported (CC BY 3.0) (<https://creativecommons.org/licenses/by/3.0/>)

Abstract

Background. Alpha-solanine (α -solanine) is the main glycoalkaloid in potato plants. It possesses anticarcinogenic properties and exerts toxic effects. Alpha-solanine can regulate the nuclear factor kappa B (NF- κ B) signaling pathway in cancer cells and macrophages. However, little is known about the anti-inflammatory effects and the related molecular mechanisms of α -solanine on endothelial cells.

Objectives. This study aims to examine the effects of α -solanine on endothelial inflammation in vitro, and to evaluate its influence on regulating the NF- κ B signaling pathway.

Materials and methods. Tumor necrosis factor alpha (TNF- α)-pcDNA3.1(+) plasmid vector was constructed and transfected into human umbilical vein endothelial cells (HUVECs). The expression of TNF- α was examined with quantitative reverse transcription polymerase chain reaction (qRT-PCR) and western blot. Following treatment with α -solanine or the specific NF- κ B inhibitor SN50 for 24 h, cell viability was detected using Cell Counting Kit-8 (CCK-8) assay. Interleukin 6 (IL-6) and TNF- α levels in cell supernatant were detected using enzyme-linked immunosorbent assay (ELISA). The relative protein levels of phospho-P65 (p-P65), phospho-inhibitor of NF- κ B α (p-I κ B α) and I κ B kinase (IKK) α / β were examined with western blot.

Results. The α -solanine inhibits TNF- α -induced inflammatory injury in HUVECs. Compared with control cells, the cell viability was significantly decreased, the levels of TNF- α and IL-6 were significantly increased, and the relative protein levels of p-P65, p-I κ B α and IKK α / β were significantly upregulated in TNF- α -overexpressed cells. The treatment with α -solanine or SN50 decreased the levels of TNF- α and IL-6, and downregulated the relative protein levels of p-P65, p-I κ B α and IKK α / β in TNF- α -overexpressed HUVECs.

Conclusions. This study demonstrated for the first time that α -solanine inhibits endothelial inflammation through the NF- κ B signaling pathway. The α -solanine was suggested to be an inhibitor of the NF- κ B signaling pathway in endothelial cells. The anti-inflammatory effect of α -solanine may provide a new perspective for the prevention and treatment of phlebitis.

Key words: TNF- α , NF- κ B signaling pathway, inflammatory reaction, α -solanine

Background

Peripheral intravenous infusion is widely used in modern medical practice. Phlebitis is a common complication associated with intravenous therapies.¹ The incidence of phlebitis with peripheral intravenous catheter use is 10.5% in hospitalized adult patients in China,¹ whereas it is as high as 53% in hospitalized pediatric patients in Jordan.² Phlebitis is a chemical or mechanical inflammation caused by a long-term intravenous infusion of high-concentration, highly irritant drugs or placement of irritant interventional catheters.^{1,3–5} The routine treatments for phlebitis, such as the external application of magnesium sulfate or mucopolysaccharide polysulfate cream, are unsatisfactory.^{6–8} Therefore, developing new strategies for the prevention and treatment of phlebitis caused by intravenous infusion is needed. Potato glycoalkaloids, the naturally occurring steroidal glycoalkaloids, are well known for their toxicity and antimicrobial activity.^{9–13} Alpha-solanine (α -solanine) is one of the major glycoalkaloids in potato plants.¹⁰ Previous studies about α -solanine mostly center on its anticarcinogenic properties and toxicant effects.^{14–16} It has been reported that α -solanine could promote tumor cell apoptosis, inhibit cell proliferation and suppress angiogenesis.^{17–22} In addition, α -solanine plays important roles in chemical protection and chemotherapy.^{23–25} Shin et al. investigated the anti-inflammatory effect of α -solanine on cultured macrophages in a mouse model of endotoxemia, and the results suggested that α -solanine may be a promising therapeutic agent against inflammatory diseases.²⁶

It has been indicated that the role of α -solanine in cancer cells and macrophages is associated with the nuclear factor kappa B (NF- κ B) signaling pathway.^{26–28} It is a prototypical pro-inflammatory signaling pathway that can be activated by various cytokines, including tumor necrosis factor alpha (TNF- α).²⁹ The NF- κ B family consists of 5 proteins: p65, cRel, RelB, p50, and p52. Among them, p65 possesses a transactivation domain and therefore can affect transcription. In resting cells, NF- κ B proteins exist in the cytoplasm as inactive forms by binding to their inhibitory proteins I κ Bs. The I κ B α is the prototypical member of the I κ B family. The activation of NF- κ B depends on I κ B α phosphorylation. The I κ B α phosphorylation can stimulate ubiquitination and proteasomal degradation, leading to the nuclear translocation of liberated NF- κ B, and subsequently the transcription of inflammatory molecules. The phosphorylation of I κ B proteins is regulated by I κ B kinases (IKK): IKK α and IKK β .^{30,31} Dysregulated NF- κ B signaling can cause an imbalance of immune homeostasis, leading to autoimmune diseases, chronic inflammatory diseases and cancers.^{32–34} In addition, the activation of the NF- κ B signaling pathway is involved in the inflammation-induced activation of the tryptophan-kynurenine metabolic system and mitochondrial impairment, which is implicated in neurodegenerative diseases and psychiatric disorders.^{35–45} The SN50 is a specific NF- κ B inhibitor that could suppress the translocation of the NF- κ B

active complex into the nucleus.^{46,47} It has been reported that SN50 can attenuate inflammation in lung injury and traumatic brain injury.^{48,49}

The anti-inflammatory effect of α -solanine has been reported in macrophages; however, the effect of α -solanine on endothelial inflammation and the related mechanisms have not been reported until now. Elucidating the effects of α -solanine on endothelial inflammation in vitro as well as evaluating its influence on the NF- κ B signaling pathway could provide an experimental basis for the clinical management of phlebitis.

Objectives

This study aims to examine the effects of α -solanine on endothelial inflammation in TNF- α -overexpressed human umbilical vein endothelial cells (HUVECs). Furthermore, whether α -solanine regulates the TNF- α -induced NF- κ B signaling pathway was explored.

Materials and methods

Cells and transfection

The HUVECs (BNCC249736) were provided by Beijing Beina Chuanglian Institute of Biotechnology (Beijing, China) and cultured in Endothelial Cell Medium (1001; ScienCell™, Carlsbad, USA). The cells were incubated at 37°C in a humidified atmosphere of 5% CO₂. The α -solanine (20562-02-1) was purchased from Shanghai Yuanye Bio-Technology Co., Ltd. (Shanghai, China), and SN50 (HY-P0151) from MedChemExpress (Monmouth Junction, USA). The pcDNA3.1(+) (P0157) was provided by Wuhan Miaoling Biotechnology Co., Ltd. (Wuhan, China). Before transfection, the TNF- α overexpression vector (TNF- α -pcDNA3.1(+) plasmid vector) was prepared. The pcDNA3.1(+) plasmid vector was digested with XhoI (ER0691; Thermo Fisher Scientific, Waltham, USA). The sequences of the TNF- α gene were amplified and inserted into the pcDNA3.1(+) vector. The ligated vector was transformed into Trans5 α Chemically Competent Cell (CD201-01; TransGen Biotech Co., Ltd.) and the positive clones were selected. The TNF- α -pcDNA3.1(+) and pcDNA3.1(+) plasmids were extracted using the Endo-free Plasmid Mini Kit II (D6950-01; Omega Bio-Tek, Norcross, USA) and verified through enzyme digestion. Cell transfection was performed using Lipofectamine 3000 (L3000015; Thermo Fisher Scientific).^{50,51} The HUVECs were seeded in 6-well plates at a density of 5 \times 10⁵ cells per well and allowed to grow to 70% confluence. Then, the cells were incubated in fresh medium without serum. Next, 5 μ L Lipofectamine 3000 was diluted with 125 μ L opti-MEM medium and incubated with the diluted plasmid (2.5 μ g plasmid DNA diluted in 125 μ L opti-MEM medium (Thermo Fisher Scientific) and 5 μ L Lipofectamine 3000) for 15 min at room temperature.

The HUVECs were incubated with 250 μ L DNA-liposome complexes (containing 10 μ L Lipofectamine 3000 and 2.5 μ g plasmid DNA) at 37°C for 4 h, and then the medium was refreshed. At 48 h following transfection, the cells were treated with 10 μ g/mL α -solanine or 5 mg/mL SN50 for 24 h.^{52,53} Cells transfected with the empty plasmid vector pcDNA3.1(+) were called the vector group.

Quantitative reverse transcription polymerase chain reaction (qRT-PCR)

Ultrapure RNA Kit (CW0581M; CWBIO, Beijing, China) was used for RNA extraction. The RNA concentrations were measured under an ultraviolet spectrophotometer (NP80, NanoPhotometer; Implen GmbH, Munich, Germany). Reverse transcription was performed to synthesize cDNA using a commercial kit (R223-0; Vazyme Biotech Co., Ltd., Nanjing, China) and qRT-PCR was performed with SYBR Green reagents (A4004M; LifeInt, Xiamen, China). The reaction system contained 1 μ L cDNA, 10 μ L 2 \times SYBR Green PCR Master Mix, 0.4 μ L upstream and downstream primers, and 8.2 μ L dH₂O without RNase. Cycling parameters were 10 min at 95°C for initial denaturation, then 40 cycles of 10 s at 95°C for denaturation, 30 s at 58°C for annealing, and 30 s at 72°C for extension. The primer sequences of *TNF- α* were 5'-CGAGTGACAAGCCTGTAGCC-3' (upstream) and 5'-TGAAGAGACCTGGGAGTAG-3' (downstream). The primer sequences of *β -actin* were 5'-TGGCACCCAGCACAATGAA-3' (upstream) and 5'-CTAAGTCAGATTCGCTAGAGAAGCA-3' (downstream). Relative *TNF- α* mRNA expression levels were calculated using the 2^{- $\Delta\Delta$ C_q} method.⁵⁴ The *β -actin* was used as the housekeeping gene.

Western blot

The cells were lysed with radioimmunoprecipitation assay (RIPA) Lysis Buffer (C1053; Applygen Technologies Inc., Beijing, China) and incubated on ice for 20 min. After centrifugation at 12,000 rpm for 10 min, the concentration of proteins in the supernatant was determined using a bicinchoninic acid (BCA) kit. Equal amounts of protein were separated using sodium dodecyl-sulfate polyacrylamide gel electrophoresis (SDS-PAGE), followed by transferring onto a polyvinylidene fluoride (PVDF) membrane (IPVH00010; Millipore, Boston, USA). The membrane was blocked in nonfat milk and incubated overnight with the specific antibody at 4°C. Mouse monoclonal anti-actin (TA-09) was purchased from Zhongshan Jinqiao Biotechnology Co., Ltd. (Beijing, China). Rabbit anti-P65 (10745-1-ap) and rabbit anti-inhibitor of NF- κ B (anti-I κ B α) (10268-1-ap) were obtained from Proteintech Group Inc. (Chicago, USA). Rabbit anti-phospho-P65 (af2006), rabbit anti-I κ B kinase (IKK) α/β (af6014), and rabbit anti-phospho-I κ B α (af2002) were purchased from Affinity Biosciences (Cincinnati, USA). These antibodies were used at a dilution of 1:1000. After washing with Tris-buffered saline with Tween 20 (TBST),

the membrane was incubated with the secondary antibody, including peroxidase-conjugated goat anti-mouse IgG (H+L) (ZB-2305) and peroxidase-conjugated goat anti-rabbit IgG (H+L) (ZB-2301) at a 1:2000 dilution for 2 h at room temperature. These secondary antibodies were from Zhongshan Jinqiao Biotechnology Co., Ltd (Beijing, China). The signals were visualized by the hypersensitive luminescent solution (RJ239676; Thermo Fisher Scientific) with a chemiluminescence imaging system (ChemiDoc™ XRS+; Bio-Rad, Hercules, USA).

CCK-8 assay

Cell Counting Kit-8 (CCK-8) assay was performed to examine cell viability. This assay uses a tetrazolium salt WST-8 (water-soluble tetrazolium 8), which produces the orange-colored formazan when 2 electrons are received from viable cells through an electron mediator, 1-Methoxy phenazinium methylsulfate (PMS), by nicotinamide adenine dinucleotide (NADH) and nicotinamide adenine dinucleotide phosphate (NADPH). The amount of formazan is dependent on the number of living cells. After washing with phosphate-buffered saline (PBS), 5 \times 10³ cells were plated into the 96-well plate. The α -solanine was dissolved in absolute ethanol. The next day, 1, 3, 6, 9, or 12 μ L of α -solanine (1 mg/mL) were added to treat the cells for 24 h. The medium was then refreshed and 10 μ L of CCK-8 was added into the wells and incubated for 2 h at 37°C. Optical densities were measured with an automatic microplate reader (WD-2102B; Beijing Liuyi Biotechnology Co., Ltd., Beijing, China) at a wavelength of 450 nm.

ELISA

The *TNF- α* and IL-6 concentrations in cell supernatant were measured with the Human *TNF- α* enzyme-linked immunosorbent assay (ELISA) Kit (MM-0122H1; Jiangsu Meimian Industrial Co., Ltd., Yancheng, China) and Human IL-6 ELISA Kit (MM-0049H1; Jiangsu Meimian Industrial Co., Ltd.), respectively, following the manufacturer's protocols. Briefly, 50 μ L standards with different concentrations or 50 μ L samples were added to the wells. Then, 100 μ L of enzyme-labeled reagents were added to each well, except for the blank well, and incubated at 37°C for 60 min. After washing with washing buffer 5 times, 50 μ L substrates A and B were added and the plates were incubated in the dark at 37°C for 15 min. Then, 50 μ L termination solution was added to each well and the optical density (OD) values at a wavelength of 450 nm were measured within 15 min.

Statistical analyses

The IBM SPSS v. 20.0 software (IBM Corp., Armonk, USA) was used to analyze statistical data. Each sample was selected independently. Kruskal–Wallis H test (K–W test) followed by Dunn–Bonferroni test (D–B test) was performed to compare the differences between multiple

Table 1. Statistic values of pairwise comparisons between the groups using the Dunn–Bonferroni test for post hoc testing

Group–group	Viability	Group–group	TNF- α		Viability	IL-6	TNF- α	p-IkBa	p-P65	IKK α / β	Group–group	Viability	IL-6	TNF- α	p-IkBa	p-P65	IKK α / β
			mRNA	protein													
0–10	6.111	C–V	0.000	0.000	13.056	1.556	-4.611	-6.833	-9.917	4.000	C–V	10.944	-10.889	-0.444	7.333	-6.667	4.667
0–30	22.000*	C–T	-9.000*	-9.000*	8.222	-5.222	-4.722	0.500	0.000	-1.083	C–T	30.222*	-32.556*	-29.278*	-21.154*	-21.167*	-15.667*
0–60	27.222*	V–T	-9.000*	-9.000*	33.778*	-37.222*	-38.222*	-25.500*	-24.833*	-20.750*	C–V+S	15.056	-5.778	-6.389	7.167	-2.833	2.333
0–90	28.111*	-	-	-	22.944*	-19.222	-17.778	-11.667	-5.417	-1.917	C–T+S	32.111*	-23.556*	-20.278*	20.333*	-15.167*	-14.751*
0–120	42.889*	-	-	-	42.333*	-28.222*	-29.000*	-19.500*	-18.833*	-18.750*	V–T	19.278*	-21.667*	-28.833*	-20.500*	-14.500*	-20.333*
10–30	15.889	-	-	-	-4.833	-6.778	-0.111	7.333	9.917	-5.083	V–V+S	4.111	5.111	-5.944	-0.167	3.833	-2.333
10–60	21.111	-	-	-	20.722	-38.778*	-33.611*	6.000	-14.917	6.000	V–T+S	21.167*	-17.778*	-19.833*	-14.500*	18.333*	-14.333*
10–90	22.000*	-	-	-	9.889	-20.778	-13.167	-4.833	4.500	-5.917	T–V+S	-15.156	9.000	9.000	-7.167	-8.500	6.000
10–120	36.778*	-	-	-	29.278*	9.000	9.222	-12.167	-8.917	-14.750	T–T+S	1.889	26.778*	22.889*	-14.333*	-14.791*	18.000*
30–60	5.222	-	-	-	25.556*	-32.000*	-33.500*	-26.000*	-24.833*	-19.667*	V+S–T+S	17.056	-12.667	-13.889	6.000	6.000	-9.667
30–90	6.111	-	-	-	14.722	-14.000	-13.056	-12.167	-5.417	-0.833	-	-	-	-	-	-	-
30–120	20.889	-	-	-	34.111*	-23.000*	-24.278*	-20.000*	-18.833*	18.833*	-	-	-	-	-	-	-
60–90	0.889	-	-	-	-10.833	18.000	20.444	13.833	6.000	-13.667	-	-	-	-	-	-	-
60–120	15.667	-	-	-	8.556	-29.778*	-24.389*	-18.667*	19.417*	-24.750*	-	-	-	-	-	-	-
90–120	14.778	-	-	-	19.389	-9.000	-11.222	-7.833	-13.417	-12.833	-	-	-	-	-	-	-

* p < 0.05; C – control; V – vector; T – TNF- α ; α – α -solanine; S – SN50; IL-6 – interleukin 6; TNF- α – tumor necrosis factor alpha; p-P65 – phospho-P65; p-IkBa – phospho-inhibitor of NF- κ B; IKK – IkB kinase.

groups. All the statistical values of pairwise comparisons between the groups using D–B test for post hoc testing are shown in Table 1. Statistical significance was defined as $p < 0.05$.

Results

Effect of different concentrations of α -solanine on the viability of HUVECs

Different concentrations of α -solanine were used to treat HUVECs for 24 h. Then, the cell viabilities were measured using the CCK-8 assay. As shown in Fig. 1A, HUVEC viability was significantly decreased by treatment with

30 $\mu\text{g/mL}$, 60 $\mu\text{g/mL}$, 90 $\mu\text{g/mL}$, and 120 $\mu\text{g/mL}$ α -solanine (K–W test: $H = 44.802$, $df = 5$, $p < 0.001$). Cell viability was not affected by treatment with 10 $\mu\text{g/mL}$ α -solanine (D–B test, $p = 1.000$). Therefore, we chose α -solanine at the concentration of 10 $\mu\text{g/mL}$ to conduct the following experiments.

Effect of α -solanine on cell viability of TNF- α -overexpressed HUVECs

The TNF- α overexpression vector was constructed and transfected into HUVECs, and TNF- α expression levels in HUVECs were examined with western blot and qRT-PCR. The results in Fig. 1B show that, compared with the TNF- α negative control vector (pcDNA3.1(+)) plasmid

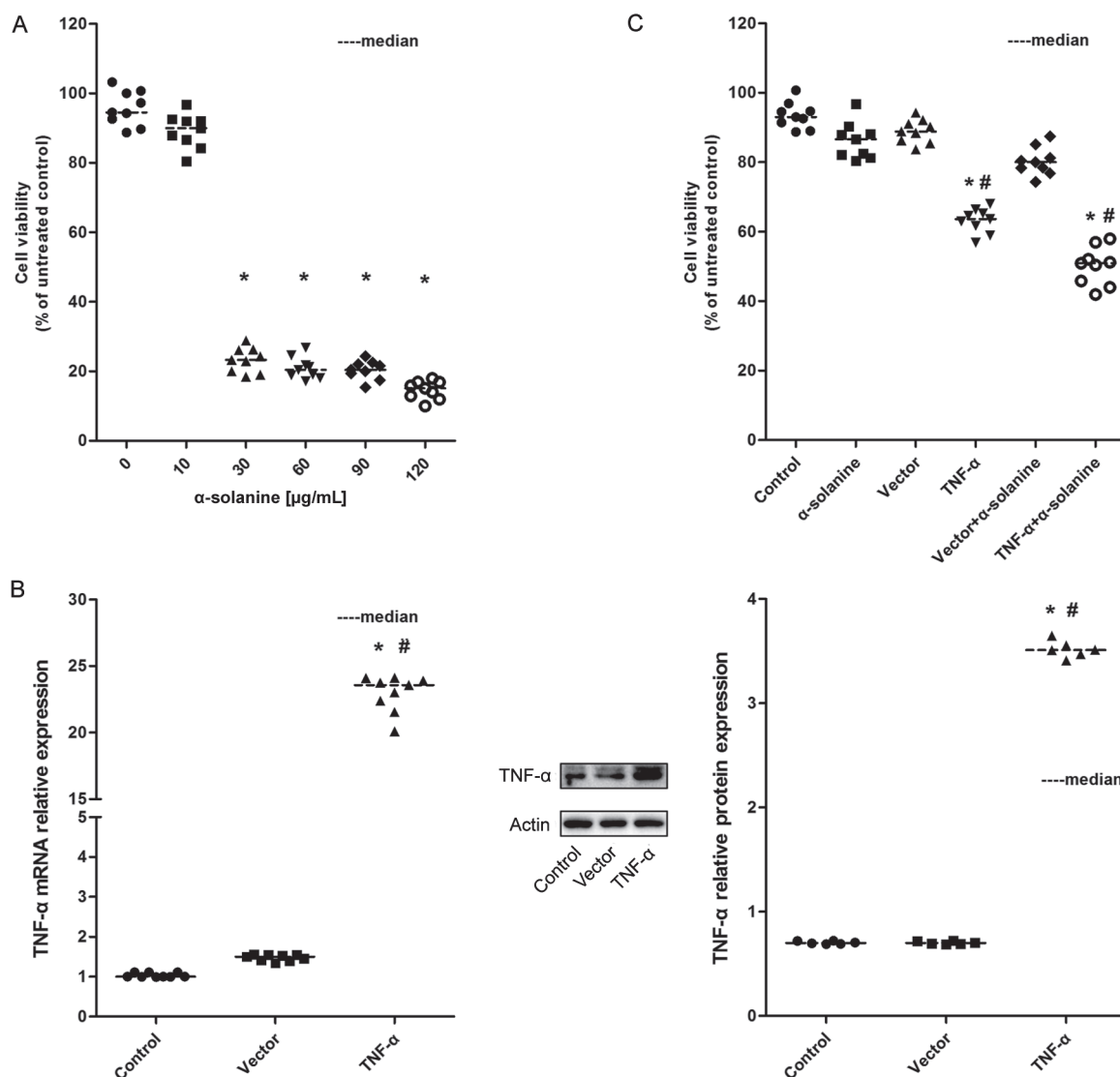


Fig. 1. Effects of α -solanine on cell viability of tumor necrosis factor alpha (TNF- α)-overexpressed human umbilical vein endothelial cells (HUVECs). A. Cell viability of HUVECs under the treatment of different concentrations of α -solanine. Data were analyzed with Kruskal–Wallis H (K–W) test followed by Dunn–Bonferroni (D–B) test (K–W test: $H = 44.802$, degrees of freedom (df) = 5, $p < 0.001$; * $p < 0.05$ compared to 0 $\mu\text{g/mL}$, $n = 5$); B. TNF- α relative mRNA expression level and TNF- α relative protein expression level in HUVECs after the transfection of the pcDNA3.1(+) plasmid vector or the TNF- α overexpression vector. Data were analyzed using K–W test followed by D–B test (K–W test: mRNA, $H = 23.143$, $df = 2$, $p < 0.001$; protein, $H = 11.439$, $df = 2$, $p = 0.003$; * $p < 0.05$ compared to vector; # $p < 0.05$ compared to TNF- α , $n = 3$); C. Effects of α -solanine treatment on the cell viability of HUVECs transfected with TNF- α vector. Data were analyzed with K–W test followed by D–B test (K–W test: $H = 46.700$, $df = 5$, $p < 0.001$; * $p < 0.05$ compared to control; # $p < 0.05$ compared to vector; $n = 5$)

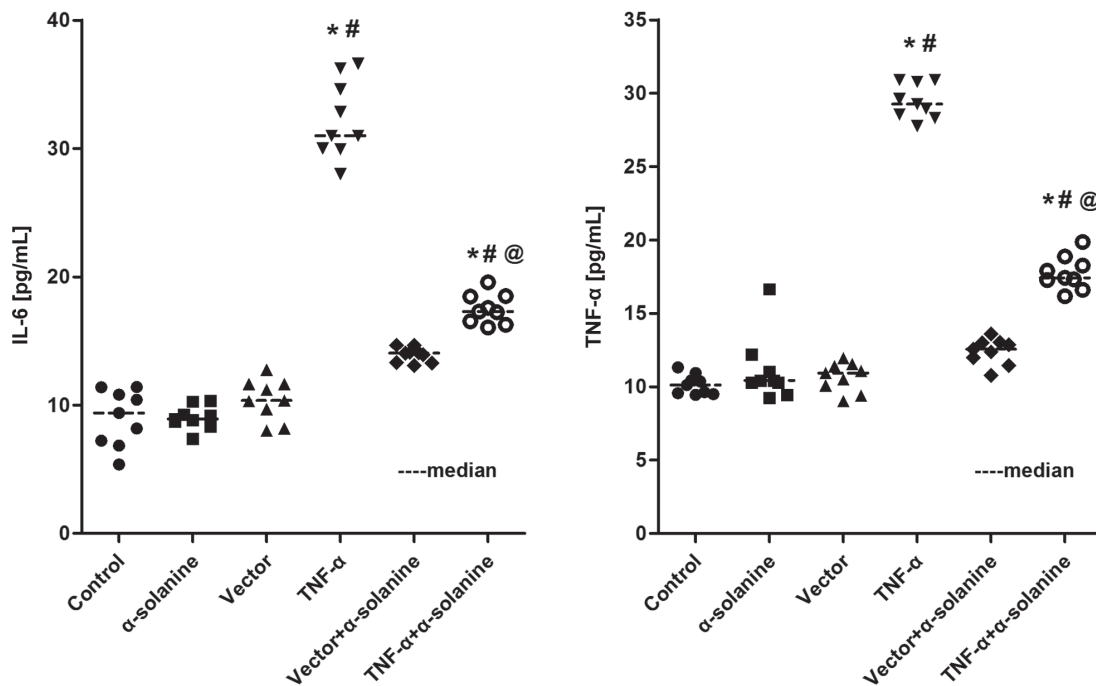


Fig. 2. Effects of α -solanine on tumor necrosis factor alpha (TNF- α) and interleukin 6 (IL-6) protein levels in TNF- α -overexpressed cells. Data were analyzed with Kruskal–Wallis H (K–W) test followed by Dunn–Bonferroni test (K–W test: TNF- α , $H = 42.863$, degrees of freedom (df) = 5, $p < 0.001$; IL-6, $H = 46.571$, df = 5, $p < 0.001$; * $p < 0.05$ compared to control; # $p < 0.05$ compared to vector; @ $p < 0.05$ compared to TNF- α ; $n = 3$)

vector)-transfected cells, both the TNF- α relative mRNA expression level (D–B test, $p = 0.048$) and the TNF- α relative protein expression level (D–B test, $p = 0.010$) in the TNF- α overexpression vector-transfected cells were significantly increased. The CCK-8 assay demonstrated that, compared with the vector group, cell viability was significantly decreased in the TNF- α group (D–B test, $p = 0.009$). The difference in cell viability between the TNF- α + α -solanine group and the TNF- α group was not significant (D–B test, $p = 1.000$) (Fig. 1C).

Effect of α -solanine on TNF- α and IL-6 protein levels in TNF- α -overexpressed HUVECs

An ELISA was used to detect TNF- α and interleukin 6 (IL-6) protein levels in the cell supernatant of HUVECs. The results presented in Fig. 2 show that, compared with the vector group, TNF- α (D–B test, $p < 0.001$) and IL-6 protein levels (D–B test, $p < 0.001$) were significantly increased in the TNF- α group. In TNF- α -overexpressed cells, α -solanine significantly decreased the elevated protein levels of TNF- α (D–B test, $p = 0.015$) and IL-6 (D–B test, $p = 0.001$).

Effect of α -solanine on phospho-inhibitor of NF- κ Ba (p-I κ Ba), phospho-P65 (p-P65) and IKK α / β relative protein expression levels in TNF- α -overexpressed HUVECs

The p-I κ Ba, p-P65 and IKK α / β relative protein expression levels in TNF- α -overexpressed HUVECs were determined using western blot assay. We found that the relative protein expression levels of p-I κ Ba (D–B test, $p < 0.001$), p-P65 (D–B test, $p = 0.001$) and IKK α / β (D–B

test, $p = 0.018$) were significantly increased in the TNF- α group compared with the vector group. However, in TNF- α -overexpressed HUVECs, the increased p-I κ Ba (D–B test, $p = 0.032$), p-P65 (D–B test, $p = 0.021$) and IKK α / β (D–B test, $p = 0.001$) relative protein expression levels were significantly suppressed by treatment with α -solanine (Fig. 3).

Effect of SN50 on cell viability, as well as IL-6 and TNF- α levels in TNF- α -overexpressed HUVECs

The SN50 is a specific NF- κ B inhibitor that could suppress the translocation of the NF- κ B active complex into the nucleus. To evaluate whether α -solanine has a similar function to that of SN50, the cells were treated with 5 mg/mL SN50 for 24 h. As shown in Fig. 4A, SN50 did not affect the cell viability of TNF- α -overexpressed HUVECs (D–B test, $p = 1.000$). As shown in Fig. 4B, both the TNF- α level (D–B test, $p < 0.001$) and the IL-6 level (D–B test, $p = 0.005$) were significantly increased in TNF- α -overexpressed HUVECs; however, SN50 treatment suppressed the elevated TNF- α (D–B test, $p = 0.002$) and IL-6 (D–B test, $p < 0.001$) levels.

Effect of SN50 on p-I κ Ba, p-P65 and IKK α / β relative protein expression levels in TNF- α -overexpressed HUVECs

The results presented in Fig. 5 demonstrate that p-I κ Ba (D–B test, $p = 0.001$), p-P65 (D–B test, $p = 0.043$) and IKK α / β (D–B test, $p = 0.001$) relative protein expression levels were increased in the cells transfected with the TNF- α vector compared with the cells transfected with the pcDNA3.1(+) vector. The SN50 treatment

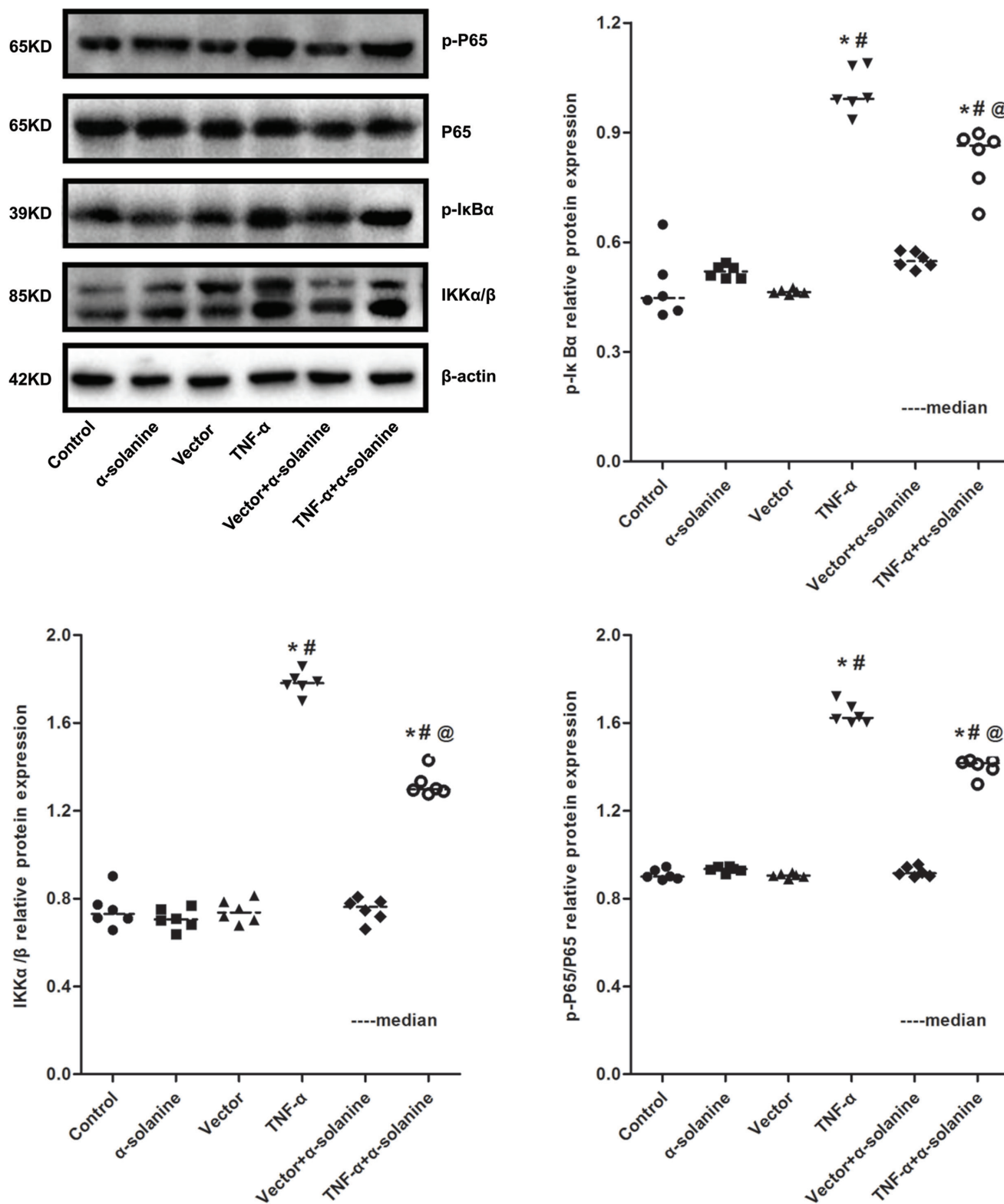


Fig. 3. Effect of α-solanine on phospho-inhibitor of NF-κBα (p-IκBα), phospho-P65 (p-P65) and IκB kinase (IKK) α/β relative protein expression levels in tumor necrosis factor alpha (TNF-α)-overexpressed cells. Data were analyzed with Kruskal–Wallis H (K–W) test followed by Dunn–Bonferroni test (K–W test: p-IκBα, H = 29.841, degrees of freedom (df) = 5, p < 0.001; p-P65, H = 28.052, df = 5, p < 0.001; IKKα/β, H = 25.441, df = 5, p < 0.001; * p < 0.05 compared to control; # p < 0.05 compared to vector; @ p < 0.05 compared to TNF-α; n = 3)

significantly suppressed the increased p-IκBα (D–B test, p = 0.048), p-P65 (D–B test, p = 0.041) and IKKα/β (D–B test, p = 0.004) relative protein expression levels in TNF-α-overexpressed HUVECs.

Discussion

The present study demonstrated the effects of α-solanine on inflammation in HUVECs. The α-solanine inhibited

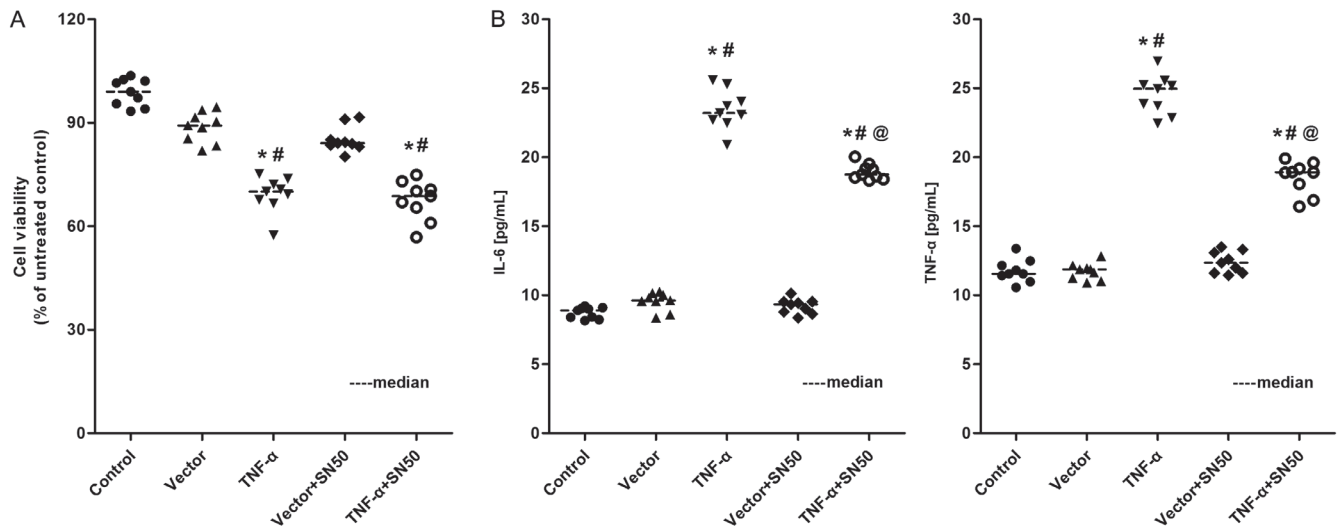


Fig. 4. Effects of SN50 on (A) cell viability (data were analyzed with Kruskal–Wallis H (K–W) test followed by Dunn–Bonferroni test (K–W test: $H = 38.110$, $df = 4$, $p < 0.001$)), as well as (B) the protein levels of tumor necrosis factor alpha (TNF- α) and interleukin 6 (IL-6) in TNF- α -overexpressed cells (data were analyzed with K–W test followed by Dunn–Bonferroni test (K–W test: TNF- α , $H = 35.143$, degrees of freedom (df) = 4, $p < 0.001$; IL-6, $H = 36.906$, $df = 4$, $p < 0.001$; * $p < 0.05$ compared to control; # $p < 0.05$ compared to vector; @ $p < 0.05$ compared to TNF- α ; $n = 5$ for cell viability and $n = 3$ for TNF- α and IL-6 protein levels))

the expression of TNF- α and IL-6 in TNF- α -overexpressed HUVECs, and these effects were related to the suppression of the NF- κ B signaling pathway.

Phlebitis is an inflammation of the vein. Vascular endothelial cells make up the innermost surface of blood vessels. Inflammatory injury and apoptosis of endothelial cells are observed in many human diseases, including phlebitis.^{55–57} In the present study, TNF- α was overexpressed in HUVECs to establish a model of venous endothelial inflammation. Consistent with the previous report revealing that TNF- α can induce inflammatory injury,⁵⁸ our study showed that TNF- α increased IL-6 expression, activated the NF- κ B signaling pathway and inhibited the proliferation of HUVECs. These results demonstrated that TNF- α can induce inflammation injury in endothelial cells.

A large number of studies have confirmed the toxic effects of α -solanine on cancers.^{14–16,23,24} Only a limited number of studies investigated the anti-inflammatory effect of α -solanine on macrophages and in endotoxemia model mice.^{26,59} Kenny et al. reported that α -solanine possesses anti-inflammatory properties in lipopolysaccharide (LPS)-induced Raw264.7 macrophages⁵⁹ by reducing the production of nitric oxide (NO) and decreasing the levels of pro-inflammatory cytokines. This study provided more evidence for the anti-inflammatory effect of α -solanine. We investigated the anti-inflammatory effect of α -solanine in endothelial cells. Similar to the effects in LPS-induced macrophages, α -solanine inhibited the expression of the pro-inflammatory mediators TNF- α and IL-6 in TNF- α -overexpressed endothelial cells. The suppression of TNF- α and IL-6 can prevent inflammatory injury and apoptosis of HUVECs.^{60,61} Taken together, this evidence suggests that α -solanine can inhibit inflammatory injury of HUVECs. It is noteworthy that the levels

of IL-6 and TNF- α in the TNF- α + α -solanine group were significantly higher than in the control group, suggesting that α -solanine may not eliminate the effect of TNF- α overexpression on IL-6 and TNF- α elevation in HUVECs. However, α -solanine could alleviate endothelial inflammation, thus showing a positive role in the treatment of phlebitis.

The NF- κ B pathway is considered the most typical inflammatory pathway, and many inflammatory mediators are found downstream of NF- κ B.^{62,63} The study by Lu et al. showed that α -solanine downregulates the nuclear content of NF- κ B in human melanoma cells.²⁸ In human hepatocellular carcinoma HepG2 cells, α -solanine-induced oxidative stress is associated with the NF- κ B pathway.²⁷ Natural or synthetic NF- κ B inhibitors could prevent LPS-induced injury in endothelial cells by decreasing the levels of inflammatory factors.^{64,65} In the current study, we investigated the effect of α -solanine on the NF- κ B signaling pathway in endothelial cells and found that α -solanine inhibited TNF- α -induced NF- κ B signaling pathway activation in HUVECs by decreasing p-I κ B α , p-P65 and IKK α / β relative protein expression levels. Our results were consistent with the reports on LPS-induced macrophages and endotoxemia model mice which demonstrated that α -solanine abrogates inflammatory responses by inhibiting the NF- κ B signaling pathway. We found that p-I κ B α was not significantly decreased in the TNF- α + α -solanine group compared with the control group. However, p-I κ B α was significantly decreased in the TNF- α + α -solanine group compared with the TNF- α group. These results indicate that α -solanine may not eliminate the effect of TNF- α overexpression on I κ B α phosphorylation in HUVECs. However, α -solanine shows an inhibitory effect on the phosphorylation of I κ B α in TNF- α -overexpressed HUVECs. Taken

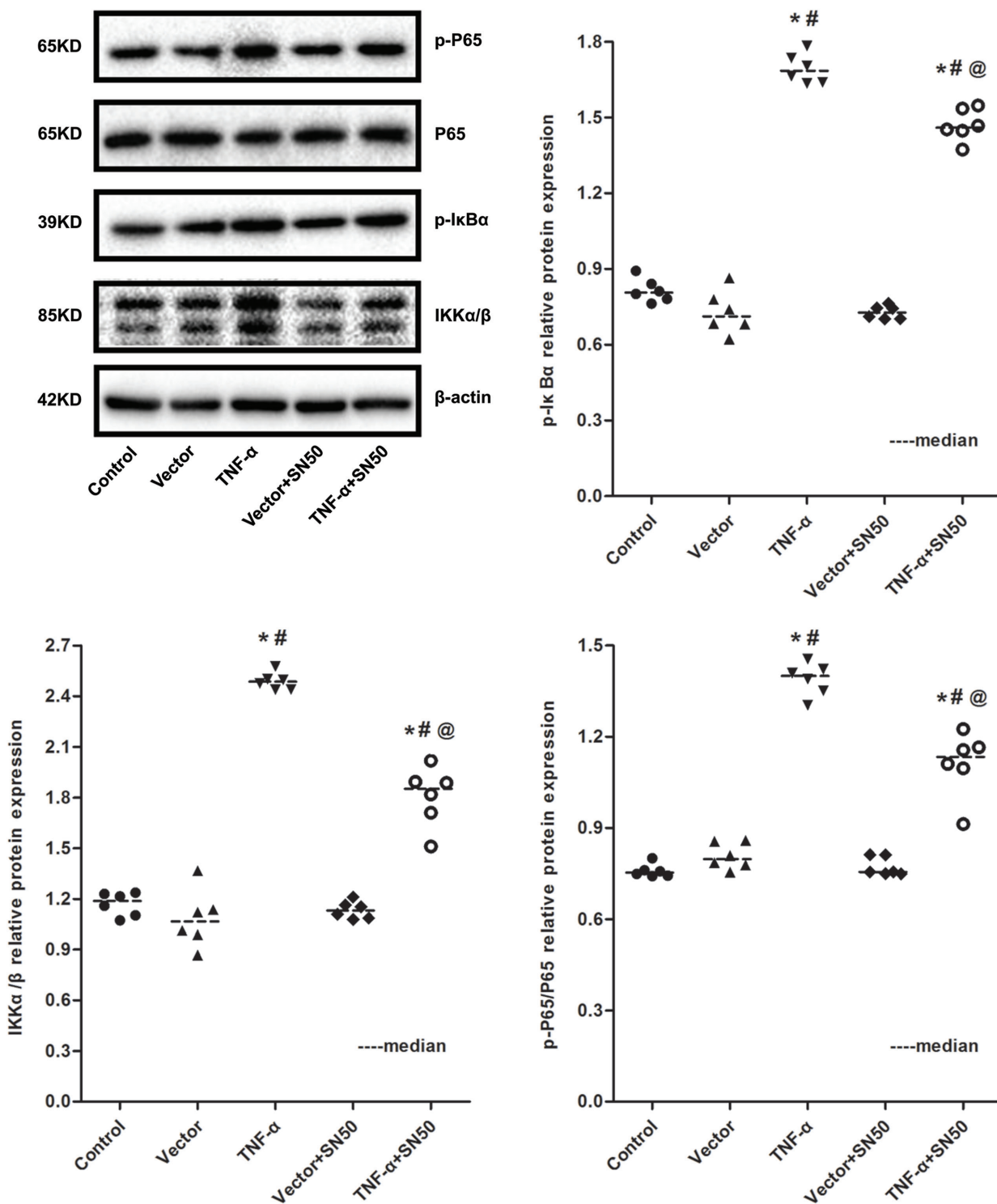


Fig. 5. Effect of SN50 on phospho-inhibitor of NF-κBα (p-IkBα), phospho-P65 (p-P65) and IκB kinase (IKK) α/β relative protein expression levels in tumor necrosis factor alpha (TNF-α)-overexpressed cells. Data were analyzed with Kruskal–Wallis H (K–W) test followed by Dunn–Bonferroni test (K–W test: p-IkBα, H = 25.011, degrees of freedom (df) = 4, p < 0.001; p-P65, H = 24.030, df = 4, p < 0.001; IKKα/β, H = 23.140, df = 4, p < 0.001; * p < 0.05 compared to control; # p < 0.05 compared to vector; @ p < 0.05 compared to TNF-α; n = 3)

p-P65 – phospho-P65; p-IkBα – phospho-inhibitor of NF-κB α; IKK – IκB kinase

together, this evidence suggests that α-solanine protects against inflammatory diseases via NF-κB suppression. Previous studies have shown other molecules and signaling pathways that were regulated by α-solanine, such as matrix metalloproteinases (MMPs), Akt/mTOR signaling

pathway, STAT3 signaling pathway, and ERK and PI3K/Akt signaling pathways.^{20,28,66–68} Whether these molecules and signaling pathways are involved in the effect of α-solanine on protecting against endothelial inflammation is still unknown. The molecular mechanisms underlying the effect

of α -solanine on endothelial inflammation need to be further explored.

In the present study, we found that the effects of α -solanine on TNF- α -overexpressed HUVECs seem to be similar to that of SN50. The activation of the NF- κ B pathway leads to the nuclear translocation of NF- κ B protein and the activation of downstream genes.⁶⁹ The SN50 is a specific NF- κ B inhibitor that could suppress the translocation of the NF- κ B active complex into the nucleus. We demonstrated that both α -solanine and SN50 could decrease the relative expression levels of proteins in the NF- κ B signaling pathway, such as p-I κ B α , p-P65 and IKK α / β . These results suggested that α -solanine can act as an NF- κ B inhibitor in the process of inflammatory injury in HUVECs. However, we did not examine the nuclear translocation of NF- κ B proteins. To confirm the possibility of α -solanine as an NF- κ B inhibitor, a study investigating the effect of α -solanine on NF- κ B nuclear translocation will be carried out in the future.

This study demonstrated the inhibitory effect of α -solanine on endothelial inflammation in vitro. Further studies need to be performed on phlebitis animal models and phlebitis patients to confirm the anti-inflammatory effect of α -solanine in vivo. Expanding the application of α -solanine on other inflammatory diseases may be a good research direction in the future. Potato glycoside alkaloids are a group of easily obtained natural steroid compounds. Studies on the function of α -solanine in inflammation will provide a new perspective for the prevention and treatment of phlebitis, as well as new ideas for the research and development of potato glycoside alkaloids.

Limitations

There are 3 major limitations to this study. First, we only investigated the anti-inflammatory effects of α -solanine in vitro. The therapeutic effect of α -solanine on phlebitis in vivo needs to be confirmed on animal models in our further studies. Second, to fully elucidate the effect of α -solanine on inflammatory response in HUVECs, more inflammatory factors and mechanisms that are related to inflammation need to be examined. Third, TNF- α -transfected cells are not a good model of inflammation. The use of endotoxin or inflammatory agents will better induce inflammation.

Conclusions

This is the first in vitro study demonstrating that α -solanine inhibits endothelial inflammation through the NF- κ B signaling pathway. The findings support the potential application of α -solanine for the clinical management of phlebitis and describe the molecular mechanism underlying the protective function of α -solanine against endothelial inflammation.

ORCID iDs

Nan Wang  <https://orcid.org/0000-0001-7362-7590>

Daquan Jiang  <https://orcid.org/0000-0003-4413-0598>

Chunxiu Zhou  <https://orcid.org/0000-0002-8274-4438>

Xi Han  <https://orcid.org/0000-0001-6616-8808>

References

- Liu C, Chen L, Kong D, Lyu F, Luan L, Yang L. Incidence, risk factors and medical cost of peripheral intravenous catheter-related complications in hospitalised adult patients. *J Vasc Access*. 2022;23(1):57–66. doi:10.1177/1129729820978124
- Suliman M, Saleh W, Al-Shiekh H, Taan W, AlBashtawy M. The incidence of peripheral intravenous catheter phlebitis and risk factors among pediatric patients. *J Pediatr Nurs*. 2020;50:89–93. doi:10.1016/j.pedn.2019.11.006
- Manrique-Rodríguez S, Heras-Hidalgo I, Pernia-López MS, et al. Standardization and chemical characterization of intravenous therapy in adult patients: A step further in medication safety. *Drugs Res Dev*. 2021;21(1):39–64. doi:10.1007/s40268-020-00329-w
- Marsh N, Webster J, Ullman AJ, et al. Peripheral intravenous catheter non-infectious complications in adults: A systematic review and meta-analysis. *J Adv Nurs*. 2020;76(12):3346–3362. doi:10.1111/jan.14565
- Nicotera R. La flebite associata alla terapia endovenosa/infusionale. *Assistenza Infermieristica e Ricerca*. 2011;30(1):34–41. doi:10.1702/620.7244
- Wan Y. Observation for clinical effect of phellodendron wet compress in treating the phlebitis caused by infusion. *Pak J Pharm Sci*. 2018;31(3 Special):1099–1102. PMID:29735457.
- Zheng GH, Yang L, Chen HY, Chu JF, Mei L. *Aloe vera* for prevention and treatment of infusion phlebitis. *Cochrane Database Syst Rev*. 2014; 2014(6):CD009162. doi:10.1002/14651858.CD009162.pub2
- Wang X, Lv X, Zhang J, Wang Y. Effect of Chahuang ointment on prevention of phlebitis from peripherally inserted central catheter: Randomized clinical trial. *Rev Esc Enferm USP*. 2021;55:e03680. doi:10.1590/s1980-220x2019008003680
- Friedman M. Chemistry and anticarcinogenic mechanisms of glycoalkaloids produced by eggplants, potatoes, and tomatoes. *J Agric Food Chem*. 2015;63(13):3323–3337. doi:10.1021/acs.jafc.5b00818
- Friedman M. Potato glycoalkaloids and metabolites: Roles in the plant and in the diet. *J Agric Food Chem*. 2006;54(23):8655–8681. doi:10.1021/jf061471t
- Korpan YI, Nazarenko EA, Skryshevskaya IV, Martelet C, Jaffrezic-Renault N, El'skaya AV. Potato glycoalkaloids: True safety or false sense of security? *Trends Biotechnol*. 2004;22(3):147–151. doi:10.1016/j.tibtech.2004.01.009
- Dhalsamant K, Singh CB, Lankapalli R. A review on greening and glycoalkaloids in potato tubers: Potential solutions. *J Agric Food Chem*. 2022;70(43):13819–13831. doi:10.1021/acs.jafc.2c01169
- Schrenk D, Bignami M, Bodin L, et al; EFSA Panel on Contaminants in the Food Chain (CONTAM). Risk assessment of glycoalkaloids in feed and food, in particular in potatoes and potato-derived products. *EFSA J*. 2020;18(8):e06222. doi:10.2903/j.efsa.2020.6222
- Hassan SH, Gul S, Zahra HS, et al. Alpha solanine: A novel natural bioactive molecule with anticancer effects in multiple human malignancies. *Nutr Cancer*. 2021;73(9):1541–1552. doi:10.1080/01635581.2020.1803932
- Luo S, Tian GJ, Yu FX, Wen ZD. A narrative review of the antitumor studies of solanine. *Transl Cancer Res*. 2021;10(3):1578–1582. doi:10.21037/tcr-20-3094
- Mohsenikia M, Alizadeh AM, Khodayari S, et al. The protective and therapeutic effects of alpha-solanine on mice breast cancer. *Eur J Pharmacol*. 2013;718(1–3):1–9. doi:10.1016/j.ejphar.2013.09.015
- Lv C, Kong H, Dong G, et al. Antitumor efficacy of α -solanine against pancreatic cancer in vitro and in vivo. *PLoS One*. 2014;9(2):e87868. doi:10.1371/journal.pone.0087868
- Yan X, Li M, Chen L, et al. α -solanine inhibits growth and metastatic potential of human colorectal cancer cells. *Oncol Rep*. 2020;43(5):1387–1396. doi:10.3892/or.2020.7519
- Zou T, Gu L, Yang L, et al. Alpha-solanine anti-tumor effects in non-small cell lung cancer through regulating the energy metabolism pathway. *Recent Pat Anticancer Drug Discov*. 2022;17(4):396–409. doi:10.2174/1574892817666220113144635

20. Shen KH, Liao A, Hung JH, et al. α -solanine inhibits invasion of human prostate cancer cell by suppressing epithelial–mesenchymal transition and MMPs expression. *Molecules*. 2014;19(8):11896–11914. doi:10.3390/molecules190811896
21. Wang L, Sun QQ, Zhang SJ, et al. Inhibitory effect of α -solanine on esophageal carcinoma in vitro. *Exp Ther Med*. 2016;12(3):1525–1530. doi:10.3892/etm.2016.3500
22. Ni X, Chen J, Lu F, et al. Anti-cancer effect of α -solanine by down-regulating S100P expression in colorectal cancer cells. *Recent Pat Anticancer Drug Discov*. 2018;13(2):240–247. doi:10.2174/1574892813666180329163945
23. Wang Y, Wu J, Guo W, et al. α -solanine modulates the radiosensitivity of esophageal cancer cells by inducing microRNA 138 expression. *Cell Physiol Biochem*. 2016;39(3):996–1010. doi:10.1159/000447807
24. Gu T, Yuan W, Li C, et al. α -solanine inhibits proliferation, invasion, and migration, and induces apoptosis in human choriocarcinoma JEG-3 cells in vitro and in vivo. *Toxins*. 2021;13(3):210. doi:10.3390/toxins13030210
25. Nie X, Dai Y, Tan J, et al. α -solanine reverses pulmonary vascular remodeling and vascular angiogenesis in experimental pulmonary artery hypertension. *J Hypertens*. 2017;35(12):2419–2435. doi:10.1097/HJH.0000000000001475
26. Shin JS, Lee KG, Lee HH, et al. Solanine isolated from *Solanum tuberosum* L. cv Jayoung abrogates LPS-induced inflammatory responses via NF- κ B inactivation in RAW 264.7 macrophages and endotoxin-induced shock model in mice. *J Cell Biochem*. 2016;117(10):2327–2339. doi:10.1002/jcb.25530
27. Gouhar SA, Abo-Elfadl MT, Gamal-Eldeen AM, El-Daly SM. Involvement of miRNAs in response to oxidative stress induced by the steroidal glycoalkaloid α -solanine in hepatocellular carcinoma cells. *Environ Toxicol*. 2022;37(2):212–223. doi:10.1002/tox.23390
28. Lu MK, Shih YW, Chang Chien TT, Fang LH, Huang HC, Chen PS. α -solanine inhibits human melanoma cell migration and invasion by reducing matrix metalloproteinase-2/9 activities. *Biol Pharm Bull*. 2010;33(10):1685–1691. doi:10.1248/bpb.33.1685
29. Hayden MS, Ghosh S. Regulation of NF- κ B by TNF family cytokines. *Semin Immunol*. 2014;26(3):253–266. doi:10.1016/j.smim.2014.05.004
30. Hayden MS, Ghosh S. NF- κ B, the first quarter-century: Remarkable progress and outstanding questions. *Genes Dev*. 2012;26(3):203–234. doi:10.1101/gad.183434.111
31. Ghosh S, Hayden MS. Celebrating 25 years of NF- κ B research. *Immunol Rev*. 2012;246(1):5–13. doi:10.1111/j.1600-065X.2012.01111.x
32. Mitchell JP, Carmody RJ. NF- κ B and the transcriptional control of inflammation. *Int Rev Cell Mol Biol*. 2018;335:41–84. doi:10.1016/bbs.ircmb.2017.07.007
33. Peng C, Ouyang Y, Lu N, Li N. The NF- κ B signaling pathway, the microbiota, and gastrointestinal tumorigenesis: Recent advances. *Front Immunol*. 2020;11:1387. doi:10.3389/fimmu.2020.01387
34. Poma P. NF- κ B and disease. *Int J Mol Sci*. 2020;21(23):9181. doi:10.3390/ijms21239181
35. Ozer M, Ince S, Gündoğdu B, et al. Effect of thiamine pyrophosphate on cyclophosphamide-induced oxidative ovarian damage and reproductive dysfunction in female rats. *Adv Clin Exp Med*. 2022;31(2):129–137. doi:10.17219/acem/142535
36. Zhou A, Zhang S, Yang C, Liao N, Zhang Y. Dandelion root extracts abolish MAPK pathways to ameliorate experimental mouse ulcerative colitis. *Adv Clin Exp Med*. 2022;31(5):529–538. doi:10.17219/acem/146234
37. Tosun M, Olmez H, Unver E, et al. Oxidative and pro-inflammatory lung injury induced by desflurane inhalation in rats and the protective effect of rutin. *Adv Clin Exp Med*. 2021;30(9):941–948. doi:10.17219/acem/136194
38. Sun B, Liu Z, Yu Z. miRNA-323a-3p promoted intracranial, aneurysm-induced inflammation via AMPK/NF- κ B signaling pathway by AdipoR1. *Adv Clin Exp Med*. 2022;31(11):1243–1254. doi:10.17219/acem/151053
39. Zhuang S, Xu Q, Li Y, Hu K, Xia Z, Zhang L. Serum TBK1 levels are correlated with inflammation, optic nerve sheath diameter and intracranial pressure in severe traumatic brain injury patients under deep sedation [published online as ahead of print on November 30, 2022]. *Adv Clin Exp Med*. 2022. doi:10.17219/acem/155040
40. Requena-Ocaña N, Flores-Lopez M, Papaseit E, et al. Vascular endothelial growth factor as a potential biomarker of neuroinflammation and frontal cognitive impairment in patients with alcohol use disorder. *Biomedicines*. 2022;10(5):947. doi:10.3390/biomedicines10050947
41. Török N, Maszlag-Török R, Molnár K, et al. Single nucleotide polymorphisms of indoleamine 2,3-dioxygenase 1 influenced the age onset of Parkinson's disease. *Front Biosci (Landmark Ed)*. 2022;27(9):265. doi:10.31083/j.fb12709265
42. Tanaka M, Szabó Á, Spekker E, Polyák H, Tóth F, Vécsei L. Mitochondrial impairment: A common motif in neuropsychiatric presentation? The link to the tryptophan–kynurenine metabolic system. *Cells*. 2022;11(16):2607. doi:10.3390/cells11162607
43. Tanaka M, Vécsei L. Editorial of Special Issue 'Dissecting Neurological and Neuropsychiatric Diseases: Neurodegeneration and Neuroprotection.' *Int J Mol Sci*. 2022;23(13):6991. doi:10.3390/ijms23136991
44. Tanaka M, Spekker E, Szabó Á, Polyák H, Vécsei L. Modelling the neurodevelopmental pathogenesis in neuropsychiatric disorders: Bioactive kynurenines and their analogues as neuroprotective agents. In celebration of 80th birthday of Professor Peter Riederer. *J Neural Transm*. 2022;129(5–6):627–642. doi:10.1007/s00702-022-02513-5
45. Tanaka M, Szabó Á, Vécsei L. Integrating armchair, bench, and bedside research for behavioral neurology and neuropsychiatry: Editorial. *Biomedicines*. 2022;10(12):2999. doi:10.3390/biomedicines10122999
46. Zhao K, Zhu BS, Gong W, et al. SN50 enhances the effects of LY294002 on cell death induction in gastric cancer cell line SGC7901. *Arch Med Sci*. 2013;6:990–998. doi:10.5114/aoms.2013.39790
47. Saika S, Miyamoto T, Yamanaka O, et al. Therapeutic effect of topical administration of SN50, an inhibitor of nuclear factor- κ B, in treatment of corneal alkali burns in mice. *Am J Pathol*. 2005;166(5):1393–1403. doi:10.1016/S0002-9440(10)62357-7
48. Sun YX, Dai DK, Liu R, et al. Therapeutic effect of SN50, an inhibitor of nuclear factor- κ B, in treatment of TBI in mice. *Neurol Sci*. 2013;34(3):345–355. doi:10.1007/s10072-012-1007-z
49. Chian CF, Chiang CH, Chuang CH, Liu SL, Tsai CL. SN50, a cell-permeable inhibitor of nuclear factor- κ B, attenuates ventilator-induced lung injury in an isolated and perfused rat lung model. *Shock*. 2016;46(2):194–201. doi:10.1097/SHK.0000000000000563
50. Shi B, Xue M, Wang Y, et al. An improved method for increasing the efficiency of gene transfection and transduction. *Int J Physiol Pathophysiol Pharmacol*. 2018;10(2):95–104. PMID:29755642.
51. Xian Z, Yanhua H, Jingyi H, Yan W, Dingming S, Chenglong L. Optimization of transfection conditions of chicken primordial germ cells. *Yi Chuan*. 2021;43(3):280–288. doi:10.16288/jyczz.20-212
52. Kao YH, Chen YC, Cheng CC, Lee TI, Chen YJ, Chen SA. Tumor necrosis factor- α decreases sarcoplasmic reticulum Ca²⁺-ATPase expressions via the promoter methylation in cardiomyocytes. *Crit Care Med*. 2010;38(1):217–222. doi:10.1097/CCM.0b013e3181b4a854
53. Qin Y, Hua M, Duan Y, et al. TNF- α expression in Schwann cells is induced by LPS and NF- κ B-dependent pathways. *Neurochem Res*. 2012;37(4):722–731. doi:10.1007/s11064-011-0664-2
54. Livak KJ, Schmittgen TD. Analysis of relative gene expression data using real-time quantitative PCR and the 2^{- $\Delta\Delta$ CT} method. *Methods*. 2001;25(4):402–408. doi:10.1006/meth.2001.1262
55. Bosseboeuf E, Raimondi C. Signalling, metabolic pathways and iron homeostasis in endothelial cells in health, atherosclerosis and Alzheimer's disease. *Cells*. 2020;9(9):2055. doi:10.3390/cells9092055
56. Ribatti D, Tamma R, Annesse T. The role of vascular niche and endothelial cells in organogenesis and regeneration. *Exp Cell Res*. 2021;398(1):112398. doi:10.1016/j.yexcr.2020.112398
57. Wang Y, Wang J, Yang J, et al. Study on protection of human umbilical vein endothelial cells from amiodarone-induced damage by intermediate through activation of Wnt/ β -catenin signaling pathway. *Oxid Med Cell Longev*. 2021;2021:8889408. doi:10.1155/2021/8889408
58. Xue M, Qiqige C, Zhang Q, et al. Effects of tumor necrosis factor α (TNF- α) and interleukin 10 (IL-10) on intercellular cell adhesion molecule-1 (ICAM-1) and cluster of differentiation 31 (CD31) in human coronary artery endothelial cells. *Med Sci Monit*. 2018;24:4433–4439. doi:10.12659/MSM.906838
59. Kenny OM, McCarthy CM, Brunton NP, et al. Anti-inflammatory properties of potato glycoalkaloids in stimulated Jurkat and Raw 264.7 mouse macrophages. *Life Sci*. 2013;92(13):775–782. doi:10.1016/j.lfs.2013.02.006
60. Liu Y, Tie L. Apolipoprotein M and sphingosine-1-phosphate complex alleviates TNF- α -induced endothelial cell injury and inflammation through PI3K/AKT signaling pathway. *BMC Cardiovasc Disord*. 2019;19(1):279. doi:10.1186/s12872-019-1263-4

61. Gao H, Zhang Q, Chen J, et al. Porcine IL-6, IL-1 β , and TNF- α regulate the expression of pro-inflammatory-related genes and tissue factor in human umbilical vein endothelial cells. *Xenotransplantation*. 2018;25(5):e12408. doi:10.1111/xen.12408
62. Yu H, Lin L, Zhang Z, Zhang H, Hu H. Targeting NF- κ B pathway for the therapy of diseases: Mechanism and clinical study. *Sig Transduct Target Ther*. 2020;5(1):209. doi:10.1038/s41392-020-00312-6
63. Dorrington MG, Fraser IDC. NF- κ B signaling in macrophages: Dynamics, crosstalk, and signal integration. *Front Immunol*. 2019;10:705. doi:10.3389/fimmu.2019.00705
64. Deng HF, Wang S, Li L, et al. Puerarin prevents vascular endothelial injury through suppression of NF- κ B activation in LPS-challenged human umbilical vein endothelial cells. *Biomed Pharmacother*. 2018;104:261–267. doi:10.1016/j.biopha.2018.05.038
65. Cheng J, Chen T, Li P, et al. Sodium tanshinone IIA sulfonate prevents lipopolysaccharide-induced inflammation via suppressing nuclear factor- κ B signaling pathway in human umbilical vein endothelial cells. *Can J Physiol Pharmacol*. 2018;96(1):26–31. doi:10.1139/cjpp-2017-0023
66. Hasanain M, Bhattacharjee A, Pandey P, et al. α -solanine induces ROS-mediated autophagy through activation of endoplasmic reticulum stress and inhibition of Akt/mTOR pathway. *Cell Death Dis*. 2015;6(8):e1860. doi:10.1038/cddis.2015.219
67. Wen Z, Huang C, Xu Y, et al. α -solanine inhibits vascular endothelial growth factor expression by downregulating the ERK1/2-HIF-1 α and STAT3 signaling pathways. *Eur J Pharmacol*. 2016;771:93–98. doi:10.1016/j.ejphar.2015.12.020
68. Karaboğa Arslan A, Yerer M. α -chaconine and α -solanine inhibit RL95-2 endometrium cancer cell proliferation by reducing expression of Akt (Ser473) and ER α (Ser167). *Nutrients*. 2018;10(6):672. doi:10.3390/nu10060672
69. Zinatizadeh MR, Schock B, Chalbatani GM, Zarandi PK, Jalali SA, Miri SR. The nuclear factor kappa B (NF- κ B) signaling in cancer development and immune diseases. *Genes Dis*. 2021;8(3):287–297. doi:10.1016/j.gendis.2020.06.005

Bone tissue 3D bioprinting in regenerative dentistry through the perspective of the diamond concept of healing: A narrative review

Karolina Fiona Osypko^{1,A–F}, Michał Piotr Ciszynski^{2,B–F}, Paweł Kubasiewicz-Ross^{2,E,F}, Jakub Hadzik^{2,E,F}

¹ Klinika Platinum, Wrocław, Poland

² Department of Oral Surgery, Wrocław Medical University, Poland

A – research concept and design; B – collection and/or assembly of data; C – data analysis and interpretation;

D – writing the article; E – critical revision of the article; F – final approval of the article

Advances in Clinical and Experimental Medicine, ISSN 1899–5276 (print), ISSN 2451–2680 (online)

Adv Clin Exp Med. 2023;32(8):921–931

Address for correspondence

Michał Piotr Ciszynski
michal.ciszynski@umw.edu.pl

Funding sources

None declared

Conflict of interest

None declared

Received on April 11, 2022

Reviewed on December 22, 2022

Accepted on January 8, 2023

Published online on February 8, 2023

Abstract

Three-dimensional bioprinting technology appears to be a promising solution for the treatment and reconstruction of a wide range of maxillofacial bone defects. In this review, the authors discuss different bioprinting solutions and options in the context of the 4 factors of bone healing: structures or scaffolds, osteogenic cells, growth factors, and stabilization (diamond concept of healing), as well as the influence of a 5th factor – vascularization. Bone is a complex tissue; hence, bone bioprinting may require different technical approaches and mixed methods. Ultraviolet (UV) crosslinkable hydrogels, such as gelatin methacryloyl (GelMA), are among the most promising bioinks; they are enhanced by hydroxyapatite or 1–2.5 mm beta-tricalcium phosphate (β -TCP) granules and porous scaffolds with recommended pore sizes greater than 300 μ m. The advantages of mesenchymal stem cells (MSCs) are their significant availability, low tumorigenicity, and great potential for differentiation into osteoblasts or endothelial cells (ECs). Although growth factors require advanced delivery systems, they provide excellent improvement in the functionality of printed tissues. A proper vasculature system supplies cells with oxygen and nutrients, removes waste products, promotes osteogenesis, prevents ischemic necrosis, and improves the mechanical properties of bone. With all of these aspects perfectly balanced and working in synergy, the clinical use of bioprinting is only a matter of time.

Key words: bioprinting, augmentation, tissue engineering, regenerative dentistry, regenerative medicine

Cite as

Osypko KF, Ciszynski MP, Kubasiewicz-Ross P, Hadzik J.
Bone tissue 3D bioprinting in regenerative dentistry
through the perspective of the diamond concept of healing:
A narrative review. *Adv Clin Exp Med.* 2023;32(8):921–931.
doi:10.17219/acem/159091

DOI

10.17219/acem/159091

Copyright

Copyright by Author(s)

This is an article distributed under the terms of the
Creative Commons Attribution 3.0 Unported (CC BY 3.0)
(<https://creativecommons.org/licenses/by/3.0/>)

Introduction

Three-dimensional (3D) printing has long been used in efforts to not only achieve bone regeneration but also restore lost dentition. Computer-aided design and computer-aided manufacturing (CAD/CAM)-produced titanium mesh can be used for guided bone regeneration procedures, allowing for more predictable outcomes.^{1,2} Furthermore, 3D technology can be used to manufacture custom-made, precisely fitting scaffolds out of porous hydroxyapatite blocks.³ Titanium dental implants created through the process of direct laser metal forming, a particular method of additive manufacturing, have already proven to be predictable. Moreover, although their properties still need to be confirmed, they could potentially surpass conventional, machined dental implants in many ways.^{4–10}

Since its inception over a decade ago, the “diamond concept”, a conceptual framework of what is necessary to achieve successful bone healing, has been acknowledged. This framework includes the following: 1) sufficient mechanical stabilization and biological competence of the organism; 2) osteogenic cells; 3) osteoconductive structures or scaffolds; and 4) growth factors.^{11,12} Additionally, sufficient vascularization of newly formed tissue should be considered a 5th element required for successful bone regeneration (Fig. 1).

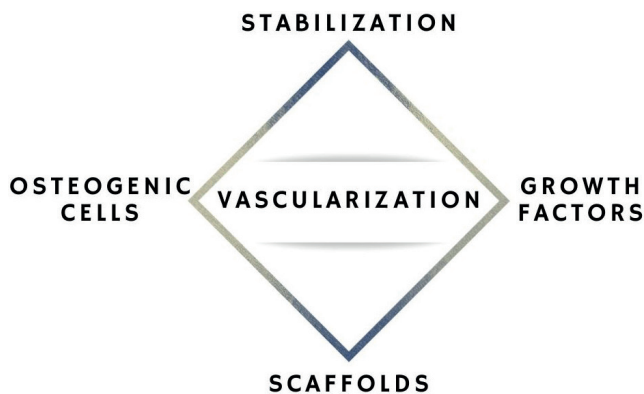


Fig. 1. Diagram of 5 elements promoting successful bone tissue regeneration

Autogenous grafts are considered the “gold standard” in bone tissue regeneration due to their osteogenic, osteoconductive and osteoinductive properties.¹³ Unfortunately, harvesting autogenous bone grafts usually causes pain at the donor site. It may also result in other, less frequently encountered complications, including nerve injury, hematoma, infection, and damage to neighboring tissues.¹⁴ An emerging solution to this problem is 3D bioprinting technology, which has the ability to create living autogenous grafts that are designed and manufactured in adequate form and dimensions to perfectly fit the shape of the defect. The creation of 3D tissue constructs is achievable using bioink deposition (specifically, jetting, extrusion

or laser-assisted evaporation) and then crosslinking with a 3D bioprinter. This technology facilitates the design of complex constructs – individualized forms and shapes of the target tissue structure that simultaneously contain multiple cell types.¹⁵

Objectives

The available scientific literature is relatively lacking in original studies and review articles on the use of bioprinting in dental procedures. Nevertheless, knowledge of this topic is important to refine the practice and development of this technology. This review aims to summarize the current state of knowledge on contemporary bioprinting treatment in dentistry. Current regenerative practices and studies in the field of regenerative dentistry are also discussed.

Methods

An electronic database search was conducted using MEDLINE via PubMed and Google Scholar. The database was searched for in vitro and in vivo studies involving different approaches to certain topics (i.e., types of cells, bioinks, growth factors, and answers to vascularization needs). The especially valued studies were those that contradicted or proved the limitations of factors and methods used in previous studies.

The search terms included all combinations of the following keywords: bioprinting OR 3D bioprinting OR stem cells OR mesenchymal stem cells OR growth factors OR GelMA AND bone regeneration OR bone OR clinical use OR regenerative medicine OR regenerative dentistry. Since 3D bioprinting refers to a variety of scientific fields, the following exclusion criteria were applied: 1) 3D printing not related to medicine; 2) 3D printing of medical materials; 3) studies related to hard tissues other than bone; 4) studies on bone regenerated with different techniques; and 5) other 3D applications in medicine.

Two researchers (KO and MC) independently reviewed the titles and abstracts to determine whether they met the inclusion and exclusion criteria. Disagreements were resolved via consensus. Collected titles and corresponding abstracts without duplicates were imported into Sciwheel citation manager program (Sciwheel Ltd., London, UK). The reference lists of the imported articles were screened for other relevant studies (Fig. 2). In turn, the collected studies were screened to search for bias in article selection. They were then grouped into the following 5 categories depending on the type of experiment conducted: 1) scaffold and bioinks; 2) stem cells; 3) growth factors and differentiation factors; 4) vasculature; and 5) stabilization. Although some studies addressed 2 or more categories, the authors tried to cite the results in such a way that

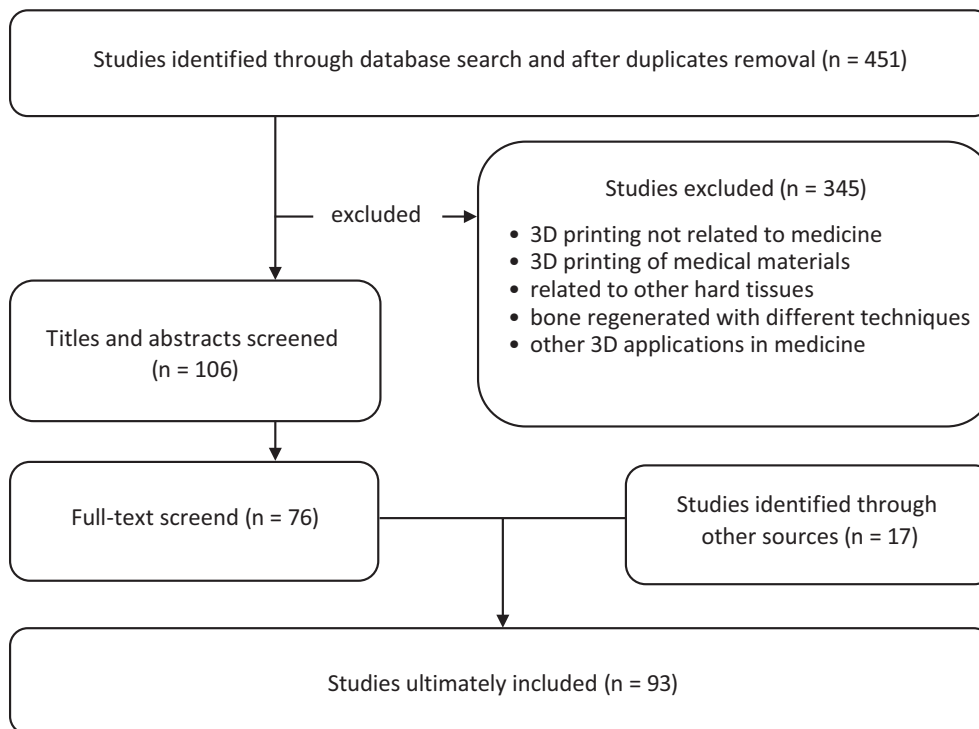


Fig. 2. Flowchart of the search strategy, exclusion criteria and study selection

the main points and significance of the results could be easily understood. Sometimes, one study was mentioned multiple times, as it pointed to various findings.

Scaffolds and bioinks

Bioprinting offers the possibility of printing cell suspensions into a tissue construct, regardless of the presence of a scaffold support. The most common bioinks are cell-laden hydrogels, decellularized extracellular matrix (dECM)-based solutions and cell suspensions.¹⁶ When choosing a suitable bioink, certain technical aspects must be considered, as it should: 1) provide chemical conditions mimicking those of the targeted tissue; 2) be biocompatible; 3) have controlled biodegradability to allow for cellular remodeling; 4) present shear-thinning behavior that allows extrusion with minimal stress to the encapsulated cells; 5) enable sol–gel transition; 6) be able to be extruded without clogging the nozzle; 7) provide suitable durability and stiffness; 8) provide adequate shape fidelity with proper stacking ability; and 9) feature proper density and porosity for the diffusion of gasses and nutrients.¹⁷ No perfect, flawless bioink exists; the compromise between suitability for fabrication and ability to accommodate encapsulated cells should be established. This compromise is known as the “biofabrication window”.¹⁸ Bioprinting of bone requires the use of bioinks with the ability to transform from a liquid state to a more dense structure while simultaneously preserving cell viability and bioactivity.¹⁹ Moreover, the density of the newly formed construct has an impact not only on the durability of the scaffold itself but also directly influences the activity of the cells.²⁰ Precalcified

bone with a maximum stiffness of approx. 50 kPa is the most rigid matrix that can host stem cells,²¹ which is still over 10,000 times less rigid than mature calcified bone.²² Bone marrow mesenchymal stem cells (MSCs) are the softest stem cell niche,²³ with a nearly liquid extracellular space and elasticity of 0.3 kPa.²⁰ Such a difference may be overcome *in vitro*, but it presents a challenge for *in vivo* experiments. A promising solution seems to be integrating different technical approaches for different bone compartments (i.e., scaffold-based and non-scaffolding methods).¹⁵

The biomaterials currently used in 3D bioprinting can be assigned to one of 3 main categories: 1) non-hygroscopic polymers; 2) hydrogels; and 3) dECM.¹⁹

Curable polymers comprise the 1st category; they display good durability and mechanical properties suitable for adequate structure and scaffolding. Processing of this kind of material, however, requires extraordinary conditions, including high temperature or the presence of toxic solvents, which mostly excludes them from being printed collectively with cells. Therefore, these materials are usually used for scaffold production, with cells seeded upon the surface.²⁴

The 2nd category consists of hydrogels, i.e., soft biomaterials that can absorb and maintain large loads of water.²⁵ These can be made of synthetic or natural polymers and do not present the same levels of mechanical features as curable support polymers, although cells are capable of residing within them.²⁴ Synthetic hydrogels include polyethylene glycol (PEG)-based materials, such as PEG diacrylate, and polyacrylamide-based gels. Naturally derived hydrogels, which employ polymers, are often polysaccharides obtained and purified from natural sources. Additionally, they can be composed of peptides or proteins. Hydrogels commonly used in laboratories include collagen,

hyaluronic acid, alginate, agarose, chitosan, fibrin, and Matrigel.^{19,24}

As the majority of bone tissue's extracellular matrix (ECM) (approx. 95%) consists of collagen (COL) type I,²⁶ and since collagen is one of the most widely available bioinks, it might seem to be a logical initial choice from the viewpoint of bone bioprinting.²⁷ Although not ideal, COL has the qualities to be a potential bioprinting material. It has a variety of different characteristics, including being liquid at low temperatures; when faced with an increase in temperature or neutral pH, it creates a fibrous structure.²⁵ As a consequence of losing its typical, organized structure, COL becomes gelatin (denatured COL).²⁸

Gelatin, being the degraded form of collagen, contains many arginine–glycine–aspartic acid sequences, which display cell-responsive properties,²⁹ as well as the target sequences of matrix metalloproteinases (MMPs) responsible for tissue and cell remodeling.³⁰ Pore sizes greater than 300 μm are recommended, as they enhance the formation of bone tissue and capillaries. Larger pores are better vascularized and cause immediate osteogenesis, without the preceding formation of cartilage. Smaller pores, on the other hand, tend to cause hypoxic conditions and favor osteochondral formation. In addition, gelatin is easily soluble and less antigenous than collagen.³¹

Gelatin methacryloyl (GelMA) is a synthetically modified gelatin-based material containing methacrylamide groups and methacrylate groups.³² Most importantly, GelMA is an inexpensive, cell-responsive hydrogel utilized to create cell-laden microtissues and microfluidic devices. Synthetically derived hydrogels have the advantage of allowing easy modification of their mechanical features and having cell-adhesive properties.³³ Gelatin methacryloyl hydrogels could be useful for creating complex, cell-responsive microtissues with endothelialized microvasculature. They have been patterned down to 100 μm resolution and proven to have accuracy and functionality similar to other commonly used hydrogels. However, unlike other synthetic ultraviolet (UV) crosslinkable hydrogels, they have been shown to have cell-adhesive properties; cells adhere to them, migrate within them, proliferate, and organize in both 2D and 3D in GelMA micropatterns. These data suggest possible applications in creating endothelial-lined vasculature within engineered tissues.³³

Conveniently, methacryloyl substituent groups provide gelatin with the ability to photo-cross-link when exposed to light and a photoinitiator.³⁴ This process of polymerization does not require extraordinary conditions and allows a certain level of control over the reaction. For this reason, the photo-curing properties of hydrogels are considered a significant upgrade compared to other common materials. Gao et al. created a particular bioink composed of GelMA hydrogel cross-linked with PEG-gelatin and MSCs incorporated within its structure as a way to obtain mechanical properties ideal for creating bone and cartilage.³⁵ After 21 days, different types of constructs were compared:

human MSC-PEG-GelMA and cell-laden PEG or GelMA. The first type demonstrated an elastic modulus improvement of 100% compared to the others. The authors proved that multimaterial hydrogels with photo-cross-linking features may introduce new solutions and promising advances in the composition of bioinks, in particular in the context of producing cartilage and bone substitutes.¹⁹ Additionally, GelMA has already been used in several studies on printing functioning vascular networks and bone-tissue substitutes, which will be discussed later in this article.^{36–38}

The 3rd category of biomaterials is dECM, which has the native ECM components retained. Its premanufacturing requires all cells to be removed from a tissue while preserving only the ECM. This is achieved through a series of chemical and enzymatic processes.³⁹ The dECM is then solubilized to a desired concentration until a gel-like substance appropriate for 3D bioprinting is obtained.¹⁹ Once isolated, bone dECM can be co-printed with biocompatible hydrogels or molecules.^{40–42} Moreover, in order to promote osteogenesis, small particles of hydroxyapatite or beta-tricalcium phosphate (β -TCP) can be dispersed in the hydrogel-based bioink.⁴³

Factors such as the macrostructural and geometrical properties of a material have a major impact on more than just the resilience of a scaffold. Studies have shown that materials characterized by numerous pores of variable sizes and connectivities facilitate the passage of oxygen, nutrients and cellular wastes.¹⁹ As porosity promotes the oxygenation of MSCs in printed hydrogel scaffolds, it also supports their viability and osteogenic differentiation.⁴⁴ Lower porosity has been shown to suppress cell proliferation and force cell aggregation *in vitro*, thus stimulating osteogenesis. On the contrary, significantly greater ingrowth of bone tissue can be achieved *in vivo*, thanks to larger pore size and higher porosity. However, the increased size and number of pores results in worsened mechanical properties. This fact sets an upper limit to pore size and porosity.⁴⁵ Pore sizes greater than 300 μm are recommended, as they enhance the formation of bone tissue and capillaries. Larger pores are better vascularized and cause immediate osteogenesis, without the preceding cartilage formation. Smaller pores, on the other hand, tend to cause hypoxic conditions and favor osteochondral formation.⁴⁵ A study by Lee et al. compared porosity of and cell cultures on 3 different scaffolds: COL, COL/dECM (CE) and COL/dECM/silk fibroin (CES). After 7 days, scanning electron microscope (SEM) images showed the highest concentration of cells on CES, followed by a medium concentration on CE and comparatively the lowest concentration on pure COL. Furthermore, the researchers analyzed the pore aspect ratio (length/width), and almost 100% of CES pores had a ratio of less than 3. In the case of CE, approx. 70% of pores had a ratio lower than 3, 20% had a ratio of 3–6 and 10% had a ratio greater than 6. The majority of pure COL pores had a ratio of 3–6. In light of these data, it seems that longer and narrower pores provide inferior conditions for cell cultures compared to more proportional ones.⁴²

Stem cells

Stem cells have major advantages over adult cells (i.e., self-renewing potential and ability to differentiate when exposed to specific stimuli).⁴⁶ Tissue engineering and regenerative medicine need to embrace these abilities to fulfill the following tasks: such as: 1) providing architectural and hierarchical arrangement of the cell–biomaterial complex; 2) patterning living cells in 3D; and 3) mimicking the complex patterns of tissue organization.⁴⁷ Before selecting stem cells for a bioprinted model, their experimental and therapeutic boundaries, origin, immunocompetence, and long-term engraftment potential dictated by the potency of the cell must be taken into consideration.⁴⁸

Three major classes of stem cells can be distinguished: 1) induced pluripotent stem cells (iPSCs), which can be reprogrammed from somatic cells isolated from the patient's tissue with ease of access; 2) embryonic stem cells (ESCs), which originate from the inner cell mass of blastocysts and have the potential to differentiate into any cell type; and 3) adult stem cells, which are located in specific tissues and take an active role in repair processes.⁴⁷

The initial creation of iPSCs was accomplished through the ectopic expression of 4 specific genes (*OCT4*, *KLF4*, *SOX2*, and *c-Myc*; all 4 are abbreviated as OSKM). Thus far, iPSCs have been successfully acquired from a variety of different cell types and species, suggesting a universal molecular mechanism. The abundance of sources of iPSCs in contrast to other pluripotent stem cell sources may suggest their forthcoming usefulness in the development of tissues and organs.⁴⁹ Moreover, autologous iPSCs provide cells considered the least dangerous in terms of the risk of immune rejection. However, in research into age-related macular degeneration therapy, 2 major drawbacks were encountered: financial limitations and the duration of treatment. The process of generating iPSCs, confirming their safety and differentiating them into retinal cells used for transplantation took approx. 1 year and cost almost 1 million USD.⁴⁹

In the 2nd group are ESCs, which provide extraordinary proliferative potential and are directly responsible for the formation and growth of the embryo and the 3 different germ layers – ectoderm, endoderm and mesoderm – which are essentially employed in the formation and generation of any type of tissue.⁴⁷ There has been extensive research on utilizing ESCs to achieve regeneration of bone tissue. However, due to the risk of immune rejection and existing ethical issues, the application of ESCs under nonlethal orthopedic conditions is considerably limited.⁵⁰ Furthermore, ESCs isolated from mice and then later from humans featured not only pluripotency but also tumorigenicity.⁵¹ In the context of regenerative medicine, the extent of their application for printing tissue constructs is largely limited by their low approachability, questionable safety and ethical issues.⁵²

Unlike ESCs, MSCs have the advantage of being available throughout the entire life of an individual and at all

stages of development, including adulthood. Moreover, they may also be obtained as a result of differentiation of other types of stem cells (iPSCs and ESCs).⁵³ A meta-analysis by Wang et al. showed that tumorigenesis, which might potentially occur in MSC therapy, has rarely been reported.⁵⁴ The MSCs constitute a class of cells displaying significant heterogeneity and the possibility to be isolated from many different sites, including adipose tissue, the umbilical cord and the placenta,⁵⁴ as well as from bone marrow in the form of an aspirate.⁴⁵ One of the natural pathways for the development of MSCs is differentiation into osteoblasts, although this requires key differentiation factors, such as ascorbic acid, β -glycerophosphate, dexamethasone/vitamin D3, and galectins. This process results in the expression of certain markers, including an increase in alkaline phosphatase, calcium accumulation and RUNX2.⁵³ However, research on the potential of MSCs in scaffold models should concentrate not only on osteogenic capabilities, as they can actually play 2 different roles. The first and most obvious role is as a source of a specific type of cell, which in this case means subsequent differentiation into osteoblasts. An alternative role of MSCs is as a supplemental population of cells, either as a native population or as an additional population that can be recruited to the tissue in order to perform a different function. In osteochondral constructs within the same model, MSCs are meant to differentiate into bone lineages and cartilage.⁵³ Cidonio et al. highlighted that the patterning of endothelial cells (ECs) and using MSCs for printing are crucial for the proper functioning of engineered bone tissue, while new clinical solutions targeting bone defects may fail due to poor interconnection between the graft and host tissues and possible necrosis of the graft caused by insufficient nutrient supplies.⁵⁵ An in vitro study by Wang et al. demonstrated successful MSC differentiation into ECs. Factors such as vascular endothelial growth factor (VEGF), basic fibroblast growth factor, insulin-like growth factor (IGF), epidermal growth factor, ascorbic acid, and heparin were used to impact MSCs. In addition, real-time quantitative polymerase chain reaction (qPCR) showed elevated expression of certain indicators, such as vascular endothelial cadherin, von Willebrand factor and VEGF receptor-2, in an induced MSC group compared with an uninduced MSC group.⁵⁶ The ability of MSCs to create vasculature was examined in a recent in vivo study of canines by producing small artificial vessels. The researchers employed autologous MSCs of bone marrow origin and biodegradable polycaprolactone (PCL). After MSC culturing and confirmation of differentiation into endothelial-like cells, 3-layered artificial vessels were created and subsequently implanted into the arteries of the canines. In comparison to the control vessels, the cell-derived vessels showed that their inner surfaces were covered with more ECs, whereas fibrinous clots exhibited little to even no inflammation. The authors of that study suggested that the immune system only minimally

rejected these artificial vessels due to the autologous origin of the MSCs.⁵⁷

Although the presented studies depict MSCs as currently the best candidate for tissue engineering and regenerative medicine, there are always drawbacks. In this case, more research needs to be conducted on the exact mechanism of differentiation into other cell types, as this process remains unknown.⁵³

Growth and differentiation factors

Growth factors are endogenous signaling molecules that regulate the cellular responses required for wound healing processes, including migration, proliferation and differentiation.^{58,59}

These signaling molecules can be divided into 3 groups: 1) pro-inflammatory cytokines; 2) transforming growth factor beta (TGF- β) superfamily and other growth factors; and 3) metalloproteinases and angiogenic factors.⁶⁰

All of these molecules, including the interleukins (IL-1 and IL-6), tumor necrosis factor alpha (TNF- α), fibroblast growth factor, IGF, platelet-derived growth factor, and VEGF, are naturally found in abundant quantities in a fracture hematoma. These biologically active molecules are secreted not only by a variety of cell types, including ECs, platelets, macrophages, and monocytes, but also MSCs. Bone morphogenetic proteins (BMPs) are well-known signaling molecules that possess osteoinductive properties.¹² Bone morphogenetic protein 2 and BMP-7 are already approved for clinical use in orthopedic and trauma surgery.⁶¹ Additionally, the activity of BMPs and other proteins that triggers cell differentiation into osteoblasts, which in turn results in bone formation, is also affected by the micro- and nanostructural properties of the scaffold used.⁶²

Vascular endothelial growth factor is known to be a key regulator of physiological angiogenesis during embryogenesis.⁶³ This makes it one of the best examined growth factors in regard to this topic. In fact, a different approach to promoting vascularization is to enrich 3D constructs with growth factors, thus causing the fabrication of a vascular network in tissue-engineered bone.⁶⁴ Unfortunately, growth factors display very low *in vivo* stability, which significantly reduces their effectiveness in clinical settings.⁵⁸ The effective use of growth factors is highly dependent on available delivery systems. Some researchers have targeted this aspect of therapy with novel delivery platforms, such as polymer gels, coated dressings, chamber devices, and nanoparticles.^{65,66}

Gelatin microparticles have been tested as a way of controlling the release of VEGF so that it is active for a longer period of time at a specific part of the 3D-bioprinted scaffold. Gelatin microparticles enabled the prolonged release of VEGF during 3 weeks of *in vitro* studies. Perhaps more importantly, with the help of human endothelial progenitor cells, the bioactivity of VEGF was successfully

confirmed. Moreover, *in vivo* experiments on mice compared Matrigel scaffolds containing endothelial progenitor cells and VEGF that were released in one of 2 ways – fast or sustained – through the application of gelatin microparticles. The results after 7 days showed significantly higher levels of vessel formation in the sustained-release VEGF group compared to the fast-release VEGF group.⁶⁷ A study by Kim et al. tested the chitosan gel/gelatin microsphere dual delivery system as a method of enhancing osteoblast differentiation through the sequential release of 2 osteogenetically important molecules – BMP-2 and IGF-1. In their research, BMP-2 was released at the beginning, with a succeeding sustained slow release of IGF-1. Significantly higher alkaline phosphatase activity, which is usually associated with ongoing osteoblast activity, was observed among cells that received the sequential delivery system when compared with cells that underwent other treatment methods ($p < 0.05$).⁶⁸

A study by Jeon et al. examined the effect of transforming growth factor beta 1 (TGF- β 1) and angiopoietin (Ang-1) on human bone marrow-derived MSCs, both in monoculture and in direct contact with ECs. They demonstrated that the effect of these molecules is dependent on direct heterotypic cell–cell contact. Furthermore, they found a significant increase in the amount of α -smooth muscle actin in microvascular networks with added VEGF and TGF- β 1 or VEGF and Ang-1 compared to networks with added VEGF alone. The addition of Ang-1 resulted in the creation of fully functional networks, while the microvasculature initiated by TGF- β 1 lacked interconnections and thus was not satisfactory. The addition of Ang-1 to human bone marrow-derived MSCs caused an increase in the number of network branches and a reduction in mean vessel diameter compared to EC-only vasculature.⁶⁹ In conclusion, more actin-rich networks originated with VEGF + TGF- β 1 or VEGF + Ang-1 compared to VEGF alone; in particular, Ang-1 developed more complex networks than TGF- β 1.

Platelet-rich fibrin, with its advantage of being of autologous origin, does not face the legal problems of its predecessors and has been applied for a variety of different surgical indications.⁷⁰

A recent study by Lafiti et al. showed that platelet rich plasma/heparin sulfate (PRP/HS) improved adipose MSC differentiation and accelerated osteoblast differentiation, regardless of the presence of an osteogenic medium. Moreover, HS has a positive effect on the induction of osteoblast differentiation. Hydroxyapatite, PRP and HS showed synergistic effects on the formation of a 3D scaffold, especially in the presence of chemical induction. The ZrO₂ increased mechanical strength without any detrimental effects on bone formation. All things considered, it seems that hydroxyapatite/ZrO₂/PRP/HS scaffolds provide a better osteoconductive microenvironment for stem cells to differentiate into osteoblasts.⁷¹

Bone morphogenetic proteins provide proper stimulation for osteoblasts or progenitor cells toward osteogenic

differentiation. However, some biomaterials can induce intrinsic osteoinduction, in which MSCs differentiate into osteoblasts, even without the contribution of BMPs, thereby avoiding the potential adverse effects of BMP treatment.¹⁹

The process of osteogenic differentiation may be directly triggered by surface topography and inorganic ion release (in the case of calcium phosphate-based ceramics).⁶² When implanted within a coralline hydroxyapatite scaffold, adipose tissue-derived MSCs promoted the formation of new bone and enhanced bone healing of critical-size defects in rat mandibles. Descriptive histology and histomorphometry revealed a significant ($p < 0.05$) increase in bone regeneration values in the cell-treated defects at 3 and 6 weeks.⁷²

An *in vitro* study by Gao et al. demonstrated that β -TCP granules affected bone mesenchymal stem cells (BMSCs) by improving their proliferation and osteogenic genes through promoting their expression and the formation of related proteins. Additionally, the 1–2.5-millimeter granule scaffolds exhibited superior function compared to the 1-millimeter β -TCP granules. Furthermore, an *in vivo* study demonstrated that the 1–2.5-millimeter β -TCP granules facilitated new bone formation without the application of any exogenous cells or growth factors.⁴³

Another cell line that plays an important role in bone tissue regeneration is macrophages. Studies on animal models have proven that macrophage–MSC communication is essential for bone regeneration, and that macrophages probably play the most important role during the early stages of fracture healing.⁷³ However, many studies have shown seemingly contradictory results, which is suggested to be the result of technical differences among the studies (i.e., different sources of cells, maturity of the monocytes/macrophages, and specific co-culture conditions). In point of fact, all subpopulations of monocytes and macrophages have the ability to promote MSC-mediated osteogenesis, although their relevance fluctuates depending on the ambient physiological conditions: while M0 macrophages are the most important in physiological bone homeostasis, M1 and M2 macrophages show greater significance in particular stages of fracture healing. Presumably, the timing and duration of the M1 macrophage-mediated inflammatory reaction is a critical determinant in the outcome of subsequent bone regeneration.⁷³

Vasculature

Since free grafts do not have a proper vascular connection with the rest of the host, and oxygen diffusion reaches only cells located 100–200 μm from blood vessels, fabricated constructs may face oxygenation problems if the layer between vessels is thicker than 400 μm . Observations following *in vivo* implantations have shown relatively slow and insufficient capillary ingrowth into

thick constructs.⁷⁴ Therefore, tissue engineers must first create functional vasculatures into the engineered tissue to provide nutrient and oxygen supply, as well as to effectively remove waste products.⁷⁵ Highly developed vascularization in engineered bone tissue was shown to positively impact osteogenesis, lower the risk of ischemic necrosis and enhance mechanical properties.⁷⁶ Additionally, adequate vascularization promoted successive recruitment, differentiation and proliferation of osteoprogenitor cells as well as efficient gas exchange with subsequent bone homeostasis.⁷⁷

The creation of new blood vessels is possible through 2 processes. First, angiogenesis is the formation of new capillaries from existing blood vessels.⁶⁴ Vasculogenesis, on the other hand, is the formation of a primitive vascular network by differentiation of endothelial progenitor cells or angioblastic progenitor cells into ECs.⁷⁸

The maturation of newly formed vasculature through angiogenesis or vasculogenesis requires meeting certain conditions: 1) recruitment of mural cells; 2) generation of an ECM; and 3) specialization of the vessel wall for structural support and regulation of vessel function. In addition, parenchymal cells require an adequate nutrient supply, which can only be achieved when there is proper organization of the vascular network. All of these processes are finely regulated by a variety of receptors and ligands and their expression or concentration, as well as the influence of physical forces. Physical or biochemical disturbances of these factors result in abnormal vasculature, which may underlie future pathologies.⁷⁹

As mentioned earlier in this review, there are many different ways to ameliorate vasculature nascence and growth. Angiogenesis can be promoted through the influence of MSCs, as they cause an increase in the number of vascular branches.⁵³

An *in vitro* and *in vivo* study by Temple et al. tested varying internal porosities in anatomically shaped PCL scaffolds. The properties of these scaffolds were compared in terms of influencing human adipose-derived stem cells into producing vasculature and bone, which are 2 essential elements of bone tissue. The researchers demonstrated large scaffolds of maxillary and mandibular bone printed with precise details gathered from patients' computed tomography (CT) scans.⁸⁰ As another construct example, a functioning model of a fabricated vascular network was created with GelMA hydrogels. The authors of that study confirmed that the channels they produced were lined with endothelial monolayers. This suggests that GelMA is potentially an adequate substance for printing vascular networks.³⁶ Byambaa et al. gave another example of GelMA application in constructing whole vasculature within large-scale 3D-printed constructs. The co-culture of human bone marrow-derived MSCs and human umbilical vein endothelial cells (HUVECs) was integrated into bone-like tissue matrices with a perfusable vascular lumen. In order to print perfusable vessels within the construct,

the authors formed a cylinder with 5% GelMA hydrogel at low methacryloyl substitution (GelMA_{LOW}). They also loaded GelMA hydrogel with silicate nanoplatelets to induce osteogenesis, and synthesized hydrogel formulations with chemically conjugated VEGF to promote vascular spreading. The whole construct successfully supported proliferation and cell survival and remained structurally stable for 21 days of *in vitro* tests.³⁷ Anada et al. bioprinted 2 GelMA rings, creating a vascularized bone-mimetic construct with a central ring and peripheral ring to mimic bone marrow and cortical bone, respectively. The central ring contained HUVEC spheroids, and the peripheral ring contained octacalcium phosphate. As a result, octacalcium phosphate induced osteoblastic differentiation of the MSCs, while in the center, the HUVEC spheroids stimulated capillary network formation. In conclusion, both osteoblastic and angiogenic differentiation can be successfully achieved in the hydrogel environment.³⁸

As for directly printing vasculature, Dolati et al. printed conduits with carbon nanotubes as an additional mechanical reinforcement and a way to improve bioprintability. Their study became the foundation for more advanced constructs where, instead of carbon nanotubes, natural protein nanofibers could be used in large-scale tissue fabrication.⁸¹

Jusoh et al. prepared a vascularized bone tissue model made of ECM with incorporated hydroxyapatite. Not only did various hydroxyapatite concentrations in the ECM result in varying mechanical properties, but mechanically modulated hydroxyapatite–ECM interactions affected sprouting angiogenesis. Furthermore, hydroxyapatite improved not only sprouting speed but also lumen diameter, length and number of newly formed vessels.⁸²

Not only chemical particles but also physical factors affect vascularization. A study by Kuss et al. regarding the influence of oxygen levels showed that long-term hypoxia resulted in less vascularization and lower cell viability, while short-term hypoxia promoted vascularization-related gene expression. Experiments were conducted on stromal vascular fraction-derived cell (SVFC)-laden hydrogels and 3D-bioprinted composite scaffolds with polycaprolactone/hydroxyapatite (PCL/HAp). The results proved that short-term hypoxia accelerated microvessel development both *in vitro* and *in vivo* and helped merge with the host vasculature, although no osteogenic effect on SVFCs was proven. This effect could be embraced to promote *in vitro* prevascularization in order to rapidly achieve *in vivo* anastomosis.⁸³

Another aspect worth considering is the application of spheroids. Spheroids can contain high concentrations of cells from the outset, while encapsulated cells require time to proliferate.⁸⁴ This could be incredibly useful in regard to printing complex vascular networks. Norotte et al. successfully 3D-printed tubular vascular scaffold-free grafts with multicellular spheroids. Closely placed spheroids, used as building blocks, were assembled, fused and used to create a branched vascular tree. Moreover, when

comparing tissue spheroids and multicellular cylinders, the latter showed improved precision of the construct over a shorter period of time.⁸⁵

Stabilization

Bone grafts should be designed to adapt precisely to the recipient site. Importantly, in order to increase blood supply for the graft, it is recommended to perforate the recipient site with a round bur of 1.0 mm in diameter.⁸⁶ Afterwards, the bone block can be placed in a passive manner and fixed without any excessive tension to the alveolar bone, usually with titanium miniscrews. The length and number of screws depended greatly on the clinical situation, such as recipient bone conditions and the thickness of the block.⁸⁷ Improper fixation of the graft may cause tension within forming tissues and eventually constrain bone healing. A thorough surgical procedure strategy and fine management of soft tissues, including adequate flap design, are essential for osseointegration and more predictable wound healing.⁸⁶

Currently, titanium osteosynthesis and screws are the default choice in orthognathic surgery and maxillofacial traumatology.^{88–90}

Alternatively, resorbable pins can be used.⁹¹ Biodegradable systems reduce the number of necessary surgical interventions, as there is no need to remove them after the initial procedure. However, it has been reported that the degradation products of these systems may cause adverse tissue reactions.⁹⁰ Additionally, prolonged resorption time and greater screw diameter should be taken into consideration.⁸⁷

As bioprinting technology offers new regeneration possibilities, it may also introduce new solutions for fixation that are different from screws.

Discussion

The clinical use of 3D bioprinting is another step forward toward personalized medicine. This blend of different areas of sciences, such as engineering, biotechnology, medicine, and material sciences, is persistently being developed, as each of them presents new discoveries every day that can escalate the progress of the others. With innovative solutions, tissue engineering may be able to lower its costs, which is a necessary condition for achieving broad public access to this technology. Hopefully, patients with maxillofacial bone defects, tumor diseases, bone fractures, or alveolar atrophy will soon be easily able to benefit from the potential of 3D bioprinting.

Limitations

A possible limitation of this study is selection bias. The process of choosing the articles to be included in the paper was conducted independently by 2 researchers.

Despite the steps taken to prevent it, it is possible that some studies that deserved to be included in this review may have been omitted.

Conclusions

All crucial elements of the diamond concept of healing are achievable through the use of 3D bioprinting, which has been both discussed theoretically and applied clinically with promising outcomes. Among the most promising scaffolds and bioinks are COL I, GelMA and dECM. The most accessible and suitable stem cells are MSCs. As for growth factors and differentiation factors, various substances and particles may empower the final results, such as VEGF, TGF- β 1, Ang-1, hydroxyapatite, and β -TCP. In order to build functioning vasculature, researchers have used GelMA hydrogel scaffolds, carbon nanotubes, hydroxyapatite properties, different oxygen levels, and spheroids as building blocks. The stabilization issue is still to be resolved, and the newly created tissue should be precisely fitted and fixed without excessive tension (i.e., using titanium miniscrews or resorbable pins). Despite these advances, as this study shows, there is still room for improvement in all aspects of clinical bioprinting.

ORCID iDs

Karolina Fiona Osypko  <https://orcid.org/0000-0001-9953-1669>
 Michał Piotr Ciszynski  <https://orcid.org/0000-0002-3515-8479>
 Paweł Kubasiewicz-Ross  <https://orcid.org/0000-0001-7305-7161>
 Jakub Hadzik  <https://orcid.org/0000-0002-2353-3198>

References

- Ciocca L, Lizio G, Baldissara P, Sambuco A, Scotti R, Corinaldesi G. Prosthetically CAD-CAM-guided bone augmentation of atrophic jaws using customized titanium mesh: Preliminary results of an open prospective study. *J Oral Implantol*. 2018;44(2):131–137. doi:10.1563/aaid-joi-D-17-00125
- Sagheb K, Schiegnitz E, Moergel M, Walter C, Al-Nawas B, Wagner W. Clinical outcome of alveolar ridge augmentation with individualized CAD-CAM-produced titanium mesh. *Int J Implant Dent*. 2017;3(1):36. doi:10.1186/s40729-017-0097-z
- Mangano F, Macchi A, Shibli JA, et al. Maxillary ridge augmentation with custom-made CAD/CAM scaffolds: A 1-year prospective study on 10 patients. *J Oral Implantol*. 2014;40(5):561–569. doi:10.1563/AAID-JOI-D-12-00122
- Mangano C, Piattelli A, d'Avila S, et al. Early human bone response to laser metal sintering surface topography: A histologic report. *J Oral Implantol*. 2010;36(2):91–96. doi:10.1563/AAID-JOI-D-09-00003
- Shibli JA, Mangano C, D'Avila S, et al. Influence of direct laser fabrication implant topography on type IV bone: A histomorphometric study in humans. *J Biomed Mater Res*. 2010;93(2):607–914. doi:10.1002/jbm.a.32566
- Mangano C, Mangano F, Shibli JA, et al. Prospective clinical evaluation of 201 direct laser metal forming implants: Results from a 1-year multicenter study. *Lasers Med Sci*. 2012;27(1):181–189. doi:10.1007/s10103-011-0904-3
- Tunchel S, Blay A, Kolerman R, Mijiritsky E, Shibli JA. 3D printing/additive manufacturing single titanium dental implants: A prospective multicenter study with 3 years of follow-up. *Int J Dent*. 2016;2016(6):1–9. doi:10.1155/2016/8590971
- Mangano C, Mangano FG, Shibli JA, et al. Immediate loading of mandibular overdentures supported by unsplinted direct laser metal-forming implants: Results from a 1-year prospective study. *J Periodontol*. 2012;83(1):70–78. doi:10.1902/jop.2011.110079
- Mangano F, Luongo F, Shibli JA, Anil S, Mangano C. Maxillary overdentures supported by four splinted direct metal laser sintering implants: A 3-year prospective clinical study. *Int J Dent*. 2014;2014:252343. doi:10.1155/2014/252343
- Pingueiro J, Piattelli A, Paiva J, et al. Additive manufacturing of titanium alloy could modify the pathogenic microbial profile: An in vitro study. *Braz Oral Res*. 2019;33(Suppl 1):e065. doi:10.1590/1807-3107bor-2019.vol33.0065
- Giannoudis PV, Einhorn TA, Marsh D. Fracture healing: The diamond concept. *Injury*. 2007;38(Suppl 4):S3–S6. doi:10.1016/S0020-1383(08)70003-2
- Calori GM, Giannoudis PV. Enhancement of fracture healing with the diamond concept: The role of the biological chamber. *Injury*. 2011;42(11):1191–1193. doi:10.1016/j.injury.2011.04.016
- Ortega-Oller I, Padiá-Molina M, Galindo-Moreno P, O'Valle F, Jódar-Reyes AB, Peula-García JM. Bone regeneration from PLGA micro-nanoparticles. *Biomed Res Int*. 2015;2015:415289. doi:10.1155/2015/415289
- Myeroff C, Archdeacon M. Autogenous bone graft: Donor sites and techniques. *J Bone Joint Surg*. 2011;93(23):2227–2236. doi:10.2106/JBJS.J.01513
- Khoeini R, Nosrati H, Akbarzadeh A, et al. Natural and synthetic bioinks for 3D bioprinting. *Adv Nanobio Res*. 2021;1(8):2000097. doi:10.1002/anbr.202000097
- Ji S, Guvendiren M. Recent advances in bioink design for 3D bioprinting of tissues and organs. *Front Bioeng Biotechnol*. 2017;5:23. doi:10.3389/fbioe.2017.00023
- Veiga A, Silva IV, Duarte MM, Oliveira AL. Current trends on protein driven bioinks for 3D printing. *Pharmaceutics*. 2021;13(9):1444. doi:10.3390/pharmaceutics13091444
- Chimene D, Lennox KK, Kaunas RR, Gaharwar AK. Advanced bioinks for 3D printing: A materials science perspective. *Ann Biomed Eng*. 2016;44(6):2090–2102. doi:10.1007/s10439-016-1638-y
- Genova T, Roato I, Carossa M, Motta C, Cavagnetto D, Mussano F. Advances on bone substitutes through 3D bioprinting. *Int J Mol Sci*. 2020;21(19):7012. doi:10.3390/ijms21197012
- Winer JP, Janmey PA, McCormick ME, Funaki M. Bone marrow-derived human mesenchymal stem cells become quiescent on soft substrates but remain responsive to chemical or mechanical stimuli. *Tissue Eng Part A*. 2009;15(1):147–154. doi:10.1089/ten.tea.2007.0388
- Engler AJ, Sen S, Sweeney HL, Discher DE. Matrix elasticity directs stem cell lineage specification. *Cell*. 2006;126(4):677–689. doi:10.1016/j.cell.2006.06.044
- Discher DE, Mooney DJ, Zandstra PW. Growth factors, matrices, and forces combine and control stem cells. *Science*. 2009;324(5935):1673–1677. doi:10.1126/science.1171643
- Shin JW, Swift J, Ivanovska I, Spinler KR, Buxboim A, Discher DE. Mechanobiology of bone marrow stem cells: From myosin-II forces to compliance of matrix and nucleus in cell forms and fates. *Differentiation*. 2013;86(3):77–86. doi:10.1016/j.diff.2013.05.001
- Skardal A, Atala A. Biomaterials for integration with 3-D bioprinting. *Ann Biomed Eng*. 2015;43(3):730–746. doi:10.1007/s10439-014-1207-1
- Hospodiuk M, Dey M, Sosnoski D, Ozbolat IT. The bioink: A comprehensive review on bioprintable materials. *Biotechnol Adv*. 2017;35(2):217–239. doi:10.1016/j.biotechadv.2016.12.006
- Panwar P, Lamour G, Mackenzie NCW, et al. Changes in structural-mechanical properties and degradability of collagen during aging-associated modifications. *J Biol Chem*. 2015;290(38):23291–23306. doi:10.1074/jbc.M115.644310
- Marques CF, Diogo GS, Pina S, Oliveira JM, Silva TH, Reis RL. Collagen-based bioinks for hard tissue engineering applications: A comprehensive review. *J Mater Sci Mater Med*. 2019;30(3):32. doi:10.1007/s10856-019-6234-x
- Echavez MC, Hernández-Moya R, Iturriaga L, et al. Recent advances in gelatin-based therapeutics. *Exp Opin Biol Ther*. 2019;19(8):773–779. doi:10.1080/14712598.2019.1610383
- Liu Y, Chan-Park MB. A biomimetic hydrogel based on methacrylated dextran-graft-lysine and gelatin for 3D smooth muscle cell culture. *Biomaterials*. 2010;31(6):1158–1170. doi:10.1016/j.biomaterials.2009.10.040
- Van den Steen PE, Dubois B, Nelissen I, Rudd PM, Dwek RA, Opdenakker G. Biochemistry and molecular biology of gelatinase B or matrix metalloproteinase-9 (MMP-9). *Crit Rev Biochem Mol Biol*. 2002;37(6):375–536. doi:10.1080/10409230290771546

31. Gorgieva S, Kokol V. Collagen- vs. gelatine-based biomaterials and their biocompatibility: Review and perspectives. In: Pignatello R, ed. *Biomaterials Applications for Nanomedicine*. London, UK: InTech Open; 2011. doi:10.5772/24118
32. Yue K, Trujillo-de Santiago G, Alvarez MM, Tamayo A, Annabi N, Khademhosseini A. Synthesis, properties, and biomedical applications of gelatin methacryloyl (GelMA) hydrogels. *Biomaterials*. 2015;73:254–271. doi:10.1016/j.biomaterials.2015.08.045
33. Nichol JW, Koshy ST, Bae H, Hwang CM, Yamanlar S, Khademhosseini A. Cell-laden microengineered gelatin methacrylate hydrogels. *Biomaterials*. 2010;31(21):5536–5544. doi:10.1016/j.biomaterials.2010.03.064
34. Van Den Bulcke AI, Bogdanov B, De Rooze N, Schacht EH, Cornelissen M, Berghmans H. Structural and rheological properties of methacrylamide modified gelatin hydrogels. *Biomacromolecules*. 2000;1(1):31–38. doi:10.1021/bm990017d
35. Gao G, Schilling AF, Hubbell K, et al. Improved properties of bone and cartilage tissue from 3D inkjet-bioprinted human mesenchymal stem cells by simultaneous deposition and photocrosslinking in PEG-GelMA. *Biotechnol Lett*. 2015;37(11):2349–2355. doi:10.1007/s10529-015-1921-2
36. Bertassoni LE, Cecconi M, Manoharan V, et al. Hydrogel bioprinted microchannel networks for vascularization of tissue engineering constructs. *Lab Chip*. 2014;14(13):2202–2211. doi:10.1039/C4LC00030G
37. Byambaa B, Annabi N, Yue K, et al. Bioprinted osteogenic and vasculogenic patterns for engineering 3D bone tissue. *Adv Healthcare Mater*. 2017;6(16):1700015. doi:10.1002/adhm.201700015
38. Anada T, Pan CC, Stahl A, et al. Vascularized bone-mimetic hydrogel constructs by 3D bioprinting to promote osteogenesis and angiogenesis. *Int J Mol Sci*. 2019;20(5):1096. doi:10.3390/ijms20051096
39. Ott HC, Matthiesen TS, Goh SK, et al. Perfusion-decellularized matrix: Using nature's platform to engineer a bioartificial heart. *Nat Med*. 2008;14(2):213–221. doi:10.1038/nm1684
40. Jang J, Kim TG, Kim BS, Kim SW, Kwon SM, Cho DW. Tailoring mechanical properties of decellularized extracellular matrix bioink by vitamin B2-induced photo-crosslinking. *Acta Biomater*. 2016;33:88–95. doi:10.1016/j.actbio.2016.01.013
41. Pati F, Jang J, Ha DH, et al. Printing three-dimensional tissue analogues with decellularized extracellular matrix bioink. *Nat Commun*. 2014;5(1):3935. doi:10.1038/ncomms4935
42. Lee H, Yang GH, Kim M, Lee J, Huh J, Kim G. Fabrication of micro/nanoporous collagen/dECM/silk-fibroin biocomposite scaffolds using a low temperature 3D printing process for bone tissue regeneration. *Mater Sci Eng C Mater Biol Appl*. 2018;84:140–147. doi:10.1016/j.msec.2017.11.013
43. Gao P, Zhang H, Liu Y, et al. Beta-tricalcium phosphate granules improve osteogenesis in vitro and establish innovative osteo-regenerators for bone tissue engineering in vivo. *Sci Rep*. 2016;6(1):23367. doi:10.1038/srep23367
44. Fedorovich NE, Kuipers E, Gawlitta D, Dhert WJA, Alblas J. Scaffold porosity and oxygenation of printed hydrogel constructs affect functionality of embedded osteogenic progenitors. *Tissue Eng Part A*. 2011;17(19–20):2473–2486. doi:10.1089/ten.tea.2011.0001
45. Karageorgiou V, Kaplan D. Porosity of 3D biomaterial scaffolds and osteogenesis. *Biomaterials*. 2005;26(27):5474–5491. doi:10.1016/j.biomaterials.2005.02.002
46. Lutolf MP, Gilbert PM, Blau HM. Designing materials to direct stem cell fate. *Nature*. 2009;462(7272):433–441. doi:10.1038/nature08602
47. Scognamiglio C, Soloperto A, Ruocco G, Cidonio G. Bioprinting stem cells: Building physiological tissues one cell at a time. *Am J Physiol Cell Physiol*. 2020;319(3):C465–C480. doi:10.1152/ajpcell.00124.2020
48. Li J, Chi J, Liu J, et al. 3D printed gelatin-alginate bioactive scaffolds combined with mice bone marrow mesenchymal stem cells: A biocompatibility study. *Int J Clin Exp Pathol*. 2017;10(6):6299–6307. <https://e-century.us/files/ijcep/10/6/ijcep0053203.pdf>
49. Karagiannis P, Takahashi K, Saito M, et al. Induced pluripotent stem cells and their use in human models of disease and development. *Physiol Rev*. 2019;99(1):79–114. doi:10.1152/physrev.00039.2017
50. Park S, Im GI. Embryonic stem cells and induced pluripotent stem cells for skeletal regeneration. *Tissue Eng Part B Rev*. 2014;20(5):381–391. doi:10.1089/ten.teb.2013.0530
51. Knoepfler PS. Deconstructing stem cell tumorigenicity: A roadmap to safe regenerative medicine. *Stem Cells*. 2009;27(5):1050–1056. doi:10.1002/stem.37
52. Blau HM, Daley GQ. Stem cells in the treatment of disease. *N Engl J Med*. 2019;380(18):1748–1760. doi:10.1056/NEJMra1716145
53. Afflerbach AK, Kiri MD, Detinis T, Maoz BM. Mesenchymal stem cells as a promising cell source for integration in novel in vitro models. *Biomolecules*. 2020;10(9):1306. doi:10.3390/biom10091306
54. Wang Y, Yi H, Song Y. The safety of MSC therapy over the past 15 years: A meta-analysis. *Stem Cell Res Ther*. 2021;12(1):545. doi:10.1186/s13287-021-02609-x
55. Cidonio G, Glinka M, Dawson JI, Oreffo ROC. The cell in the ink: Improving biofabrication by printing stem cells for skeletal regenerative medicine. *Biomaterials*. 2019;209:10–24. doi:10.1016/j.biomaterials.2019.04.009
56. Wang C, Li Y, Yang M, et al. Efficient differentiation of bone marrow mesenchymal stem cells into endothelial cells in vitro. *Eur J Vasc Endovasc Surg*. 2018;55(2):257–265. doi:10.1016/j.ejvs.2017.10.012
57. Jang E, Kim JH, Lee J, Kim DH, Youn YN. Enhanced biocompatibility of multi-layered, 3D bio-printed artificial vessels composed of autologous mesenchymal stem cells. *Polymers*. 2020;12(3):538. doi:10.3390/polym12030538
58. Park J, Hwang S, Yoon IS. Advanced growth factor delivery systems in wound management and skin regeneration. *Molecules*. 2017;22(8):1259. doi:10.3390/molecules22081259
59. Midha S, Murab S, Ghosh S. Osteogenic signaling on silk-based matrices. *Biomaterials*. 2016;97:133–153. doi:10.1016/j.biomaterials.2016.04.020
60. Tsiroidis E, Upadhyay N, Giannoudis P. Molecular aspects of fracture healing: Which are the important molecules? *Injury*. 2007;38(Suppl 1):S11–S25. doi:10.1016/j.injury.2007.02.006
61. Schmidmaier G, Schwabe P, Strobel C, Wildemann B. Carrier systems and application of growth factors in orthopaedics. *Injury*. 2008;39(Suppl 2):S37–S43. doi:10.1016/S0020-1383(08)70014-7
62. Barradas A, Yuan H, van Blitterswijk C, Habibovic P. Osteoinductive biomaterials: Current knowledge of properties, experimental models and biological mechanisms. *Eur Cell Mater*. 2011;21:407–429. doi:10.22203/eCM.v021a31
63. Ferrara N, Gerber HP, LeCouter J. The biology of VEGF and its receptors. *Nat Med*. 2003;9(6):669–676. doi:10.1038/nm0603-669
64. Xing F, Xiang Z, Rommens PM, Ritz U. 3D bioprinting for vascularized tissue-engineered bone fabrication. *Materials (Basel)*. 2020;13(10):2278. doi:10.3390/ma13102278
65. Moura LIF, Dias AMA, Carvalho E, de Sousa HC. Recent advances on the development of wound dressings for diabetic foot ulcer treatment: A review. *Acta Biomater*. 2013;9(7):7093–7114. doi:10.1016/j.actbio.2013.03.033
66. Smith DM, Simon JK, Baker Jr JR. Applications of nanotechnology for immunology. *Nat Rev Immunol*. 2013;13(8):592–605. doi:10.1038/nri3488
67. Poldervaart MT, Gremmels H, van Deventer K, et al. Prolonged presence of VEGF promotes vascularization in 3D bioprinted scaffolds with defined architecture. *J Control Release*. 2014;184:58–66. doi:10.1016/j.jconrel.2014.04.007
68. Kim S, Kang Y, Krueger CA, et al. Sequential delivery of BMP-2 and IGF-1 using a chitosan gel with gelatin microspheres enhances early osteoblastic differentiation. *Acta Biomater*. 2012;8(5):1768–1777. doi:10.1016/j.actbio.2012.01.009
69. Jeon JS, Bersini S, Whisler JA, et al. Generation of 3D functional microvascular networks with human mesenchymal stem cells in microfluidic systems. *Integr Biol (Camb)*. 2014;6(5):555–563. doi:10.1039/C3IB40267C
70. Yamakawa S, Hayashida K. Advances in surgical applications of growth factors for wound healing. *Burns Trauma*. 2019;7:10. doi:10.1186/s41038-019-0148-1
71. Latifi M, Sani M, Salmannejad M, Kabir-Salmani M, Babakhanzadeh Bavanati H, Talaei-Khozani T. Synergistic impact of platelet rich plasma-heparin sulfate with hydroxyapatite/zirconia on the osteoblast differentiation potential of adipose-derived mesenchymal stem cells. *Cell Tissue Bank*. 2022;23(4):669–683. doi:10.1007/s10561-021-09966-0
72. Barrientos-Lezcano FJ, Redondo-González LM, Alberca-Zeballos M, Sánchez-García AM, García-Sancho J. Mandibular bone regeneration with autologous adipose-derived mesenchymal stem cells and coraline hydroxyapatite: Experimental study in rats. *Br J Oral Maxillofac Surg*. 2021;59(10):1192–1199. doi:10.1016/j.bjoms.2021.01.013

73. Pajarinen J, Lin T, Gibon E, et al. Mesenchymal stem cell-macrophage crosstalk and bone healing. *Biomaterials*. 2019;196:80–89. doi:10.1016/j.biomaterials.2017.12.025
74. Shahabipour F, Ashammakhi N, Oskuee RK, et al. Key components of engineering vascularized 3-dimensional bioprinted bone constructs. *Transl Res*. 2020;216:57–76. doi:10.1016/j.trsl.2019.08.010
75. Cui X, Boland T. Human microvasculature fabrication using thermal inkjet printing technology. *Biomaterials*. 2009;30(31):6221–6227. doi:10.1016/j.biomaterials.2009.07.056
76. Yu H, VandeVord PJ, Mao L, Matthew HW, Wooley PH, Yang SY. Improved tissue-engineered bone regeneration by endothelial cell mediated vascularization. *Biomaterials*. 2009;30(4):508–517. doi:10.1016/j.biomaterials.2008.09.047
77. Kanczler J, Oreffo R. Osteogenesis and angiogenesis: The potential for engineering bone. *Eur Cell Mater*. 2008;15:100–114. doi:10.22203/eCM.v015a08
78. Vaill e B, Vittet D, Feige JJ. In vitro models of vasculogenesis and angiogenesis. *Lab Invest*. 2001;81(4):439–452. doi:10.1038/labinvest.3780252
79. Jain RK. Molecular regulation of vessel maturation. *Nat Med*. 2003;9(6):685–693. doi:10.1038/nm0603-685
80. Temple JP, Hutton DL, Hung BP, et al. Engineering anatomically shaped vascularized bone grafts with hASCs and 3D-printed PCL scaffolds. *J Biomed Mater Res A*. 2014;10(12):4317–4325. doi:10.1002/jbm.a.35107
81. Dolati F, Yu Y, Zhang Y, Jesus AMD, Sander EA, Ozbolat IT. In vitro evaluation of carbon-nanotube-reinforced bioprintable vascular conduits. *Nanotechnology*. 2014;25(14):145101. doi:10.1088/0957-4484/25/14/145101
82. Jusoh N, Oh S, Kim S, Kim J, Jeon NL. Microfluidic vascularized bone tissue model with hydroxyapatite-incorporated extracellular matrix. *Lab Chip*. 2015;15(20):3984–3988. doi:10.1039/C5LC00698H
83. Kuss MA, Harms R, Wu S, et al. Short-term hypoxic preconditioning promotes prevascularization in 3D bioprinted bone constructs with stromal vascular fraction derived cells. *RSC Adv*. 2017;7(47):29312–29320. doi:10.1039/C7RA04372D
84. Ozbolat IT. Scaffold-based or scaffold-free bioprinting: Competing or complementing approaches? *J Nanotechnol Eng Med*. 2015;6(2):024701. doi:10.1115/1.4030414
85. Norotte C, Marga FS, Niklason LE, Forgacs G. Scaffold-free vascular tissue engineering using bioprinting. *Biomaterials*. 2009;30(30):5910–5917. doi:10.1016/j.biomaterials.2009.06.034
86. Nguyen TTH, Eo MY, Kuk TS, Myoung H, Kim SM. Rehabilitation of atrophic jaw using iliac onlay bone graft combined with dental implants. *Int J Implant Dent*. 2019;5(1):11. doi:10.1186/s40729-019-0163-9
87. Dominiak M, Dominiak S, Targonska S, Gedrange T. Three-dimensional bone block planning for mandibular sagittal bone defect reconstruction. *J Healthcare Eng*. 2020;2020:8829288. doi:10.1155/2020/8829288
88. Atef M, Osman AH, Hakam M. Autogenous interpositional block graft vs onlay graft for horizontal ridge augmentation in the mandible. *Clin Implant Dent Relat Res*. 2019;21(4):678–685. doi:10.1111/cid.12809
89. Hollensteiner M, Augat P, F rst D, et al. Bone surrogates provide authentic onlay graft fixation torques. *J Mech Behav Biomed Mater*. 2019;91:159–163. doi:10.1016/j.jmbbm.2018.12.013
90. Gareb B, van Bakelen NB, Buijs GJ, et al. Comparison of the long-term clinical performance of a biodegradable and a titanium fixation system in maxillofacial surgery: A multicenter randomized controlled trial. *PLoS One*. 2017;12(5):e0177152. doi:10.1371/journal.pone.0177152
91. Sukegawa S, Kawai H, Nakano K, et al. Feasible advantage of bioactive/bioresorbable devices made of forged composites of hydroxyapatite particles and poly-L-lactide in alveolar bone augmentation: A preliminary study. *Int J Med Sci*. 2019;16(2):311–317. doi:10.7150/ijms.27986

